Supporting Information

Tandem Synthesis of Enantioenriched Spirolactones via One-Pot Heck-Matsuda Reactions Directly from Nitroarenes

Tomaz H. D. Chorro+ [a,b], Clemens Kaussler+ [b], Julia V. Kolodiazhnaia [b], Frank Jensen,[c] Troels Skrydstrup*[b], and Carlos Roque D. Correia*[a]

Abstract: We report herein a novel, efficient, and expeditious approach for enantioselective intramolecular carbonylative Heck-Matsuda reaction, employing highly accessible, stable, and cost-effective nitroarenes as a masked electrophiles. This tandem process combines the one-pot reduction of nitroarenes to the respective anilines, diazotization, Heck-Matsuda, carbonylation, and cyclization, enabling the synthesis of enantioenriched spirolactones. The method achieves overall yields of up to 76% with excellent enantiomeric ratios of up to 96:4 under mild conditions. Isotopically labeled products are readily obtained with near stoichiometric 13C carbon monoxide. Importantly, nitroarenes are used as masked electrophiles, which serve as an advantageous alternative to anilines and aryldiazonium salts for the Heck-Matsuda reaction. This approach thereby avoids the isolation of sensitive aryldiazonium salt intermediates and, consequently, the dangers associated with them. Density Functional Theory (DFT) calculations provide precise insights into the enantioenrichment mechanism, highlighting the significance of Pd carbonyl complexes for efficient diastereoconvergence. Microkinetic modeling of the computationally obtained reaction network results in an enantioenrichment of sub-kcal-accuracy in comparison to the experiment. This work not only showcases the level of complexity achievable in the field of tandem reactions but also highlights the utility of nitroarenes in complex organic transformations, demonstrating their potential for both academic and industrial applications..

Table of Contents

General Remarks

Handling Of Carbon Monoxide

All carbonylation reactions were performed in a two-chamber system, in which gaseous CO was released in one chamber and utilized in a second chamber. The two-chamber system (COWare®) is depicted to the right and is composed of two glass vials (Chamber A and B) connected with a glass tube to allow gas transfer. Chambers can be sealed with a screw cap and a Teflon® coated silicone seal. CO-gas was released from methyldiphenylsilanecarboxylic acid (SilaCOgen) in a fluoride catalyzed decarbonylation with potassium fluoride. Precise conditions are given in the general procedures.

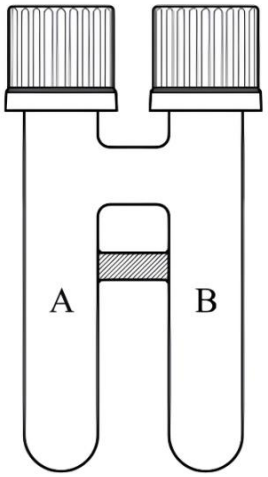

WARNING: Glassware under pressure!

- Glass equipment should always be examined for damages to its surface, which may weaken its strength.
- One must abide to all laboratory safety procedures and always work behind a shield when working with glass equipment under pressure.
- COware is pressure tested to 224 psi but should under no circumstances be operated above 60 psi (5 bar).

Solvents

Solvents THF, CH_2Cl_2 and MeCN were retrieved from a MBraun SP800 purification system, degassed by bubbling with argon for at least 30 minutes and stored over 4 Å molecular sieves for at least 16 hours prior to use. The remaining solvents were purchased from Sigma-Aldrich and used without further purification.

Analytical methods

Analytical thin layer chromatography (TLC) was performed employing Merck® Silica gel 60 F254 plates. Visualization was accomplished with UV light (254 nm), $KMnO_4$, *para*-anisaldehyde, and phosphomolybdic acid staining solutions followed by heating. Flash column chromatography was carried out utilizing Interchim puriflash system XS520Plus operating in a gradient mode (EtOAc/heptane). The ^{1}H NMR spectra were recorded at 400 MHz, ^{13}C NMR spectra were recorded at 101 MHz, and ^{19}F NMR spectra were recorded at 377 MHz on a Bruker 400 spectrometer. 1,3-Bis(trifluoromethyl)-5-bromobenzene was used as an internal standard for the determination of chemical yields by ^{1}H NMR. Chemical shifts (δ) are reported in ppm using residual undeuterated solvent as an internal standard ($CHCl_3$ at 7.26 ppm for ^{1}H NMR spectra and $CDCl_3$ at 77.16 ppm for ^{13}C NMR spectra). Multiplicity data are reported as follows: s = singlet, d = doublet, t = triplet, q = quartet, quint = quintet, sext = sextet, br s = broad singlet, dd = doublet of doublets, dt = doublet of triplets, ddd = doublet of doublet of doublets, ddt = doublet of doublet of triplets, dtd = doublet of triplet of doublets, dqd = doublet of quartet of

doublets, and m = multiplet. The multiplicity is followed by the coupling constant(s) in Hz and integration. HRMS spectra were recorded on a LC TOF (ES) apparatus. Enantiomeric ratios (*er*) were calculated through the integration of enantiomers corresponding signals, set by racemic samples. The products were analyzed by Ultra Performance Convergence Chromatography (UPC2) using Daicel Chiralpak IB-3 or ID-3 columns as chiral stationary phases. Gradient runs were performed with supercritical CO_2/solvent until the compound has been eluted. Racemic samples of the compounds were prepared following the general procedure A - *Synthesis of Standard Product*. Optical rotations were measured on a Bellingham+Stanley ADP440+ polarimeter, and $[\alpha]_D^T$ values are given in deg cm^3 g^{-1} dm^{-1}; concentrations, c, are listed in g 100 mL^{-1}.

Synthesis of Starting Materials

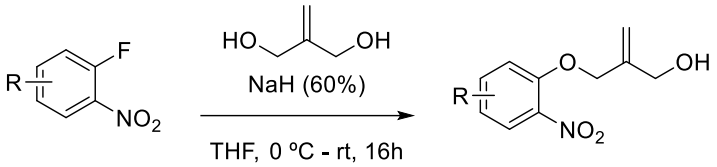

General Procedure A

According to a procedure adapted from the literature,[1] in a round bottom flask with a magnetic stirring bar was added NaH 60% (2.0 equiv) and anhydrous THF (3 mL/mmol), under N_2 atmosphere. The reaction was then cooled to 0 °C and 2-methylenepropane-1,3-diol (4.0 equiv) was added dropwise. This mixture was stirred for 30 min, warmed to room temperature and stirred for additional 30 min. Then, the mixture was cooled to 0 °C and the respective nitro-fluorobenzene (1.0 equiv) was added dropwise. The mixture was stirred for 30 min at 0 °C and overnight at room temperature. After 16 hours, water was added, and the organic layer was separated. The aqueous layer was extracted twice with DCM and the combined organic layers were washed with brine, dried over Na_2SO_4 and the solvent was evaporated under reduced pressure. The residue was purified by flash chromatography to afford the respective desired products.

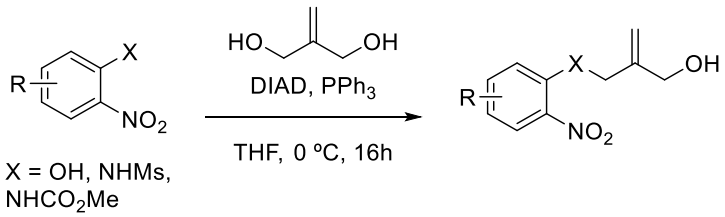

General Procedure B

According to a procedure adapted from the literature,[1] a round bottom flask with a magnetic stirring bar was charged with di-*tert*-butyl azodicarboxylate (2.0 equiv) and THF (5 mL/mmol) the mixture was cooled to 0 °C and triphenylphosphine (2.0 equiv) was added, followed by the addition of the aromatic phenol or protected aniline (1.0 equiv) and 2-methylenepropane-1,3-diol (4.0 equiv). The reaction was stirred overnight at room temperature. After 16 hours, the reaction mixture was diluted with ethyl acetate

and water and the organic layer was separated. The aqueous layer was extracted three times with ethyl acetate and the combined organic layers were washed with brine, dried over Na_2SO_4 and the solvent was evaporated under reduced pressure. The residue was purified by flash chromatography to afford the respective desired products.

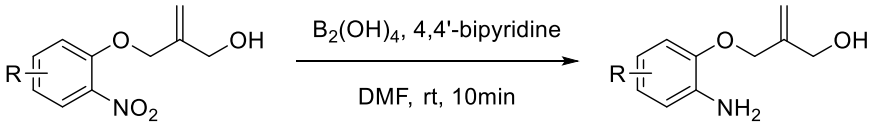

General Procedure C

According to a procedure adapted from the literature,[2] a round bottom flask with a magnetic stirring bar was charged with the respective nitroarene (1 equiv), $B_2(OH)_4$ (4 equiv) and DFM (0.95 mL/mmol). The reaction mixture was stirred at room temperature for 5 min and then, 4,4-bipyridine solution (1 mM stock solution in DMF, 5 mol % relative to nitroarene) was added and let stir at room temperature for 10 min. After, the reaction mixture was diluted with water and ethyl acetate and the organic layer was separated. The aqueous layer was extracted three times with ethyl acetate and the combined organic layers were washed three times with water and brine, dried over Na_2SO_4 and the solvent was evaporated under reduced pressure. The residue was purified by flash chromatography to afford the respective desired products.

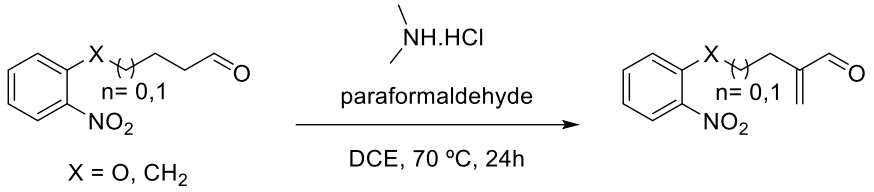

General Procedure D

According to a procedure adapted from the literature,[3] a round bottom flask with a magnetic stirring bar was charged with the respective aldehyde (1.0 equiv) and paraformaldehyde (10.0 equiv) in DCE (0.45 mL/ mmol). To this solution was added dimethylammonium chloride (5.0 equiv). The reaction mixture was stirred at 70 °C for 24 hours. After this time, the reaction mixture was then cooled, filtered, the residue was washed three times with DCM and the solvent removed under reduced pressure. The residue was purified by flash chromatography to afford the respective desired products.

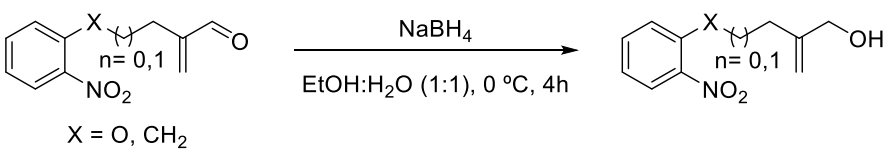

General Procedure E

According to a procedure adapted from the literature,[3] a round bottom flask with a magnetic stirring bar was charged with the respective aldehyde and EtOH (0.68 mL/mmol). To this solution, a solution of

$NaBH_4$ (5 equiv) in cold water (0.68 mL/mmol) was added at 0 ºC dropwise. The rection mixture was stirred at 0 ºC for 4 hours (monitored by TLC). After this time, saturated solution of NH_4Cl (3 mL/mmol) was added and the organic layer was separated. The aqueous layer was extracted twice with ethyl acetate and the combined organic layers were washed with brine, dried over Na_2SO_4 and the solvent was evaporated under reduced pressure. The residue was purified by flash chromatography to afford the respective desired products.

Substrates

2-((2-nitrophenoxy)methyl)prop-2-en-1-ol – 1a

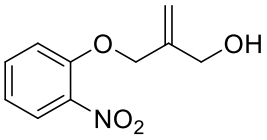

The title compound was synthesized according to general procedure A**. Yield:** 59% (490 mg, 2.34 mmol). **Rf:** 0.31 (Pentane/EtOAc 6:4). **Physical state:** Pale yellow solid. **^{1}H NMR (400 MHz, $CDCl_3$)** – δ 7.88 (dd, J = 8.1, 1.7 Hz, 1H), 7.54 (ddd, *J* = 8.8, 7.4, 1.7 Hz, 1H), 7.11 (dd, *J* = 8.5, 1.2 Hz, 1H), 7.05 (ddd, *J* = 8.4, 7.5, 1.2 Hz, 1H), 5.33 (t, *J* = 1.2 Hz, 2H), 4.75 (s, 2H), 4.30 (s, 2H), 2.07 (s, 1H). **^{13}C NMR (101 MHz, $CDCl_3$)** – δ 152.0, 142.9, 139.9, 134.5, 126.1, 120.8, 115.3, 114.7, 70.7, 64.2. **HRMS (ESI+)** *m*/*z* calculated for [$C_{10}H_{11}NNaO_4^+$]: 232.0580 [*M*+Na]$^+$; found: 232.0579.

2-((4-chloro-2-nitrophenoxy)methyl)prop-2-en-1-ol – 1b

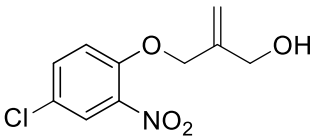

The title compound was synthesized according to general procedure A. **Yield:** 83% (606 mg, 2.49 mmol). **Rf:** 0.25 (Pentane/EtOAc 6:4). **Physical state:** Yellow solid. **^{1}H NMR (400 MHz, $CDCl_3$)** – δ 7.87 (d, *J* = 2.6 Hz, 1H), 7.49 (dd, *J* = 9.0, 2.6 Hz, 1H), 7.07 (d, *J* = 9.0 Hz, 1H), 5.36 – 5.29 (m, 2H), 4.74 (s, 2H), 4.28 (d, *J* = 5.8 Hz, 2H), 2.01 (t, *J* = 6.1 Hz, 1H). **^{13}C NMR (101 MHz, $CDCl_3$)** – δ 150.7, 142.5, 139.9, 134.3, 125.9, 125.9, 116.1, 115.5, 70.9, 64.1. **HRMS (ESI+)** *m*/*z* calculated for [$C_{10}H_{10}ClNNaO_4^+$]: 266.0191 [M+Na]$^+$; found: 266.0188.

2-((2-nitro-4-(trifluoromethyl)phenoxy)methyl)prop-2-en-1-ol – 1c

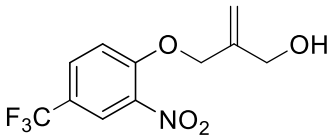

The title compound was synthesized according to general procedure A. **Yield:** 92% (1.041 mg, 3.66 mmol). **Rf:** 0.28 (Pentane/EtOAc 6:4). **Physical state:** Yellow solid. **^{1}H NMR (400 MHz, $CDCl_3$)** – δ 8.14 (d, *J* = 2.3 Hz, 1H), 7.79 (dd, *J* = 8.8, 2.3 Hz, 1H), 7.24 (d, *J* = 9.2 Hz, 1H), 5.38 – 5.31 (m, 2H), 4.81 (s,

2H), 4.28 (d, *J* = 5.8 Hz, 2H), 2.21 (t, *J* = 6.0 Hz, 1H). **^{13}C NMR (101 MHz, $CDCl_3$) –** δ 154.3, 142.1, 139.4, 131.2 (q, *J* = 3.5 Hz), 123.7 (q, *J* = 3.9 Hz), 123.3 (q, J = 34.5 Hz), 123.1 (q, *J* = 271.8 Hz), 115.7, 115.1, 70.8, 63.9. **^{19}F NMR (376 MHz, $CDCl_3$) –** δ -62.1. **HRMS (ESI+)** *m/z* calculated for [$C_{11}H_{10}F_3NNaO_4^+$]: 300.0454 [M+Na]$^+$; found: 300.0449.

2-((3-methoxy-2-nitrophenoxy)methyl)prop-2-en-1-ol – 1d

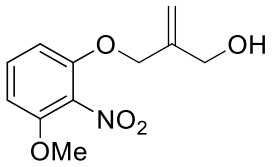

The title compound was synthesized according to general procedure A. **Yield:** 25% (237 mg, 0.989 mmol). **Rf:** 0.25 (Pentane/EtOAc 6:4). **Physical state:** Brown oil. **^{1}H NMR (400 MHz, $CDCl_3$)** – δ 7.27 (t, *J* = 8.6 Hz, 1H), 6.61 (dd, *J* = 8.5, 6.3 Hz, 2H), 5.19 (dd, *J* = 17.2, 1.2 Hz, 2H), 4.61 (s, 2H), 4.13 (s, 2H), 3.82 (s, 3H), 2.63 (s, 1H).**^{13}C NMR (101 MHz, $CDCl_3$)** – δ 151.8, 150.7, 142.8, 132.2, 131.3, 114.3, 105.7, 104.8, 69.9, 63.3, 56.5. **HRMS (ESI+)** *m/z* calculated for [$C_{11}H_{13}NNaO_5^+$]: 262.0686 [M+Na]$^+$; found: 262.0687.

2-((2-amino-3-methoxyphenoxy)methyl)prop-2-en-1-ol – 2d

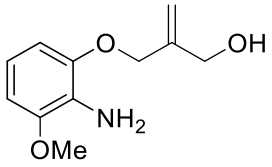

The title compound was synthesized according to general procedure C. **Yield:** 33% (126.2 mg, 0.60 mmol). **Rf:** 0.14 (Pentane/EtOAc 4:6). **Physical state:** Brown oil. **^{1}H NMR (400 MHz, $CDCl_3$)** – δ 6.68 (t, *J* = 8.2 Hz, 1H), 6.54 (ddd, *J* = 8.1, 5.6, 1.2 Hz, 2H), 5.23 (dq, *J* = 3.8, 1.1 Hz, 2H), 4.59 (d, *J* = 1.4 Hz, 2H), 4.22 (t, *J* = 1.1 Hz, 2H), 3.84 (s, 5H), 2.93 (s, 1H). **^{13}C NMR (101 MHz, $CDCl_3$)** – δ 147.9, 146.7, 144.6, 125.6, 117.3, 113.5, 105.9, 104.4, 69.9, 63.7, 55.9. **HRMS (ESI+)** *m/z* calculated for [$C_{11}H_{16}NO3+$]: 210.1125 [M+H]$^+$; found: 210.1127.

3-((2-(hydroxymethyl)allyl)oxy)-4-nitrobenzonitrile – 1e

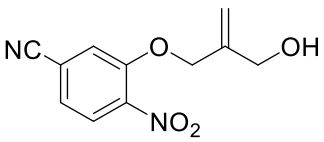

The title compound was synthesized according to general procedure A. **Yield:** 30% (280 mg, 1.19 mmol). **Rf:** 0.51 (Pentane/EtOAc 6:4). **Physical state:** Yellow solid. **^{1}H NMR (400 MHz, DMSO-d_6)** – δ 8.06 (d, *J* = 8.3 Hz, 1H), 7.95 (d, *J* = 1.6 Hz, 1H), 7.63 (dd, *J* = 8.3, 1.5 Hz, 1H), 5.24 (d, *J* = 2.0 Hz, 1H), 5.18 (q, *J* = 1.5 Hz, 1H), 5.01 (t, *J* = 5.4 Hz, 1H), 4.81 (s, 2H), 3.99 (d, *J* = 5.0 Hz, 2H). **^{13}C NMR (101**

MHz, (DMSO-d_6) – δ 150.4, 143.9, 142.3, 125.7, 124.9, 119.4, 117.3, 116.0, 112.3, 70.1, 61.2. **HRMS (ESI+)** *m*/*z* calculated for [$C_{11}H_{10}N_2NaO_4^+$]: 257.0533 [M+Na]$^+$; found: 257.0528.

2-((5-methoxy-2-nitrophenoxy)methyl)prop-2-en-1-ol – 1f

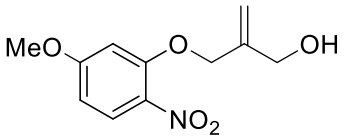

The title compound was synthesized according to general procedure A. **Yield:** 74% (708 mg, 2.96 mmol). **Rf:** 0.26 (Pentane/EtOAc 6:4). **Physical state:** Yellow solid. **^{1}H NMR (400 MHz, $CDCl_3$)** – δ 8.01 (d, *J* = 9.1 Hz, 1H), 6.55 (d, *J* = 2.5 Hz, 1H), 6.52 (dd, *J* = 9.1, 2.5 Hz, 1H), 5.49 – 5.24 (m, 2H), 4.72 (t, *J* = 1.1 Hz, 2H), 4.29 (dd, *J* = 6.1, 1.2 Hz, 2H), 3.87 (s, 3H), 2.44 (t, *J* = 6.2 Hz, 1H). **^{13}C NMR (101 MHz, $CDCl_3$)** – δ 165.0, 154.6, 142.7, 132.9, 128.7, 115.5, 105.5, 100.5, 70.9, 64.3, 56.1. **HRMS (ESI+)** *m*/*z* calculated for [$C_{11}H_{13}NNaO_5^+$]: 262.0686 [*M*+Na]$^+$; found: 262.0689.

2-((2-amino-5-methoxyphenoxy)methyl)prop-2-en-1-ol – 2f

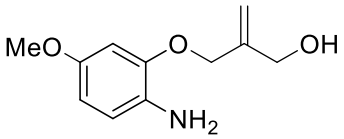

The title compound was synthesized according to general procedure C. **Yield:** 50% (136.0 mg, 0.65 mmol)**. Rf:** 0.17 (Pentane/EtOAc 4:6). **Physical state:** Brown oil. **^{1}H NMR (400 MHz, $CDCl_3$)** - δ 6.64 (d, *J* = 8.5 Hz, 1H), 6.47 (d, *J* = 2.6 Hz, 1H), 6.35 (dd, *J* = 8.5, 2.6 Hz, 1H), 5.42 – 5.11 (m, 2H), 4.56 (s, 2H), 4.20 (s, 2H), 3.72 (s, 3H), 3.30 (bs, 3H). **^{13}C NMR (101 MHz, $CDCl_3$)** - δ 153.3, 147.5, 144.4, 129.7, 116.0, 113.8, 105.1, 100.9, 69.5, 63.7, 55.8. **HRMS (ESI+)** *m*/*z* calculated for [$C_{11}H_{16}NO_3^+$]: 210.1125 [*M*+H]$^+$; found: 210.1126.

2-((4-methyl-2-nitrophenoxy)methyl)prop-2-en-1-ol – 1g

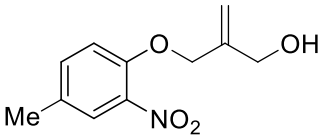

The title compound was synthesized according to general procedure A. **Yield:** 56% (496 mg, 2.22 mmol). **Rf:** 0.33 (6:4, Pentane:EtOAc). **Physical state:** White solid. **^{1}H NMR (400 MHz, $CDCl_3$)** – δ 7.84 (d, *J* = 8.3 Hz, 1H), 6.90 (s, 1H), 6.84 (ddd, *J* = 8.3, 1.7, 0.8 Hz, 1H), 5.43 – 5.26 (m, 2H), 4.74 (s, 2H), 4.31 (d, *J* = 6.2 Hz, 2H), 2.41 (s, 3H), 2.25 – 2.15 (m, 1H).**^{13}C NMR (101 MHz, $CDCl_3$)** – δ 152.3, 146.3, 143.0, 137.4, 126.3, 121.5, 115.3, 115.1, 70.8, 64.4, 22.1. **HRMS (ESI+)** *m*/*z* calculated for [$C_{11}H_{13}NNaO_4^+$]: 246.0737 [M+Na]$^+$; found: 246.0738.

2-((5-bromo-4-fluoro-2-nitrophenoxy)methyl)prop-2-en-1-ol – 1h

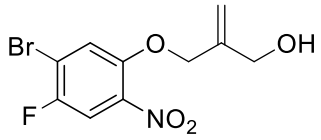

The title compound was synthesized according to general procedure A. **Yield:** 73% (467 mg, 1.52 mmol). **Rf:** 0.45 (6:4, Pentane:EtOAc). **Physical state:** Yellow Solid. **^{1}H NMR (400 MHz, $CDCl_3$) -** δ 7.74 (d, *J* = 7.6 Hz, 1H), 7.35 (d, *J* = 5.5 Hz, 1H), 5.38 – 5.32 (m, 2H), 4.73 (s, 2H), 4.30 (d, *J* = 5.9 Hz, 2H), 1.97 – 1.87 (m, 1H). **^{13}C NMR (101 MHz, $CDCl_3$)** - δ 153.7, 151.2, 148.8 (d, J = 2.9 Hz), 142.2, 119.8, 116.0 (d, J = 22.6 Hz), 115.8, 113.8 (d, J = 28.1 Hz), 71.5, 64.1. **^{19}F NMR** (376 MHz, $CDCl_3$) – δ -114.1. **HRMS (ESI+)** *m/z* calculated for [$C_{10}H_9BrFNNaO_4^+$]: 327.9591 [*M*+Na]$^+$; found: 327.9583.

2-((3-fluoro-2-nitrophenoxy)methyl)prop-2-en-1-ol – 1i

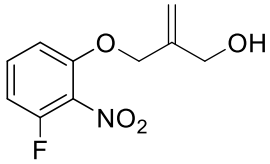

The title compound was synthesized according to a procedure adapted from the literature.[4] In a round bottom flask with a magnetic stirring bar was added 2-(bromomethyl)prop-2-en-1-ol (synthesized according to the literature,[5] 1.2 equiv, 4.8 mmol, 724.0 mg), K_2CO_3 (3 equiv, 12 mmol, 1.66 g), 3-fluoro-2-nitrophenol (1 equiv, 4 mmol, 628.4 mg) and MeCN (20 mL). The reaction mixture was stirred at 70 ºC overnight. After 16 hours, the reaction mixture was diluted with ethyl acetate and water and the organic layer was separated. The aqueous layer was extracted three times with ethyl acetate and the combined organic layers were washed with brine, dried over Na_2SO_4 and the solvent was evaporated under reduced pressure. The residue was purified by flash chromatography to give the title compound as a white solid (79%, 718 mg, 3.16 mmol). **Rf:** 0.20 (Pentane/EtOAc 6:4). **^{1}H NMR (400 MHz, $CDCl_3$)** – δ 7.39 (td, *J* = 8.6, 6.2 Hz, 1H), 6.91 – 6.78 (m, 2H), 5.28 (d, *J* = 18.4 Hz, 2H), 4.71 (s, 2H), 4.22 (s, 2H), 1.97 (bs, 1H). **^{13}C NMR (101 MHz, $CDCl_3$) –** δ 154.69 (d, *J* = 257.2 Hz), 151.62 (d, *J* = 2.5 Hz), 142.48, 132.12 (d, *J* = 9.7 Hz), 131.2, 115.15, 109.45 (d, J = 3.3 Hz), 108.97 (d, *J* = 19.1 Hz), 70.55, 63.72. **^{19}F NMR** (376 MHz, $CDCl_3$) – δ -122.2. **HRMS (ESI+)** *m/z* calculated for [$C_{10}H_{10}FNNaO_4^+$]: 250.0486 [M+Na]$^+$; found: 250.0482.

2-((5-methyl-2-nitrophenoxy)methyl)prop-2-en-1-ol – 1j

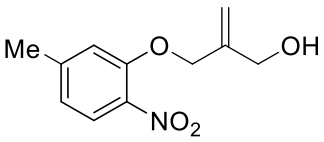

The title compound was synthesized according to general procedure B. **Yield:** 68% (761 mg, 3.41 mmol). **Rf:** 0.30 (Pentane/EtOAc 6:4). **Physical state:** Yellow Solid. **^{1}H NMR (400 MHz, $CDCl_3$)** – δ 7.69 (d, *J* = 2.3 Hz, 1H), 7.33 (dd, *J* = 8.5, 2.3 Hz, 1H), 7.00 (d, *J* = 8.6 Hz, 1H), 5.31 (s, 2H), 4.72 (s,

2H), 4.29 (d, *J* = 5.7 Hz, 2H), 2.35 (s, 3H), 2.09 (t, *J* = 6.2 Hz, 1H). **^{13}C NMR (101 MHz, $CDCl_3$)** – δ 150.0, 143.1, 139.5, 135.1, 130.8, 126.2, 115.3, 114.7, 70.9, 64.3, 20.4. **HRMS (ESI+)** *m/z* calculated for [$C_{11}H_{13}NNaO_4^+$]: 246.0737 [M+Na]$^+$; found: 246.0738.

2-((5-chloro-4-methyl-2-nitrophenoxy)methyl)prop-2-en-1-ol – 1k

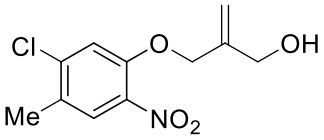

The title compound was synthesized according to general procedure A. **Yield:** 76% (979 mg, 3.79 mmol). **Rf:** 0.23 (8:2, Pentane:EtOAc). **Physical state:** Pale Yellow solid. **^{1}H NMR (400 MHz, $CDCl_3$)** – δ 7.81 (s, 1H), 7.12 (s, 1H), 5.34 (s, 2H), 4.72 (s, 2H), 4.30 (d, *J* = 6.1 Hz, 2H), 2.36 (s, 3H), 2.09 – 1.99 (m, 1H). **^{13}C NMR (101 MHz, $CDCl_3$)** – δ 150.7, 142.5, 140.6, 137.8, 129.0, 127.8, 115.7, 115.6, 71.1, 64.2, 19.2. **HRMS (ESI+)** *m/z* calculated for [$C_{11}H_{12}ClNNaO_4^+$]: 280,0347 [M+Na]$^+$; found: 280,0342.

2-(((2-nitronaphthalen-1-yl)oxy)methyl)prop-2-en-1-ol – 1l

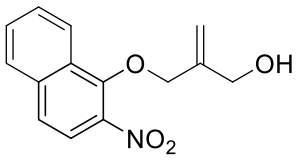

The title compound was synthesized according to general procedure B. **Yield:** 62% (801 mg, 3.10 mmol). **Rf:** 0.62 (Pentane/EtOAc 6:4). **Physical state:** Brown solid. **^{1}H NMR (400 MHz, $CDCl_3$)** - δ 8.30 (ddt, *J* = 7.3, 2.4, 0.8 Hz, 1H), 8.06 – 7.82 (m, 2H), 7.80 – 7.45 (m, 3H), 5.87 – 5.24 (m, 2H), 4.77 (s, 2H), 4.42 (s, 2H), 2.04 (s, 1H). **^{13}C NMR (101 MHz, $CDCl_3$)** - δ 150.3, 144.0, 139.5, 136.6, 129.7, 128.7, 128.4, 127.9, 124.8, 124.2, 121.0, 115.5, 77.1, 64.1. **HRMS (ESI+)** *m/z* calculated for [$C_{14}H_{13}NNaO_4^+$]: 282.0737 [M+Na]$^+$; found: 282.0738.

Synthesis of 2-(((2-nitrobenzyl)oxy)methyl)prop-2-en-1-ol – 1m

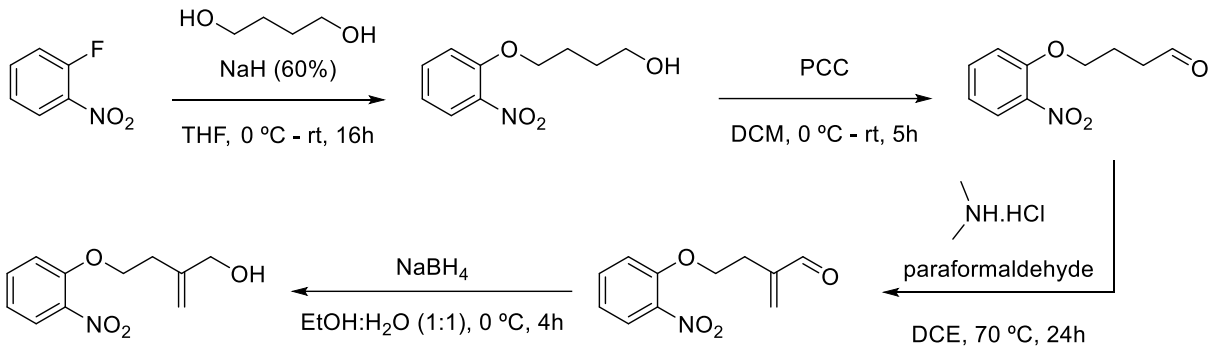

Step 1: 4-(2-nitrophenoxy)butan-1-ol – S1

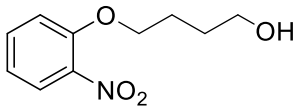

The title compound was prepared according to a procedure adapted from the literature.[1] In a round bottom flask with a magnetic stirring bar was added NaH 60% (2.0 equiv, 60 mmol, 2.4 g) and anhydrous THF (3 mL/mmol), under N_2 atmosphere. The reaction was then cooled to 0 °C and butane-1,4-diol (4.0 equiv, 120 mmol, 10.6 g) was added dropwise. This mixture was stirred for 30 min, warmed to room temperature and stirred for additional 30 min. Then, the mixture was cooled to 0 °C and 1-fluoro-2-nitrobenzene (1.0 equiv, 30 mmol, 4.23 g) was added dropwise. The mixture was stirred for 30 min at 0 °C and overnight at room temperature. After 16 hours, water was added, and the organic layer was separated. The aqueous layer was extracted twice with DCM and the combined organic layers were washed with brine, dried over Na_2SO_4 and the solvent was evaporated under reduced pressure. The residue was purified by flash chromatography to give the title compound as a yellow oil (76%, 4.81 g, 22.77 mmol). **Rf:** 0.26 (Pentane/EtOAc 4:6). **^{1}H NMR (400 MHz, $CDCl_3$)** – δ 7.82 (dd, *J* = 8.1, 1.7 Hz, 1H), 7.51 (ddd, *J* = 8.4, 7.4, 1.7 Hz, 1H), 7.07 (dd, *J* = 8.4, 1.2 Hz, 1H), 7.01 (ddd, *J* = 8.4, 7.4, 1.2 Hz, 1H), 4.15 (t, *J* = 6.1 Hz, 2H), 3.73 (q, *J* = 5.8 Hz, 2H), 1.95 (tt, *J* = 8.2, 5.7 Hz, 2H), 1.78 (tt, *J* = 7.2, 6.0 Hz, 2H), 1.74 – 1.68 (m, 1H). **^{13}C NMR (101 MHz, $CDCl_3$)** – δ 152.5, 139.9, 134.3, 125.8, 120.3, 114.5, 69.5, 62.4, 29.4, 25.6. **HRMS (ESI+)** *m/z* calculated for $[C_{10}H_{14}NO_4^+]$: 212.0917 $[M+H]^+$; found: 212.0914.

Step 2: 4-(2-nitrophenoxy)butanal – S2

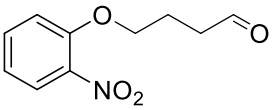

The title compound was prepared according to the following procedure.[1] To a suspension of the 4-(2-nitrophenoxy)butan-1-ol (1 equiv, 22.77 mmol, 4.81g) in DCM (68 mL) at 0 ºC, PCC (1.3 equiv, 29.6 mmol, 6.38 g) was added. The reaction mixture was stirred for 3 hours at 0 ºC and 2 hours at room temperature. After this time, the residue was filtered through a short pad of silica gel, washed with DCM and the solvent was evaporated under reduced pressure. The residue was purified by flash chromatography to give the title compound as a yellow oil (50%, 2.38 g, 11.38 mmol). **Rf:** 0.21 (Pentane/EtOAc 2:8). **^{1}H NMR (400 MHz, $CDCl_3$) –** δ 9.87 – 9.82 (m, 1H), 7.83 (dt, *J* = 8.1, 1.8 Hz, 1H), 7.51 (ddd, *J* = 8.4, 7.4, 1.7 Hz, 1H), 7.11 – 6.98 (m, 2H), 4.15 (t, *J* = 5.9 Hz, 2H), 2.77 (ddt, *J* = 7.8, 6.8, 1.0 Hz, 2H), 2.16 (p, *J* = 6.5 Hz, 2H). **^{13}C NMR (101 MHz, $CDCl_3$)** – δ 201.7, 152.2, 140.0, 134.3, 125.8, 120.6, 114.5, 68.2, 40.3, 21.7. **HRMS (ESI+)** *m/z* calculated for $[C_{10}H_{11}NNaO_4^+]$: 232.0580 $[M+Na]^+$; found: 232.0579.

Step 3: 2-methylene-4-(2-nitrophenoxy)butanal – S3

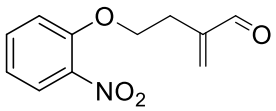

The title compound was synthesized according to general procedure D. **Yield:** 33% (837 mg, 3.78 mmol). **Rf:** 0.41 (Pentane/EtOAc 2:8). **Physical state:** Yellow oil. **^{1}H NMR (400 MHz, $CDCl_3$)** – δ 9.56 (s, 1H), 7.82 (dd, *J* = 8.1, 1.7 Hz, 1H), 7.51 (ddd, *J* = 8.4, 7.4, 1.7 Hz, 1H), 7.09 – 6.97 (m, 2H), 6.57 (s, 1H), 6.20 (s, 1H), 4.19 (t, *J* = 6.1 Hz, 2H), 2.80 (td, *J* = 6.1, 1.1 Hz, 2H). **^{13}C NMR (101 MHz, $CDCl_3$) –** δ 194.5, 152.1, 145.4, 140.0, 138.1, 134.3, 125.8, 120.6, 114.5, 67.1, 28.2. **HRMS (ESI+)** *m/z* calculated for [$C_{11}H_{11}NNaO_4^+$]: 244.0580 [M+Na]$^+$; found: 244.0580.

Step 4: 2-(((2-nitrobenzyl)oxy)methyl)prop-2-en-1-ol – 1m

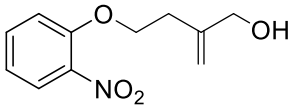

The title compound was synthesized according to general procedure E. **Yield:** 47% (393 mg, 1.76 mmol) **Rf:** 0.26 (Pentane/EtOAc 4:6). **Physical state:** Yellow oil. **^{1}H NMR (400 MHz, $CDCl_3$) –** δ 7.83 (dd, *J* = 8.1, 1.8 Hz, 1H), 7.52 (ddd, *J* = 8.7, 7.4, 1.7 Hz, 1H), 7.08 (dd, *J* = 8.4, 1.1 Hz, 1H), 7.06 – 6.97 (m, 1H), 5.16 (s, 1H), 5.01 (s, 1H), 4.24 (t, *J* = 6.4 Hz, 2H), 4.17 (d, *J* = 4.5 Hz, 2H), 2.64 (t, *J* = 6.4 Hz, 2H), 1.94 (s, 1H). **^{13}C NMR (101 MHz, $CDCl_3$)** – δ 152.3, 145.3, 139.9, 134.4, 125.9, 120.5, 114.5, 113.1, 69.0, 66.3, 32.7. **HRMS (ESI+)** *m/z* calculated for [$C_{11}H_{13}NNaO_4^+$]: 246.0737 [M+Na]$^+$; found: 246.0738.

2-(((2-nitrobenzyl)oxy)methyl)prop-2-en-1-ol – 1n

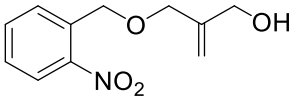

The title compound was prepared according to a procedure adapted from the literature.[1] In a round bottom flask with a magnetic stirring bar was added NaH 60% (239 mg, 1.5 equiv, 6 mmol) and anhydrous THF (18 mL), under N_2 atmosphere. The reaction was then cooled to 0 °C and 2-methylenepropane-1,3-diol (1.06 g, 3 equiv, 12 mmol) was added dropwise. This mixture was stirred for 30 min, warmed to room temperature and stirred for additional 30 min. Then, the mixture was cooled to 0 °C and 1-(bromomethyl)-2-nitrobenzene (1 equiv, 4 mmol, 864 mg) was added dropwise. The mixture was stirred for 30 min at 0 °C and overnight at room temperature. After 16 hours, water was added, and the organic layer was separated. The aqueous layer was extracted three times with ethyl acetate and the combined organic layers were washed with brine, dried over Na_2SO_4 and the solvent was evaporated under reduced pressure. The residue was purified by flash chromatography (EtOAc 30% in heptane) and then columned again (EtOAc 30% in DCM) to give the title compound as an orange oil (21%, 187.2 mg, 0.838 mmol). **Rf:** 0.40 (Pentane/EtOAc 6:4). **^{1}H NMR (400 MHz, $CDCl_3$)** – δ 8.06 (dd, *J* = 8.2, 1.3 Hz, 1H), 7.78 (dd, *J* = 7.8, 1.3 Hz, 1H), 7.65 (td, *J* = 7.6, 1.3 Hz, 1H), 7.49 – 7.40 (m, 1H), 5.27 – 5.17 (m, 2H), 4.90 (s, 2H), 4.22 (s, 2H), 4.19 (s, 2H), 1.76 (bs, 1H). **^{13}C NMR (101 MHz, $CDCl_3$)** – δ 147.5,

144.8, 134.9, 133.8, 128.8, 128.2, 124.9, 113.9, 72.5, 69.1, 64.4. **HRMS (ESI+)** *m/z* calculated for $[C_{11}H_{13}NNaO_4^+]$: 246.0737 $[M+Na]^+$; found: 246.0736.

Synthesis of *N*-(2-(hydroxymethyl)allyl)-4-methyl-*N*-(2-nitrophenyl)benzenesulfonamide – 1o

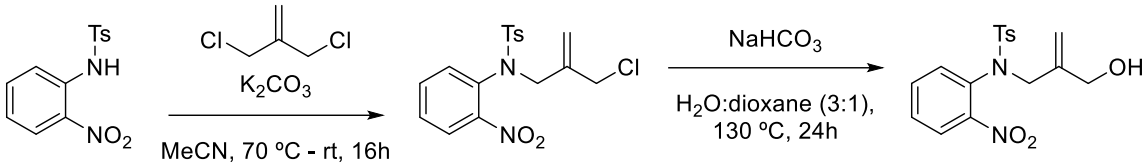

Step 1: *N*-(2-(chloromethyl)allyl)-4-methyl-*N*-(2-nitrophenyl)benzenesulfonamide – S4

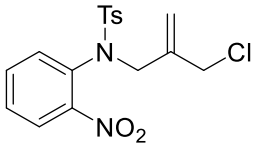

The title compound was prepared according to a procedure adapted from the literature.[4] In a round bottom flask with a magnetic stirring bar was added 3-chloro-2-(chloromethyl)prop-1-ene (1.99 g, 4 equiv, 16 mmol), K_2CO_3 (1.66 g, 3 equiv, 12 mmol), 4-methyl-*N*-(2-nitrophenyl)benzenesulfonamide (1.17g, 1 equiv, 4 mmol) and MeCN (16 mL). The reaction mixture was stirred at 70 ºC overnight. After 16 hours, the reaction mixture was diluted with ethyl acetate and water and the organic layer was separated. The aqueous layer was extracted three times with ethyl acetate and the combined organic layers were washed with brine, dried over Na_2SO_4 and the solvent was evaporated under reduced pressure. The residue was used next step without further purification**.**

Step 2: *N*-(2-(hydroxymethyl)allyl)-4-methyl-*N*-(2-nitrophenyl)benzenesulfonamide – 1o

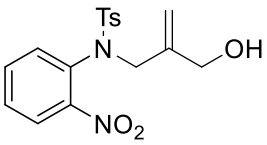

The title compound was prepared according to a procedure adapted from the literature.[6] Sealed tube with a magnetic stirring bar was charged with *N*-(2-(chloromethyl)allyl)-4-methyl-*N*-(2-nitrophenyl)benzenesulfonamide (1.52 g, 4 mmol, 1.0 equiv) and H_2O/dioxane (3:1, v/v, 60 mL). To this solution was added $NaHCO_3$ (2.0 g, 6 equiv, 24 mmol). The reaction mixture was stirred at 130 ºC for 24 h (monitored by TLC), and then cooled down to room temperature. The organic fraction of the crude was concentrated under reduced pressure. The aqueous fraction was extracted with three times with DCM. The combined organic layers were washed with brine, dried over Na_2SO_4, and concentrated under reduced pressure. The residue was purified by flash chromatography to give the title compound as a yellow solid (88% (two steps), 646.7 mg, 3.53 mmol). **Rf:** 0.38 (4:6, Pentane:EtOAc). **^{1}H NMR (400 MHz, $CDCl_3$) –** δ 7.87 (dd, *J* = 8.0, 1.7 Hz, 1H), 7.58 – 7.42 (m, 4H), 7.31 – 7.25 (m, 2H), 7.10 (dd, *J* = 7.9, 1.5 Hz, 1H), 5.08 (d, *J* = 1.4 Hz, 1H), 4.81 (q, *J* = 1.0 Hz, 1H), 4.37– 4.10 (m, 4H), 2.44 (s, 3H), 2.32 (t, *J* = 6.6 Hz, 1H). **^{13}C NMR (101 MHz, $CDCl_3$) –** δ 149.1, 144.6, 143.1, 134.7, 133.0, 132.1, 131.1, 129.9,

129.2, 128.0, 125.8, 117.0, 63.6, 53.5, 21.8. **HRMS (ESI+)** *m/z* calculated for [$C_{17}H_{19}N_2O_5S^+$]: 363.1009 $[M+H]^+$; found: 363.1007.

_N_-(2-(hydroxymethyl)allyl)-_N_-(2-nitrophenyl)methanesulfonamide – 1p

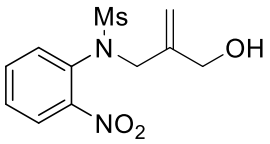

The title compound was synthesized according to general procedure B (*N*-(2-nitrophenyl)methanesulfonamide was synthesized according to the literature[1]). **Yield:** 71% (1.01 g, 3.53 mmol). **Rf:** 0.15 (4:6, Pentane:EtOAc). **Physical state:** Pale yellow solid. **^{1}H NMR (400 MHz, $CDCl_3$)** – δ 7.93 (dd, *J* = 8.5, 1.5 Hz, 1H), 7.68 – 7.59 (m, 1H), 7.51 (td, *J* = 7.8, 1.1 Hz, 2H), 5.09 (q, *J* = 1.3 Hz, 1H), 4.83 (q, *J* = 1.0 Hz, 1H), 4.21 (d, *J* = 6.5 Hz, 4H), 3.09 (s, 3H), 2.33 (td, *J* = 6.6, 1.2 Hz, 1H). **^{13}C NMR (101 MHz, $CDCl_3$) –** δ 147.9, 142.7, 133.8, 133.7, 131.6, 129.5, 125.7, 117.8, 63.6, 53.2, 40.1. **HRMS (ESI+)** *m/z* calculated for [$C_{11}H_{14}N_2NaO_5S^+$]: 309.0516 $[M+Na]^+$; found: 309.0515.

Methyl (2-(hydroxymethyl)allyl)(2-nitrophenyl)carbamate – 1q

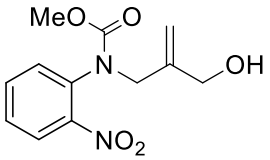

The title compound was synthesized according to general B (methyl (2-nitrophenyl)carbamate was synthesized according to the literature[7]). **Yield (2 steps):** 46% (614 mg, 2.31 mmol). **Rf:** 0.43 (4:6, Pentane:EtOAc). **Physical state:** Yellow Oil. **^{1}H NMR (400 MHz, $CDCl_3$) –** δ 7.99 (dd, *J* = 8.2, 1.6 Hz, 1H), 7.61 (td, *J* = 7.7, 1.6 Hz, 1H), 7.46 (t, *J* = 7.8 Hz, 1H), 7.31 (d, *J* = 7.9 Hz, 1H), 5.12 (s, 1H), 4.86 (s, 1H), 4.61 (d, *J* = 15.5 Hz, 1H), 4.22 (d, *J* = 6.5 Hz, 2H), 4.04 (d, *J* = 15.3 Hz, 1H), 3.62 (s, 3H), 3.12 (s, 1H). **^{13}C NMR (101 MHz, $CDCl_3$) –** δ 156.2, 146.1, 144.5, 135.2, 134.0, 129.9, 128.4, 125.6, 115.5, 63.9, 53.7, 53.3. **HRMS (ESI+)** *m/z* calculated for [$C_{12}H_{14}N_2NaO_5^+$]: 289.0795 $[M+Na]^+$; found: 289.0795.

Synthesis of 2-methylene-4-(2-nitrophenyl)butan-1-ol – 1r

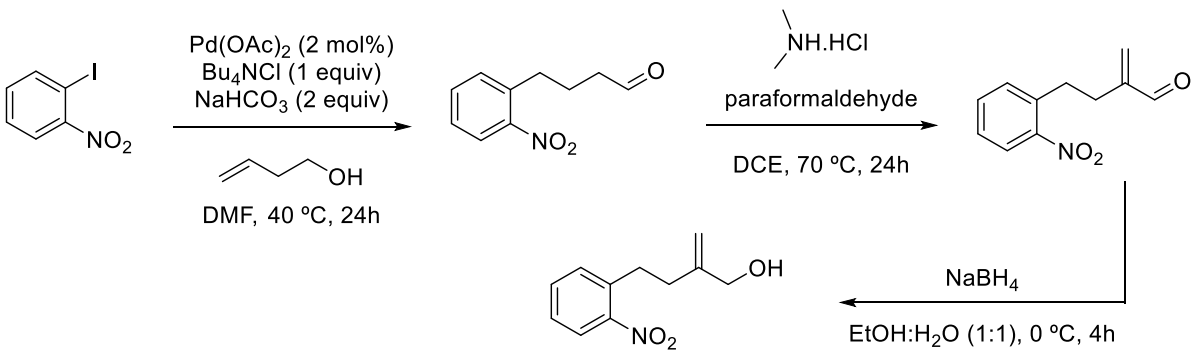

Step 1: 4-(2-nitrophenyl)butanal – S5

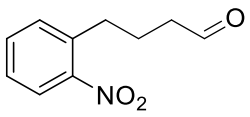

The title compound was synthesized according to the literature procedure.[8] **Yield:** 23% (881 mg, 4.56 mmol). **Rf:** 0.40 (Pentane/EtOAc 7:13). **Physical state:** Yellow oil. Spectroscopy data according to the literature.

Step 2: 2-methylene-4-(2-nitrophenyl)butanal – S6

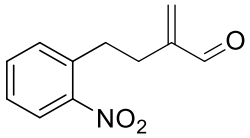

The title compound was synthesized according to general procedure D. The residue was used for the next step without further purification**.**

Step 3: 2-methylene-4-(2-nitrophenyl)butan-1-ol – 1r

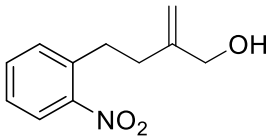

The title compound was synthesized according to general procedure E. **Yield (2 steps):** 19% (175 mg, 0.85 mmol). **Rf:** 0.40 (6:4, Pentane:EtOAc). **Physical state:** Orange oil. **^{1}H NMR (400 MHz, $CDCl_3$)** – δ 8.31 – 8.08 (m, 2H), 7.35 (d, J = 8.6 Hz, 2H), 5.09 (s, 1H), 4.89 (q, *J* = 1.2 Hz, 1H), 4.11 (s, 2H), 2.96 – 2.82 (m, 2H), 2.60 – 2.33 (m, 2H), 1.45 (s, 1H). **^{13}C NMR (101 MHz, $CDCl_3$)** – δ 149.7, 147.4, 146.6, 129.3, 123.8, 111.0, 68.0, 66.1, 34.1, 34.1, 16.6. **HRMS (ESI+)** *m/z* calculated for [$C_{11}H_{13}NNaO_3^+$]: 230.0788 [M+Na]$^+$; found: 230.0788.

Optimization of the One-pot Synthesis of Enantioenriched Spirolactones Conditions

Reactions were conducted on a 0.1 mmol scale and yields were determined by GC analysis using *n*-dodecane as an internal standard. The enantiomeric ratios were determined by UPLC analysis on a chiral stationary phase. The ligands **L1**,[9] **L2**,[10] **L3**,[9] **L4**,[11] **L5**[12] and **L6**[13] shown below were synthesized according to the literature.

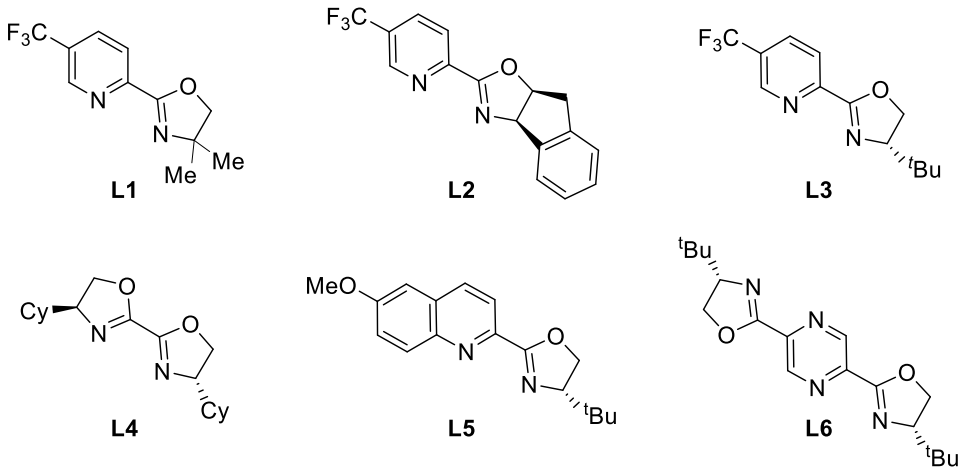

Scheme S1. Table of ligands.

Table S1. a) Radical reduction of nitroarene **1a** and b) First test of the one-pot Heck-Matsuda reaction.

a) Radical Reduction in Different Solvents

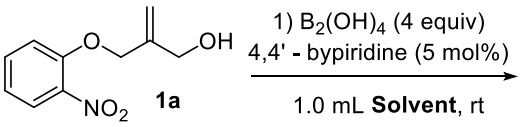

Entry	Solvent	Conv. (%)	Yield (%)
1	MeOH	20	20
2	DMF	100	100

b) Initial Test of the one-pot Heck Matsuda Reaction

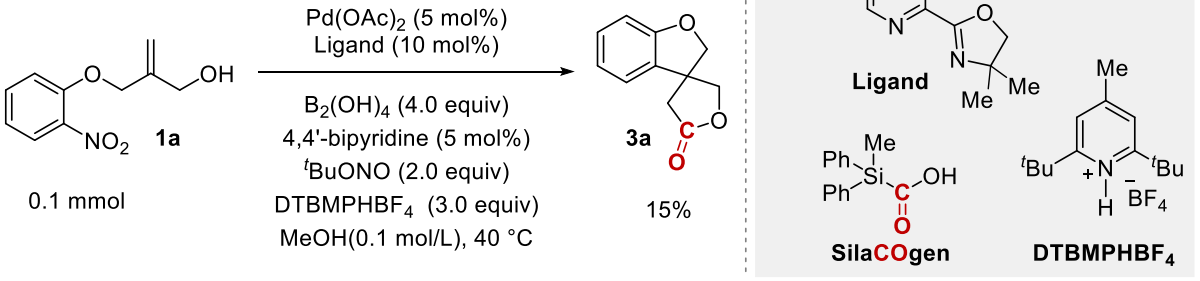

Table S2. Optimization of the amount of the acidic salt.

Optimization of the amount of the acidic salt

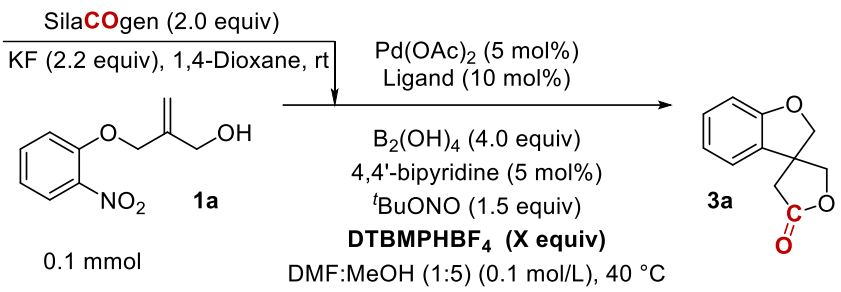

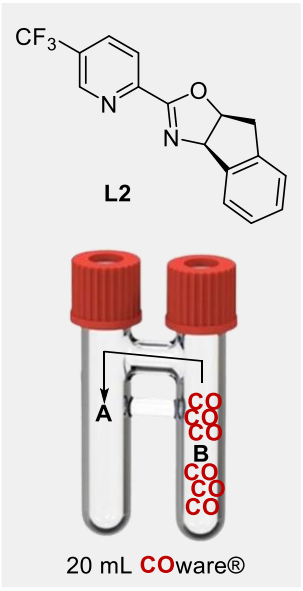

Entry	$DTBMPHBF_4$ (equiv)	Yield[a] (%)	*er*
1	0	0	-
2	1	52	-
3	2	56	-
4	3	52	-

Table S3. Optimization of the amount of CO released.

Optimization of the Amount of CO Released

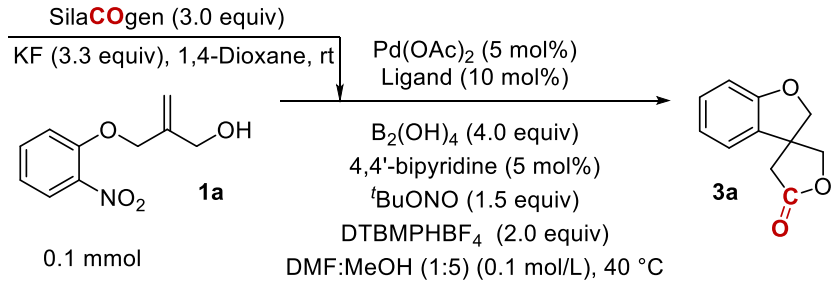

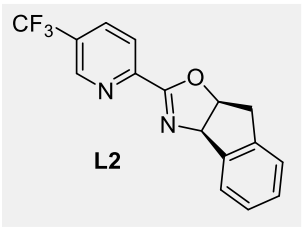

Entry	CO (equiv)	Yield[a] (%)	*er*
1	1.5	53	-
2	2.0	54	-
3	2.5	53	-
4	3.0	60	-
5	4.0	60	-

Table S4. Catalytic loading optimization.

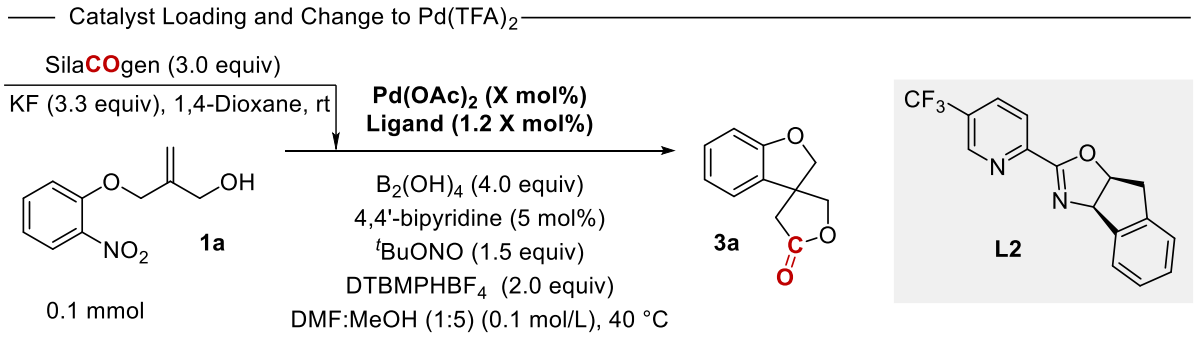

Entry	$Pd(OAc)_2$ (mol%)	Yield[a] (%)	*er*
1	1.0	23	-
2	2.5	55	-
3	5.0	60	-
4	7.5	51	-
5	10.0	57	-
6	$Pd(TFA)_2$ (5 mol%)	49	-

Table S5. Chamber B solvent screening.

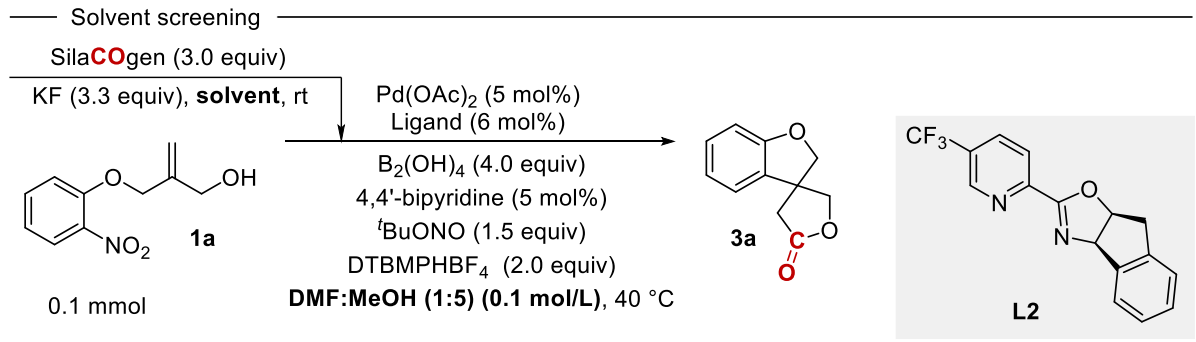

Entry	Solvent	Yield[a] (%)	*er*	
1	1,4-Dioxane (10 min)	60	-	
2	THF (5 min)	46	-	CO Release Chamber
3	DMF (1 min)	74	-	

Table S6. ^{t}BuONO equivalents optimization.

^{t}BuONO Amount Optimization

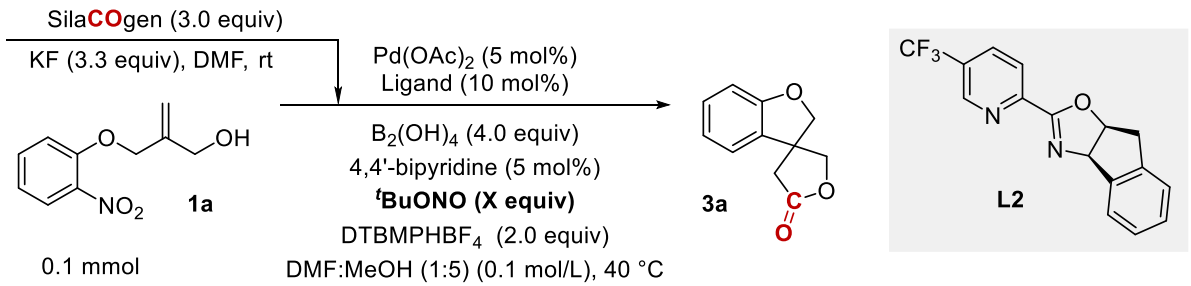

Entry	^{t}BuONO (equiv)	Yield[a] (%)	*er*
1	1.5	74	-
2	2.0	77	-
3	2.5	59	-
4	3.0	58	-

Table S7. $B_2(OH)_4$ equivalents optimization.

$B_2(OH)_4$ Amount Optimization

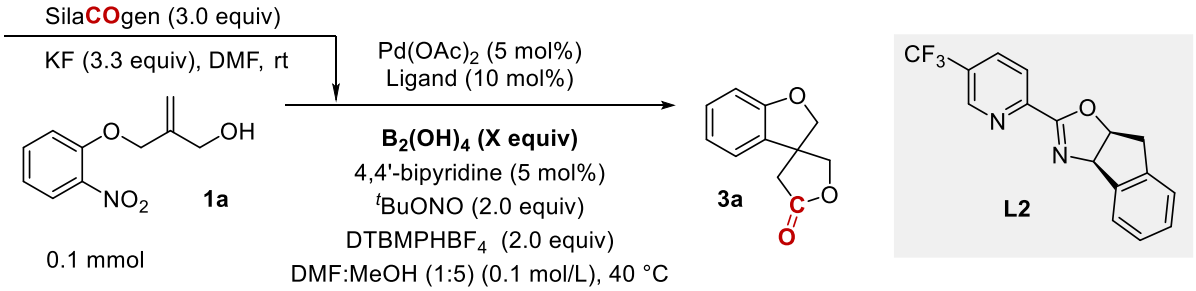

Entry	$B_2(OH)_4$ (equiv)	Yield[a] (%)	*er*
1	1.0	25	-
2	2.0	42	-
3	3.0	63	-
4	4.0	77	-

Table S8. Chiral ligand screening.

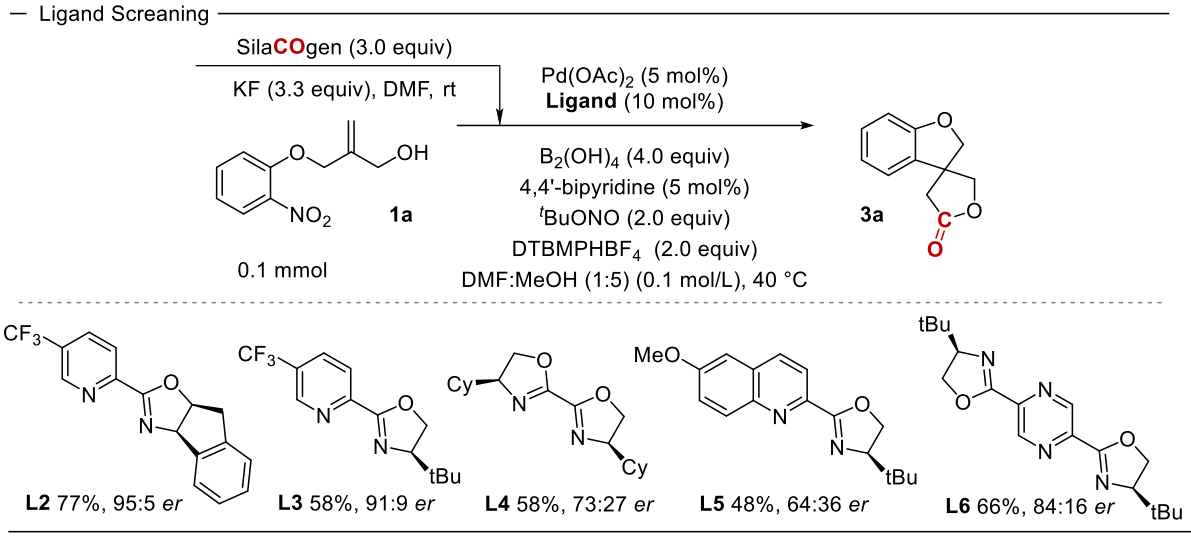

Table S9. Other parameters optimization.

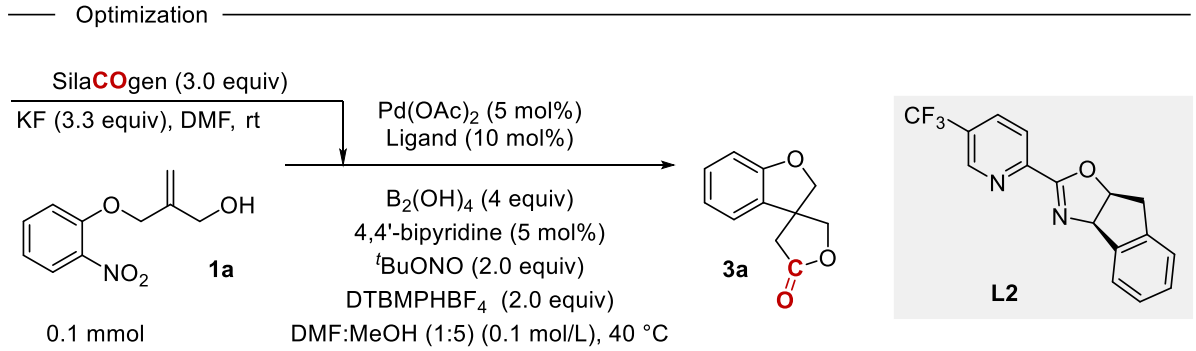

Entry	Deviation	Yield[a] (%)	*er*[b]
1	Ar atm	94	-
2	1 mol% 4,4'-bipyridine	90	-
3	2.5 mol% Pd/ 2 equiv CO	82	-
4	Reaction at 0.2 mmol	84	95:5

Synthesis of Standard Products

Catalyst Preparation Procedure

A 4 mL vial equipped with a magnetic stir bar was charged with $Pd(OAc)_2$ (2.5 mol%, 0.005 mmol, 1.12 mg), **L1** (for racemic version), **L2** or **L3** (5 mol%, 0.01 mmol), and MeOH (300 µL). The vial was capped, and the mixture was stirred at 40 °C for 15 minutes to form the precatalyst which was used without further purification.

General Procedure A

To chamber A (volume = 10 mL) of a two-chamber system was added the respective nitroarene (1 equiv, 0.2 mmol), $B_2(OH)_4$ (71.7 mg, 0.8 mmol, 4 equiv) and a stir bar. To chamber B (volume = 10 mL) of the two-chamber system was added SilaCOgen (97.0 mg, 0.4 mmol, 2 equiv) and KF (25.6 mg, 0.44 mmol, 2.2 equiv). Chamber A was then charged with 380 µL of DMF and 4,4'-bipyridine (20 µL of a 0.1 M stock solution in DMF, 2 µmol of 4,4'-bipyridine, 1 mol % relative to nitroarene). The two-chambers were then sealed and let stirring for 2 minutes at room temperature. After this time, the atmosphere was changed by purging the system with argon and 2 mL of DMF was added to chamber B. The two-chambers were then let stirring for 5 minutes at room temperature (for complete CO release). After this time, a solution of the preformed catalyst (300 µL of a freshly prepared MeOH solution – see Catalyst Preparation Procedure) was added. Next, *t*BuONO (47.6 µL, 41.2 mg, 0.4 mmol, 2.0 equiv) was added, followed by the addition of $DTBMPHBF_4$ (1 mL of a 0.4 M stock solution in MeOH, 0.4 mmol, 2 equiv. relative to nitroarene) and 0.3 mL of MeOH. The reaction mixture was then allowed to stir at 40 °C. After 16 hours, the MeOH was removed under reduced pressure, the residue was diluted with ethyl acetate and filtrated through a short pad of celite. The filtrate was diluted with ethyl acetate and water and the organic layer was separated. The aqueous layer was extracted three times with ethyl acetate and the combined organic layers were washed three times with water and brine, dried over Na_2SO_4 and the solvent was evaporated under reduced pressure. The residue was purified by flash chromatography to afford the respective desired products.

Note: after purging with argon, the system was not opened, all other reagents and solvents were added *via* syringe or microsyringe.

General Procedure B- ^{13}C

To chamber A (volume = 10 mL) of a two-chamber system was added the respective nitroarene (1 equiv, 0.2 mmol), $B_2(OH)_4$ (71.7 mg, 0.8 mmol, 4 equiv) and a stir bar. To chamber B (volume = 10 mL) of the two-chamber system was added ^{13}C-SilaCOgen (97.0 mg, 0.4 mmol, 2 equiv) and KF (25.6 mg, 0.44 mmol, 2.2 equiv). Chamber A was then charged with 380 µL of DMF and 4,4'-bipyridine (20 µL of a 0.1 M stock solution in DMF, 2 µmol of 4,4'-bipyridine, 1 mol % relative to nitroarene). The two-chambers were then sealed and let stirring for 2 minutes at room temperature. After this time, the atmosphere was changed by purging the system with argon and 2 mL of DMF was added to chamber B. The two-chambers were then and let stirring for 5 minutes at room temperature (for complete CO release). After this time, a solution of the preformed catalyst (300 µL of a freshly prepared MeOH solution – see Catalyst Preparation Procedure) was added. Next, *t*BuONO (47.6 µL, mg, 0.4 mmol, 2.0 equiv) was added, followed by the addition of $DTBMPHBF_4$ (1 mL of a 0.4 M stock solution in MeOH, 0.4 mmol, 2 equiv. relative to nitroarene) and 0.3 mL of MeOH. The reaction mixture was then allowed to stir at 40 °C. After 16 hours, the MeOH was removed under reduced pressure, the residue was diluted with ethyl acetate and filtrated through a short pad of celite. The filtrate was diluted with ethyl acetate and water and the organic layer was separated. The aqueous layer was extracted three times with ethyl acetate and the combined organic layers were washed three times with water and brine, dried over Na_2SO_4 and the

solvent was evaporated under reduced pressure. The residue was purified by flash chromatography to afford the respective desired products.

Note: after purging with argon, the system was not opened, all other reagents and solvents were added *via* syringe or microsyringe.

General Procedure C- Scale Up Reaction

To chamber A (volume = 200 mL) of a two-chamber system was added the nitroarene X (1.0 equiv, 2.0 mmol), $B_2(OH)_4$ (717 mg, 8.0 mmol, 4 equiv) and a stir bar. To chamber B (volume = 200 mL) of the two-chamber system was added SilaCOgen (970 mg, 4.0 mmol, 2.0 equiv) and KF (256 mg, 4.4 mmol, 2.2 equiv). Chamber A was then charged with 3.8 mL of DMF and 4,4'-bipyridine (200 µL of a 0.1 M stock solution in DMF, 20 µmol of 4,4'-bipyridine, 1 mol % relative to nitroarene). The two-chambers were then sealed and let stirring for 2 minutes at room temperature. After this time, the atmosphere was changed by purging the system with argon and 20 mL of DMF was added to chamber B. The two-chambers were then and let stirring for 5 minutes at room temperature (for complete CO release). After this time, a solution of the preformed catalyst (3.0 mL of a freshly prepared MeOH solution – see Catalyst Preparation Procedure) was added. Next, ^{t}BuONO (0.476 mL, 412 mg, 4.0 mmol, 2.0 equiv) was added, followed by the addition of $DTBMPHBF_4$ (10 mL of a 0.4 M stock solution in MeOH, 4.0 mmol, 2.0 equiv relative to nitroarene) and 3.0 mL of MeOH. The reaction mixture was then allowed to stir at 40 °C. After 16 hours, the MeOH was removed under reduced pressure, the residue was diluted with ethyl acetate and filtrated through a short pad of celite. The filtrate was diluted with ethyl acetate and water and the organic layer was separated. The aqueous layer was extracted three times with ethyl acetate and the combined organic layers were washed three times with water and brine, dried over Na_2SO_4 and the solvent was evaporated under reduced pressure. The residue was purified by flash chromatography to afford the respective desired products.

Note: after purging with argon, the system was not opened, all other reagents and solvents were added *via* syringe or microsyringe.

General Procedure D- Heck-Matsuda Reaction from the aniline

To chamber A (volume = 10 mL) of a two-chamber system was added the respective aniline (0.2 mmol, 1 equiv), MeOH (0.7 mL) and a stir bar. To chamber B (volume = 10 mL) of the two-chamber system was added SilaCOgen (97.0 mg, 0.4 mmol, 2 equiv) and KF (25.6 mg, 0.44 mmol, 2.2 equiv). The two-chambers were then sealed the atmosphere was changed by purging the system with argon and 2 mL of DMF was added to chamber B. The two-chambers were then let stirring for 5 minutes at room temperature (for complete CO release). After this time, a solution of the preformed catalyst (300 µL of a freshly prepared MeOH solution – see Catalyst Preparation Procedure) was added. Next, ^{t}BuONO (47.6 µL, 41.2 mg, 0.4 mmol, 2.0 equiv) was added, followed by the addition of $DTBMPHBF_4$ (1 mL of a 0.4 M stock solution in MeOH, 0.4 mmol, 2 equiv relative to aniline). The reaction mixture was then allowed to stir at 40 °C. After 16 hours, the MeOH was removed under reduced pressure, the residue was diluted with ethyl acetate and filtrated through a short pad of celite. The filtrate was diluted with ethyl acetate and water and the organic layer was separated. The aqueous layer was extracted three times with ethyl acetate and the combined organic layers were washed three times with water and brine,

dried over Na_2SO_4 and the solvent was evaporated under reduced pressure. The residue was purified by flash chromatography to afford the respective desired products.

Characterization of Standard Products

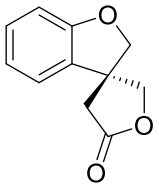

3a - Obtained from **L2**

3a - (*R*)-2*H*,2'*H*-spiro[benzofuran-3,3'-furan]-5'(4'*H*)-one - The nitroarene **1a** (mg, 0.20 mmol) was subjected to the general procedure A - the crude product was purified by column chromatography to afford pure product. The isolated yield is the average of two runs. **Yield:** 65% (24.7 mg, 0,130mmol); 95:5 *er.* **Rf:** 0.38 (8:2 Pentane:EtOAc). **Physical state:** Colorless oil. **^{1}H NMR (400 MHz, $CDCl_3$)** - δ 7.26 – 7.20 (m, 2H), 6.97 (td, *J* = 7.5, 1.0 Hz, 1H), 6.86 (dt, *J* = 8.0, 0.8 Hz, 1H), 4.59 (d, *J* = 9.3 Hz, 1H), 4.47 (d, *J* = 9.4 Hz, 1H), 4.46 – 4.35 (m, 2H), 2.95 (d, *J* = 17.7 Hz, 1H), 2.75 (d, *J* = 17.7 Hz, 1H). **^{13}C NMR (101 MHz, $CDCl_3$) -** δ 174.9, 159.8, 130.1, 128.3, 122.5, 121.8, 110.6, 81.4, 77.7, 50.0, 40.7. **HRMS (ESI+)** calculated *m/z* for $[C_{11}H_{11}O_3^+]$: 191.0703 $[M+H]^+$; found: 191.0703. **$[\alpha]_D^{24.3}$** +3.2 (*c* 0.99, $CHCl_3$, 95:5 *er*).

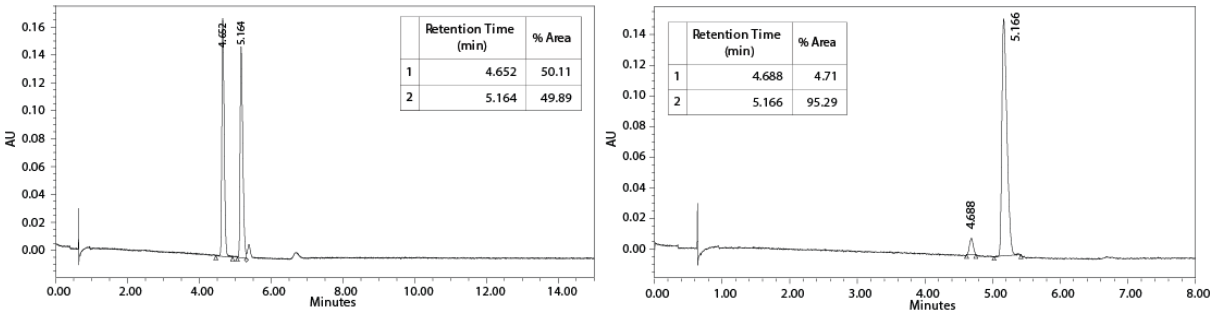

UPCC: Daicel Chiralpak® ID column (4.6 mm x 250 mm), CO_2/^{i}PrOH = 99:1 to 95:5 over 4.5 min, 3.0 mL/min, 40 °C, λ = 284 nm, tR (major) = 5.16 min; tR (minor) = 4.69 min, *er* = 95:5.

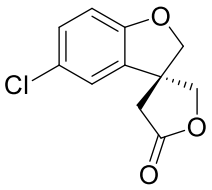

3b - Obtained from **L2**

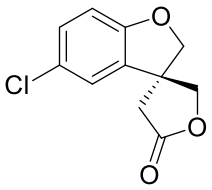

***ent*-3b -** Obtained from **L3**

3b - (*R*)-5-chloro-2H,2'H-spiro[benzofuran-3,3'-furan]-5'(4'H)-one - The nitroarene **1b** (0.20 mmol) was subjected to the general procedure A - the crude product was purified by column chromatography to afford pure product. The isolated yield is the average of two runs. **3b: Yield:** 22% (10 mg, 0.045 mmol); 11:89 *er.* ***ent*-3b: Yield:** 52% (23.4 mg, 0.104 mmol); 93:7 *er.* **Rf:** 0.38 (8:2 Pentane:EtOAc).

Physical state: White Solid. **^{1}H NMR (400 MHz, $CDCl_3$)** – δ 7.23 – 7.15 (m, 2H), 6.79 (d, *J* = 8.4 Hz, 1H), 4.61 (d, *J* = 9.5 Hz, 1H), 4.50 (d, *J* = 9.4 Hz, 1H), 4.40 (q, *J* = 9.5 Hz, 2H), 2.93 (d, *J* = 17.7 Hz, 1H), 2.76 (d, *J* = 17.7 Hz, 1H). **^{13}C NMR (101 MHz, $CDCl_3$)** – δ 174.3, 158.4, 130.3, 130.1, 126.5, 122.8, 111.7, 81.8, 77.3, 50.1, 40.6. **HRMS (ESI+)** calculated *m/z* for [$C_{11}H_{10}ClO_3^+$]: 225.0313 [M+H]$^+$; found: 225.0311. **3b: $[\alpha]_D^{24.3}$** -22.4 (c 0.93, $CHCl_3$, 11:89 *er*). ***ent*-3b: $[\alpha]_D^{24.3}$** +38.7 (c 0.93, $CHCl_3$, 93:7 *er*).

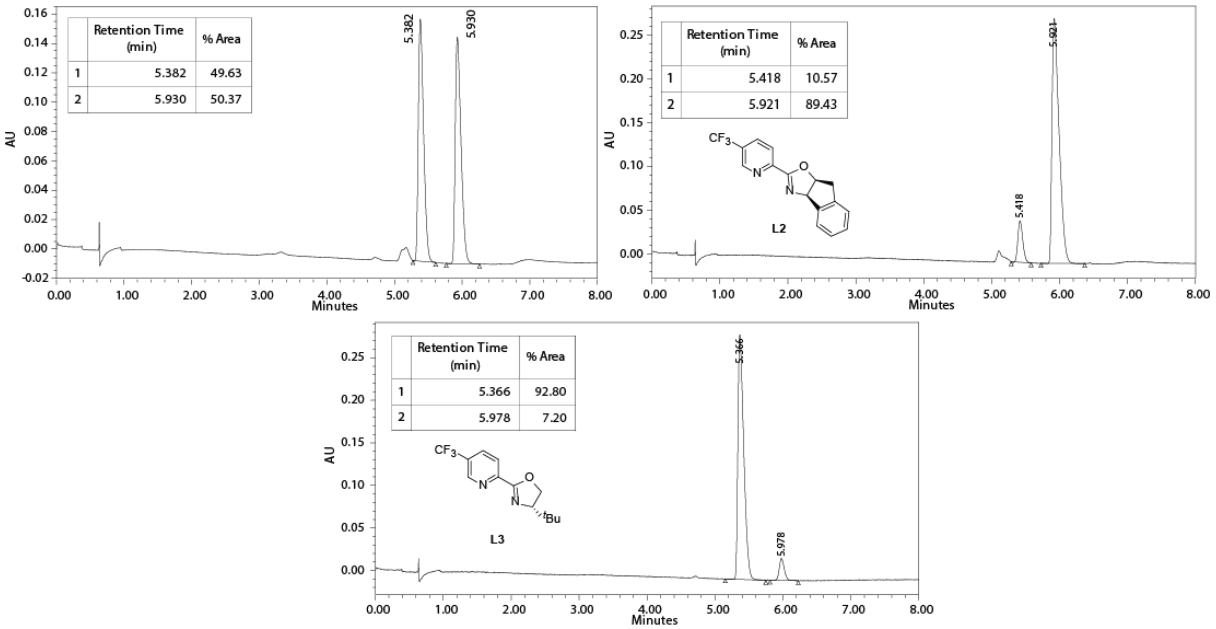

UPCC: Daicel Chiralpak® ID column (4.6 mm x 250 mm), CO_2/^{i}PrOH = 99:1 to 95:5 over 4.5 min, 3.0 mL/min, 40 °C, λ = 284 nm, **3a:** tR (major) = 5.92 min; tR (minor) = 5.42 min, *er* = 11:89. ***ent*-3a:** tR (major) = 5.37 min; tR (minor) = 5.98 min, *er* = 93:7.

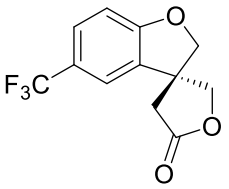

3c - Obtained from **L2**

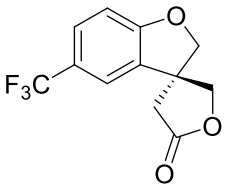

***ent*-3c -** Obtained from **L3**

3c - (*R*)-5-(trifluoromethyl)-2*H*,2'*H*-spiro[benzofuran-3,3'-furan]-5'(4'H)-one - The nitroarene **1c** (0.20 mmol) was subjected to the general procedure A - the crude product was purified by column chromatography to afford pure product. The isolated yield is the average of two runs. **3c: Yield:** 26% (13.4 mg, 0.052 mmol); 8:92 *er.* ***ent*-3c: Yield:** 60% (31.0 mg, mmol); 90:10 *er.* **Rf:** 0.41 (Pentane/EtOAc 8:2). **Physical state:** White Solid. **^{1}H NMR (400 MHz, $CDCl_3$)** - δ 7.52 (d, *J* = 8.3 Hz, 1H), 7.47 (s, 1H), 6.94 (d, *J* = 8.4 Hz, 1H), 4.68 (d, *J* = 9.6 Hz, 1H), 4.57 (d, J = 9.6 Hz, 1H), 4.48 – 4.38 (m, 2H), 2.98 (d, *J* = 17.7 Hz, 1H), 2.79 (d, *J* = 17.7 Hz, 1H). **^{13}C NMR (101 MHz, $CDCl_3$)** - δ 174.2, 162.4 (q, *J* = 1.4 Hz), 129.3, 128.1 (q, *J* = 3.8 Hz), 124.4 (q, *J* = 32.8 Hz), 124.2 (q, *J* = 271.5 Hz), 120.2 (q, *J* = 3.7 Hz), 110.8, 82.3, 77.4, 49.8, 40.7. **^{19}F NMR (376 MHz, $CDCl_3$)** - δ -61.2. **HRMS (ESI+)** *m/z* calculated for [$C_{12}H_{10}F_3O_3^+$]: 259.0577 [M+H]$^+$; found: 259.0572. **3c: $[\alpha]_D^{24.6}$** -10.3 (*c* 0.94, $CHCl_3$, 8:92 *er*). ***ent*-3c: $[\alpha]_D^{24.6}$** +10.9 (*c* 0.95, $CHCl_3$, 90:10 *er*).

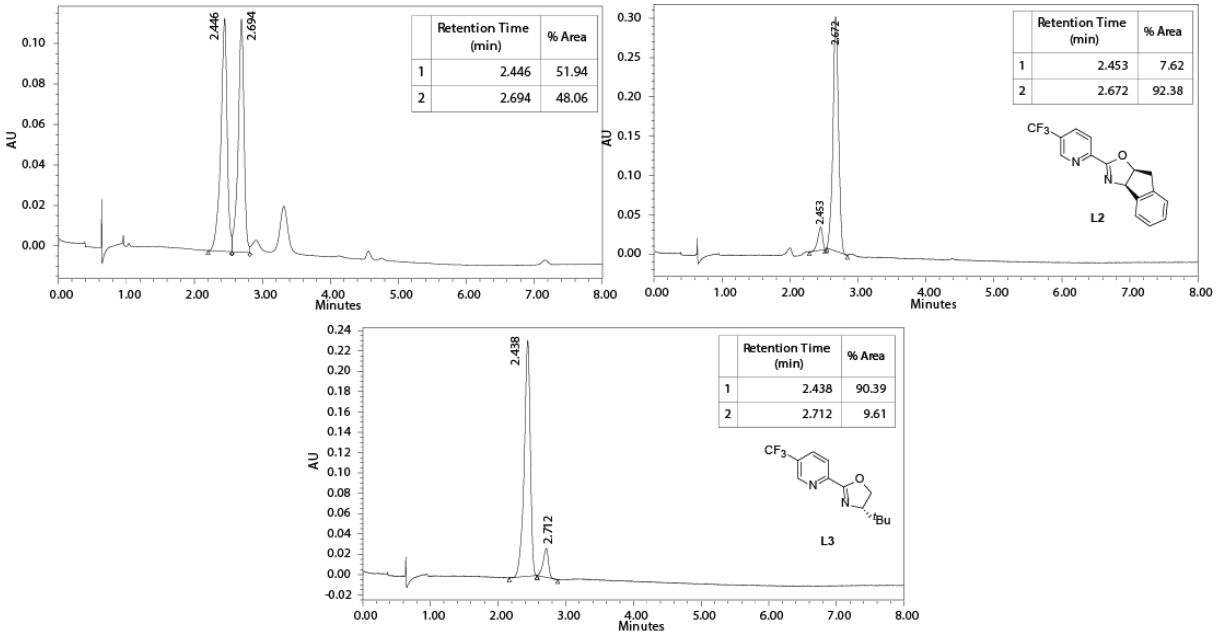

UPCC: Daicel Chiralpak® ID column (4.6 mm x 250 mm), CO_2/^{i}PrOH = 99:1 to 95:5 over 4.5 min, 3.0 mL/min, 40 °C, λ = 284 nm, **3c:** tR (major) = 2.67 min; tR (minor) = 2.45 min, *er* = 92:8. ***ent*-3c:** tR (major) = 2.43 min; tR (minor) = 2.71 min, *er* = 90:10.

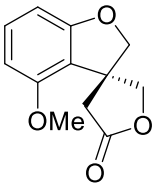

3d - Obtained from **L2**

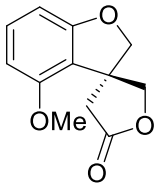

***ent*-3d -** Obtained from **L3**

3d - (*R*)-4-methoxy-2*H*,2'*H*-spiro[benzofuran-3,3'-furan]-5'(4'*H*)-one - The aniline **1d** (0.15 mmol) was subjected to the general procedure D - the crude product was purified by column chromatography to afford pure product. The isolated yield is the average of two runs. **3d: Yield:** 53% (17.5 mg, 0.079 mmol); 5:95 *er.* ***ent*-3d: Yield:** 59% (19.6 mg, 0,089 mmol); 96:4 *er.* **Rf:** 0.27 (8:2 Pentane:EtOAc). **Physical state:** White Solid. **^{1}H NMR (400 MHz, $CDCl_3$)** – δ 7.18 (t, *J* = 8.2 Hz, 1H), 6.48 (ddd, *J* = 8.1, 7.2, 0.7 Hz, 2H), 4.61 (dd, *J* = 11.1, 9.2 Hz, 2H), 4.44 (d, J = 9.3 Hz, 1H), 4.31 (d, *J* = 9.0 Hz, 1H), 3.85 (s, 3H), 3.42 (d, *J* = 17.6 Hz, 1H), 2.55 (d, *J* = 17.7 Hz, 1H). **^{13}C NMR (101 MHz, $CDCl_3$)** – δ 175.9, 161.2, 157.0, 131.3, 113.9, 103.8, 103.6, 82.9, 76.4, 55.5, 49.8, 38.7. **HRMS (ESI+)** calculated *m/z* for [$C_{12}H_{13}O_4^+$]: 221.0808 [M+H]$^+$; found: 221.0804. **3d: $[\alpha]_D^{24}$** -15.7 (c 0.84, $CHCl_3$, 5:95 *er*). ***ent*-3d: $[\alpha]_D^{24}$** +7.6 (c 0.97, $CHCl_3$, 96:4 *er*).

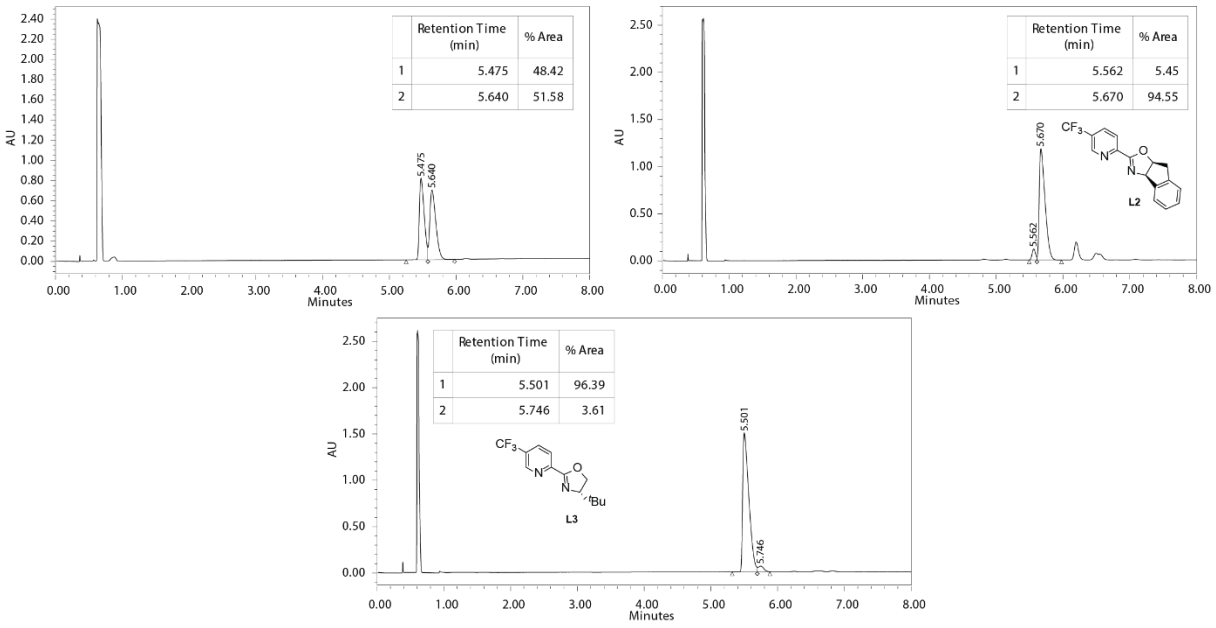

UPCC: Daicel Chiralpak® IB column (4.6 mm x 250 mm), CO_2/^{i}PrOH = 99:1 to 95:5 over 4.5 min, 3.0 mL/min, 40 °C, λ = 212 nm, **3d:** tR (major) = 5.67 min; tR (minor) = 5.56 min, *er* = 5:95. ***ent*-3d:** tR (major) = 5.50 min; tR (minor) = 5.75 min, *er* = 96:4.

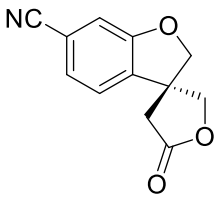

3e - Obtained from **L2**

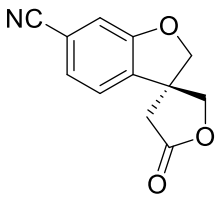

***ent*-3e -** Obtained from **L3**

3e - (*R*)-5'-oxo-4',5'-dihydro-2*H*,2'*H*-spiro[benzofuran-3,3'-furan]-6-carbonitrile - The nitroarene **1e** (0.20 mmol) was subjected to the general procedure A - the crude product was purified by column chromatography to afford pure product. The isolated yield is the average of two runs. **3e: Yield:** 28% (12.0 mg, 0.056 mmol); 92:8 *er.* ***ent*-3e: Yield:** 44% (19.0 mg, 0.088 mmol); 7:93 *er.* **Rf:** 0.11 (8:2 Pentane:EtOAc). **Physical state:** White Solid. **^{1}H NMR (400 MHz, $CDCl_3$)** – δ 7.36 – 7.27 (m, 2H), 7.11 (s, 1H), 4.66 (d, *J* = 9.6 Hz, 1H), 4.57 (d, J = 9.6 Hz, 1H), 4.42 (q, *J* = 9.5 Hz, 2H), 2.94 (d, *J* = 17.7 Hz, 1H), 2.81 (d, *J* = 17.7 Hz, 1H). **^{13}C NMR (101 MHz, $CDCl_3$)** – δ 173.9, 159.9, 134.4, 126.3, 123.5, 118.3, 113.9, 113.8, 81.6, 77.0, 49.9, 40.6. **HRMS (ESI+)** calculated *m/z* for [$C_{12}H_{10}NO_3^+$]: 216.0655 [M+H]$^+$; found: 216.0653. **3e: $[\alpha]_D^{25}$** -13.8 (c 0.64, $CHCl_3$, 92:8 er). ***ent*-3e: $[\alpha]_D^{25}$** +41.1 (c 1.07, $CHCl_3$, 7:93 er).

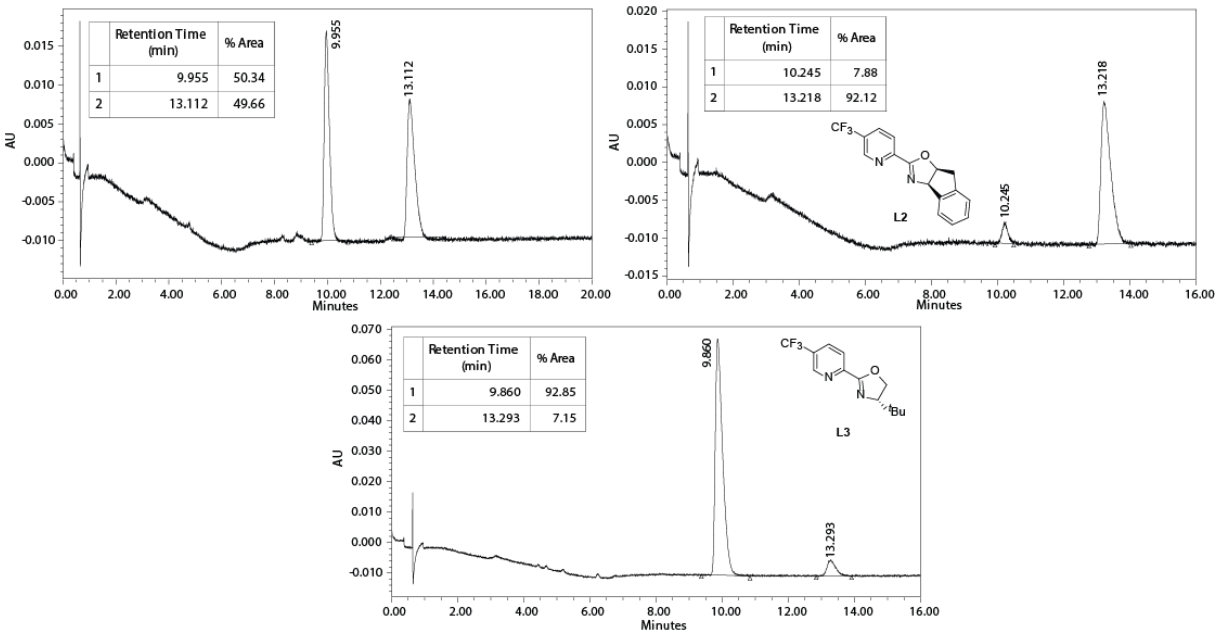

UPCC: Daicel Chiralpak® ID column (4.6 mm x 250 mm), CO_2/^{i}PrOH = 99:1 to 95:5 over 4.5 min, 3.0 mL/min, 40 °C, λ = 284 nm, **3e:** tR (major) = 13.22 min; tR (minor) = 10.25 min, *er* = 8:92. ***ent*-3e:** tR (major) = 9.86 min; tR (minor) = 13.29 min, *er* = 93:7.

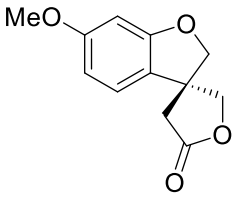

3f - Obtained from **L2**

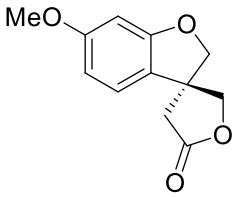

***ent*-3f -** Obtained from **L3**

3f - (*R*)-6-methoxy-2*H*,2'*H*-spiro[benzofuran-3,3'-furan]-5'(4'*H*)-one - The aniline **1f** (0.20 mmol) was subjected to the general procedure A - the crude product was purified by column chromatography to afford pure product. The isolated yield is the average of two runs. **3f: Yield:** 24% (10.5 mg, 0.048 mmol); 10:90 *er.* ***ent*-3a: Yield:** 26% (11.3 mg, 0.051 mmol); 93:7 *er.* **Rf:** 0.30 (8:2 Pentane:EtOAc). **Physical state:** Pale yellow solid. **^{1}H NMR (400 MHz, $CDCl_3$)** – δ 7.08 (d, *J* = 8.3 Hz, 1H), 6.51 (dd, *J* = 8.3, 2.3 Hz, 1H), 6.43 (d, *J* = 2.2 Hz, 1H), 4.59 (d, *J* = 9.3 Hz, 1H), 4.47 (d, *J* = 9.3 Hz, 1H), 4.43 – 4.31 (m, 2H), 3.78 (s, 3H), 2.91 (d, *J* = 17.7 Hz, 1H), 2.72 (d, *J* = 17.7 Hz, 1H). **^{13}C NMR (101 MHz, $CDCl_3$)** – δ 175.0, 161.9, 161.3, 122.8, 120.1, 107.7, 96.9, 82.3, 77.8, 55.8, 49.7, 40.8. **HRMS (ESI+)** calculated *m/z* for $[C_{12}H_{13}O_4^+]$: 221.0808 $[M+H]^+$; found: 221.0803. **3f: $[\alpha]_D^{25}$** -5.9 (c 1.02, $CHCl_3$, 10:90 *er*). ***ent*-3f: $[\alpha]_D^{25}$** 2.0 (c 1.00, $CHCl_3$, 93:7 *er*).

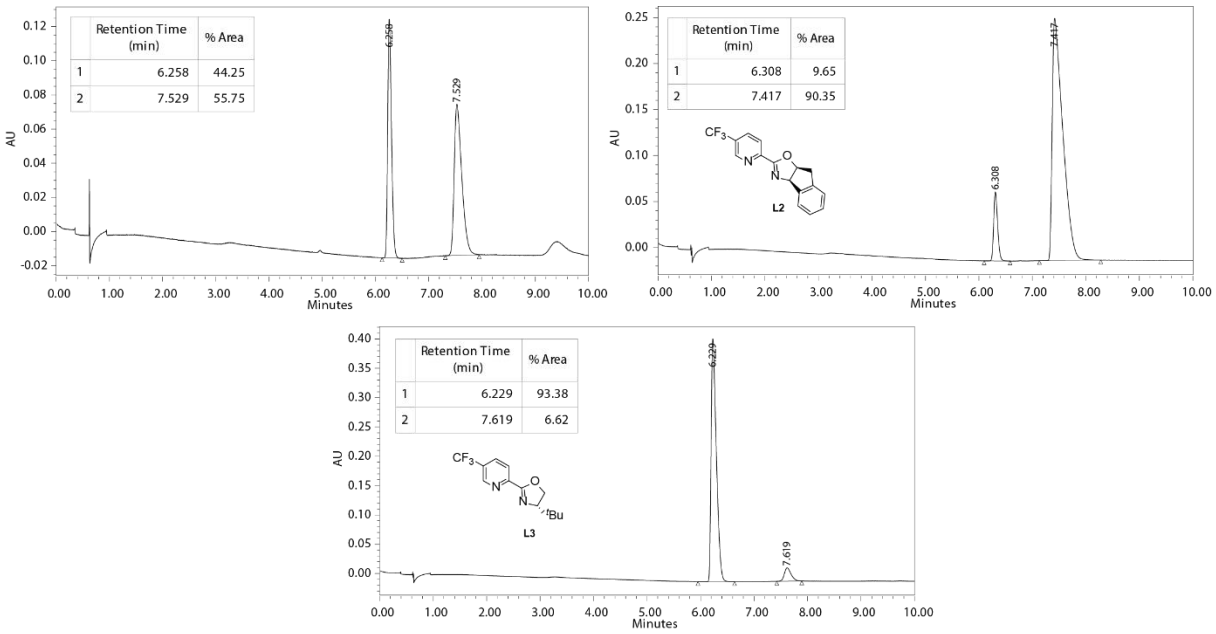

UPCC: Daicel Chiralpak® ID column (4.6 mm x 250 mm), CO_2/^{i}PrOH = 99:1 to 95:5 over 4.5 min, 3.0 mL/min, 40 °C, λ = 284 nm, **3f:** tR (major) = 7.42 min; tR (minor) = 6.31 min, *er* = 10:90. ***ent*-3f:** tR (major) = 6.23 min; tR (minor) = 7.62 min, *er* = 93:7.

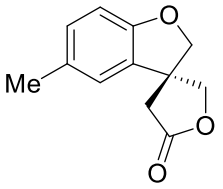

3g - Obtained from **L2**

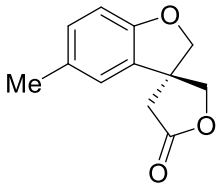

***ent*-3g -** Obtained from **L3**

3g - (*R*)-5-methyl-2*H*,2'*H*-spiro[benzofuran-3,3'-furan]-5'(4'*H*)-one - The nitroarene **1g** (0.20 mmol) was subjected to the general procedure A - the crude product was purified by column chromatography to afford pure product. The isolated yield is the average of two runs. **3g: Yield:** 58% (23.8 mg, 0.117 mmol); 4:96 *er.* ***ent*-3g: Yield:** 64% (26.0 mg, 0.127 mmol); 86:14 *er.* **Rf:** 0.41 (8:2 Pentane:EtOAc). **Physical state:** White Solid. **^{1}H NMR (400 MHz, $CDCl_3$)** - δ 7.09 (d, *J* = 7.7 Hz, 1H), 6.78 (ddd, *J* = 7.6, 1.5, 0.7 Hz, 1H), 6.71 – 6.66 (m, 1H), 4.57 (d, *J* = 9.3 Hz, 1H), 4.45 (d, *J* = 9.4 Hz, 1H), 4.38 (q, *J* = 9.3 Hz, 2H), 2.92 (d, *J* = 17.7 Hz, 1H), 2.72 (d, *J* = 17.7 Hz, 1H), 2.33 (s, 3H). **^{13}C NMR (101 MHz, $CDCl_3$)** – δ 175.0, 160.1, 140.6, 125.3, 122.5, 122.1, 111.2, 81.7, 77.8, 49.8, 40.7, 21.7. **HRMS (ESI+)** calculated *m/z* for [$C_{12}H_{13}O_3^+$]: 205.0859 [M+H]$^+$; found: 205.0858. **3g: $[\alpha]_D^{25}$** -8.3 (c 0.98, $CHCl_3$, 4:96 er). ***ent*-3g: $[\alpha]_D^{25}$** +6.4 (c 0.94, $CHCl_3$, 86:14 *er*).

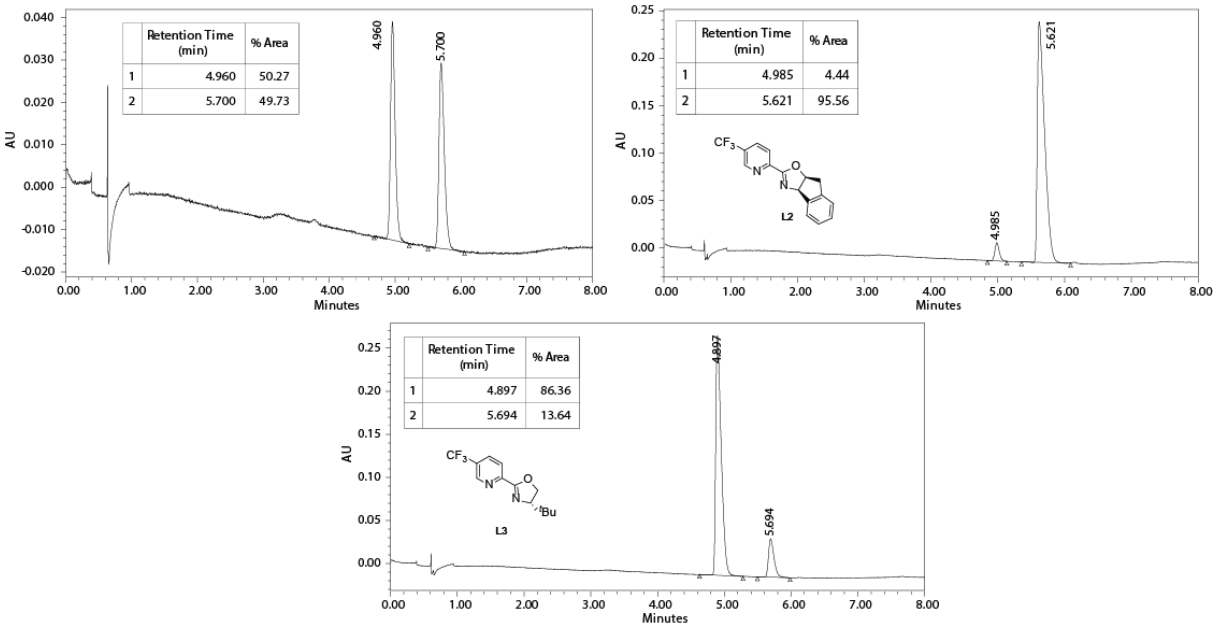

UPCC: Daicel Chiralpak® ID column (4.6 mm x 250 mm), CO_2/^{i}PrOH = 99:1 to 95:5 over 4.5 min, 3.0 mL/min, 40 °C, λ = 284 nm, **3g:** tR (major) = 5.62 min; tR (minor) = 4.99 min, *er* = 4:96, ***ent*-3g:** tR (major) = 4.90 min; tR (minor) = 5.69 min, *er* = 86:14.

Scale Up - The nitroarene **1g** (2.00 mmol) was subjected to the general procedure C - catalyst **L2** for 16 h - the crude product was purified by column chromatography to afford pure product. **Yield:** 35% (143.7 mg, 0.703 mmol); 6:94 *er*.

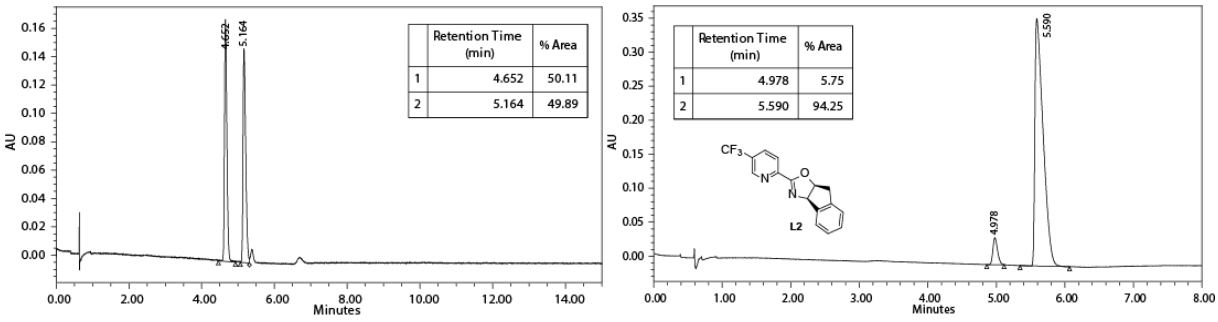

UPCC: Daicel Chiralpak® ID column (4.6 mm x 250 mm), CO_2/^{i}PrOH = 99:1 to 95:5 over 4.5 min, 3.0 mL/min, 40 °C, λ = 284 nm, tR (major) = 5.59 min; tR (minor) = 4.98 min, *er* = 6:94.

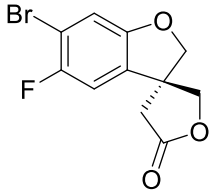

***ent*-3h -** Obtained from **L3**

***ent*-3h - (*S*)-6-bromo-5-fluoro-2*H*,2'*H*-spiro[benzofuran-3,3'-furan]-5'(4'*H*)-one -** The nitroarene **1h** (0.20 mmol) was subjected to the general procedure A - the crude product was purified by column chromatography to afford pure product. The isolated yield is the average of two runs. **3h: Yield:** traces. ***ent*-3h: Yield:** 21% (12.0 mg, 0.042 mmol); 65:35 *er*. **Rf:** 0.32 (Pentane/EtOAc 8:2). **Physical state:** Orange Solid. **^{1}H NMR (400 MHz, $CDCl_3$)** - δ 7.04 (d, J = 5.3 Hz, 1H), 6.98 (d, J = 7.4 Hz, 1H), 4.61 (d, J = 9.5 Hz, 1H), 4.51 (d, J = 9.4 Hz, 1H), 4.42 (d, J = 9.5 Hz, 1H), 4.35 (d, J = 9.5 Hz, 1H), 2.90 (d, J = 17.7 Hz, 1H), 2.77 (d, J = 17.7 Hz, 1H). **^{13}C NMR (101 MHz, $CDCl_3$)** - δ 174.0, 156.0 (d, J = 2.1 Hz), 154.5 (d, J = 241.6 Hz), 129.2 (d, J = 6.7 Hz), 115.0, 110.4 (d, J = 26.0 Hz), 110.0 (d, J = 23.5 Hz), 82.0, 76.9, 50.2 (d, J = 1.7 Hz), 40.4. **^{19}F NMR (376 MHz, $CDCl_3$)** - δ -115.2. **HRMS (ESI+)** calculated *m/z* for [$C_{11}H_8BrFNaO_3^+$]: 308.9533 [M+Na]$^+$; found: 308.9524. ***ent*-3h: $[\alpha]_D^{24}$** +2 (c 0.98, $CHCl_3$, 65:35 *er*).

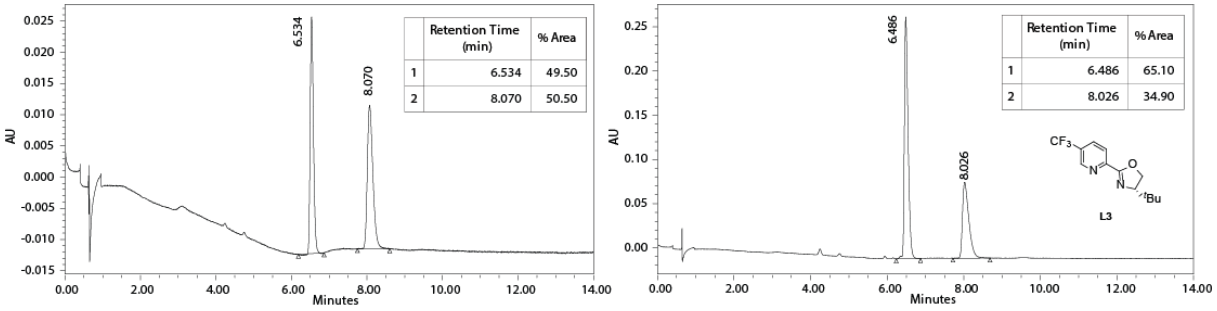

UPCC: Daicel Chiralpak® ID column (4.6 mm x 250 mm), CO_2/^{i}PrOH = 99:1 to 95:5 over 4.5 min, 3.0 mL/min, 40 °C, λ = 284 nm, ***ent*-3h:** tR (major) = 6.49 min; tR (minor) = 8.03 min, *er* = 65:35.

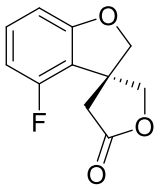

3i - Obtained from **L2**

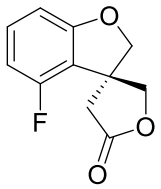

***ent*-3i -** Obtained from **L3**

3i - (*R*)-4-fluoro-2*H*,2'*H*-spiro[benzofuran-3,3'-furan]-5'(4'*H*)-one - The nitroarene **1i** (0.20 mmol) was subjected to the general procedure A - the crude product was purified by column to afford pure product. The isolated yield is the average of two runs. **3i: Yield:** 12% (4.8 mg, 0.023 mmol); 11:89 *er.* ***ent*-3i: Yield:** 19% (7.9 mg, 0.038 mmol); 90:10 *er.* **Rf:** 0.35 (Pentane/EtOAc 8:2). **Physical state:** Colorless oil. **^{1}H NMR (400 MHz, $CDCl_3$)** – δ 7.21 (td, *J* = 8.2, 5.9 Hz, 1H), 6.71 – 6.56 (m, 2H), 4.65 (d, *J* = 9.4 Hz, 1H), 4.59 (d, *J* = 9.3 Hz, 1H), 4.49 (d, *J* = 9.4 Hz, 1H), 4.42 (d, *J* = 9.3 Hz, 1H), 3.28 (d, *J* = 17.7 Hz, 1H), 2.71 (d, *J* = 17.7 Hz, 1H). **^{13}C NMR (101 MHz, $CDCl_3$)** – δ 174.7, 162.0 (d, *J* = 8.1 Hz), 159.6 (d, *J* = 248.2 Hz), 131.8 (d, *J* = 9.1 Hz), 114.0 (d, *J* = 17.6 Hz), 108.8 (d, *J* = 19.9 Hz), 106.8 (d, *J* = 3.6 Hz), 82.9, 76.1, 49.7 (d, *J* = 2.6 Hz), 39.2 (d, *J* = 1.6 Hz). **^{19}F NMR (376 MHz, $CDCl_3$)** – δ -119.9. **HRMS (ESI+)** calculated *m/z* for [$C_{11}H_{10}FO_3^+$]: 209.0608 [M+H]$^+$; found: 209.0612. **3i: $[\alpha]_D^{25}$** +33.8 (c 1.04, $CHCl_3$, 11:89 er). ***ent*-3i: $[\alpha]_D^{25}$** -9.1 (c 1.00, $CHCl_3$, 90:10 *er*).

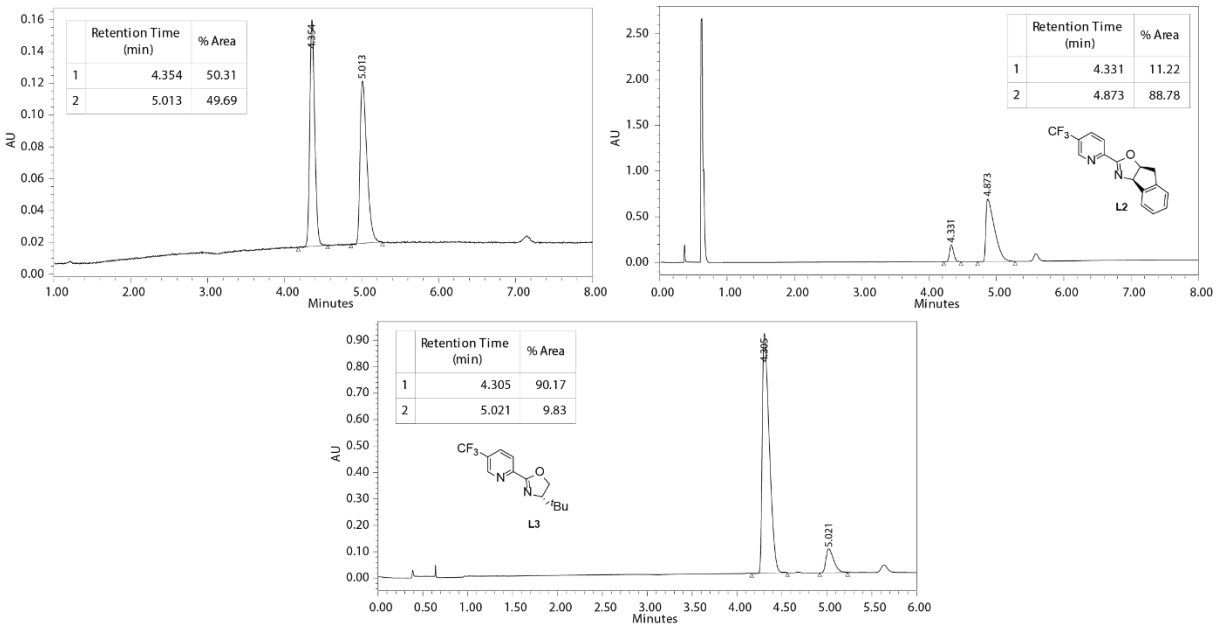

UPCC: Daicel Chiralpak® ID column (4.6 mm x 250 mm), CO_2/^{i}PrOH = 99:1 to 95:5 over 4.5 min, 3.0 mL/min, 40 °C, λ = 212 nm, **3i:** tR (major) = 4.87 min; tR (minor) = 4.33 min, *er* = 11:89. ***ent*-3i:** tR (major) = 4.31 min; tR (minor) = 5.02 min, *er* = 90:10.

3j - Obtained from **L2** ***ent*-3j -** Obtained from **L3**

3j - (*R*)-6-methyl-2*H*,2'*H*-spiro[benzofuran-3,3'-furan]-5'(4'*H*)-one - The nitroarene **1j** (0.20 mmol) was subjected to the general procedure A - the crude product was purified by column chromatography (silica gel, Heptane:EtOAc) to afford pure product. The isolated yield is the average of two runs. **3j: Yield:** 54% (22.0 mg, 0.108 mmol); 5:95 *er.* ***ent*-3j: Yield:** 76% (31.0 mg, 0.152 mmol); 89:11 *er.* **Rf:** 0.43 (8:2 Pentane:EtOAc). **Physical state:** White Solid. **^{1}H NMR (400 MHz, $CDCl_3$)** – δ 7.07 – 6.99 (m, 2H), 6.75 (d, *J* = 8.1 Hz, 1H), 4.56 (d, *J* = 9.4 Hz, 1H), 4.44 (d, *J* = 9.3 Hz, 1H), 4.43 – 4.34 (m, 2H), 2.93 (d, *J* = 17.7 Hz, 1H), 2.73 (d, *J* = 17.7 Hz, 1H), 2.31 (s, 3H). **^{13}C NMR (101 MHz, $CDCl_3$)** – δ 175.0, 157.7, 131.3, 130.5, 128.4, 122.9, 110.1, 81.3, 77.7, 50.0, 40.6, 20.9. **HRMS (ESI+)** calculated *m/z* for $[C_{12}H_{13}O_3^+]$: 205.0859 $[M+H]^+$; found: 205.0857. **3j: $[\alpha]_D^{25}$** -13.5 (c 0.95, $CHCl_3$, 5:95 *er*). ***ent*-3j: $[\alpha]_D^{25}$** +29.0 (c 0.87, $CHCl_3$, 89:11 *er*).

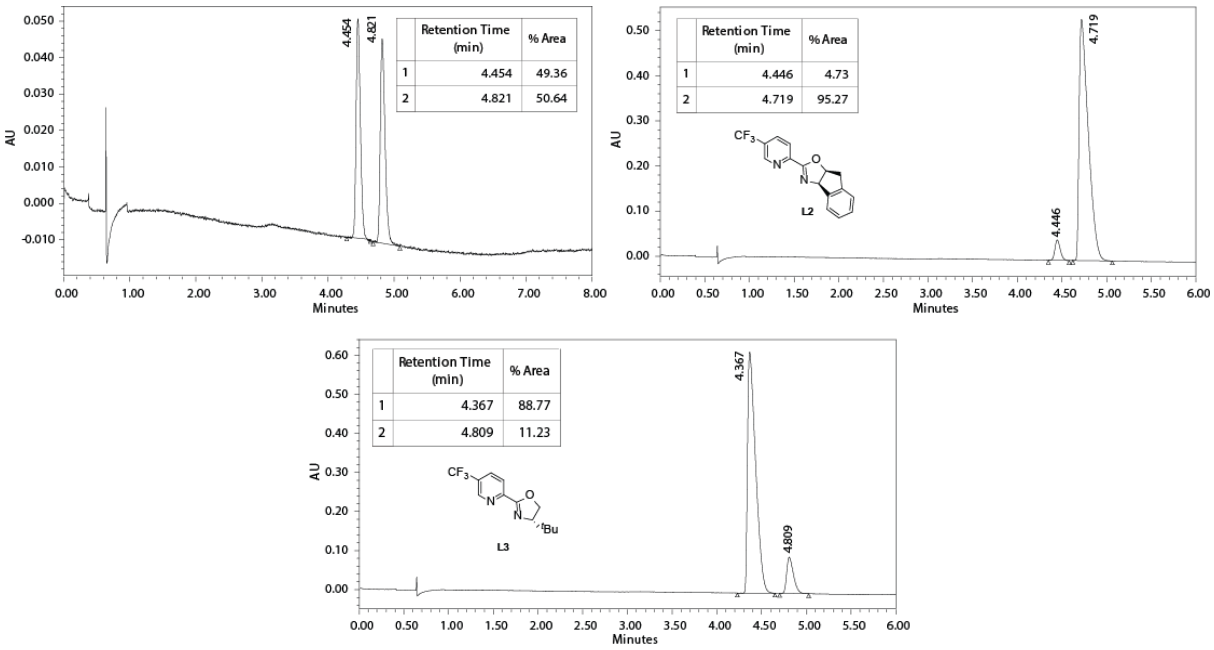

UPCC: Daicel Chiralpak® ID column (4.6 mm x 250 mm), CO_2/^{i}PrOH = 99:1 to 95:5 over 4.5 min, 3.0 mL/min, 40 °C, λ = 284 nm, **3j:** tR (major) = 4.72 min; tR (minor) = 4.45 min, *er* = 5:95, ***ent*-3j:** tR (major) = 4.37 min; tR (minor) = 4.81 min, *er* = 4:96.

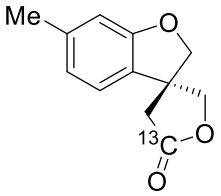

^{13}C-3j - Obtained from **L2**

^{13}C-3j - (*R*)-5-methyl-2H,2'H-spiro[benzofuran-3,3'-furan]-5'(4'H)-one-5'-^{13}C - The nitroarene **1j** (0.20 mmol) was subjected to the general procedure B - the crude product was purified by column chromatography to afford pure product. **^{13}C-3j***:* 54% (22.2 mg, 0.108 mmol); 5:95 *er.* **Rf:** 0.43 (8:2 Pentane:EtOAc). **Physical state:** White Solid. **^{1}H NMR (400 MHz, $CDCl_3$)** – δ 7.06 – 6.99 (m, 2H), 6.75 (d, *J* = 8.1 Hz, 1H), 4.56 (d, *J* = 9.3 Hz, 1H), 4.44 (d, *J* = 9.4 Hz, 1H), 4.42 – 4.35 (m, 2H), 2.93 (dd, *J* = 17.7, 6.2 Hz, 1H), 2.74 (dd, *J* = 17.7, 5.1 Hz, 1H), 2.31 (s, 3H). **^{13}C NMR (101 MHz, $CDCl_3$)** – δ 174.91 (^{13}C enriched), 157.6, 131.2, 130. 5, 128.3 (d, *J* = 2.9 Hz), 122.8, 110.0, 81.3 (d, *J* = 1.9 Hz), 77.6 (d, *J* = 2.5 Hz), 50.0 (d, *J* = 1.8 Hz), 40.5 (d, *J* = 50.5 Hz), 20.8. **HRMS (ESI+)** calculated *m/z* for [$C_{11}{}^{13}CH_{13}O_3^+$]: 206.0893 [M+H]$^+$; found: 206.0887.

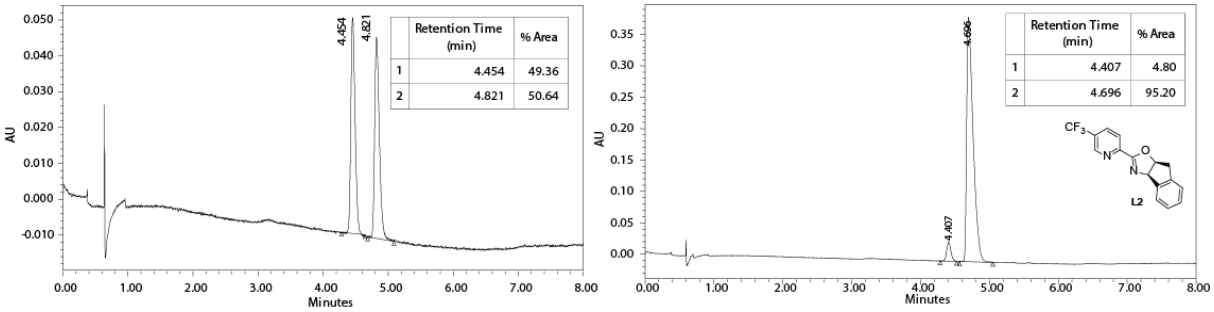

UPCC: Daicel Chiralpak® ID column (4.6 mm x 250 mm), CO_2/^{i}PrOH = 99:1 to 95:5 over 4.5 min, 3.0 mL/min, 40 °C, λ = 284 nm, tR (major) = min; tR (minor) = min, *er* = 5:95.

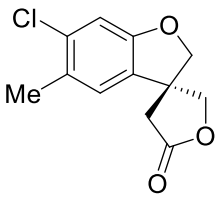

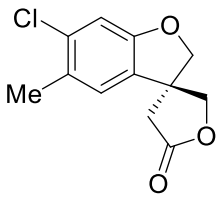

3k - Obtained from **L2** ***ent*-3k -** Obtained from **L3**

3k - (*R*)-6-chloro-5-methyl-2*H*,2'*H*-spiro[benzofuran-3,3'-furan]-5'(4'*H*)-one - The nitroarene **1k** (0.20 mmol) was subjected to the general procedure A - the crude product was purified by column to afford pure product. The isolated yield is the average of two runs. **3k: Yield:** 34% (16.1 mg, 0.067 mmol); 9:91 *er.* ***ent*-3k: Yield:** 63% (30.1 mg, 0,126 mmol); 90:10 *er.* **Rf:** 0.32 (8:2 Pentane:EtOAc). **Physical state:** White Solid. **^{1}H NMR (400 MHz, $CDCl_3$)** - δ 7.04 (s, 1H), 6.86 (s, 1H), 4.57 (d, *J* = 9.4 Hz, 1H), 4.47 (d, *J* = 9.4 Hz, 1H), 4.43 – 4.32 (m, 2H), 2.90 (d, *J* = 17.7 Hz, 1H), 2.74 (d, *J* = 17.7 Hz, 1H), 2.30 (s, 3H). **^{13}C NMR (101 MHz, $CDCl_3$)** – δ 174.7, 158.5, 135.3, 129.3, 127.4, 124.1, 111.4, 81.7, 77.4, 49.8, 40.6, 19.8. **HRMS (ESI+)** calculated *m/z* for [$C_{12}H_{12}ClO_3^+$]: 239.0469 [M+H]$^+$; found: 239.0463. **3k: $[\alpha]_D^{24}$** -23.5 (c 0.88, $CHCl_3$, 9:91 *er*). ***ent*-3k: $[\alpha]_D^{24}$** +23.3 (c 0.94, $CHCl_3$, 90:10 *er*).

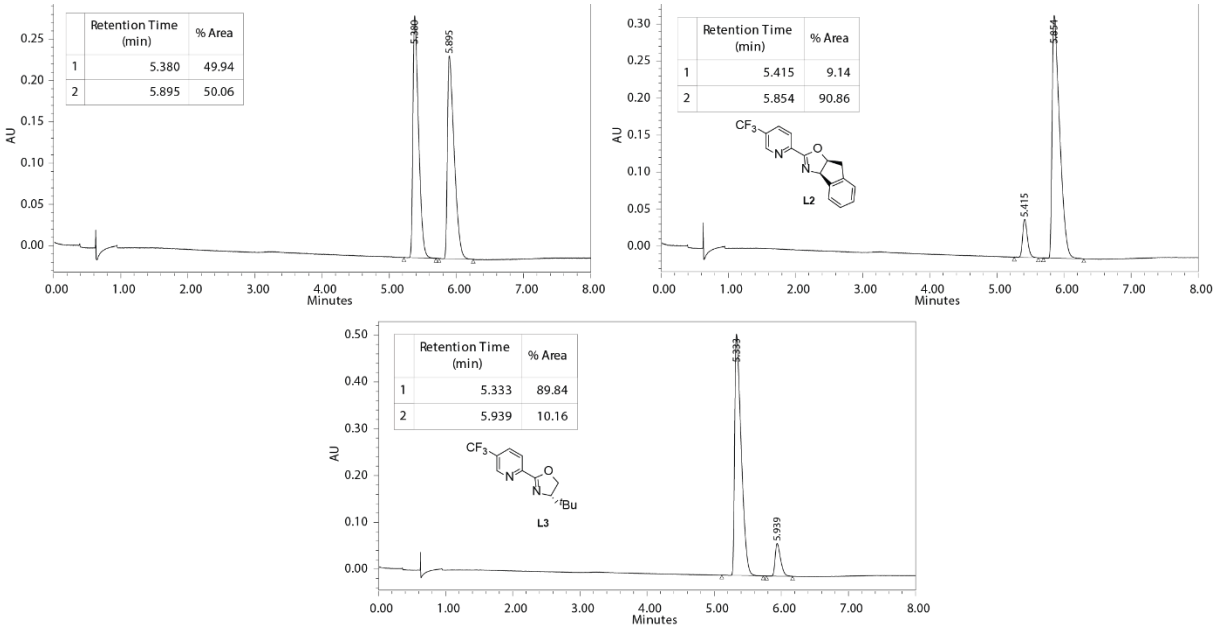

UPCC: Daicel Chiralpak® ID column (4.6 mm x 250 mm), CO_2/^{i}PrOH = 99:1 to 95:5 over 4.5 min, 3.0 mL/min, 40 °C, λ = 284 nm, **3k:** tR (major) = 5.85 min; tR (minor) = 5.42 min, *er* = 9:91. ***ent*-3k:** tR (major) = 5.33 min; tR (minor) = 5.94 min, *er* = 90:10.

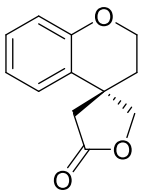

3m - Obtained from **L2**

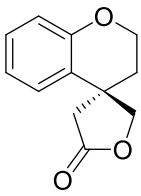

***ent*-3m -** Obtained from **L3**

3m - (*R*)-2'*H*-spiro[chromane-4,3'-furan]-5'(4'*H*)-one - The nitroarene **1m** (0.20 mmol) was subjected to the general procedure A - the crude product was purified by column chromatography to afford pure product. The isolated yield is the average of two runs. **3m: Yield:** 53% (21.8 mg, 0.107 mmol); 30:70 *er.* ***ent*-3m: Yield:** 50% (20.4 mg, 0.099 mmol); 75:25 *er.* **Rf:** 0.24 (8:2 Pentane:EtOAc). **Physical state:** Pale yellow solid. **^{1}H NMR (400 MHz, $CDCl_3$)** - δ 7.28 (dd, *J* = 7.8, 1.6 Hz, 1H), 7.18 (ddd, *J* = 8.3, 7.2, 1.6 Hz, 1H), 6.96 (ddd, *J* = 7.8, 7.2, 1.3 Hz, 1H), 6.86 (dd, *J* = 8.2, 1.3 Hz, 1H), 4.46 (d, *J* = 9.4 Hz, 1H), 4.30 (d, *J* = 9.4 Hz, 1H), 4.27 – 4.13 (m, 2H), 3.00 (d, *J* = 17.6 Hz, 1H), 2.62 (d, *J* = 17.6 Hz, 1H), 2.14 (ddd, *J* = 14.0, 6.5, 3.4 Hz, 1H), 2.04 (ddd, *J* = 14.0, 7.7, 3.8 Hz, 1H). **^{13}C NMR (101 MHz, $CDCl_3$)** – δ 175.6, 154.7, 129.1, 126.3, 123.5, 121.5, 117.9, 79.3, 63.1, 43.9, 39.8, 33.7. **HRMS (ESI+)** calculated *m/z* for [$C_{12}H_{13}O_3^+$]: 205.0859 [M+H]$^+$; found: 205.0857. **3m: $[\alpha]_D^{25}$** -10.1 (c 0.93, $CHCl_3$, 30:70 er). ***ent*-3m: $[\alpha]_D^{25}$** +2.1 (c 0.95, $CHCl_3$, 75:25 er).

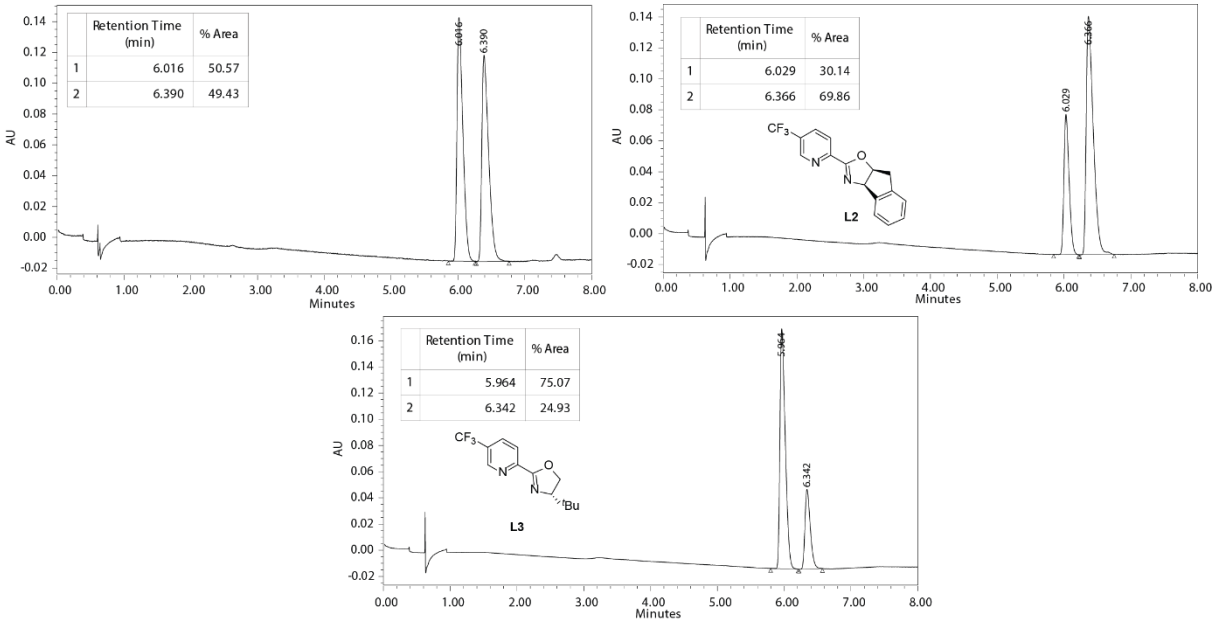

UPCC: Daicel Chiralpak® ID column (4.6 mm x 250 mm), CO_2/^{i}PrOH = 99:1 to 95:5 over 4.5 min, 3.0 mL/min, 40 °C, λ = 284 nm, **3m:** tR (major) = 6.37 min; tR (minor) = 6.03 min, *er* = 30:70. ***Ent*-3m:** tR (major) = 5.96 min; tR (minor) = 6.34 min, *er* = 75:25.

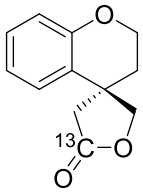

^{13}C-*ent*-3m - Obtained from **L3**

^{13}C-*ent*-3m - (*S*)-2'*H*-spiro[chromane-4,3'-furan]-5'(4'*H*)-one-5'-^{13}C - The nitroarene **1m** (0.20 mmol) was subjected to the general procedure B - the crude product was purified by column chromatography to afford pure product. **Yield:** 66% (26.9 mg, 0,132 mmol); 73:27 *er*. **Rf:** 0.24 (8:2 Pentane:EtOAc). **Physical state:** Pale yellow solid. **^{1}H NMR (400 MHz, $CDCl_3$)** – δ 7.28 (dd, *J* = 7.9, 1.6 Hz, 1H), 7.18 (ddd, *J* = 8.5, 7.2, 1.6 Hz, 1H), 6.96 (td, *J* = 7.5, 1.3 Hz, 1H), 6.86 (dd, *J* = 8.2, 1.3 Hz, 1H), 4.46 (ddd, *J* = 9.5, 2.2, 0.7 Hz, 1H), 4.30 (dd, *J* = 9.4, 4.9 Hz, 1H), 4.26 – 4.15 (m, 2H), 3.00 (dd, *J* = 17.6, 6.4 Hz, 1H), 2.62 (dd, *J* = 17.6, 5.0 Hz, 1H), 2.14 (ddd, *J* = 14.0, 6.5, 3.4 Hz, 1H), 2.05 (ddd, *J* = 14.1, 7.5, 3.8 Hz, 1H). **^{13}C NMR (101 MHz, $CDCl_3$)** – δ 175.6 (^{13}C enriched), 154.7, 129.1, 126.3, 123.5 (d, *J* = 3.1 Hz), 121.5, 117. 9, 79.3 (d, *J* = 2.6 Hz), 63.1, 43.9 (d, *J* = 50.1 Hz), 39.8 (d, *J* = 1.9 Hz), 33.7 (d, *J* = 1.3 Hz). **HRMS (ESI+)** calculated *m/z* for [$C_{11}{}^{13}CH_{13}O_3^+$]: 206.0893 [M+H]$^+$; found: 206.0895. **$[\alpha]_D^{24.3}$** +3.8 (c 0.94, $CHCl_3$, 73:27 *er*).

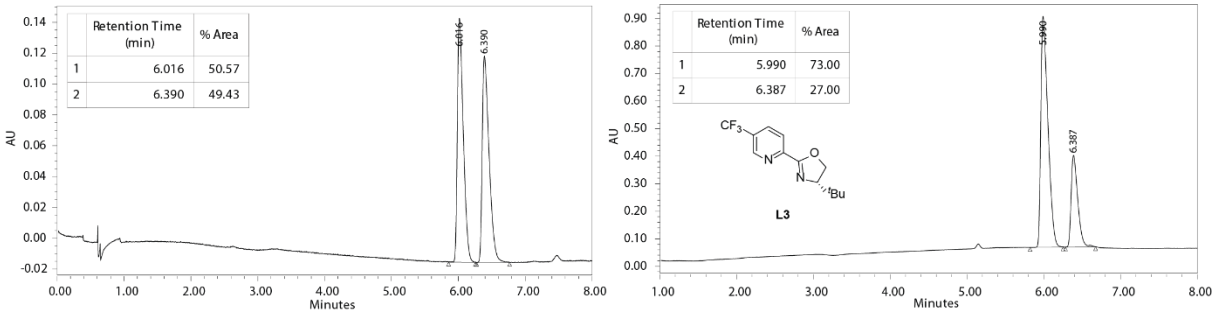

UPCC: Daicel Chiralpak® ID column (4.6 mm x 250 mm), CO_2/^{i}PrOH = 99:1 to 95:5 over 4.5 min, 3.0 mL/min, 40 °C, λ = 284 nm, tR (major) = 5.99 min; tR (minor) = 6.39 min, *er* = 73:27.

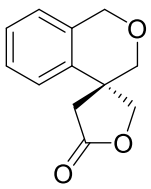

3n - Obtained from **L2**

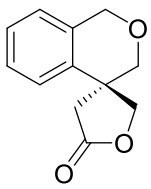

***ent*-3n -** Obtained from **L3**

3n - (*R*)-2*H*-spiro[furan-3,4'-isochroman]-5(4*H*)-one - The nitroarene **1n** (0.20 mmol) was subjected to the general procedure **A** - the crude product was purified by column to afford pure product. **3n: Yield:** 48% (19.6 mg, 0.096 mmol); 52:48 *er.* ***ent*-3n: Yield:** 67% (27.3 mg, 0.134 mmol); 37:63 *er.* **Rf:** 0.30 (8:2 Pentane:EtOAc). **Physical state:** White solid. **^{1}H NMR (400 MHz, $CDCl_3$) –** δ 7.37 (dd, *J* = 7.7, 1.6 Hz, 1H), 7.34 – 7.29 (m, 1H), 7.26 (td, *J* = 7.1, 1.6 Hz, 1H), 7.09 – 7.01 (m, 1H), 4.83 (s, 2H), 4.52 (d, *J* = 9.5 Hz, 1H), 4.32 (dd, *J* = 9.4, 1.2 Hz, 1H), 3.97 (d, *J* = 11.4 Hz, 1H), 3.73 (dd, *J* = 11.5, 1.3 Hz, 1H),

3.12 – 2.89 (m, 1H), 2.76 – 2.40 (m, 1H). **^{13}C NMR (101 MHz, $CDCl_3$) –** δ 175.8, 135.0, 134.9, 127.8, 127.7, 125.4, 124.9, 77.2, 72.3, 68.8, 42.2, 39.2. **HRMS (ESI+)** calculated *m/z* for [$C_{12}H_{13}O_3^+$]: 205.0859 [M+H]$^+$; found: 205.0856. **3n: [α]$_D^{25}$** 0.0 (c 0.07, $CHCl_3$, 52:48 *er*). ***ent*-3n: [α]$_D^{25}$** -6.0 (c 1.00, $CHCl_3$, 37:63 *er*).

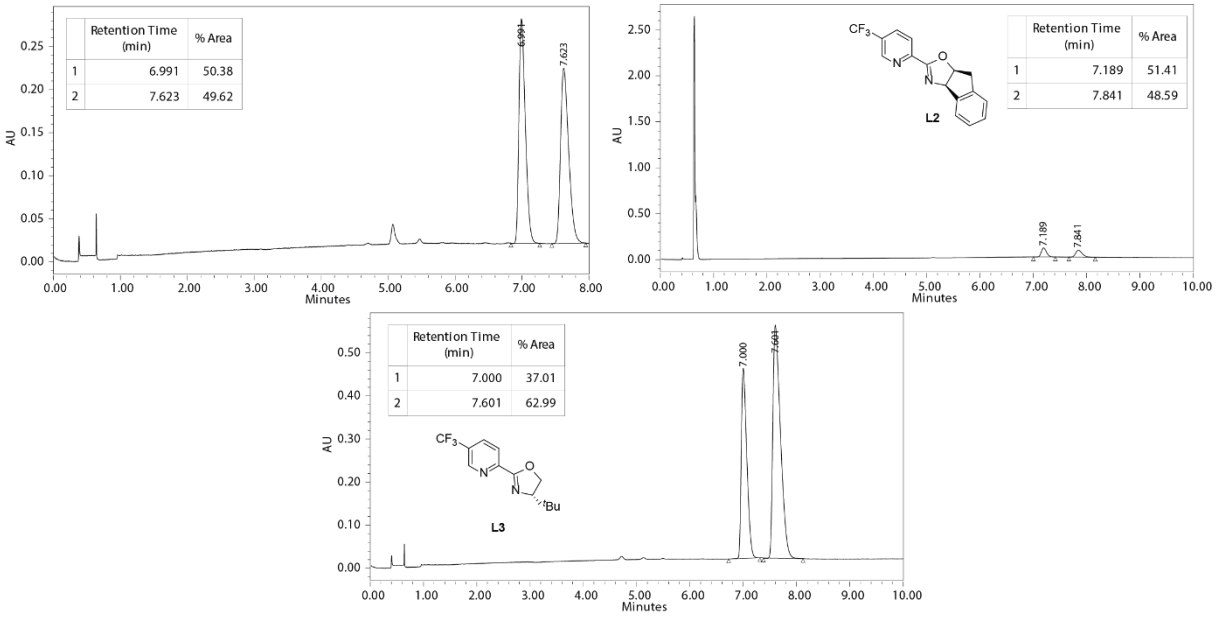

UPCC: Daicel Chiralpak® ID column (4.6 mm x 250 mm), CO_2/$_i$PrOH = 99:1 to 95:5 over 4.5 min, 3.0 mL/min, 40 °C, λ = 212 nm, **3n:** tR (major) = 7.19 min; tR (minor) = 7.84 min, *er* = 51:49. ***ent*-3n:** tR (major) = 7.60 min; tR (minor) = 7.00 min, *er* = 37:63.

3o - Obtained from **L2** ***ent*-3o -** Obtained from **L3**

3o- (*R*)-1'-tosyl-2*H*-spiro[furan-3,3'-indolin]-5(4*H*)-one - The nitroarene **1o** (0.20 mmol) was subjected to the general procedure A - the crude product was purified by column chromatography to afford pure product. The isolated yield is the average of two runs. **3o: Yield:** 59% (40.2 mg, 0.117 mmol); 67:33 *er.* ***ent*-3o: Yield:** 74% (50.7 mg, 0.148 mmol); 27:73 *er.* **Rf:** 0.6 (6:4 Pentane:EtOAc). **Physical state:** Yellow solid. **^{1}H NMR (400 MHz, $CDCl_3$)** – δ 7.72 (dt, *J* = 8.2, 0.8 Hz, 1H), 7.70 – 7.61 (m, 2H), 7.34 (ddd, *J* = 8.2, 6.8, 2.0 Hz, 1H), 7.31 – 7.26 (m, 2H), 7.18 – 7.06 (m, 2H), 4.12 – 4.02 (m, 2H), 3.99 (d, *J* = 11.2 Hz, 1H), 3.82 (d, *J* = 11.2 Hz, 1H), 2.62 (d, *J* = 17.7 Hz, 1H), 2.46 (d, *J* = 17.7 Hz, 1H), 2.39 (s, 3H). **^{13}C NMR (101 MHz, $CDCl_3$)** – δ 174.5, 145.0, 141.6, 133.4, 133.0, 130.1, 130.0, 127.4, 124.9, 122.6, 115.7, 77.4, 60.4, 48.1, 40.9, 21.7. **HRMS (ESI+)** calculated *m/z* for [$C_{18}H_{18}NO_4S^+$]: 344.0951 [M+H]$^+$; found: 344.0949. **3o: [α]$_D^{25}$** -15.0 (c 0.93, $CHCl_3$, 67:33 *er*). ***ent*-3o: [α]$_D^{25}$** +4.0 (c 1.00, $CHCl_3$, 27:73 *er*).

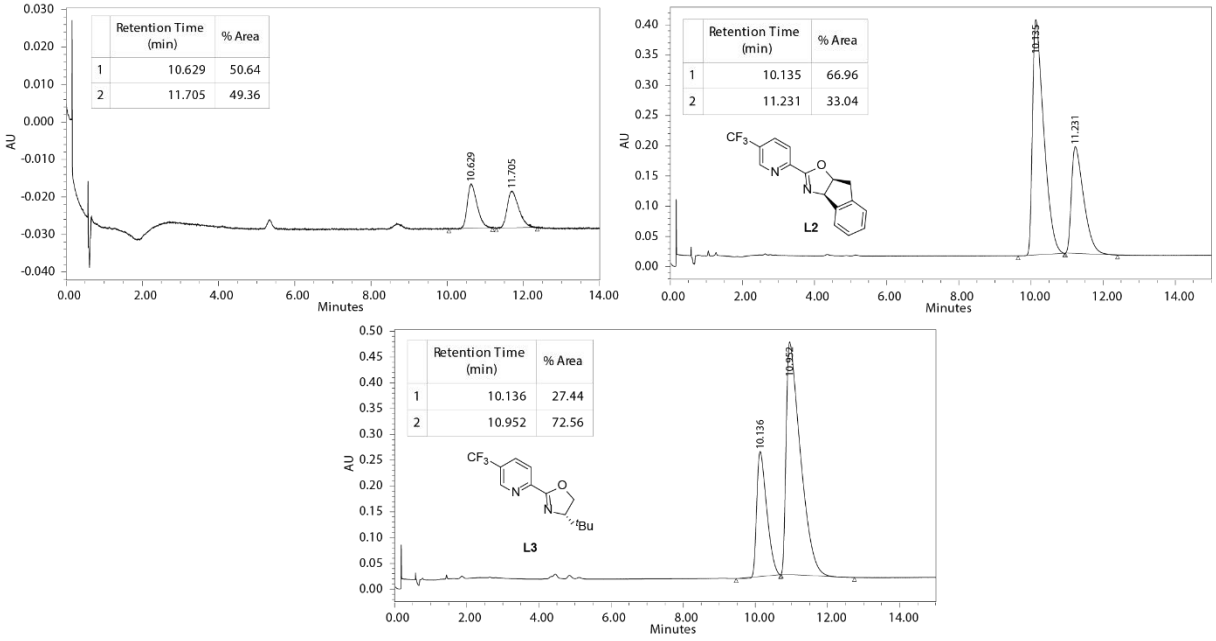

UPCC: Daicel Chiralpak® ID column (4.6 mm x 250 mm), CO_2/^{i}PrOH = 90:10, 3.0 mL/min, 40 °C, λ = 212 nm, **3o:** tR (major) = 10.14 min; tR (minor) = 11.23 min, *er* = 67:33. ***ent*-3o:** tR (major) = 10.95 min; tR (minor) = 10.14 min, *er* = 27:73.

3p - Obtained from **L2** ***ent*-3p -** Obtained from **L3**

3p- (*R*)-1'-(methylsulfonyl)-2*H*-spiro[furan-3,3'-indolin]-5(4*H*)-one - The nitroarene **1p** (0.20 mmol) was subjected to the general procedure A - the crude product was purified by column chromatography to afford pure product. The isolated yield is the average of two runs. **3p: Yield:** 40% (21.4 mg, 0.080 mmol); 67:33 *er*. ***ent*-3p: Yield:** 61% (32.5 mg, 0.122 mmol); 22:78 *er*. **Rf:** 0.3 (6:4 Pentane:EtOAc). **Physical state:** White solid. **^{1}H NMR (400 MHz, $CDCl_3$)** – δ 7.43 (dt, *J* = 8.1, 0.8 Hz, 1H), 7.33 (td, *J* = 7.8, 1.3 Hz, 1H), 7.30 – 7.26 (m, 1H), 7.14 (td, *J* = 7.5, 1.0 Hz, 1H), 4.44 (d, *J* = 9.4 Hz, 1H), 4.35 (d, *J* = 9.4 Hz, 1H), 4.07 (d, *J* = 10.5 Hz, 1H), 3.91 (d, *J* = 10.5 Hz, 1H), 2.96 – 2.90 (m, 4H), 2.79 (d, *J* = 17.6 Hz, 1H). **^{13}C NMR (101 MHz, $CDCl_3$)** – δ 174.4, 141.6, 132.3, 130.3, 124.7, 123.0, 113.8, 77.3, 61.0, 48.1, 40.8, 35.1. **HRMS (ESI+)** calculated for $[C_{12}H_{14}NO_4S^+]$: 268.0638 $[M+H]^+$; found: 268.0633. **3p: $[\alpha]_D^{25}$** +6.1 (c 0.98, $CHCl_3$, 67:33 *er*). ***ent*-3p: $[\alpha]_D^{25}$** -8.6 (c 0.98, $CHCl_3$, 22:78 *er*).

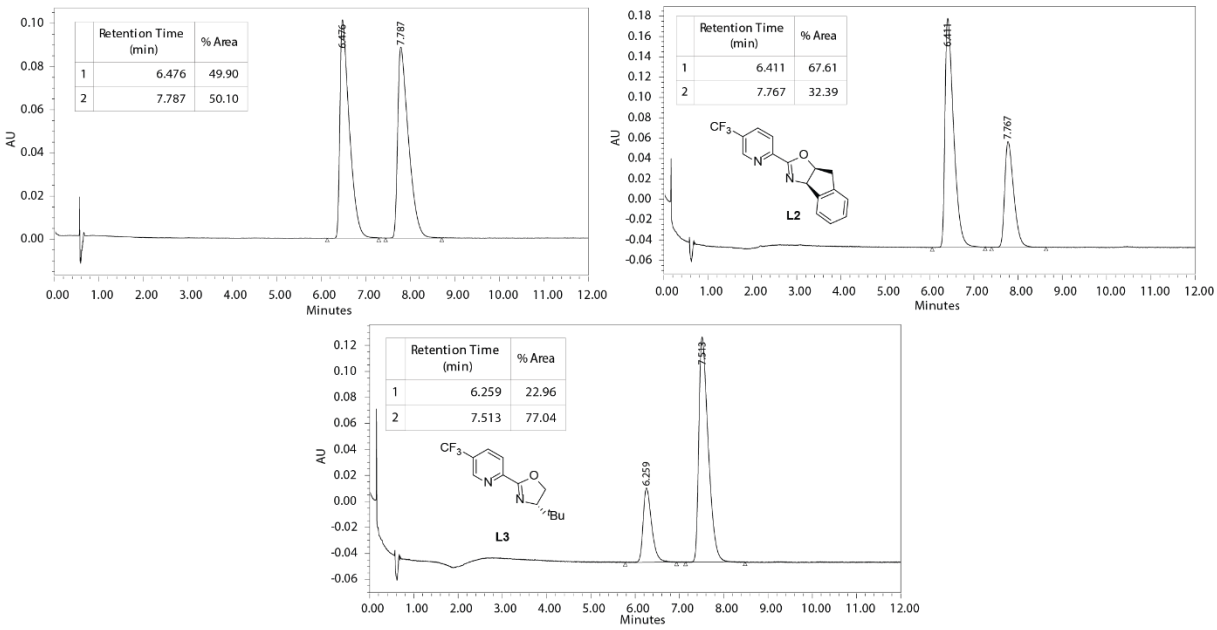

UPCC: Daicel Chiralpak® ID column (4.6 mm x 250 mm), CO_2/^{i}PrOH = 90:10, 3.0 mL/min, 40 °C, λ = 230 nm, **3p:** tR (major) = 6.41 min; tR (minor) = 7.77 min, *er* = 67:33. **ent-3p:** tR (major) = 7.51 min; tR (minor) = 6.26 min, *er* = 23:77.

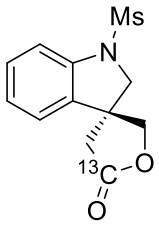

^{13}C-*ent*-3p - Obtained from **L3**

^{13}C-*ent*-3p - (*S*)-1'-(methylsulfonyl)-2*H*-spiro[furan-3,3'-indolin]-5(4*H*)-one - The nitroarene **1p** (0.20 mmol) was subjected to the general procedure B - the crude product was purified by column chromatography **Yield:** 59% (31.6 mg, 0.118 mmol); 24:76 *er*. **Physical state:** White solid. **^{1}H NMR (400 MHz, $CDCl_3$)** – δ 7.42 (dt, J = 8.2, 0.8 Hz, 1H), 7.33 (ddd, *J* = 8.3, 7.4, 1.3 Hz, 1H), 7.30 – 7.26 (m, 1H), 7.13 (td, *J* = 7.5, 1.1 Hz, 1H), 4.44 (dd, *J* = 9.4, 4.5 Hz, 1H), 4.35 (dd, *J* = 9.4, 2.6 Hz, 1H), 4.07 (d, *J* = 10.5 Hz, 1H), 3.90 (d, *J* = 10.5 Hz, 1H), 2.98 – 2.88 (m, 4H), 2.78 (dd, *J* = 17.6, 5.2 Hz, 1H). **^{13}C NMR (101 MHz, $CDCl_3$)** – δ 174.4 (^{13}C enriched), 141.6, 132.3 (d, *J* = 2.9 Hz), 130.2, 124.6, 123.0, 113.8, 77.3 (d, *J* = 2.4 Hz), 61.0 (d, *J* = 2.0 Hz), 48.1 (d, *J* = 1.8 Hz), 40.8 (d, *J* = 50.6 Hz), 35.1. **HRMS (ESI+)** calculated *m/z* for [$C_{11}{}^{13}CH_{14}NO_4S^+$]: 269.0672 $[M+H]^+$ found: 269.0668. **$[\alpha]_D^{24.2}$** -7.5 (c 0.80, $CHCl_3$, 24:76 *er*).

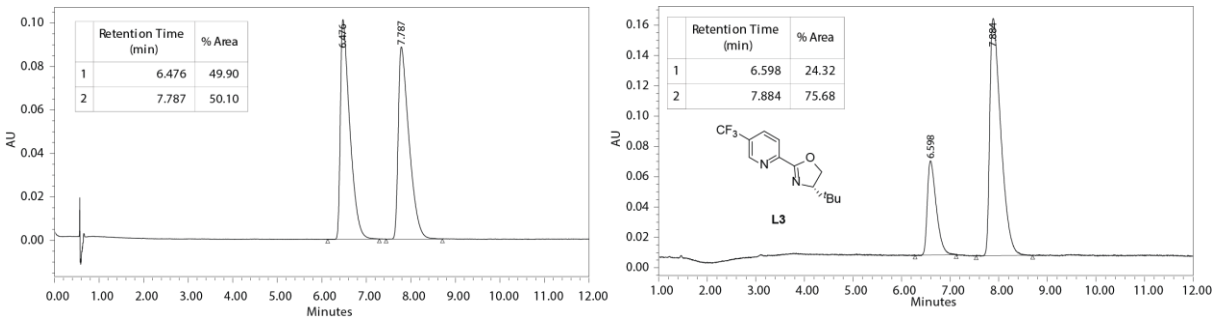

UPCC: Daicel Chiralpak® ID column (4.6 mm x 250 mm), CO_2/^{i}PrOH = 90:10, 3.0 mL/min, 40 °C, λ = 230 nm, tR (major) = 7.88 min; tR (minor) = 6.60 min, *er* = 24:76.

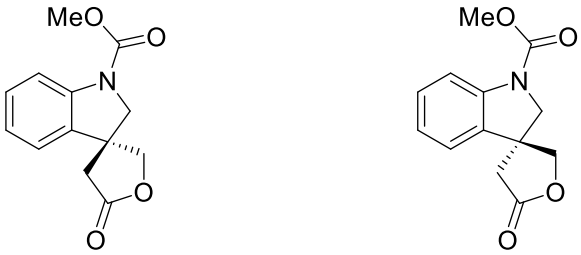

3q - Obtained from **L2** ***ent*-3q** - Obtained from **L3**

3q- Methyl (*R*)-5-oxo-4,5-dihydro-2*H*-spiro[furan-3,3'-indoline]-1'-carboxylate - The nitroarene **1q** (0.20 mmol) was subjected to the general procedure A - the crude product was purified by column chromatography to afford pure product. The isolated yield is the average of two runs. **3q: Yield:** 29% (14.3 mg, 0.058 mmol); 27:73 *er.* ***ent-3q*: Yield:** 51% (25.4 mg, 0.103 mmol); 84:16 *er.* **Rf:** 0.54 (6:4 Pentane:EtOAc). **Physical state:** White solid. **^{1}H NMR (400 MHz, $CDCl_3$)** – 1H NMR (400 MHz, CDCl3) δ 7.90 (s, 1H), 7.35 – 7.26 (m, 1H), 7.22 (dd, *J* = 7.6, 1.3 Hz, 1H), 7.07 (td, *J* = 7.5, 1.1 Hz, 1H), 4.41 – 4.31 (m, 2H), 4.15 (d, *J* = 11.6 Hz, 1H), 4.01 (d, *J* = 11.6 Hz, 1H), 3.85 (s, 3H), 2.91 (d, *J* = 17.6 Hz, 1H), 2.74 (d, *J* = 17.5 Hz, 1H). **^{13}C NMR (101 MHz, $CDCl_3$) –** δ 174.8, 153.2, 142.2, 131.7, 129.8, 123.7, 122.3, 115.3, 78.4, 59.5, 53.1, 47.8, 41.8. **HRMS (ESI+)** *m/z* calculated for [$C_{13}H_{14}NO_4^+$]: 248.0917 [M+H]$^+$; found: 248.0916. **3q: $[\alpha]_D^{25}$** +0.6 (c 0.93, $CHCl_3$, 27:73 *er*). ***ent*-3q: $[\alpha]_D^{25}$** -18.2 (c 0.97, $CHCl_3$, 84:16 *er*).

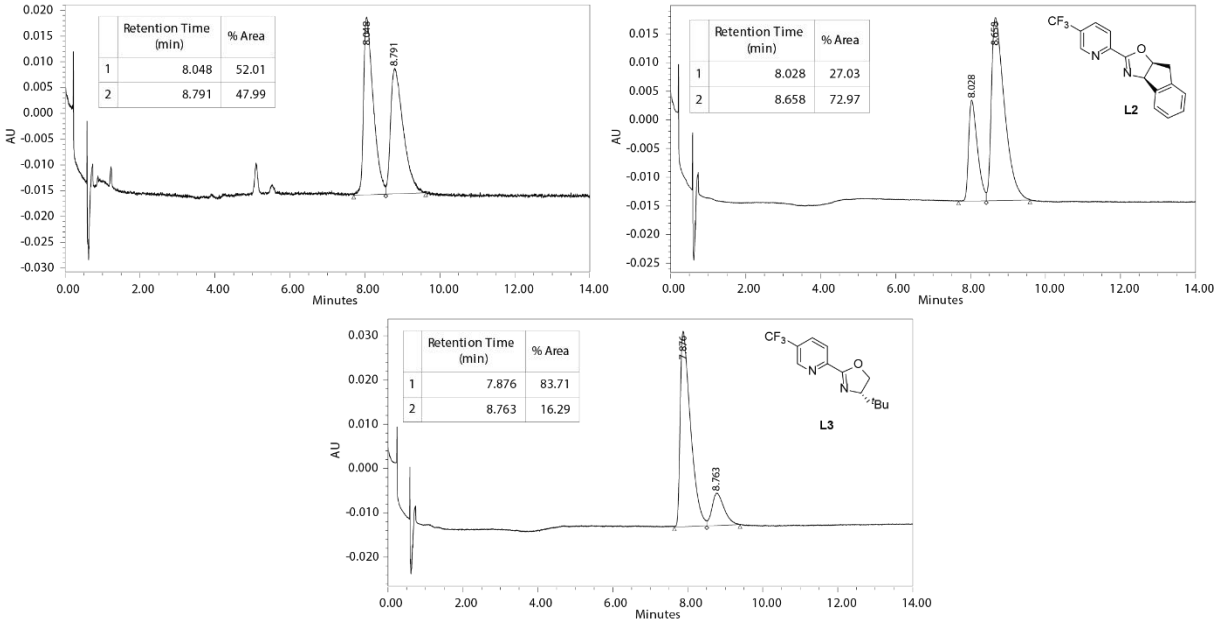

UPCC: Daicel Chiralpak® ID column (4.6 mm x 250 mm), CO_2/^{i}PrOH = 95:5, 3.0 mL/min, 40 °C, λ = 284 nm, **3q:** tR (major) = 8.66 min; tR (minor) = 8.03 min, *er* =27:73. ***ent*-3q:** tR (major) = 7.88 min; tR (minor) = 8.76 min, *er* = 84:16.

Experimental Bibliography

[1] T. H. D. Chorro, E. L. Scarpa de Souza, O. D. Köster, E. C. Polo, R. C. Carmona, V. H. Menezes da Silva, J. M. Batista Junior, C. R. Duarte Correia, *Adv. Synth. Catal.* **2023**, *365*, 211–223.

[2] M. Jang, T. Lim, B. Y. Park, M. S. Han, *J. Org. Chem.* **2022**, *87*, 910–919.

[3] S. D. Karyakarte, C. Um, I. A. Berhane, S. R. Chemler, *Angew. Chemie - Int. Ed.* **2018**, *57*, 12921–12924.

[4] akeyuki S. and M. A. Yuta Sato, Tsuyoshi Matsuzaki, Tsunayoshi Takehara, Makoto Sako, *Chem. Commun.* **2022**, *58*, 415–418.

[5] I. Massad, H. Sommer, I. Marek, *Angew. Chemie - Int. Ed.* **2020**, *59*, 15549–15553.

[6] M. Xuan, I. Paterson, S. M. Dalby, *Org. Lett.* **2012**, *14*, 5492–5495.

[7] F. A. Siqueira, J. G. Taylor, C. R. D. Correia, *Tetrahedron Lett.* **2010**, *51*, 2102–2105.

[8] B. Jiang, M. Zhao, S. Sen Li, Y. H. Xu, T. P. Loh, *Angew. Chemie - Int. Ed.* **2018**, *57*, 555–559.

[9] M. S. McCammant, M. S. Sigman, *Chem. Sci.* **2015**, *6*, 1355–1361.

[10] W. Huang, X. Wan, Q. Shen, *Angew. Chemie - Int. Ed.* **2017**, *56*, 11986–11989.

[11] R. Melot, M. Zuccarello, D. Cavalli, N. Niggli, M. Devereux, T. Bürgi, O. Baudoin, *Angew. Chemie - Int. Ed.* **2021**, *60*, 7245–7250.

[12] Y. Li, Y. Li, L. Peng, D. Wu, L. Zhu, G. Yin, *Chem. Sci.* **2020**, *11*, 10461–10464.

[13] C. C. Oliveira, A. Pfaltz, C. R. D. Correia, *Angew. Chemie - Int. Ed.* **2015**, *54*, 14036–14039.

Single Crystal X-Ray Crystallography

Crystallographic Methods

Data were either collected on an XtaLAB Synergy-S (compound *R*-**3g**) or on an Agilent SuperNova (compound *R*-**3e**) single-crystal X-ray diffractometer. The former is equipped with a Hybrid Pixel Array detector (HyPix-Arc 100) and a PhotonJet micro-focus sealed tube source that emits Mo Kα radiation (λ = 0.71073 Å). The Agilent instrument features an Atlas CCD detector and a SuperNova micro-focus source (also Mo Kα). Both diffractometers are operated with CrysAlisPro.[1] The measurements were performed on single crystals coated with Paratone N, at 100 K under a stream of dry nitrogen (Oxford Cryostream Plus). Absorption correction was performed using the SCALE3 ABSPACK multi-scan method. The space group assignment was based upon systematic absences, E statistics, and successful refinement of the structures. The structures were solved by intrinsic phasing using SHELXT[2] and were refined against all data using SHELXL[3] in conjunction with Olex2 v1.5.[4] Hydrogen atoms were calculated in ideal positions by placing them in initial, calculated positions and refining them using a riding model with methyl, methylene and aromatic C−H distances of 0.98, 0.99, and 0.95 Å, respectively, and $U_{iso}(H) = 1.2U_{eq}(C)$. All nonhydrogen atoms were refined with anisotropic displacement parameters. Full-matrix least-squares refinements were carried out by minimizing $\Sigma w(F_o^2 - F_c^2)^2$ with the SHELXL weighting scheme.[3] Neutral atom scattering factors for all atoms and anomalous dispersion corrections for the non-hydrogen atoms were taken from International Tables for Crystallography.[5] Images of the crystal structures were generated with Olex2.[4] Deposition numbers 2376544-2376545 contain the supplementary crystallographic data for this paper. These data are provided free of charge by the Cambridge Crystallographic Data Centre (CCDC).

Absolute configurations were determined by calculating Bayesian statistics on Bijvoet differences,[6] as implemented in PLATON v60720.[7] High Bijvoet pair coverage was achieved by choosing data collection strategies for *P*1, despite higher symmetry in the crystal structure. Racemic twinning as well as accidentally picking of a minor enantiomer crystal could be excluded for both crystals by redissolving these very crystals that have been used for diffraction experiments (*R*-**3e**: ~50 µg; *R*-**3g**: ~7 µg) in 50 µL acetonitrile each (after Paratone removal with pentane) and performing chiral UPLC measurements on the obtained solutions.

Crystallographic Bibliography

[1] Rigaku Oxford Diffraction, **2022**.
[2] G. M. Sheldrick, *Acta Cryst. A* **2015**, *71*, 3–8.
[3] G. M. Sheldrick, *Acta Cryst. C* **2015**, *71*, 3–8.
[4] O. V. Dolomanov, L. J. Bourhis, R. J. Gildea, J. a. K. Howard, H. Puschmann, *J. Appl. Cryst.* **2009**, *42*, 339–341.
[5] A. J. C. Wilson, Ed. , *International Tables for Crystallography Volume C : Mathematical, Physical and Chemical Tables*, Kluwer Academic Publishers, Dordrecht/Boston/London, **1992**.
[6] R. W. W. Hooft, L. H. Straver, A. L. Spek, *J. Appl. Cryst.* **2008**, *41*, 96–103.
[7] A. L. Spek, *J. Appl. Cryst.* **2003**, *36*, 7–13.

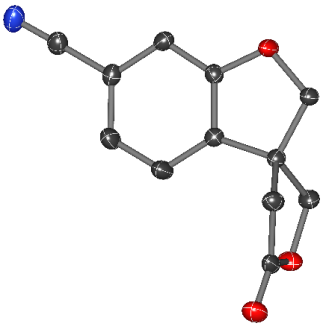

Figure S1. Molecular structure of *R*-**3e** with thermal ellipsoids displayed at the 50% probability level. Hydrogen atoms are omitted for clarity. Color code: C (black), N (blue), O (red).

Table S10. Crystal data, data collection, and structure refinement for *R*-**3e** (CCDC: 2376545)

Molecular Formula		$C_{12}H_9NO_3$	
Formula Weight	[g mol^{-1}]	215.20	
Crystal Dimensions	[mm^3]	0.6 x 0.6 x 0.1	
Crystal Habit		colorless, clear plate	
Crystal System		orthorhombic	
Space Group		$P2_12_12_1$	
Unit Cell Dimensions	[Å / °]	a = 15.8376(6) b = 8.7353(3) c = 6.9909(3)	α = 90 β = 90 γ = 90
Volume	[Å^3]	967.16(6)	
Z		4	
Density (calculated)	[g cm^{-3}]	1.478	
Absorption Coefficient μ	[mm^{-1}]	0.108	
F(000)	[e^{-1}]	448.0	
Temperature	[K]	100	
Diffractometer		SuperNova	
Wavelength	[Å]	0.71073	
Number of Frames		1499	
Exposure Time	[h]	3.3	
Θ Range	[°]	3.473 to 29.596	
Index Ranges		-21 ≤ h ≤ 21, -11 ≤ k ≤ 12, -9 ≤ l ≤ 9	
Reflections Collected		42883	
Independent Reflections		2603 [*R*(int) = 0.0565]	
Bijvoet Pairs Collected		1055	
Bijvoet Pair Coverage	[%]	93	
Coverage to Θ	[% / °]	99.7 / 25.242	
Max. and min. Transmission		1.00000, 0.49232	
Data / Restraints / Parameters		2603 / 0 / 145	
Goodness-of-fit on F^2		1.035	
Δ/σ$_{max}$		0.000	
Final *R* indices	2378 data; *I*>2σ(*I*) all data	R_1 = 0.0436, wR_2 = 0.1145 R_1 = 0.0497, wR_2 = 0.1200	
Largest Diff. Peak/Hole	[eÅ^{-3}]	0.557 / -0.203	
R.M.S. Deviation from Mean	[eÅ^{-3}]	0.051	

Table S11. Bayesian Statistics for Absolute Stereochemistry Determination of **3e** synthesized with **L2**.

	P3 (*R* = true)	**P3** (racemic twin)	**P3** (*R* = false)
probability	98.1%	1.9%	0.002%
note		Excluded by UPLC of redissolved crystal	

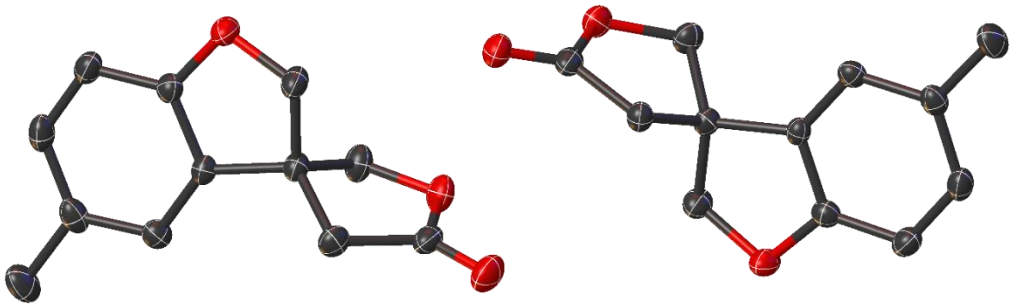

Figure S2. Asymmetric unit of *R*-**3g** with thermal ellipsoids displayed at the 50% probability level. Hydrogen atoms are omitted for clarity. Color code: C (black), O (red).

Table S12. Crystal data, data collection, and structure refinement for *R*-**3g** (CCDC: 2376544)

Molecular Formula		2x $C_{12}H_{12}O_3$	
Formula Weight	[g mol^{-1}]	190.20	
Crystal Dimensions	[mm^3]	1.0 x 0.1 x 0.05	
Crystal Habit		colorless, clear needle	
Crystal System		monoclinic	
Space Group		$P2_1$	
Unit Cell Dimensions	[Å / °]	a = 13.3053(4) b = 5.6172(1) c = 14.4165(4)	α = 90 β = 111.784(4) γ = 90
Volume	[Å^3]	1000.53(3)	
Z		2	
Density (calculated)	[g cm^{-3}]	1.356	
Absorption Coefficient μ	[mm^{-1}]	0.097	
F(000)	[e^{-1}]	432.0	
Temperature	[K]	110(10)	
Diffractometer		Synergy-S	
Wavelength	[Å]	0.71073	
Number of Frames		2142	
Exposure Time	[h]	0.6	
Θ Range	[°]	2.626 to 30.591	
Index Ranges		-18 ≤ h ≤ 18, -7 ≤ k ≤ 7, -20 ≤ l ≤ 18	
Reflections Collected		43628	
Independent Reflections		5352 [*R*(int) = 0.0517]	
Bijvoet Pairs Collected		2267	
Bijvoet Pair Coverage	[%]	82	
Coverage to Θ	[% / °]	99.9 / 25.242	
Max. and min. Transmission		1.00000, 0.35887	
Data / Restraints / Parameters		5352 / 1 / 273	
Goodness-of-fit on F^2		1.074	
Δ/σ$_{max}$		0.000	
Final *R* indices	4790 data; *I*>2σ(*I*) all data	R_1 = 0.0413, wR_2 = 0.1092 R_1 = 0.0477, wR_2 = 0.1125	
Largest Diff. Peak/Hole	[eÅ^{-3}]	0.422 / -0.232	
R.M.S. Deviation from Mean	[eÅ^{-3}]	0.047	

Table S13. Bayesian Statistics for Absolute Stereochemistry Determination of **3g** synthesized with **L2**.

	P3 (*R* = true)	**P3** (racemic twin)	**P3** (*R* = false)
probability	97.9%	2.1%	0.003%
note		Excluded by UPLC of redissolved crystal	

Computational Investigation of the Enantioselectivity

Introduction / Problem Definition

The computational study in the framework of this work was initiated to form a model for the experimentally observed enantioenrichment. To that end, we were expecting to find an enantioselectivity-determining transition state, to which the barriers would differ between the transition metal complex diastereomers. However, the system turned out to be more complex, making the implementation of a microkinetic model necessary, that additionally describes various diastereoisomerization pathways.

PyOx ligand **L3** together with the simplest substrate **1a** were chosen as model compounds for this study. Using the optimized standard conditions, an enantiomeric ratio of 91:9 *S*:*R* is obtained for this combination in the laboratory, which is typical for the experimental substrate scope of 2,3-dihydrobenzofuran products. Experimental studies of the enantioselectivity-determining step turned out to be difficult because other parts of this cascade reaction are rate-limiting overall. Nonetheless, some supplementary experiments were added as controls for the DFT-based microkinetic model.

Following a brief description of the computational method and its benchmarking (see below), the mechanistic investigation is discussed in detail (page S46). Finally, the above mentioned microkinetic model implementation is described in this supplementary discussion (page S52).

Computational Method

Unless noted otherwise, calculations were performed in ORCA 5.0.4,[1,2] parallelized with OpenMPI 4.0.3,[3] using TightSCF and DefGrid3 keywords, as well as the CPCM solvent model,[4] simulating methanol. Triple or quadruple-zeta Karlsruhe basis sets were used,[5] applying an effective core potential to palladium atoms.[6] Where applicable, the RIJCOSX approximation with respective auxiliary basis sets was utilized, which is the default setting in Orca 5.[7,8] Grimme's D4 dispersion correction was added to all DFT calculations.[9–11] Transition state optimizations were augmented with analytical Hessians every 10 iterations. Optimized geometries were confirmed to be either true ground states without imaginary modes, or – in case of transition states - first order saddle points by following up with frequency calculations at the same level of theory as the optimization. Gibbs free energies were corrected to 313.15 K. Chemcraft 1.8[12] and Gaussview 6.0.16[13] were employed for manipulation and visualization of geometries as well as for the analysis of vibrational modes.

Following recommendations from a recent "best practice" paper by Bursch, Mewes, Hansen, and Grimme in Angewandte,[14] a double hybrid functional in conjunction with quadruple-zeta basis sets was selected for the calculation of reaction energies and barriers of this transition metal catalyzed mechanism. Checinski's comprehensive benchmark on closed-shell metal organic reactions from 2018[15] was consulted to identify PWPB95[16] as a highly accurate double hybrid functional, which was therefore used as the default.

Geometries and frequencies were calculated at the PBE0[17] / triple-zeta level of theory, which was chosen owing to its robustness, as it generally is one of the best-performing global hybrid functionals when it comes to geometry fidelity.[18]
Summarized: PWPB95 / def2-QZVPP / D4 / CPCM(MeOH) // PBE0 / def2-TZVP / D4 / CPCM(MeOH)

Method Benchmarking

Ten DLPNO-CCSD(T)[19] / def2-QZVPP / CPCM(MeOH) single point calculations (thereof four transition states) were performed to benchmark the PWPB95 double hybrid functional on this system (Table S14). The DLPNO implementation agrees with canonical CCSD(T) calculations to a mean absolute deviation (MAD) of 0.2 kcal/mol in many cases (generally <0.4 kcal/mol),[20] and is therefore well-suited as an accurate but computationally affordable benchmark. The structures were selected because of their suspected role in overall rate-controlling elementary steps at that point in the study. An MAD of 0.58 kcal/mol far exceeds expectations set by the referenced benchmark paper (1.9 kcal/mol),[15] which might partially be ascribed to the use of D4 over D3 dispersion correction in this study.

Table S14. Benchmarking of selected PWPB95 single point enthalpies against DLPNO-CCSD(T), using the same geometries. All enthalpies are given relative to **RI-C** in order to account for differences in the absolute enthalpy between the individual levels of theory that will cancel out in the subtraction.

structure	SPE (PWPB95 // PBE0) [kcal/mol]	SPE (CCSD(T)-DLPNO // PBE0) [kcal/mol]	ΔSPE [kcal/mol]
L3-RI-C	0.00	0.00	0.00
L3-TS-RI-C—β	15.64	16.37	-0.72
L3-RI-β	12.67	12.83	-0.16
L3-RI-B_{intra}	14.90	14.01	0.88
L3-TS-RI-B_{intra}—β	23.81	23.73	0.08
L3-SI-C	8.78	8.74	0.04
L3-TS-SI-C—β	19.26	20.60	-1.33
L3-SI-β	11.64	11.88	-0.24
L3-SI-B_{intra}	13.36	11.76	1.61
L3-TS-SI-B_{intra}—β	18.94	19.64	-0.71
mean absolute deviation (MAD)			**0.58**

Three ground-state double-hybrid optimization runs for benchmarking of the PBE0 geometries were computed in Gaussian 16 rev. C.01.[21] The software was switched for this application because of Gaussian's higher queue priority for large jobs on our cluster which was required due to the unavailability of Hessian calculations for double-hybrid functionals and the sluggish performance of numerical gradients in ORCA 5. No additional frequency calculations were performed for the double-hybrid geometries. Transition states could not be converged in Gaussian at this high level of theory, which was chosen as mPW2PLYP-D[22,23] / def2-TZVP / CPCM(MeOH). The geometries were compared to their PBE0 equivalents by comparison of the respective PWPB95 quadruple-zeta single point energies (Table S15). A minor deviation of only MAD = 0.18 kcal/mol points to satisfactory accuracy of the PBE0 geometries, especially considering the much shorter runtime.

Table S15. Benchmarking of selected PBE0 geometries against mPW2PLYP-D double hybrid geometries by comparison of the geometries' PWPB95 single point enthalpies.

structure	SPE (PWPB95 // PBE0) [Eh]	SPE (PWPB95 // mPW2PLYP-D) [Eh]	ΔSPE [kcal/mol]
L2-RI-B_{CO}	-1767.664734	-1767.664901	0.104
L2-RI-B_{CO}	-1767.663175	-1767.662880	-0.185
L2-RI-β	-1654.319164	-1654.318779	-0.242
mean absolute deviation (MAD)			**0.18**

Both benchmarks indicate that a high degree of chemical accuracy is achievable with the chosen methodology on the investigated Pd-PyOX system.

Mechanistic Investigation

Qualitative consideration of the proposed mechanism (main paper, Scheme 3) limits the eligible steps for enantioenrichment to oxidative addition, olefin complexation, and migratory insertion, after which the stereocenter of the spiro-product is irreversibly formed (see supplementary section *Intramolecular Addition*). All enthalpies and free energies are therefore given with respect to the energetically most favorable isomer of **C**, as this is positioned in the center of the suspected relevant steps and consequently minimizes the risk of introducing systematic errors to the investigation.

Oxidative Addition

Some of us have previously demonstrated computationally that the oxidative addition for comparable *N*,*N'*-chelated palladium-pyrimidine-oxazoline complexes into arenediazonium salts is highly exothermic (approx. -70 kcal/mol) and exergonic (approx. -60 kcal/mol).[24] According to the Hammond-Leffler postulate, the transition states for highly exothermic reactions are geometrically close to the starting materials, suggesting little to no enantioselectivity for this step. In order to be certain about this assumption, we set out to optimize the low-valent, T-shaped oxidative addition products $\mathbf{B_{LV}}$ that result from the reaction between **A** and **4a** after the dissociation of dinitrogen. It is worth noting that four distinguishable diastereomers are formed in this step, where it can be distinguished between distal (I) and proximal (II) positions of the aryl group with respect to the ligand's chiral center (in this case: the *tert*-butyl group). Furthermore, the dangling olefin might point into the same or opposite half space of the *tert*-butyl group relative to the equatorial square plane of the transition metal (Figure S3). Although there is a trend, with I-isomers being favored over II-isomers, and *S*-destined isomers being favored over *R*-destined ones, the free energy differences are low (standard deviation 0.15 kcal/mol when excluding $\mathbf{RII\text{-}B_{LV}}$ which is the most unfavored isomer due to a direct clash with the ligand's *tert*-butyl group). As explicitly shown in the supplementary section *Diastereomer Interconversion*, barriers for the interconversion between these low-valent states are rather high. With this consideration as well as the highly exothermic oxidative addition in mind, we assume an initial uniform distribution (1:1:1:1 ratio) between the four resulting, low-valent oxidative addition products $\mathbf{RI\text{-}B_{LV}}$, $\mathbf{RII\text{-}B_{LV}}$, $\mathbf{SI\text{-}B_{LV}}$, and $\mathbf{SII\text{-}B_{LV}}$. Owing to a large excess of methanol (80 vol% of the solvent mixture), rapid coordination of a methanol molecule is also assumed, leading to the corresponding $\mathbf{B_{MeOH}}$ analogs with 16 valence electrons.

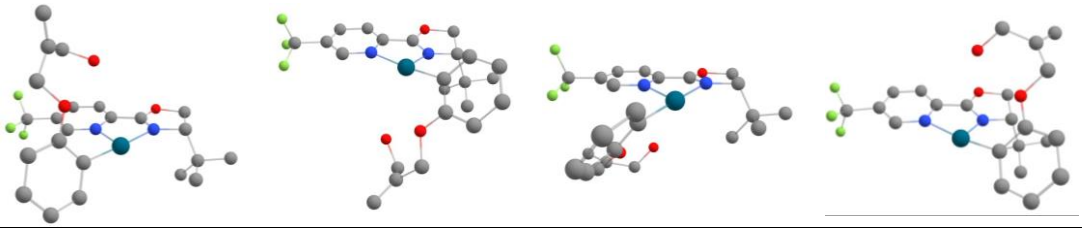

ΔG	28.4 kcal/mol	29.0 kcal/mol	28.1 kcal/mol	28.3 kcal/mol
Name	**RI-B_{LV}**	**RII-B_{LV}**	**SI-B_{LV}**	**SII-B_{LV}**

Figure S3. Low-valent products $\mathbf{B_{LV}}$ from the oxidative addition of **A** into the arenediazonium salt **4a**. Color code: C (grey), F (green), N (blue), O (red), Pd (turquoise). Hydrogen atoms omitted for clarity. Free energy shown at the PWPB95 / def2-QZVPP / D4 / CPCM(MeOH) // PBE0 / def2-TZVP / D4 / CPCM(MeOH) level of theory. All structures are mono-cationic singlets. Both color code as well as level of theory are valid for all subsequent structures too.

Intramolecular Addition (Migratory Insertion)

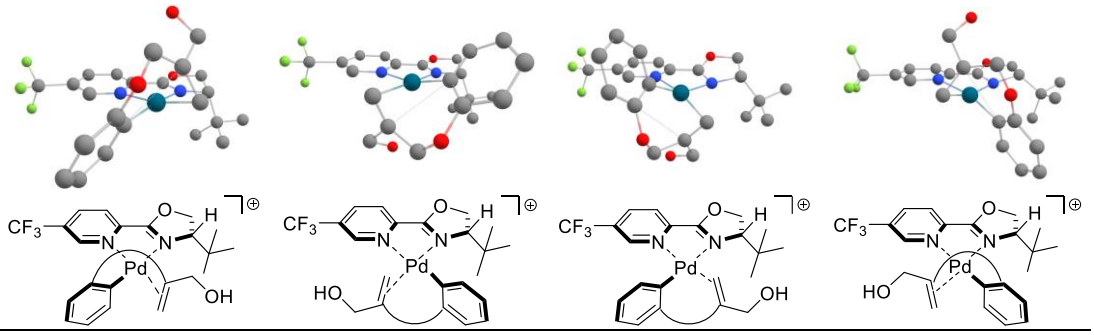

$C_{Ar}\cdots C_{olefin}$	2.93 Å	2.94 Å	3.02 Å	2.88 Å
AoA	72.9°	72.5°	77.2°	81.0°
ΔG	1.2 kcal/mol	0.0 kcal/mol	8.6 kcal/mol	9.2 kcal/mol
Name	**RI-C**	**RII-C**	**SI-C**	**SII-C**

Figure S4. Four thermodynamically favorable isomers of olefin-coordinated compounds **C** prior to intramolecular ring closure. Distances between the nucleophilic aryl carbon atom and the electrophile as well as the angle of attack (AoA) for intramolecular addition are given in addition to the structures' free energies.

Having concluded that the oxidative addition does not significantly contribute to this Heck-Matsuda reaction's enantioselectivity, the next focus of this study is the intramolecular addition, which connects structures **C** (chelating substrate with olefin coordinated to Pd, shown in Figure S4) and **D** (benzofuranyl-methanol with developed stereocenter). It becomes clear that there is a pronounced energetic difference between the *S*- and *R*-destined isomers of **C**. This is likely a result of the increased cyclic strain combined with reduced degrees of freedom compared to **B**, which leads to greater steric clash between substrate and ligand.

Furthermore, it is apparent that the intramolecular distance between nucleophilic and electrophilic sites is too high for a direct migratory insertion and that the angle of attack is too low. Instead of the present 73-81°, the Bürgi-Dunitz angle of 109° would be optimal for the experimentally observed 5-*endo*-*trig* ring closure. Therefore, further isomerization is necessary for all diastereoisomers in order to make the intramolecular addition feasible. It was found that this transformation mainly proceeds via rotation around the Pd—C_{Ar} bond. In a first step, the metallacyclic strain is increased even further (**β**), whereas in the second step, the olefin rotates into the equatorial coordination plane, effectively creating a pentagonal-planar coordination sphere for the palladium center (**γ**). This set of intermediates has significantly decreased distances between nucleophilic aryl and electrophilic olefin carbon atom (2.47-2.54 Å), as well as increased angles of attack (113-114°), thus enabling the facile intramolecular addition towards **D**. It is important to note that instead of a low-valent 14 electron species, the resulting product is square planar, being stabilized by an additional η^2-coordination mode of the emerging dihydrobenzofuran. The optimized structures for this reaction sequence are exemplarily shown for **RI** in Figure S5.

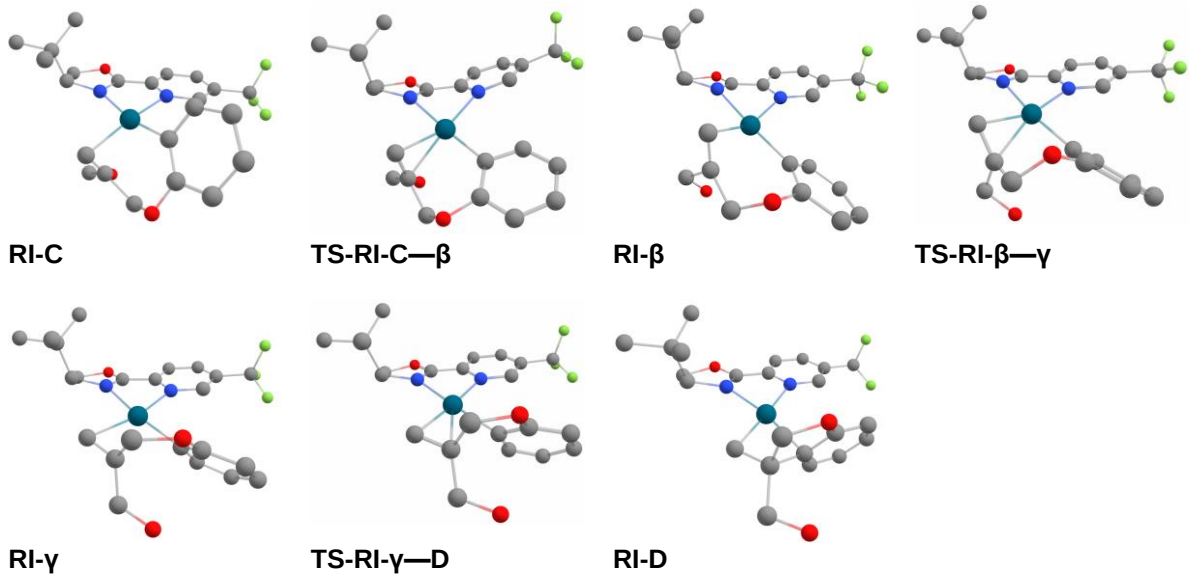

Figure S5. Intramolecular addition sequence from thermodynamically favorable metallacycle **C** towards dihydrobenzofuran **D** shown exemplarily for **RI**. The other three diastereomers behave analogously. All structures are closed-shell mono cations.

A comparison of the energetic profiles of intramolecular addition for all four diastereomers is displayed in Figure S6. Surprisingly, the first substrate rotation step **TS-C—β** is rate limiting for most diastereomers rather than the actual ring closure **TS-γ—D** which was expected to be challenging according to Baldwin's rules.

Table S16. Free energies of activation

TS-C—β	ΔG‡ [kcal/mol]
RI	16.4
RII	18.0
SI	12.5
SII	5.6

The free energies of activation for this step are displayed in Table S16. While they show a clear enantioselectivity, this observation is not sufficient to explain the experimentally observed enantiomeric ratio. A barrier difference of 4 kcal/mol as calculated between RI and SI would lead to essentially exclusive formation of the *S*-enantiomer, if there is facile diastereomer interconversion. In case of no interconversion, all products would form, because the barriers are all easily accessible at the experimental temperature of 40 °C, the reaction time of 16 h, and TONs <40: $t_{0.5}$(18 kcal/mol) = 0.39 s.

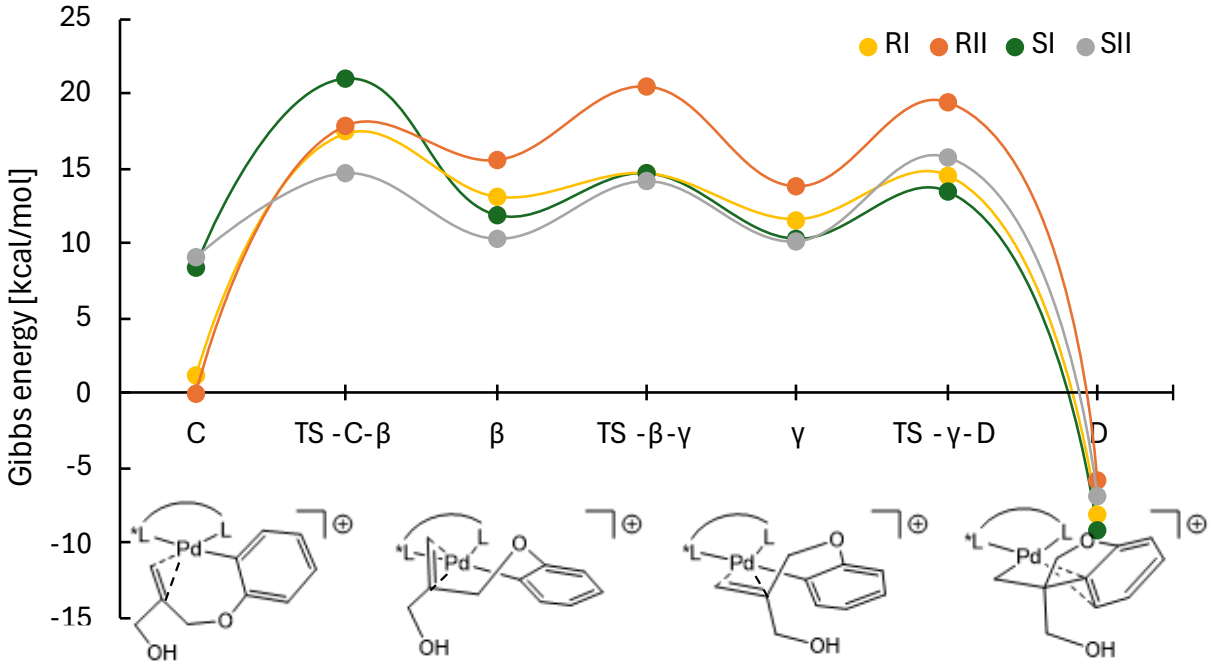

Figure S6. Free energy profiles for intramolecular addition of all four diastereomers. For clarity, ligand **L3** is abbreviated as L—L* in this depiction, which will be used for the subsequent figures too.

The absence of diastereomer interconversion would therefore lead to a racemic mixture, which is clearly wrong too. Assuming negligible racemization after formation of the stereocenter, everything points to diastereointerconversion that is affected by significant barriers compared to the ring closure reaction. This topic will be explored in the ensuing supplementary section.

A final remarkable aspect of the above calculations is the *de facto* irreversibility of the ring closure, as the activation barriers in the reverse direction (**TS-D—γ**) are $\Delta G^{\ddagger} \geq 22.5$ kcal/mol for all diastereomers, corresponding to half-lives in excess of 9 minutes for the ring opening reaction (per catalytic turnover). Considering the possibility of further substitution of **D** with either methanol or carbon monoxide, the irreversibility of the ring closure reaction is safe to assume.

Olefin Coordination

Before diving into the details of diastereomer interconversion, a reaction network for the connection between complexes **B** and **C** is set up, in order to model the relevant olefin coordination mechanisms (Figure S7a). Although there are pronounced energetic differences between the four diastereomers in olefin coordination, the barriers discussed in this section are difficult to qualitatively relate to the experimentally observed enantioenrichment. Therefore, an in-depth discussion of the individual barriers will be omitted in favor of a quantitative description in the scope of microkinetic modeling later on. All

free energies are shown in the main paper Figure 1 as well as the supplementary Table S20 at the end of this section.

Immediately following oxidative addition, a low valent complex will be formed on dissociation of N_2 (**B_{LV}**, see Figure S7a). As described above it will be assumed in the scope of this study that only methanol will coordinate to saturate the vacant site in **B_{LV}**, as it is present in large excess. Other possibilities would be the coordination of carbon monoxide (**B_{CO}**) or the intramolecular coordination of the substrate's dangling alcohol (**B_{intra}**). Associative interconversion transition states (trigonal-bipyramidal, **TS-B_X—B_Y**, example shown in Figure S7b) between the abovementioned 16 valence electron variants of **B** are modelled, rather than the dissociative version via **B_{LV}** that is disfavored in free energy.

Olefin coordination to **B_{MeOH}** and **B_{CO}** is found to proceed stepwise through a square-pyramidal intermediate, **α_X** (examples for transition states shown in Figure S7c,d), whereas the same transformation proceeds without intermediate for **B_{intra}** (Figure S7e), presumably because of the increased strain in a hypothetical tridentate square planar coordination mode of the substrate. Interestingly, the connection **TS-B_{intra}'—C** ($\Delta G^{\ddagger}$ between 18.7 and 20.0 kcal/mol) is energetically disfavored over **TS-B_{intra}—β** ($\Delta G^{\ddagger}$ between 5.5 and 10.1 kcal/mol), which is why only the latter will be modelled (not shown in main paper Figure 1).

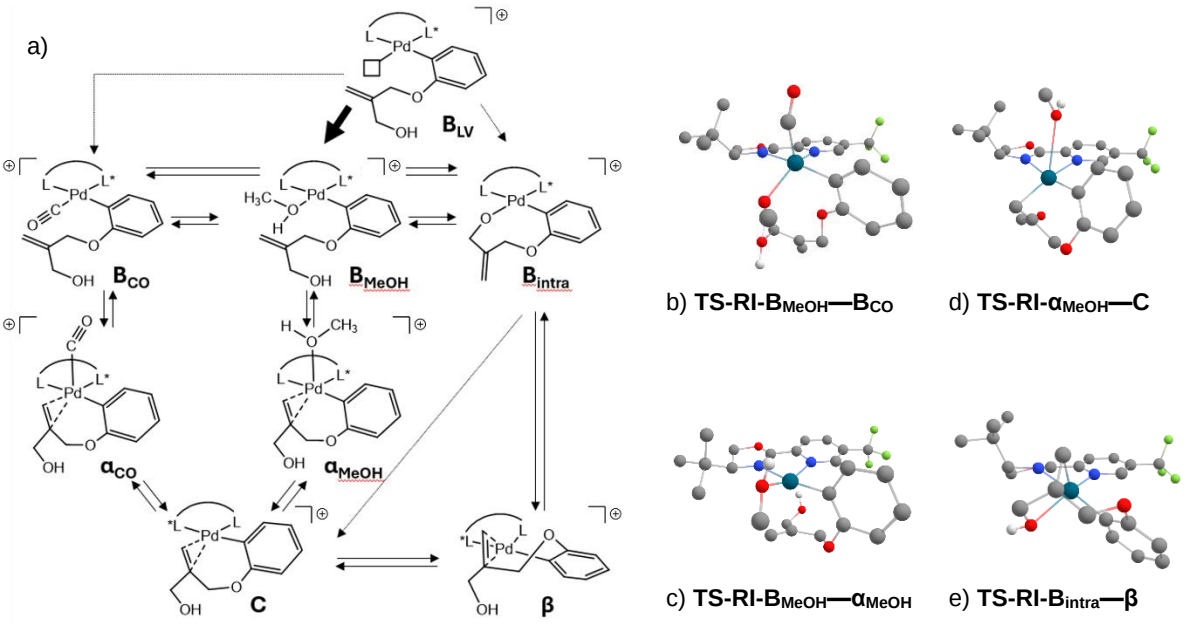

Figure S7. a) Reaction network for the olefin coordination modes that connect **B** with **C**. Note that every drawn structure represents four diastereomers. b) Trigonal-bipyramidal **TS-RI-B_{MeOH}—B_{CO}** is exemplarily shown for the horizontal connections between the 16 valence electron isomers of **B**. Furthermore, c) **TS-RI-B_{MeOH}—α_{MeOH}**, d) **TS-RI-α_{MeOH}—C** and e) **TS-RI-B_{intra}—β** are shown as examples for the vertical connections.

Out of the 32 transition states in this olefin coordination reaction network, only **TS-RII-α_{CO}—C** could not be found. In order to fully model the network despite the single missing transition state, the lacking barrier is estimated as $\Delta G^{\ddagger}$ = 3.5 kcal/mol (measured from **α**), which is slightly higher than the analogous

transition states for **RI**, **SI**, and **SII** that have free energies of activation between 0.2 and 2.5 kcal/mol, but still in the realm of an entropic barrier.

Diastereomer Interconversion

As evident from the main paper Figure 1, plausible resting states of this part of the catalytic cycle are $\mathbf{B_{CO}}$ and **C** (thermodynamic sinks). Therefore, these are obvious starting points for diastereomer interconversion calculations.

Investigations began by looking into turnstile rotations of **C** (simplified illustration in Figure S8, bottom right),[25] however no accessible transition states could be found. The same was true for attempted turnstile rotations of **ω**, which is $\mathbf{B_{CO}}$ but with another carbon monoxide molecule associated. The conversion of square planar geometries into see-saw coordination modes was frequently observed at reasonable free energies, but without offering sensible reaction pathways moving forward. These ideas were therefore abandoned.

Rotations are the simplest interconversion mechanisms; however, they are not applicable to complexes with a chelated substrate (lacking degree of flexibility). They can also not interconvert between I and II isomers, which – looking at the profiles in Figure 1 – is a necessary interconversion pathway for enantioenrichment. Furthermore, the presence of a fourth, strongly bound substituent in the palladium square plane is essential, because a weakly bound ligand (such as methanol) is prone to dissociation upon the steric pressure during rotation. The aryl-oxygen atom will then coordinate to palladium, inhibiting further rotation. This is also true for rotations involving the T-shaped $\mathbf{B_{Lv}}$. Therefore, rotations were considered for $\mathbf{B_{CO}}$ and **ω**, that both fulfill the abovementioned criteria (Figure S8). Main barriers for the former are the repulsion between the substrate aryl group and the chiral ligand, whereas in the latter case, repulsion between substrate and CO are decisive. Barriers can be found in the main paper Figure 1b as well as supplementary Table S20.

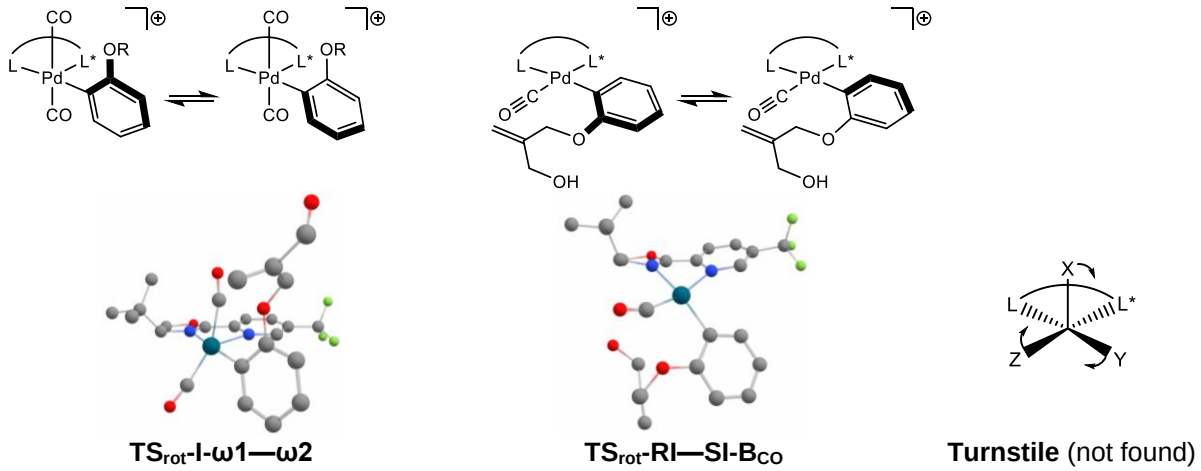

$\mathbf{TS_{rot}}$**-I-ω1—ω2** $\mathbf{TS_{rot}}$**-RI—SI-**$\mathbf{B_{CO}}$ **Turnstile** (not found)

Figure S8. Relevant rotations for the interconversion between *S*- and *R*-destined diastereomers of **ω** (top left) and $\mathbf{B_{CO}}$ (top center), with exemplary transition states for the rotations (below). All explicit interconversions are depicted in the main paper. Simplified illustration for turnstile rotation with square-planar coordination geometry (bottom right).

As mentioned above, interconversion pathways between I and II isomers are important for the explanation of the experimentally observed enantioenrichment. Apart from the turnstile mechanism, the most straightforward route would be the so-called 'lever mechanism', in which the aryl group migrates between the distal and proximal positions with respect to the chiral center of the ligand. However, the corresponding transition states for $\mathbf{B_{LV}}$ were found to have free energies of activation $\Delta G^{\ddagger}$>30 kcal/mol, which are not relevant at 40 °C (Figure S9, left). Gratifyingly, a very similar mechanism was found to proceed smoothly between I and II isomers of **ω**. It converts between the analogous square-pyramidal structures via trigonal-bipyramidal transition state (Figure S9, right). Since the square-pyramidal complex **ω** can be envisioned as an octahedral coordination sphere with an empty site (despite its saturated 18 valence electron ligand field), a comparable mechanism has been dubbed 'octahedral switch' in a previous study on d^7 complexes.[26] The corresponding free energies are shown in the main paper Figure 1b.

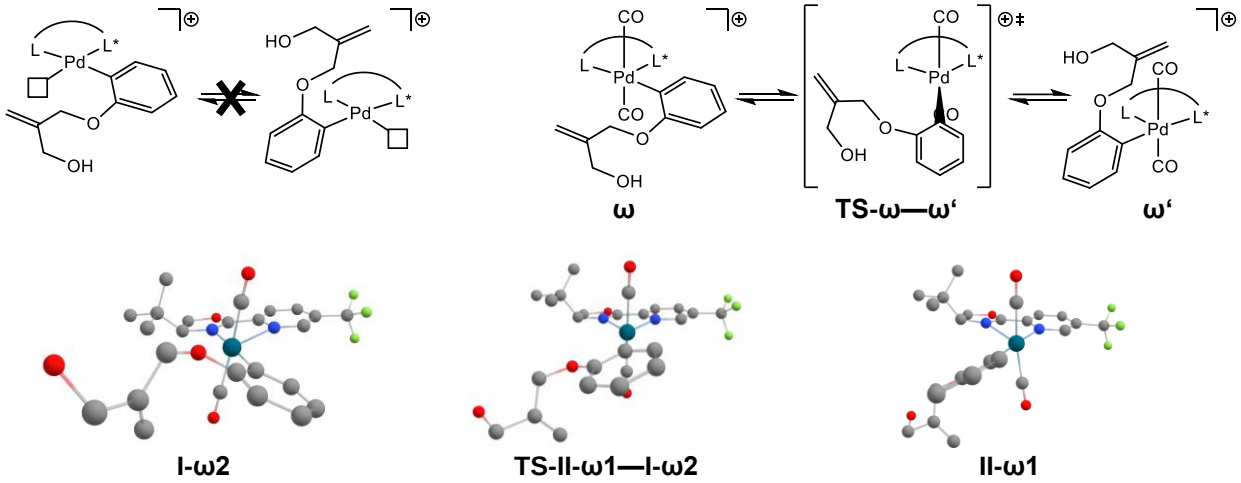

Figure S9. Lever mechanism (left, unfeasible), and 'octahedral switch' mechanism (right, feasible), with exemplary interconversion in the 'octahedral switch' mechanism shown in the bottom. There are two additional interconversions which are mentioned in the main paper.

Microkinetic Model

The microkinetic model was assembled in COPASI 4.42[27] and tasks on the model were performed with the deterministic LSODA method using the following, Eyring equation-based rate law for all chemical reactions:

$$v_{\mathrm{SM}\leftrightarrows\mathrm{P}} = \Pi_n c(\mathrm{SM}_n)\frac{\kappa k_\mathrm{B} T}{h}\mathrm{e}^{\frac{\Sigma \mathrm{G_{SM}}-\mathrm{G_{TS}}}{\mathrm{RT}}} - \Pi_n c(\mathrm{P}_n)\frac{\kappa k_\mathrm{B} T}{h}\mathrm{e}^{\frac{\Sigma \mathrm{G_{P}}-\mathrm{G_{TS}}}{\mathrm{RT}}}$$

wherein

c	concentration	
κ	transmission coefficient	(assumed to be 1)
k_B	Boltzmann constant	
T	temperature	(313.15 K)
h	Planck constant	

R	ideal gas constant
G	Gibbs energy
SM	starting material
P	product

In case of bimolecular reactions, unit correction factors of 1 mL/µmol were added in COPASI.

Concentration Estimations

The standard conditions are the following: 0.2 mmol substrate scale in 2 mL 4:1 MeOH:DMF with 2.5 mol% Pd (c = 2.5 µmol/mL). The reaction vessel is a 20 mL two-chamber reactor. Considering the volume of 2 mL dioxane which is used for the release of 4 mmol (2 equiv.) CO, as well as two standard stirring bars (0.15 mL volume each), there is a headspace volume of 15.7 mL.

According to considerations discussed in the *Oxidative Addition* section, a uniform, initial 1:1:1:1 ratio of **RI-B$_{MeOH}$**, **RII-B$_{MeOH}$**, **SI-B$_{MeOH}$**, and **SII-B$_{MeOH}$** is assumed, which amounts to concentrations of 0.625 µmol/mL for each species.

The Henry constant for the solubility of CO in pure MeOH at 313.15 K and an approximate CO partial pressure of $P_{CO} \approx 66$ kPa (from the ideal gas law) is calculated from the following equation, as stated in ref.[28]

$$\ln(\mathrm{H}^{Px}_{\mathrm{CO-MeOH}}) = 203.6 - \frac{9475.8}{T} - 29.2 \cdot \ln(T) + 1.65 \cdot 10^{-4} P_{\mathrm{CO}}$$

$$\mathrm{H}^{Px}_{\mathrm{CO-MeOH}} = 256.8\ \mathrm{MPa}$$

The Henry constant for CO in DMF under equal conditions is obtained from ref.[29]

$$\ln(\mathrm{H}^{cP}_{\mathrm{CO-DMF}}) = -6.79 - \frac{730.1}{T}$$

$$\mathrm{H}^{cP}_{\mathrm{CO-DMF}} = 1.093 \cdot 10^{-4}\ \frac{\mathrm{kmol}}{\mathrm{m^3 \cdot Pa}}$$

This concentration-based Henry constant can be transformed into the mixing-ratio-based one with the density ($\rho_{40\,°C}$ = 0.944 g/mL) and molecular weight (M = 73.09 g/mol) of DMF.

$$\mathrm{H}^{Px}_{\mathrm{CO-DMF}} = \frac{P}{x} = \frac{P}{\frac{c(\mathrm{CO})}{c(\mathrm{DMF})}} = \frac{P \cdot c(\mathrm{DMF})}{\mathrm{H}^{cP}_{\mathrm{CO-DMF}} \cdot P} = \frac{c(\mathrm{DMF})}{\mathrm{H}^{cP}} = \frac{\rho_{40\,°C}(\mathrm{DMF})}{M(\mathrm{DMF}) \cdot \mathrm{H}^{cP}_{\mathrm{CO-DMF}}}$$

$$\mathrm{H}^{Px}_{\mathrm{CO-DMF}} = 118.2\ \mathrm{MPa}$$

With the molar ratios x of MeOH and DMF in the 4:1 volumetric mixture as derived from Table S17, it is possible to estimate a Henry constant for the reaction solvent mixture. The interaction parameter for the system DMF-MeOH is assumed to be 0.

Table S17. Calculation of concentrations and molar ratios of solvent components in the reaction solvent mixture.

	V%	$\rho_{40\,°C}$ [g/mL][30]	wt%	M [g/mol]	n/n = *x*	*c* [mmol/mL]
MeOH	80	*0.773*	76.9	*32.04*	0.884	19.44
DMF	20	*0.930*	23.1	*73.09*	0.116	2.56
mix		*0.810*				22.0

$$\ln \mathrm{H}_{\mathrm{mix}} = x_{\mathrm{DMF}} \ln \mathrm{H}^{Px}_{\mathrm{CO-DMF}} + x_{\mathrm{DMF}} \ln \mathrm{H}^{Px}_{\mathrm{CO-DMF}}$$

$$\mathrm{H}_{\mathrm{mix}} = 234.7\ \mathrm{MPa}$$

Finally, the solubility of CO in the releasing reaction is estimated from the Henry constant 1,4-dioxane-CO.[31]

$$\ln(\mathrm{H}^{Px}_{\mathrm{CO-dioxane}}) = 5.688 + \frac{594.6}{T}$$

$$\mathrm{H}^{Px}_{\mathrm{CO-dioxane}} = 1972\ \mathrm{atm} = 197.2\ \mathrm{MPa}$$

In order to obtain the equilibrium concentration of CO in the reaction mixture, the dissolution equilibrium of 400 µmol CO between 2 mL dioxane, 2 mL MeOH/DMF 4 : 1 and 15.7 mL headspace is solved for its steady state in COPASI, in which the CO partial pressure again follows ideal gas law and the dissolution rates v are modeled with the following set of equations:

$$v_{\mathrm{CO-dissolution-solvent}} = \frac{P_{\mathrm{CO}} \cdot c(\mathrm{solvent})}{\mathrm{H}^{Px}_{\mathrm{CO-solvent}}} - c(\mathrm{CO_{solvent}})$$

Table S18. Result of the COPASI steady state calculation

	c(CO) [µmol/mL]	*P*(CO) [kPa]
2 mL 1,4-dioxane	3.73	
2 mL MeOH : DMF 4 : 1 mix	5.92	
15.7 mL headspace	24.25	66.3

Time Course Analysis for Determination of Enantioselectivity

The steady state of a microkinetic model with all the intermediates and transition states discussed in the **Mechanistic Investigation** section implemented with Eyring equations was sought after, as it would reveal the computational enantiomeric ratio. Because no analytical steady state solution could be found for this large microkinetic model that encompasses 44 ground states species as well as 59 transition states, a time course analysis was chosen instead. As evident both from the main paper Figure 1c as well as Figure S10 below, one catalytic turnover from $\mathbf{B_{MeOH}}$ to **D** is completed after approximately 3 seconds.

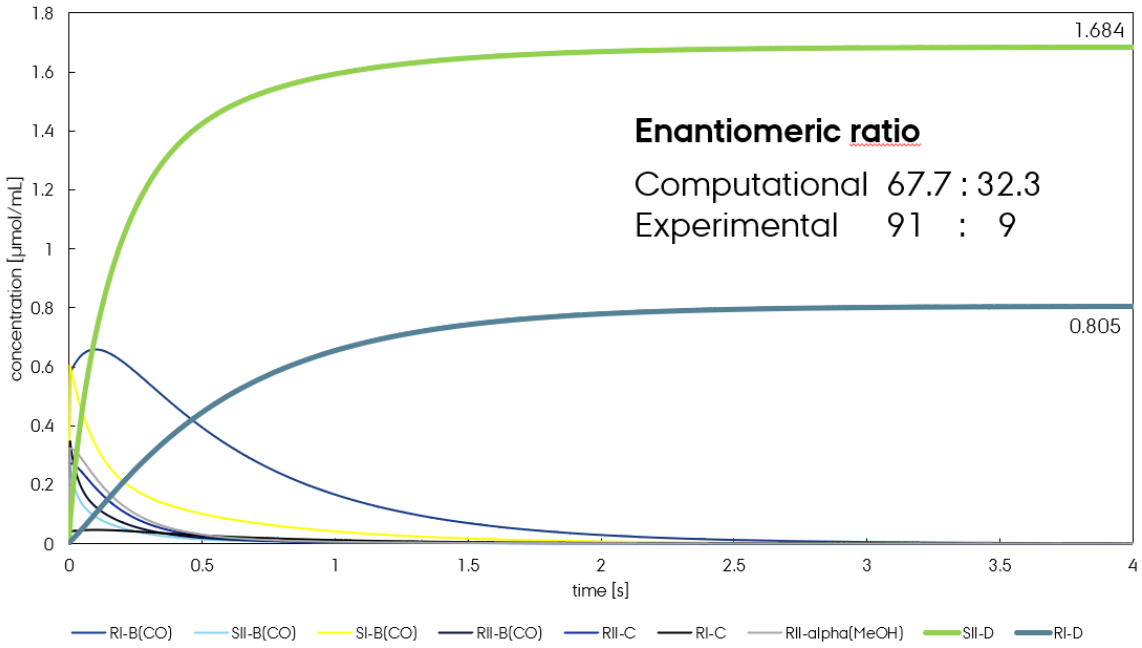

Figure S10. Time course analysis that highlights species with notable transient concentrations.

It can further be concluded that $\mathbf{B_{CO}}$ is indeed an important resting state, as suspected from its low free energy. Also, **C** and $\boldsymbol{\alpha_{MeOH}}$ are resting states for the ligand-substrate mismatch situation, evident from the significant concentrations of **RI-** and **RII-C**, as well as **RII-**$\boldsymbol{\alpha_{MeOH}}$. This is due to the relatively high barriers imposed by both transition states leading to **β** and $\boldsymbol{\alpha_{CO}}$, which would need to be overcome for either product generation or diastereomer interconversion.

The enantioselectivity can then directly be derived from the relative concentrations of the four **D** diastereomers at steady state conditions, where it is noteworthy that only **SII** and **RI** provide productive pathways, whereas the other two diastereomers are efficiently interconverted before completing the intramolecular addition.

Parameter Sensitivity Tests

As a result of the proposed high dependence on the CO partial pressure, a parameter scan with respect to the initial concentration of CO in the reaction solution is performed in COPASI. Figure S11 shows the development of enantioselectivity with CO concentration. In the relevant range between 1 and 50 µmol/mL, the model predicts increased enantioenrichment with rising CO concentrations. This prediction is consistent with additional experiments that replace the 2.0 equiv CO from SilaCOgen (partial pressure ~660 mbar, see above) with a CO balloon (1 atm CO). In these experiments, an increased enantiomeric ratio of 95:5 (compared to 91:9 with SilaCOgen) is observed for **L3** and **1a**.

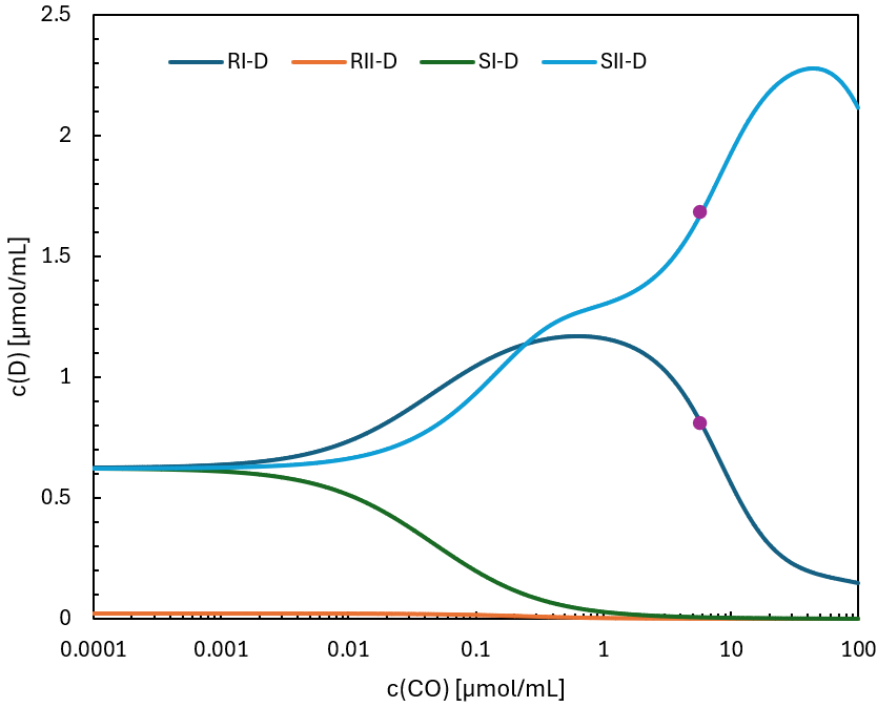

Figure S11. Semi-log plot of parameter scan, showing the concentrations of the four product species at various CO concentrations after 4 seconds. Note that for low CO concentrations, this is likely not the steady state.

Furthermore, the sensitivity to the effective palladium concentration in solution is tested, since it is likely that the concentration of $\mathbf{B_{MeOH}}$ which has been modeled as 0.625 µmol/mL per diastereomer is lower in the experiment. This might be due to other parts of the Heck-Matsuda mechanism (e.g. carbonylation, product release), being slower than the investigated part of the mechanism. Therefore, the overall resting state might well be different from **B** or **C**. Since only mononuclear reaction pathways have been considered, no dependence on the Pd concentration was expected. And indeed, this is reflected in the linear relationship of the steady-state concentration in Figure S12.

This fits well with the screening observation in main Table 2 (entries 10 and 12), that the *e.r.* does not change between 5 and 2.5 mol% Pd. Even in an experiment with 1 mol% $Pd(OAc)_2$, the level of enantioenrichment remains constant. This confirms the assumption of mononuclear pathways and is in strong support of the microkinetic results obtained in this study.

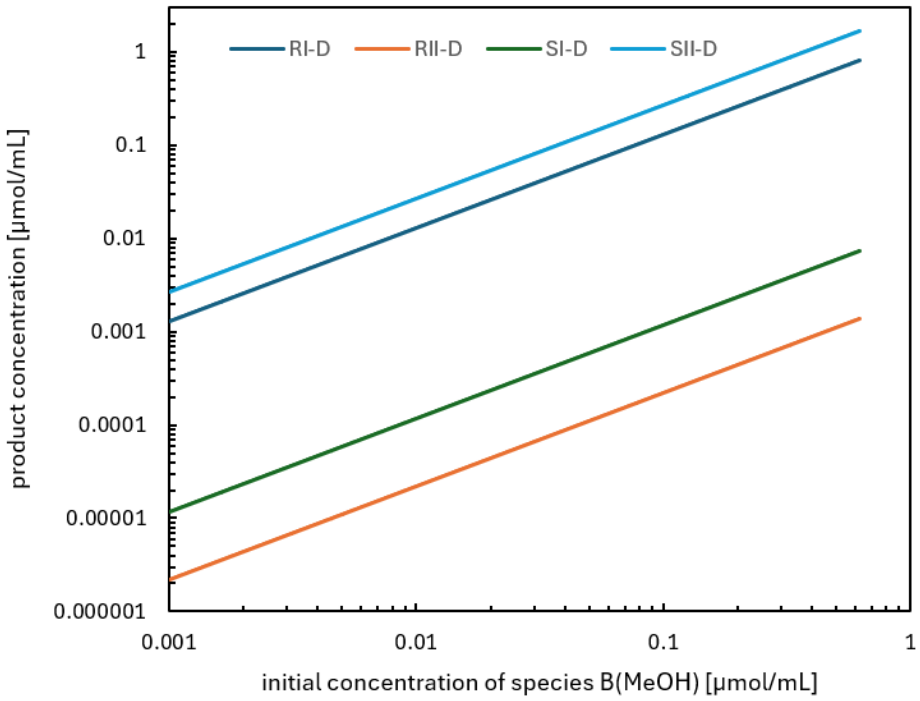

Figure S12. Log-log plot of parameter scan regarding the initial concentration of $\mathbf{B_{MeOH}}$ with respect to the steady state concentrations of the four **D** diastereomers.

Comparison with Experimental Results

Both the computationally obtained enantiomeric ratio as well as the experimentally observed one can be translated into an apparent barrier difference between two hypothetically enantioselectivity-determining transition states, assuming a simplified situation (*S*-Y ← X → *R*-Y). This allows for the direct barrier difference $\Delta\Delta G^{\ddagger}_{RS}$ comparison between experiment and calculation.

$$K = \frac{[\mathrm{R}]_\mathrm{t}}{[\mathrm{S}]_\mathrm{t}} = \frac{k_\mathrm{R}}{k_\mathrm{S}} = \frac{\frac{\kappa k_\mathrm{B} T}{h} \cdot \mathrm{e}^{-\frac{\Delta G^{\ddagger}_{R}}{RT}}}{\frac{\kappa k_\mathrm{B} T}{h} \cdot \mathrm{e}^{-\frac{\Delta G^{\ddagger}_{S}}{RT}}} = \mathrm{e}^{-\frac{\Delta G^{\ddagger}_{R}}{RT}+\frac{\Delta G^{\ddagger}_{S}}{RT}} = \mathrm{e}^{-\frac{\Delta\Delta G^{\ddagger}_{RS}}{RT}}$$

$$\mathrm{Selectivity(R)} = \frac{[\mathrm{R}]_\mathrm{t}}{[\mathrm{S}]_\mathrm{t} + [\mathrm{R}]_\mathrm{t}} = \frac{1}{\frac{1}{K} + 1} = \frac{1}{\mathrm{e}^{\frac{\Delta\Delta G^{\ddagger}_{RS}}{RT}} + 1}$$

$$\Delta\Delta G^{\ddagger}_{RS} = RT \cdot \ln\left(\frac{-\mathrm{Selectivity}}{\mathrm{Selectivity} - 1}\right)$$

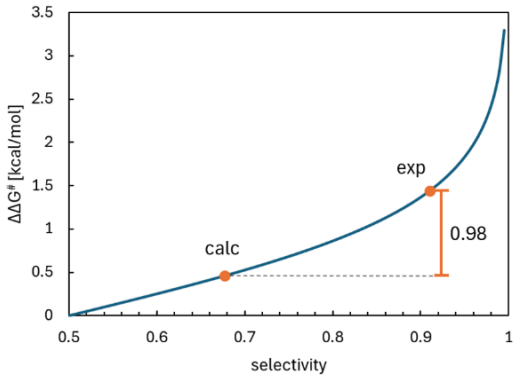

Figure S13. Visualization of the relationship between apparent barrier difference and selectivity.

Table S19. Comparison of apparent barrier differences between experiment and calculation.

	Selectivity(R)	$\Delta\Delta G^{\ddagger}_{RS}$	
experimental	0.090	6032 J/mol	1.44 kcal/mol
computational	0.323	1927 J/mol	0.46 kcal/mol
apparent barrier difference			0.98 kcal/mol

Conclusion

It can be summarized that the reaction network – which includes olefin coordination, diastereomer interconversion, and migratory insertion – is able to explain the experimentally observed enantioenrichment with a very favorable sub-kcal accuracy. With respect to improvements of the ligand, the computations would suggest that the quarter space of the complex that is occupied by the substrate in the RI diastereomer should be blocked more efficiently by ligand design, which could lead to improved enantioselectivities.

Data Availability

Important parameters for all structures are summarized below in Table S20. All geometries are attached separately as an .xyz file, including most of the parameters detailed below. The microkinetic models can be obtained from the authors as .cps files upon reasonable request.

Table S20 Summary of important computationally obtained parameters.

Structure	PWPB95 Single Point Energy [Eh]	PBE0 Single Point Energy [Eh]	PBE0 Entropy Corr. (313.15 K) [Eh]	Imaginary Mode [cm^{-1}]	Free Energy H(PWPB95) - T*S(PBE0) [Eh]	Relative Free Energy [kcal/mol]
RI-B_{LV}	-1654.2922	-1653.0270	-0.0957	None	-1654.3879	28.44
RI-B_{MeOH}	-1770.0524	-1768.6627	-0.1023	None	-1770.1547	12.79
TS-RI-B_{MeOH}—α_{MeOH}	-1770.0325	-1768.6437	-0.1025	-72.75	-1770.1350	25.16
RI-α_{MeOH}	-1770.0598	-1768.6670	-0.1026	None	-1770.1624	7.97
TS-RI-α_{MeOH}—C	-1770.0586	-1768.6675	-0.1015	-25.96	-1770.1602	9.38
RI-C	-1654.3394	-1653.0719	-0.0919	None	-1654.4312	1.24
TS-RI-C—β	-1654.3144	-1653.0464	-0.0906	-39.15	-1654.4051	17.66
RI-β	-1654.3192	-1653.0499	-0.0930	None	-1654.4121	13.22
TS-RI-β—γ	-1654.3183	-1653.0501	-0.0912	-24.63	-1654.4096	14.84
RI-γ	-1654.3214	-1653.0526	-0.0933	None	-1654.4147	11.63
TS-RI-γ—D	-1654.3179	-1653.0517	-0.0921	-168.60	-1654.4100	14.55
RI-D	-1654.3541	-1653.0889	-0.0917	None	-1654.4459	-7.94
TS_{rot}-RI—SI-B_{CO}	-1767.6379	-1766.2900	-0.0972	-23.40	-1767.7351	19.11
RI-B_{CO}	-1767.6647	-1766.3153	-0.0997	None	-1767.7645	0.70
TS-RI-B_{CO}—α_{CO}	-1767.6444	-1766.2966	-0.0970	-50.94	-1767.7414	15.18
RI-α_{CO}	-1767.6496	-1766.2980	-0.0985	None	-1767.7481	10.96
TS-RI-α_{CO}—C	-1767.6483	-1766.2961	-0.0995	-50.77	-1767.7478	11.15
RI-B_{intra}	-1654.3156	-1653.0478	-0.0933	None	-1654.4090	15.21
TS-RI-B_{intra}—β	-1654.3014	-1653.0353	-0.0915	-137.53	-1654.3930	25.26
RII-B_{LV}	-1654.2917	-1653.0252	-0.0953	None	-1654.3870	28.97
RII-B_{MeOH}	-1770.0533	-1768.6621	-0.1018	None	-1770.1552	12.52
TS-RII-B_{MeOH}—α_{MeOH}	-1770.0330	-1768.6423	-0.1010	-88.89	-1770.1340	25.76
RII-α_{MeOH}	-1770.0622	-1768.6689	-0.1033	None	-1770.1655	6.04
TS-RII-α_{MeOH}—C	-1770.0606	-1768.6688	-0.1021	-22.14	-1770.1627	7.77
RII-C	-1654.3399	-1653.0714	-0.0933	None	-1654.4332	0.00
TS-RII-C—β	-1654.3136	-1653.0452	-0.0910	-46.23	-1654.4046	17.95
RII-β	-1654.3158	-1653.0472	-0.0924	None	-1654.4082	15.72
TS-RII-β—γ	-1654.3092	-1653.0413	-0.0911	-29.31	-1654.4003	20.65
RII-γ	-1654.3186	-1653.0489	-0.0923	None	-1654.4109	13.97
TS-RII-γ—D	-1654.3103	-1653.0442	-0.0918	-185.98	-1654.4021	19.54
RII-D	-1654.3500	-1653.0848	-0.0923	None	-1654.4423	-5.73
TS_{rot}-RII—SII-B_{CO}	-1767.6449	-1766.2960	-0.0974	-17.49	-1767.7423	14.59
RII-B_{CO}	-1767.6643	-1766.3139	-0.0998	None	-1767.7640	0.97
TS-RII-B_{CO}—α_{CO}	-1767.6395	-1766.2914	-0.0982	-95.87	-1767.7377	17.49
RII-α_{CO}	-1767.6501	-1766.2976	-0.0992	None	-1767.7493	10.22
TS-RII-α_{CO}—C	structure has not been found (see supplementary discussion)					
RII-B_{intra}	-1654.3139	-1653.0471	-0.0931	None	-1654.4071	16.41
TS-RII-B_{intra}—β	-1654.3003	-1653.0351	-0.0919	-135.43	-1654.3922	25.76
SI-B_{LV}	-1654.2938	-1653.0290	-0.0946	None	-1654.3884	28.09
SI-B_{MeOH}	-1770.0525	-1768.6621	-0.1017	None	-1770.1543	13.08
TS-SI-B_{MeOH}—α_{MeOH}	-1770.0318	-1768.6427	-0.1016	-99.03	-1770.1334	26.16

Structure	PWPB95 Single Point Energy [Eh]	PBE0 Single Point Energy [Eh]	PBE0 Entropy Corr. (313.15 K) [Eh]	Imaginary Mode [cm^{-1}]	Free Energy H(PWPB95) - T*S(PBE0) [Eh]	Relative Free Energy [kcal/mol]
SI-α_{MeOH}	-1770.0496	-1768.6579	-0.1026	None	-1770.1522	14.40
TS-SI-α_{MeOH}—C	-1770.0461	-1768.6559	-0.1029	-23.23	-1770.1490	16.39
SI-C	-1654.3254	-1653.0589	-0.0942	None	-1654.4196	8.54
TS-SI-C—β	-1654.3087	-1653.0414	-0.0910	-50.02	-1654.3996	21.08
SI-β	-1654.3208	-1653.0541	-0.0934	None	-1654.4143	11.90
TS-SI-β—γ	-1654.3179	-1653.0517	-0.0917	-33.30	-1654.4096	14.81
SI-γ	-1654.3227	-1653.0549	-0.0939	None	-1654.4166	10.42
TS-SI-γ—D	-1654.3195	-1653.0537	-0.0920	-174.77	-1654.4115	13.63
SI-D	-1654.3557	-1653.0904	-0.0921	None	-1654.4478	-9.14
SI-B_{CO}	-1767.6632	-1766.3142	-0.0999	None	-1767.7631	1.55
TS-SI-B_{CO}—α_{CO}	-1767.6406	-1766.2921	-0.0976	-76.57	-1767.7382	17.17
SI-α_{CO}	-1767.6417	-1766.2917	-0.1008	None	-1767.7425	14.45
TS-SI-α_{CO}—C	-1767.6372	-1766.2858	-0.1014	-21.95	-1767.7386	16.92
SI-B_{intra}	-1654.3181	-1653.0514	-0.0931	None	-1654.4112	13.82
TS-SI-B_{intra}—β	-1654.3092	-1653.0435	-0.0911	-134.50	-1654.4003	20.66
SII-B_{LV}	-1654.2932	-1653.0276	-0.0950	None	-1654.3882	28.25
SII-B_{MeOH}	-1770.0500	-1768.6606	-0.1031	None	-1770.1531	13.83
TS-SII-B_{MeOH}—α_{MeOH}	-1770.0263	-1768.6374	-0.1019	-72.67	-1770.1282	29.43
SII-α_{MeOH}	-1770.0495	-1768.6579	-0.1019	None	-1770.1515	14.83
TS-SII-α_{MeOH}—C	-1770.0465	-1768.6569	-0.1030	-73.97	-1770.1495	16.08
SII-C	-1654.3259	-1653.0596	-0.0927	None	-1654.4186	9.19
TS-SII-C—β	-1654.3188	-1653.0511	-0.0909	-33.50	-1654.4097	14.75
SII-β	-1654.3238	-1653.0559	-0.0929	None	-1654.4167	10.34
TS-SII-β—γ	-1654.3194	-1653.0526	-0.0910	-36.60	-1654.4104	14.30
SII-γ	-1654.3235	-1653.0545	-0.0933	None	-1654.4168	10.30
TS-SII-γ—D	-1654.3161	-1653.0507	-0.0918	-210.05	-1654.4080	15.84
SII-D	-1654.3518	-1653.0870	-0.0921	None	-1654.4439	-6.73
SII-B_{CO}	-1767.6640	-1766.3143	-0.0997	None	-1767.7637	1.16
TS-SII-B_{CO}—α_{CO}	-1767.6439	-1766.2948	-0.0972	-84.31	-1767.7412	15.31
SII-α_{CO}	-1767.6474	-1766.2965	-0.0983	None	-1767.7458	12.43
TS-SII-α_{CO}—C	-1767.6423	-1766.2896	-0.1001	-20.67	-1767.7424	14.56
SII-B_{intra}	-1654.3182	-1653.0506	-0.0936	None	-1654.4118	13.42
TS-SII-B_{intra}—β	-1654.3111	-1653.0445	-0.0920	-134.00	-1654.4031	18.89
MeOH	-115.7134	-115.5904	-0.0285	None	-115.7419	—
CO	-113.3088	-113.2237	-0.0235	None	-113.3324	—
TS-RI-$B_{CO—MeOH}$	-1883.3538	-1881.8834	-0.1087	-135.28	-1883.4625	28.23
TS-RII-$B_{CO—MeOH}$	-1883.3536	-1881.8818	-0.1082	-145.72	-1883.4618	28.67
TS-SI-$B_{CO—MeOH}$	-1883.3541	-1881.8825	-0.1081	-121.29	-1883.4622	28.38
TS-SII-$B_{CO—MeOH}$	-1883.3561	-1881.8847	-0.1085	-131.03	-1883.4646	26.91
TS-RI-$B_{intra—MeOH}$	-1770.0257	-1768.6361	-0.1018	-81.41	-1770.1275	29.85
TS-RII-$B_{intra—MeOH}$	-1770.0285	-1768.6395	-0.1026	-73.45	-1770.1311	27.64
TS-SI-$B_{intra—MeOH}$	-1770.0259	-1768.6359	-0.1022	-64.15	-1770.1281	29.50
TS-SII-$B_{intra—MeOH}$	-1770.0298	-1768.6397	-0.1021	-86.42	-1770.1319	27.12

Structure	PWPB95 Single Point Energy [Eh]	PBE0 Single Point Energy [Eh]	PBE0 Entropy Corr. (313.15 K) [Eh]	Imaginary Mode [cm^{-1}]	Free Energy H(PWPB95) - T*S(PBE0) [Eh]	Relative Free Energy [kcal/mol]
TS-RI-$B_{CO—intra}$	-1767.6200	-1766.2717	-0.0998	-113.38	-1767.7198	28.72
TS-RII-$B_{CO—intra}$	-1767.6238	-1766.2754	-0.0988	-122.67	-1767.7226	26.96
TS-SI-$B_{CO—intra}$	-1767.6220	-1766.2744	-0.0989	-139.48	-1767.7209	28.04
TS-SII-$B_{CO—intra}$	-1767.6241	-1766.2751	-0.0992	-140.48	-1767.7233	26.55
TS-II-ω1—I-ω2	-1880.9547	-1879.5245	-0.1073	-77.39	-1881.0621	22.51
TS-II-ω2—I-ω1	-1880.9589	-1879.5299	-0.1068	-73.64	-1881.0658	20.19
TS-II-ω2—I-ω3	-1880.9589	-1879.5298	-0.1062	-72.60	-1881.0651	20.58
II-ω1	-1880.9632	-1879.5307	-0.1079	None	-1881.0711	16.82
II-ω2	-1880.9635	-1879.5329	-0.1081	None	-1881.0716	16.55
I-ω1	-1880.9686	-1879.5376	-0.1067	None	-1881.0753	14.21
I-ω2	-1880.9664	-1879.5362	-0.1089	None	-1881.0753	14.20
I-ω3	-1880.9669	-1879.5367	-0.1080	None	-1881.0749	14.44
TS-SII-B_{CO}—ω1	-1880.9587	-1879.5255	-0.1065	-102.19	-1881.0652	20.55
TS-SII-B_{CO}—ω2	-1880.9525	-1879.5197	-0.1068	-90.01	-1881.0594	24.21
TS-RII-B_{CO}—ω2	-1880.9599	-1879.5267	-0.1064	-106.16	-1881.0663	19.82
TS-SI-B_{CO}—ω1	-1880.9615	-1879.5298	-0.1070	-68.80	-1881.0685	18.46
TS-SI-B_{CO}—ω2	-1880.9624	-1879.5300	-0.1066	-82.11	-1881.0689	18.19
TS-RI-B_{CO}—ω2	-1880.9585	-1879.5263	-0.1070	-77.01	-1881.0655	20.35
TS-RI-B_{CO}—ω3	-1880.9641	-1879.5319	-0.1069	-85.80	-1881.0710	16.92
TS_{rot}-II-ω1—2	-1880.9506	-1879.5209	-0.1060	-27.06	-1881.0566	25.97
TS_{rot}-I-ω-1—2	-1880.9540	-1879.5240	-0.1053	-35.09	-1881.0593	24.26
TS_{rot}-I-ω-2—3	-1880.9538	-1879.5242	-0.1060	-34.97	-1881.0598	23.93

Computational Bibliography

[1] F. Neese, *Wiley Interdiscip. Rev. Comput. Mol. Sci.* **2012**, *2*, 73–78.
[2] F. Neese, *Wiley Interdiscip. Rev. Comput. Mol. Sci.* **2022**, *12*, e1606.
[3] R. L. Graham, T. S. Woodall, J. M. Squyres, in *Parallel Processing and Applied Mathematics* (Eds.: R. Wyrzykowski, J. Dongarra, N. Meyer, J. Waśniewski), Springer, Berlin, Heidelberg, **2006**, pp. 228–239.
[4] V. Barone, M. Cossi, *J. Phys. Chem. A* **1998**, *102*, 1995–2001.
[5] F. Weigend, R. Ahlrichs, *Phys. Chem. Chem. Phys.* **2005**, *7*, 3297–3305.
[6] D. Andrae, U. Häußermann, M. Dolg, H. Stoll, H. Preuß, *Theoret. Chim. Acta* **1990**, *77*, 123–141.
[7] A. Hellweg, C. Hättig, S. Höfener, W. Klopper, *Theor. Chem. Acc.* **2007**, *117*, 587–597.
[8] F. Weigend, *Phys. Chem. Chem. Phys.* **2006**, *8*, 1057–1065.
[9] E. Caldeweyher, C. Bannwarth, S. Grimme, *J. Chem. Phys.* **2017**, *147*, 034112.
[10] E. Caldeweyher, S. Ehlert, A. Hansen, H. Neugebauer, S. Spicher, C. Bannwarth, S. Grimme, *J. Chem. Phys.* **2019**, *150*, 154122.
[11] E. Caldeweyher, J.-M. Mewes, S. Ehlert, S. Grimme, *Phys. Chem. Chem. Phys.* **2020**, *22*, 8499–8512.
[12] G. A. Zhurko, **2005**.
[13] R. Dennington, T. A. Keith, J. M. Millam, **2016**.
[14] M. Bursch, J.-M. Mewes, A. Hansen, S. Grimme, *Angew. Chem. Int. Ed.* **2022**, *61*, e202205735.
[15] S. Dohm, A. Hansen, M. Steinmetz, S. Grimme, M. P. Checinski, *J. Chem. Theory Comput.* **2018**, *14*, 2596–2608.
[16] L. Goerigk, S. Grimme, *J. Chem. Theory Comput.* **2011**, *7*, 291–309.
[17] C. Adamo, V. Barone, *J. Chem. Phys.* **1999**, *110*, 6158–6170.
[18] É. Brémond, M. Savarese, N. Q. Su, Á. J. Pérez-Jiménez, X. Xu, J. C. Sancho-García, C. Adamo, *J. Chem. Theory Comput.* **2016**, *12*, 459–465.
[19] C. Riplinger, B. Sandhoefer, A. Hansen, F. Neese, *J. Chem. Phys.* **2013**, *139*, 134101.
[20] D. G. Liakos, Y. Guo, F. Neese, *J. Phys. Chem. A* **2020**, *124*, 90–100.
[21] M. J. Frisch, G. W. Trucks, H. B. Schlegel, G. E. Scuseria, M. A. Robb, J. R. Cheeseman, G. Scalmani, V. Barone, G. A. Petersson, H. Nakatsuji, X. Li, M. Caricato, A. V. Marenich, J. Bloino, B. G. Janesko, R. Gomperts, B. Mennucci, H. P. Hratchian, J. V. Ortiz, A. F. Izmaylov, J. L. Sonnenberg, Williams, F. Ding, F. Lipparini, F. Egidi, J. Goings, B. Peng, A. Petrone, T. Henderson, D. Ranasinghe, V. G. Zakrzewski, J. Gao, N. Rega, G. Zheng, W. Liang, M. Hada, M. Ehara, K. Toyota, R. Fukuda, J. Hasegawa, M. Ishida, T. Nakajima, Y. Honda, O. Kitao, H. Nakai, T. Vreven, K. Throssell, J. A. Montgomery Jr., J. E. Peralta, F. Ogliaro, M. J. Bearpark, J. J. Heyd, E. N. Brothers, K. N. Kudin, V. N. Staroverov, T. A. Keith, R. Kobayashi, J. Normand, K. Raghavachari, A. P. Rendell, J. C. Burant, S. S. Iyengar, J. Tomasi, M. Cossi, J. M. Millam, M. Klene, C. Adamo, R. Cammi, J. W. Ochterski, R. L. Martin, K. Morokuma, O. Farkas, J. B. Foresman, D. J. Fox, **2016**.
[22] T. Schwabe, S. Grimme, *Phys. Chem. Chem. Phys.* **2006**, *8*, 4398–4401.
[23] T. Schwabe, S. Grimme, *Phys. Chem. Chem. Phys.* **2007**, *9*, 3397–3406.
[24] V. H. M. da Silva, C. C. Oliveira, C. R. D. Correia, A. A. C. Braga, *Theor. Chem. Acc.* **2020**, *139*, 77.
[25] I. Ugi, D. Marquarding, H. Klusacek, P. Gillespie, F. Ramirez, *Acc. Chem. Res.* **1971**, *4*, 288–296.
[26] R. Asatryan, E. Ruckenstein, J. Hachmann, *Chem. Sci.* **2017**, *8*, 5512–5525.
[27] S. Hoops, S. Sahle, R. Gauges, C. Lee, J. Pahle, N. Simus, M. Singhal, L. Xu, P. Mendes, U. Kummer, *Bioinformatics* **2006**, *22*, 3067–3074.
[28] Liu Q., *Journal of the MESJ* **1998**, *33*, 300–305.
[29] M. M. T. Khan, S. B. Halligudi, S. Shukla, *J. Chem. Eng. Data* **1989**, *34*, 353–355.
[30] C. Yang, Y. Sun, Y. He, P. Ma, *J. Chem. Eng. Data* **2008**, *53*, 293–297.
[31] E. Veleckis, D. S. Hacker, *J. Chem. Eng. Data* **1984**, *29*, 36–39.

NMR Spectra

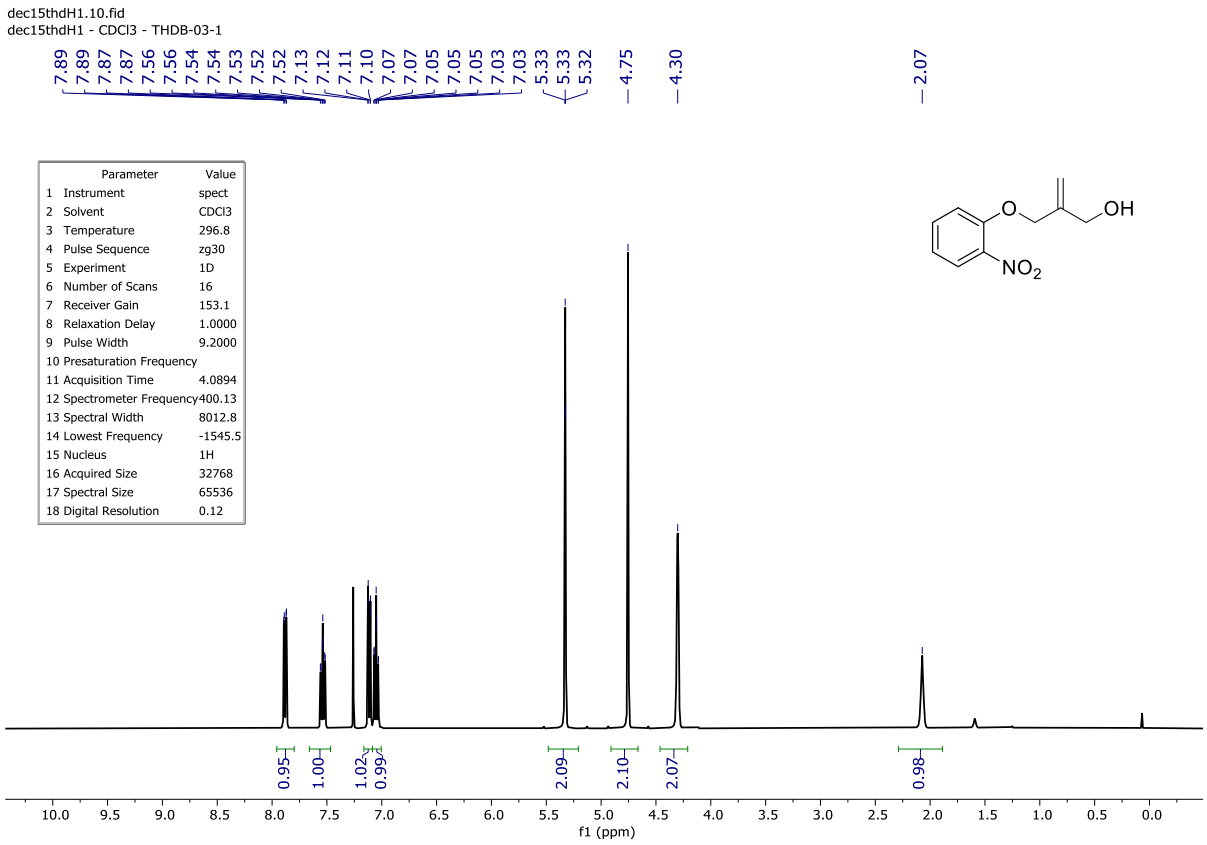

Figure S14. ^{1}H NMR spectrum ($CDCl_3$, 400 MHz) of 2-((2-nitrophenoxy)methyl)prop-2-en-1-ol – **1a**

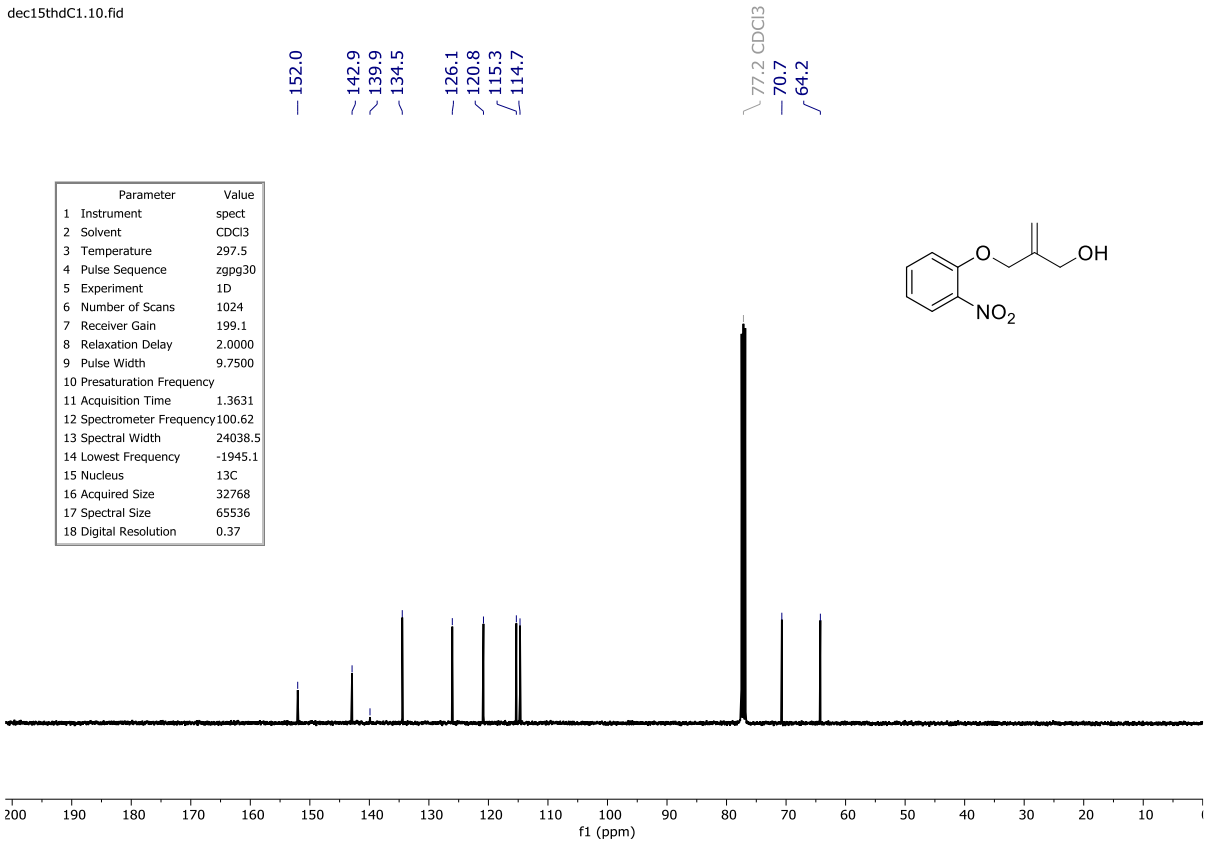

Figure S15. ^{13}C NMR spectrum ($CDCl_3$, 101 MHz) of 2-((2-nitrophenoxy)methyl)prop-2-en-1-ol – **1a**

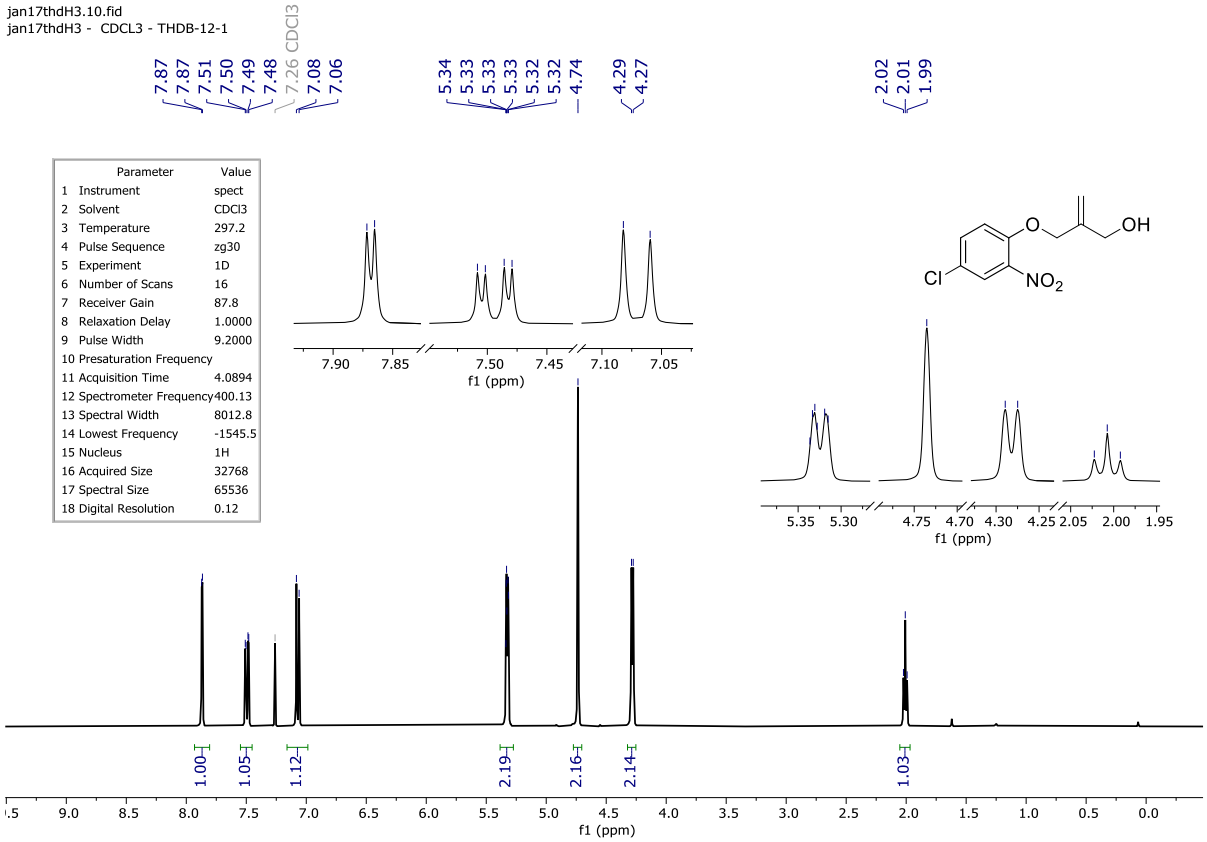

Figure S16. ^{1}H NMR spectrum ($CDCl_3$, 400 MHz) of 2-((4-chloro-2-nitrophenoxy)methyl)prop-2-en-1-ol – **1b**

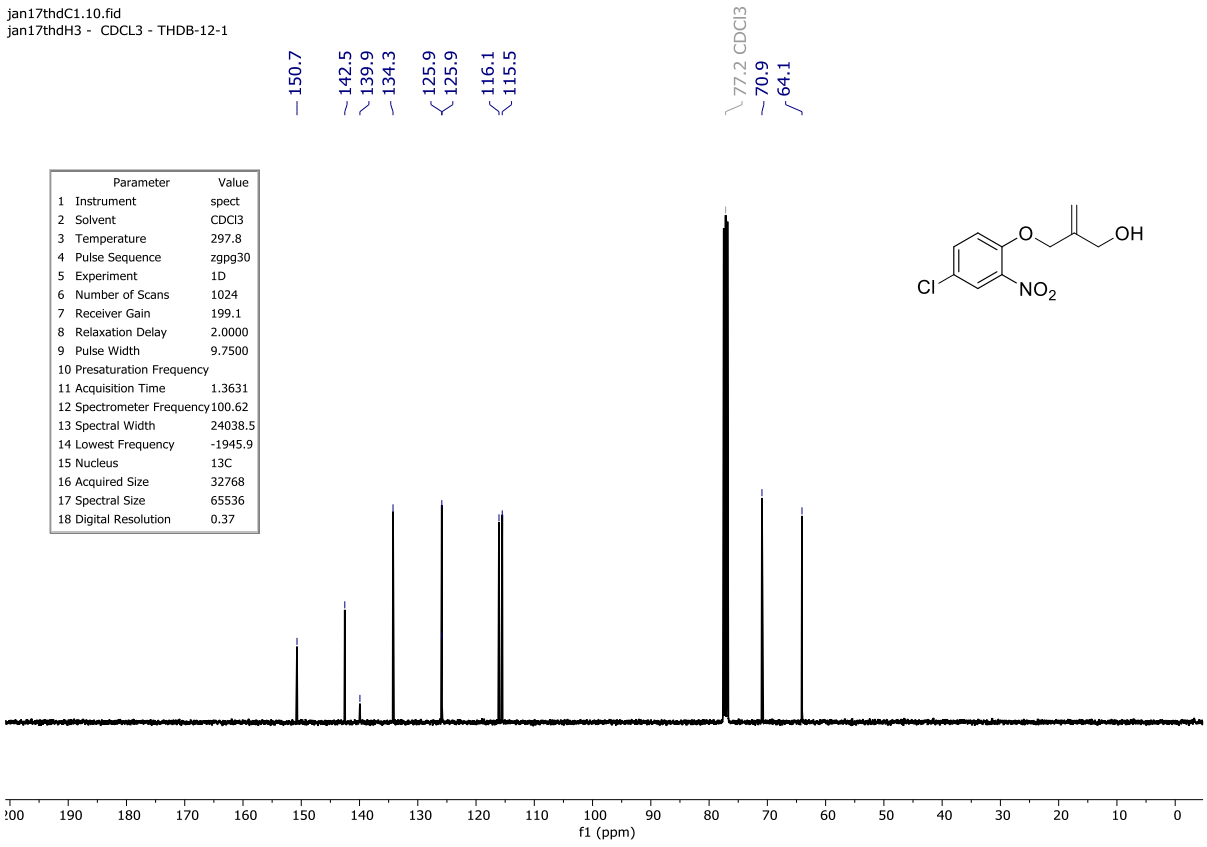

Figure S17. ^{13}C NMR spectrum ($CDCl_3$, 101 MHz) of 2-((4-chloro-2-nitrophenoxy)methyl)prop-2-en-1-ol – **1b**

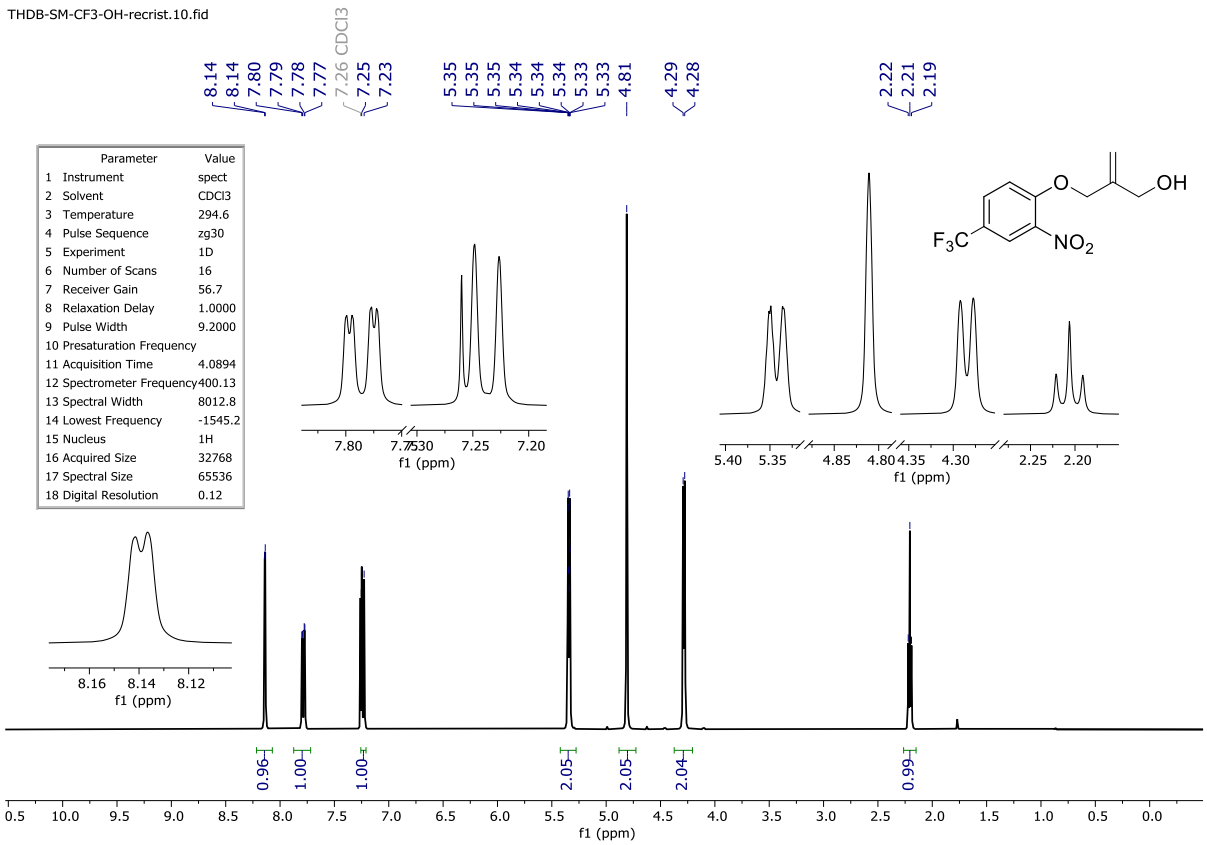

Figure S18. ^{1}H NMR spectrum ($CDCl_3$, 400 MHz) of 2-((2-nitro-4-(trifluoromethyl)phenoxy)methyl)prop-2-en-1-ol – **1c**

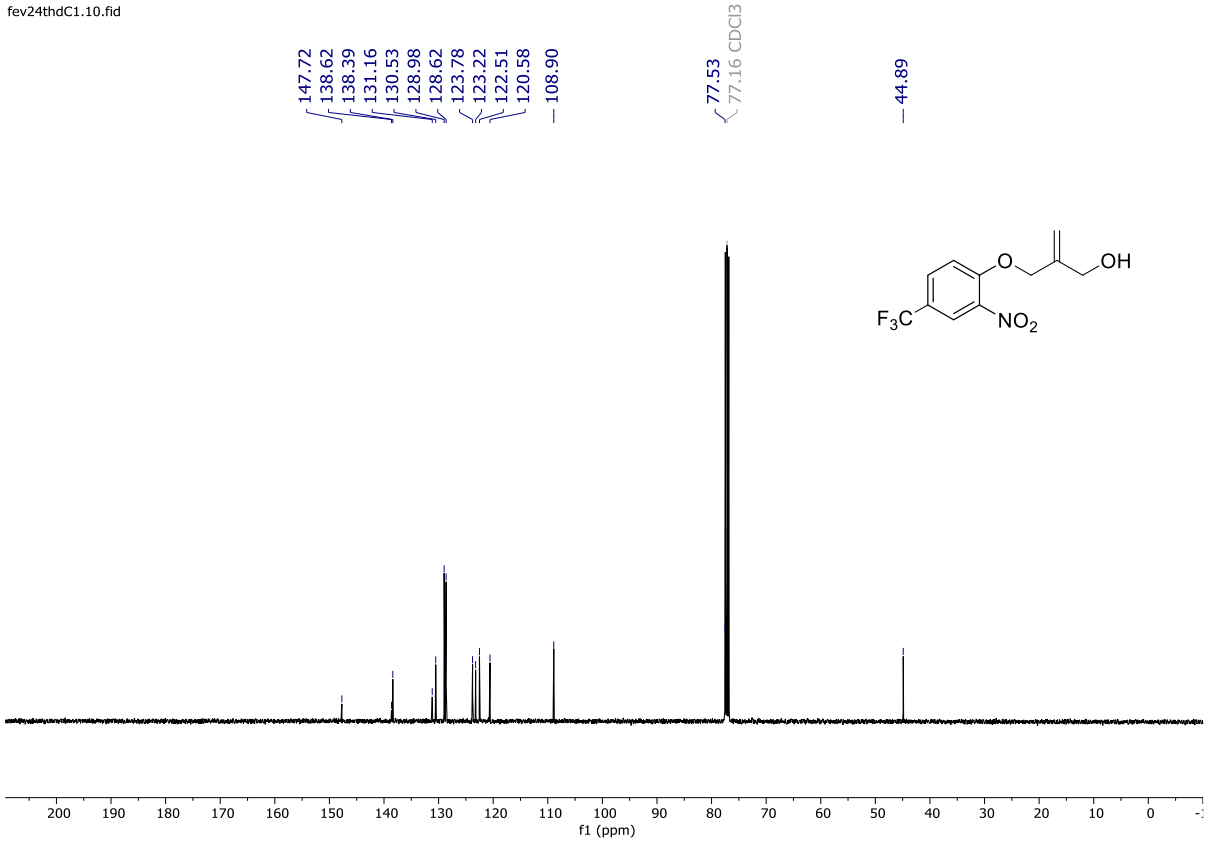

Figure S19. ^{13}C NMR spectrum ($CDCl_3$, 101 MHz) of 2-((2-nitro-4-(trifluoromethyl)phenoxy)methyl)prop-2-en-1-ol – **1c**

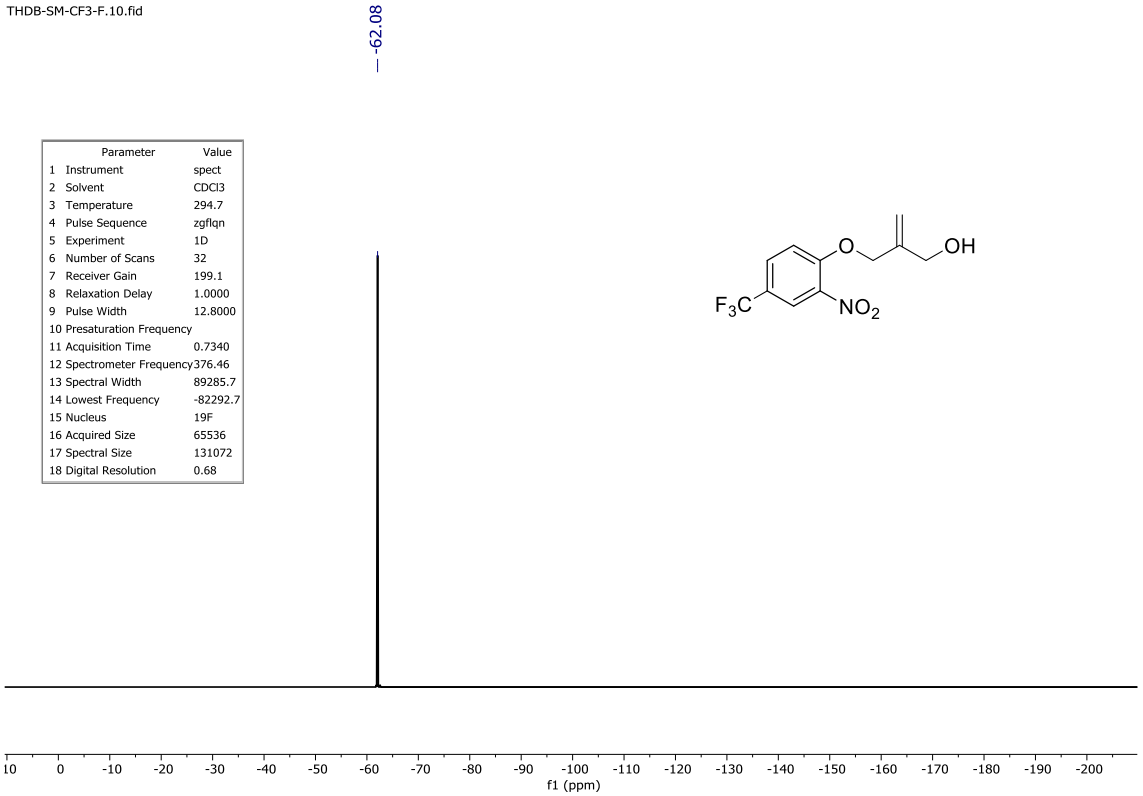

Figure S20. ^{19}F NMR spectrum (376 MHz, $CDCl_3$) of 2-((2-nitro-4-(trifluoromethyl)phenoxy)methyl)prop-2-en-1-ol – **1c**

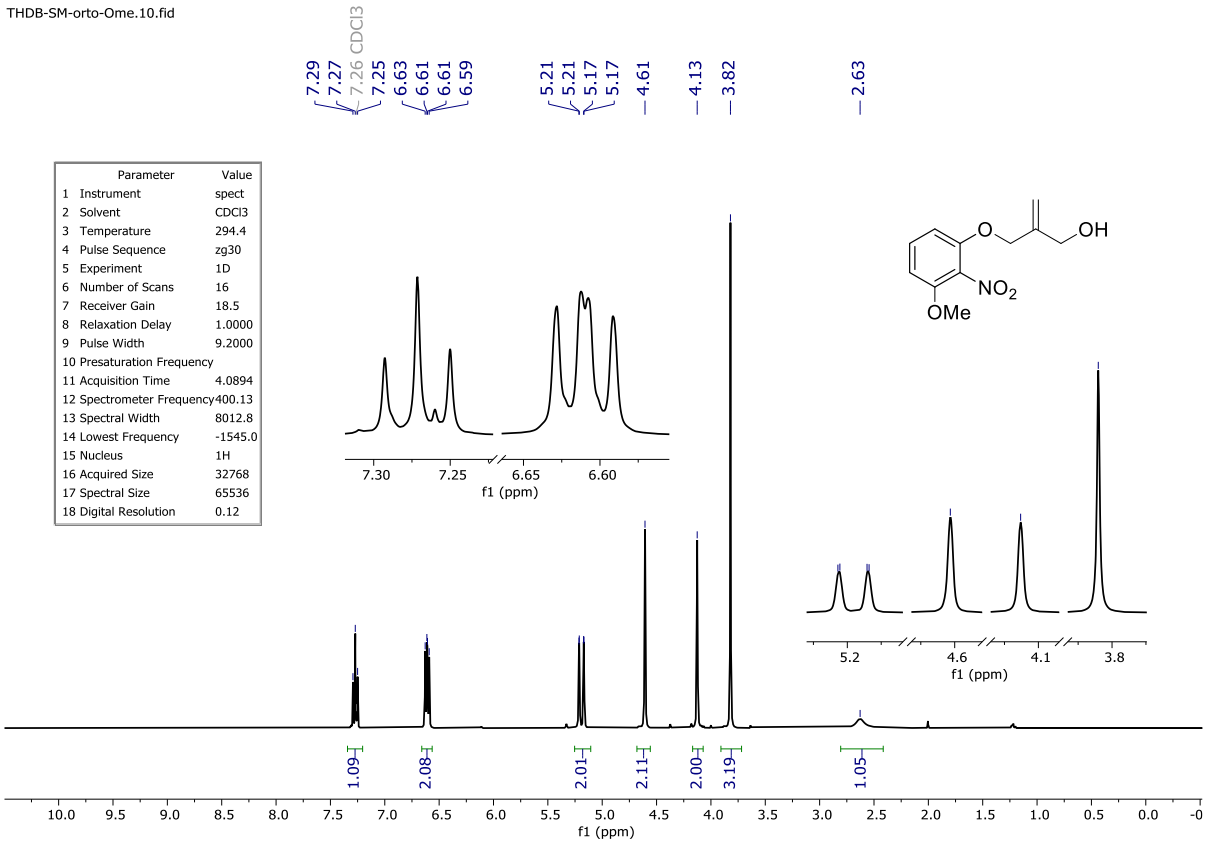

Figure S21. ^{1}H NMR spectrum ($CDCl_3$, 400 MHz) of 2-((3-methoxy-2-nitrophenoxy)methyl)prop-2-en-1-ol – **1d**

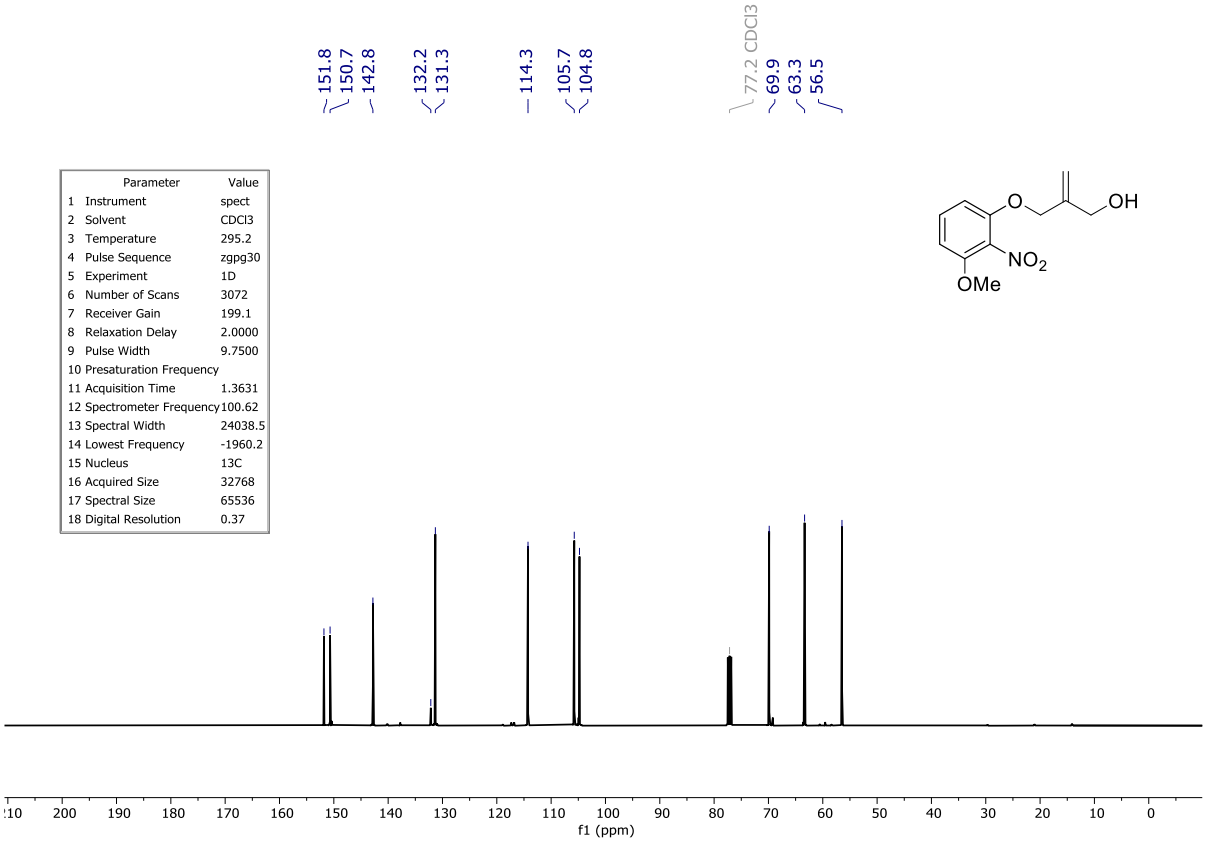

Figure S22. ^{13}C NMR spectrum ($CDCl_3$, 101 MHz) of 2-((3-methoxy-2-nitrophenoxy)methyl)prop-2-en-1-ol – **1d**

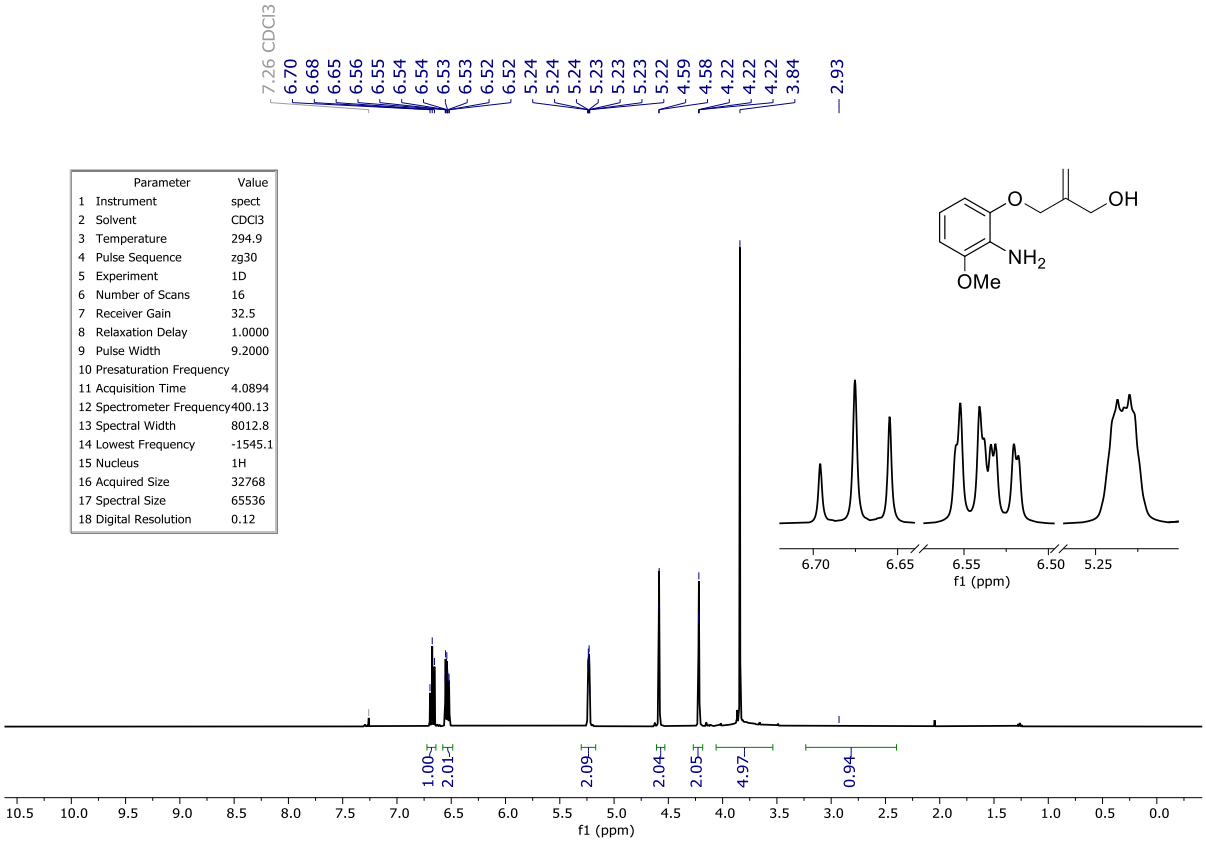

Figure S23. ^{1}H NMR spectrum ($CDCl_3$, 400 MHz) of 2-((2-amino-3-methoxyphenoxy)methyl)prop-2-en-1-ol – **2d**

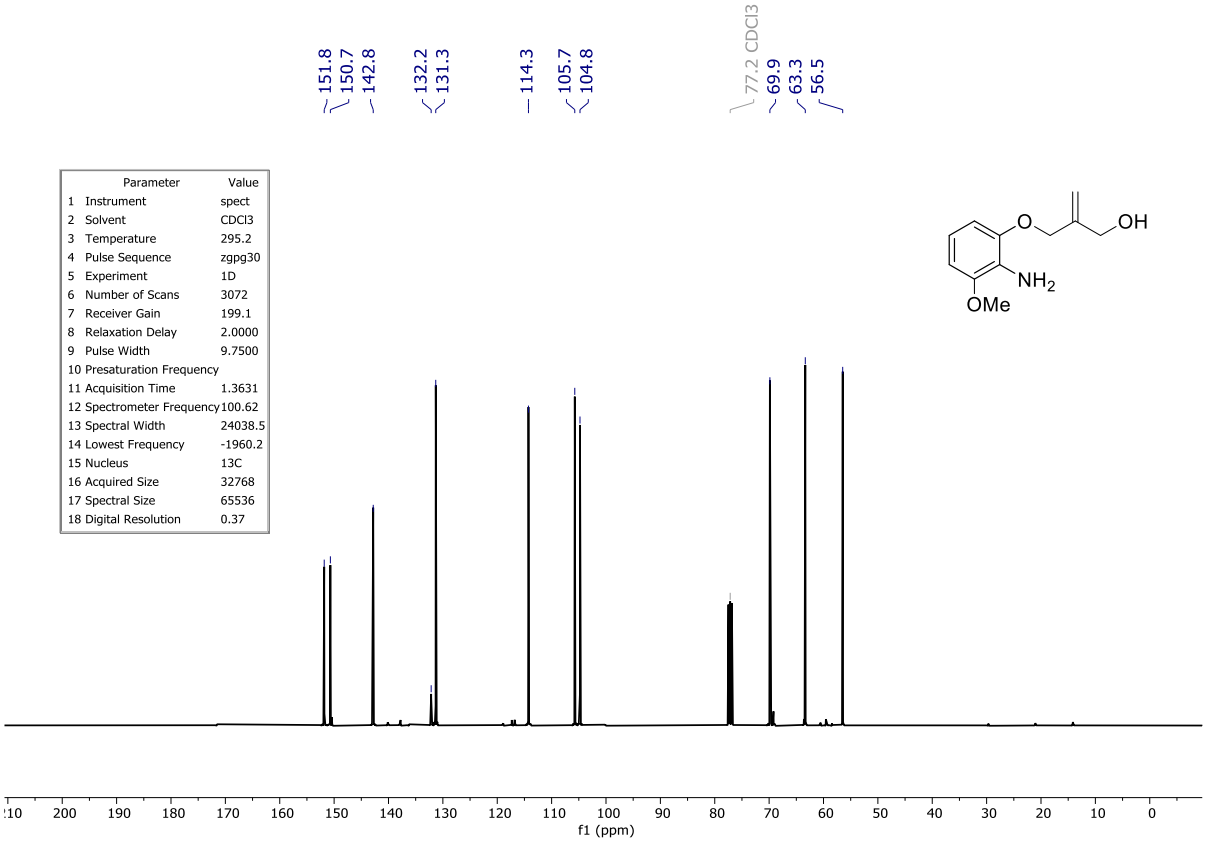

Figure S24. ^{13}C NMR spectrum ($CDCl_3$, 101 MHz) of 2-((2-amino-3-methoxyphenoxy)methyl)prop-2-en-1-ol – **2d**

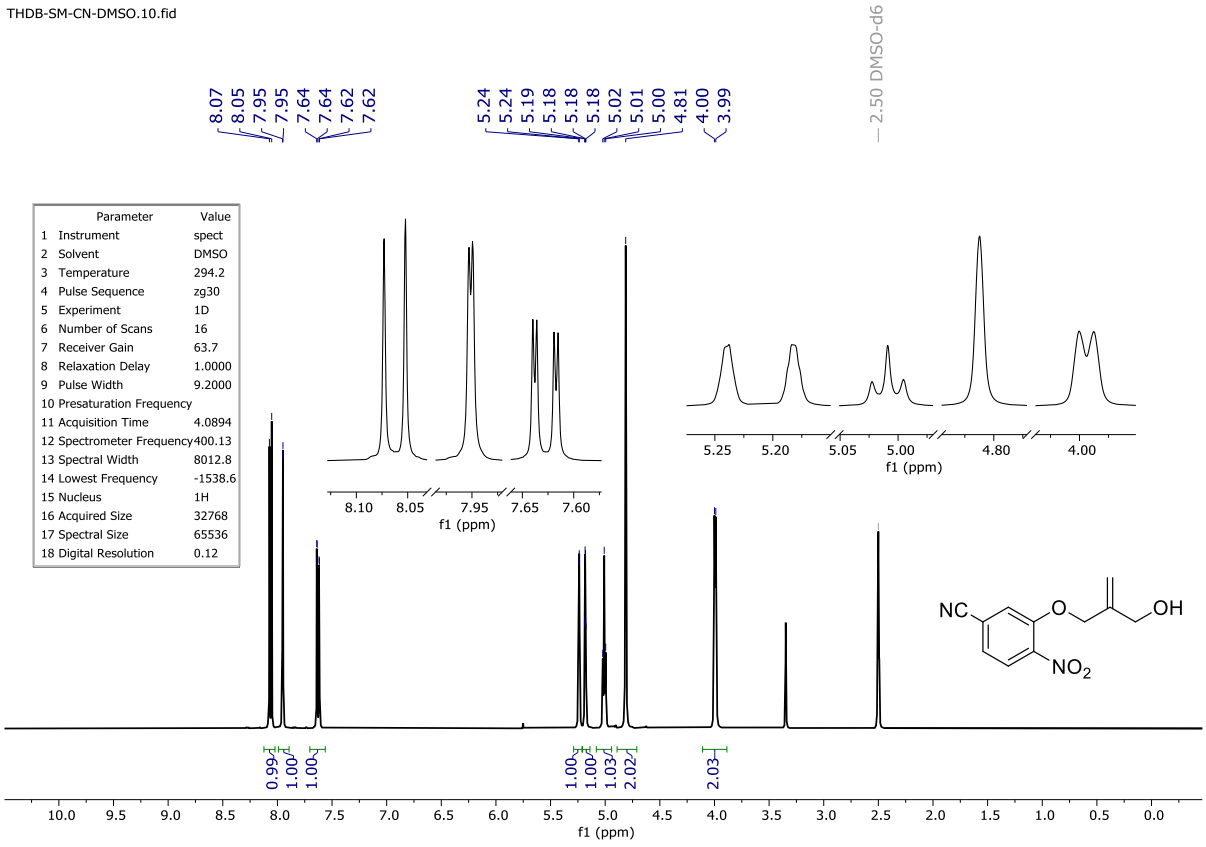

Figure S25. ^{1}H NMR spectrum (DMSO-d_6, 400 MHz) of 3-((2-(hydroxymethyl)allyl)oxy)-4-nitrobenzonitrile – **1e**

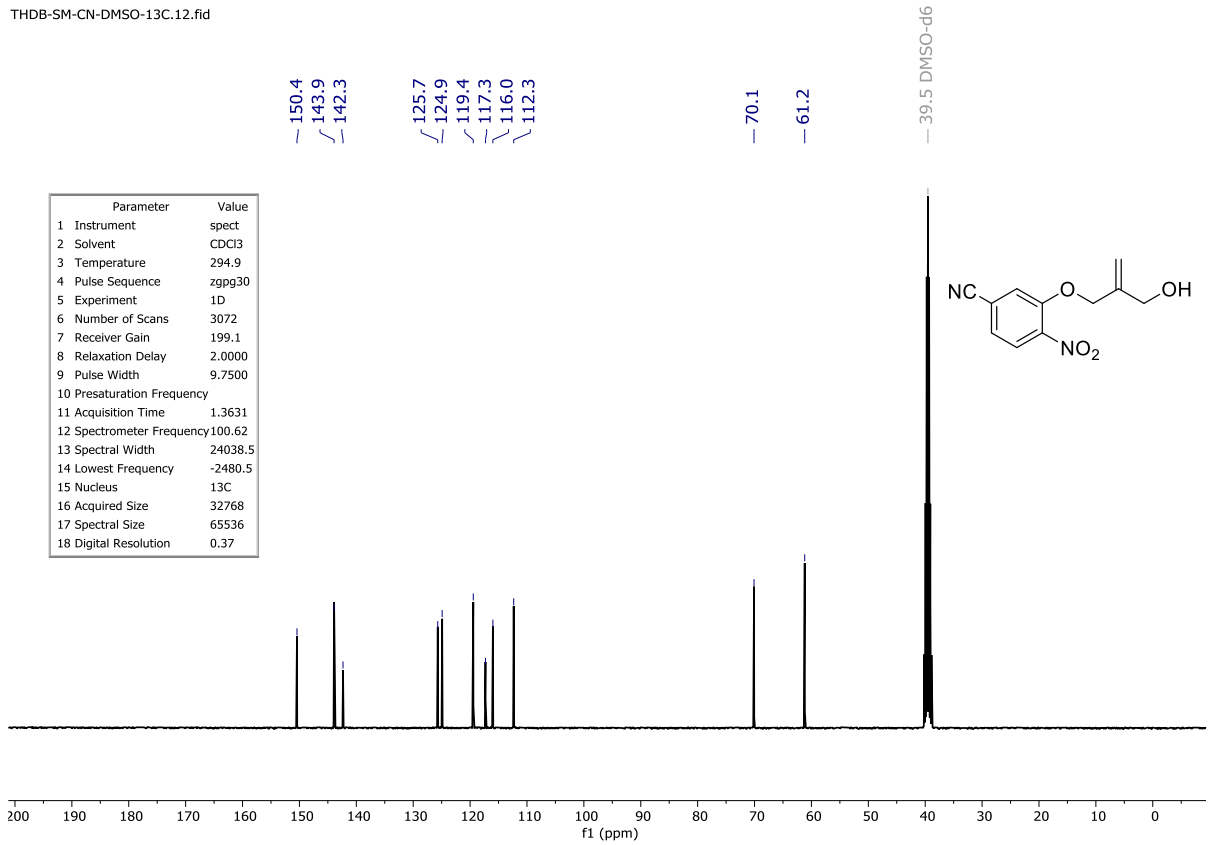

Figure S26. ^{13}C NMR spectrum (DMSO-d_6, 101 MHz) of 3-((2-(hydroxymethyl)allyl)oxy)-4-nitrobenzonitrile – **1e**

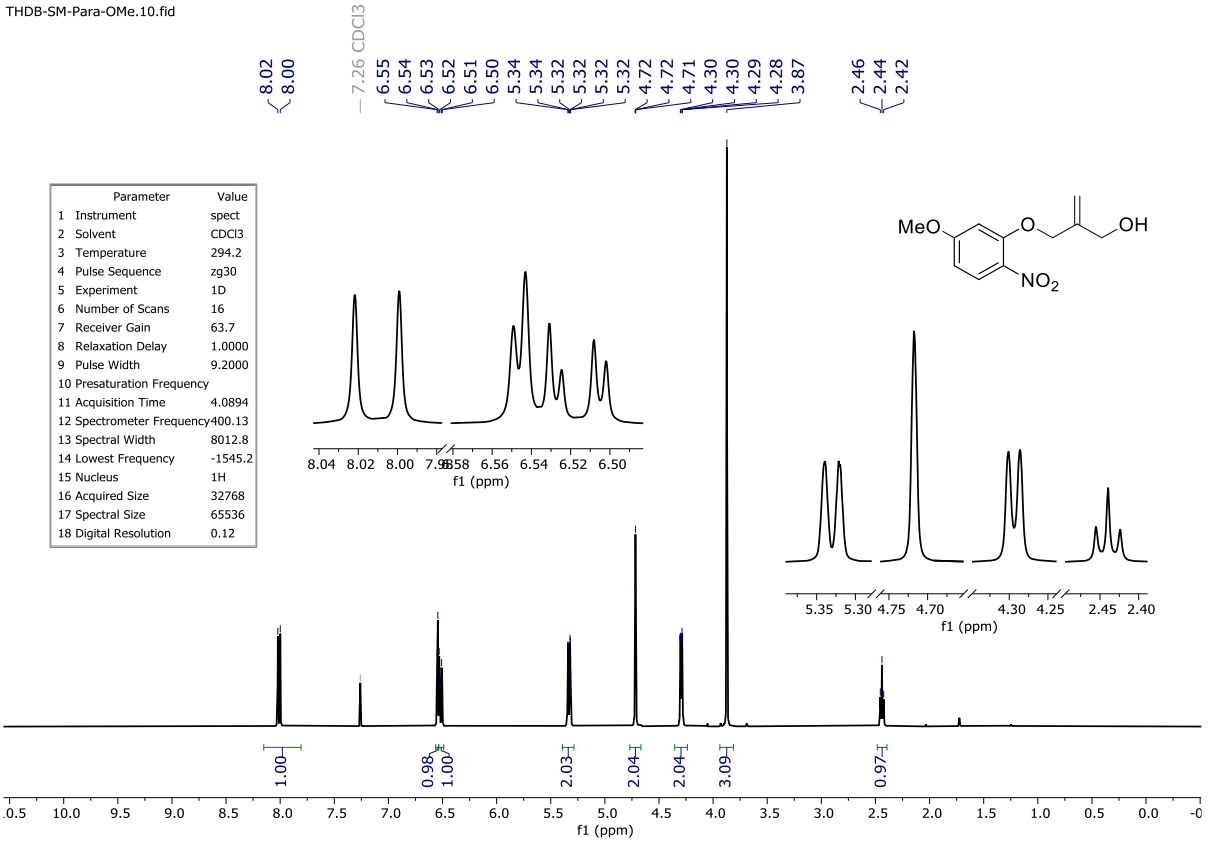

Figure S27. ^{1}H NMR spectrum ($CDCl_3$, 400 MHz) of 2-((5-methoxy-2-nitrophenoxy)methyl)prop-2-en-1-ol – **1f**

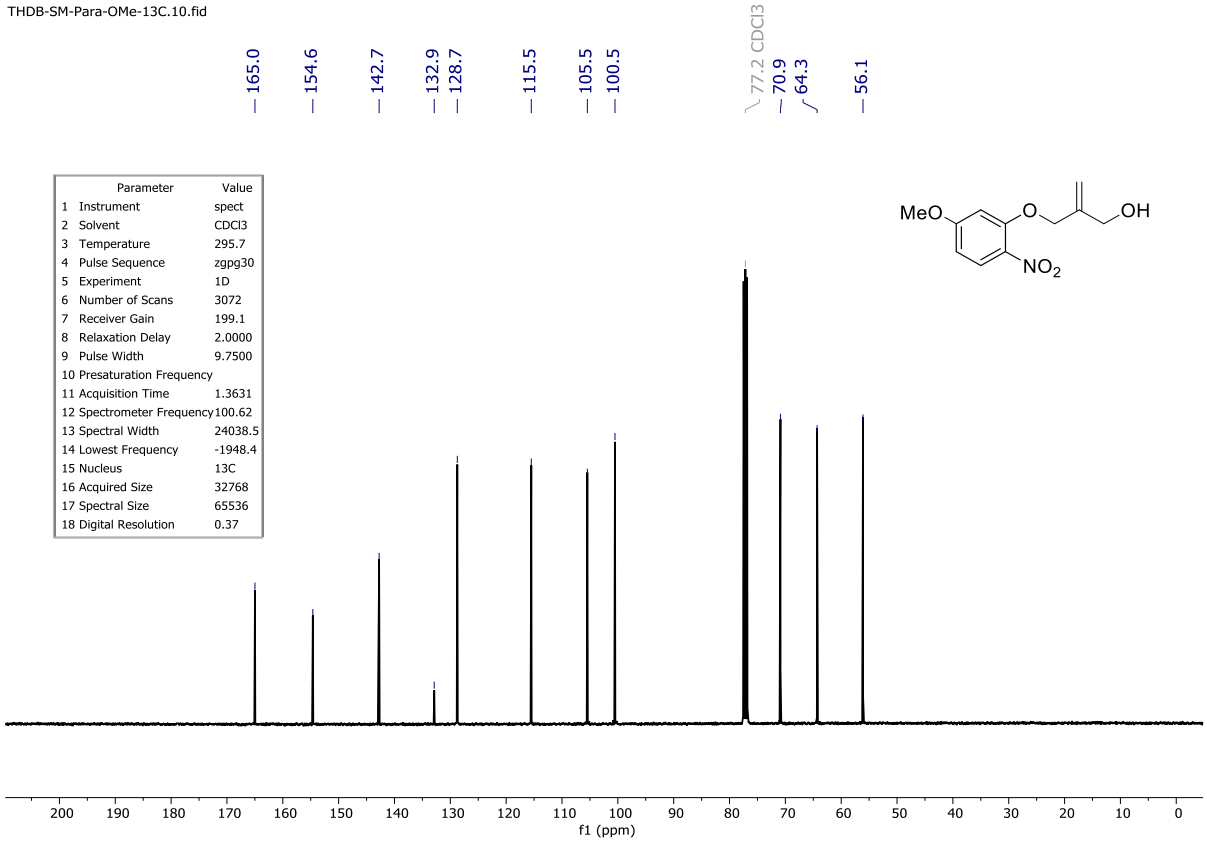

Figure S28. ^{13}C NMR spectrum ($CDCl_3$, 101 MHz) of 2-((5-methoxy-2-nitrophenoxy)methyl)prop-2-en-1-ol – **1f**

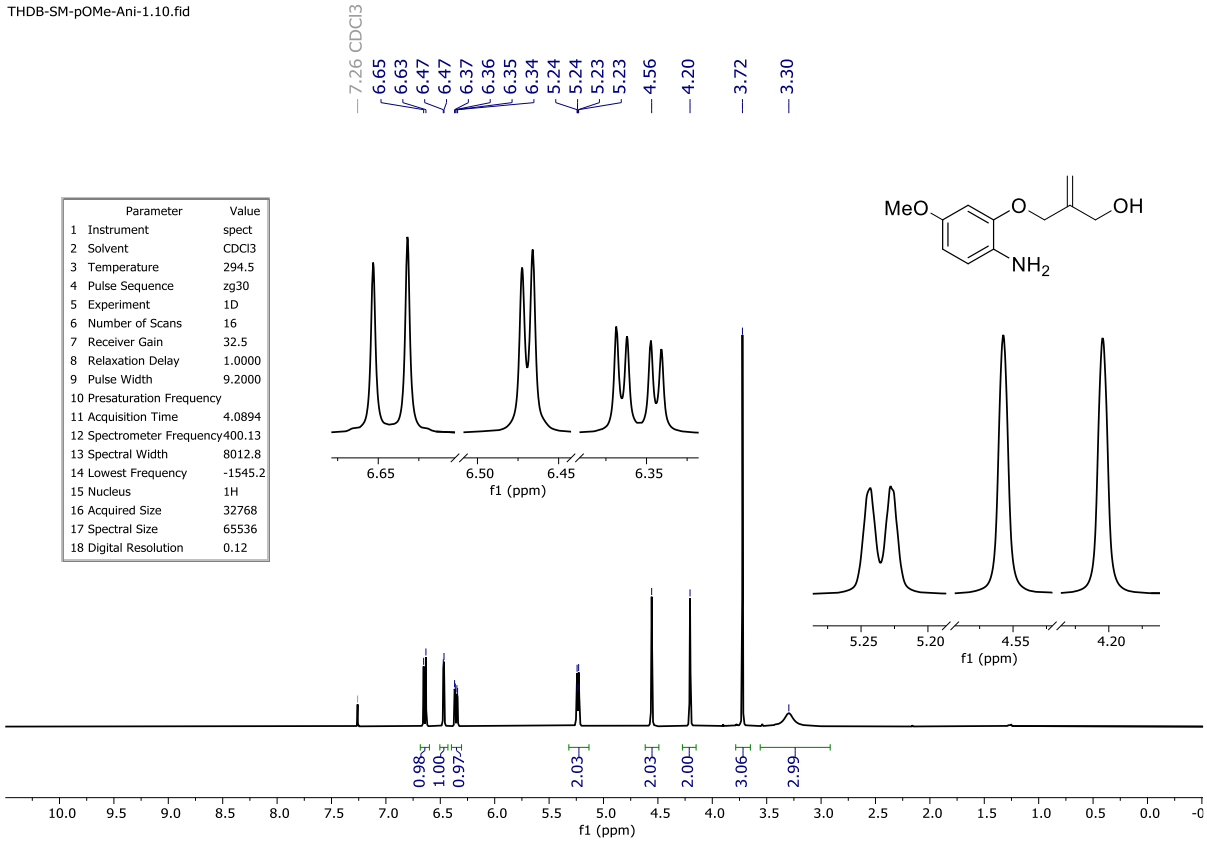

Figure S29. ^{1}H NMR spectrum ($CDCl_3$, 400 MHz) of 2-((2-amino-5-methoxyphenoxy)methyl)prop-2-en-1-ol – **2f**

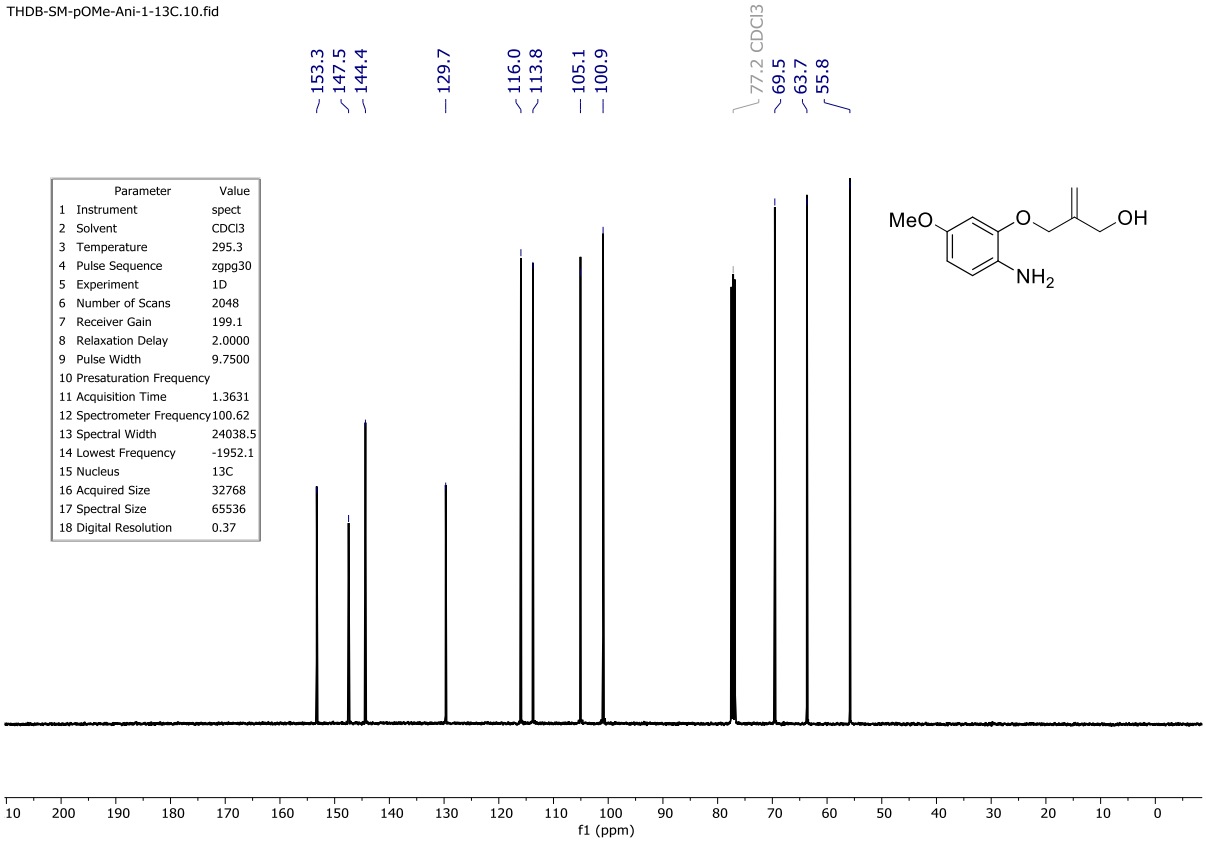

Figure S30. ^{13}C NMR spectrum ($CDCl_3$, 101 MHz) of 2-((2-amino-5-methoxyphenoxy)methyl)prop-2-en-1-ol – **2f**

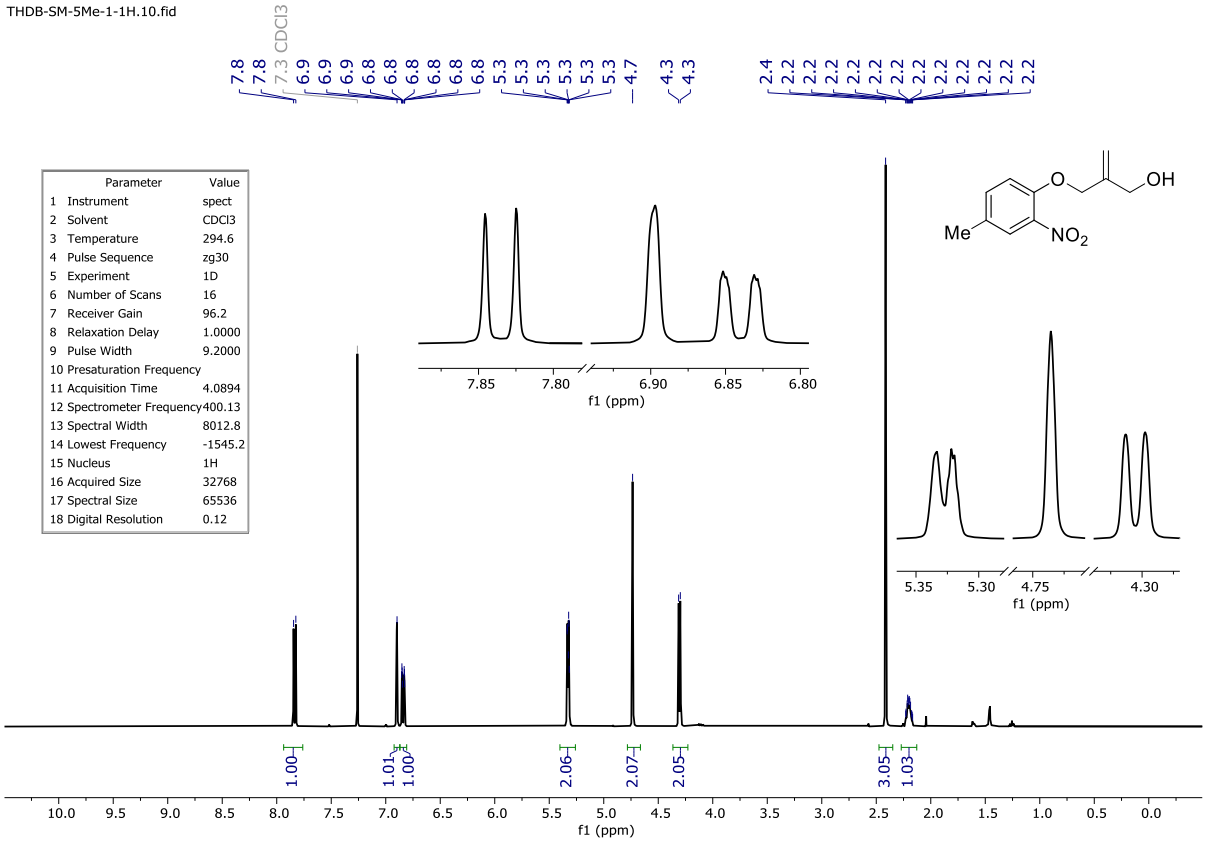

Figure S31. ^{1}H NMR spectrum ($CDCl_3$, 400 MHz) of 2-((4-methyl-2-nitrophenoxy)methyl)prop-2-en-1-ol – **1g**

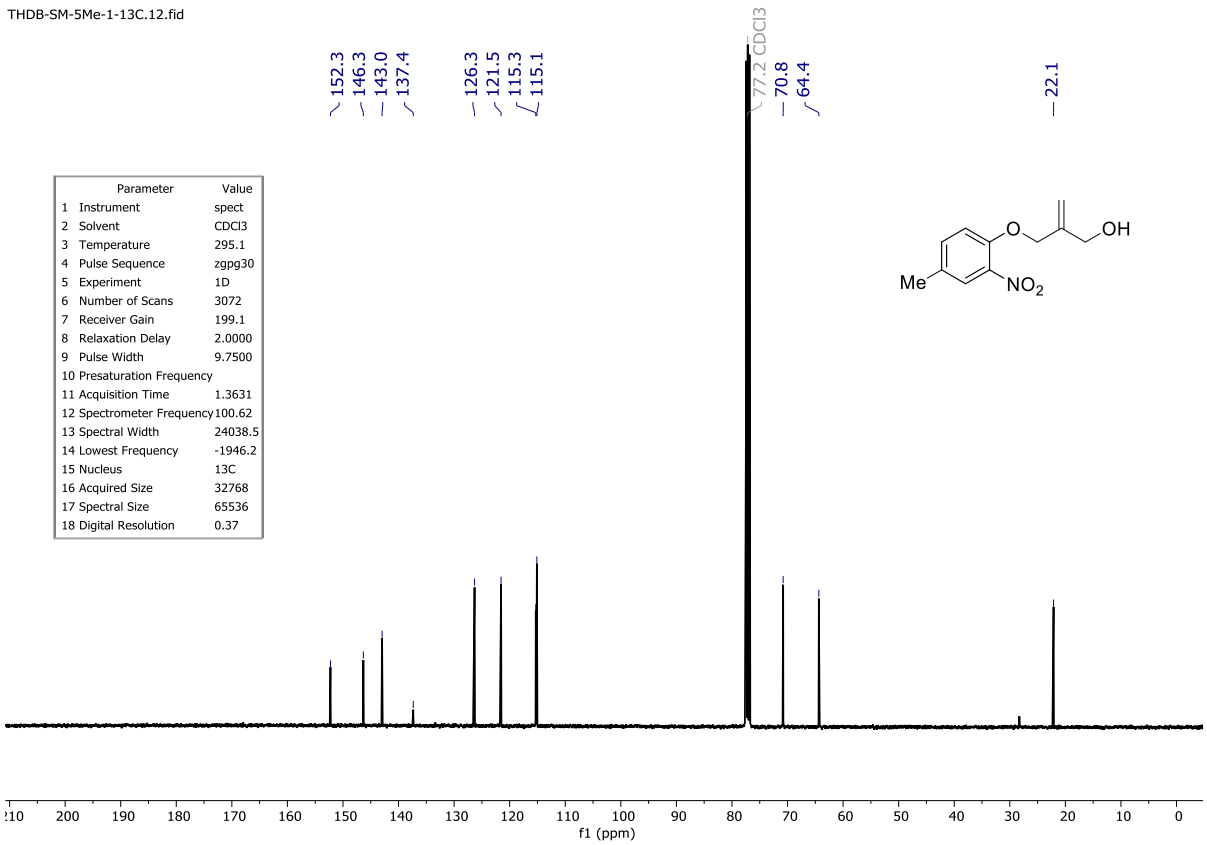

Figure S32. ^{13}C NMR spectrum ($CDCl_3$, 101 MHz) of 2-((4-methyl-2-nitrophenoxy)methyl)prop-2-en-1-ol – **1g**

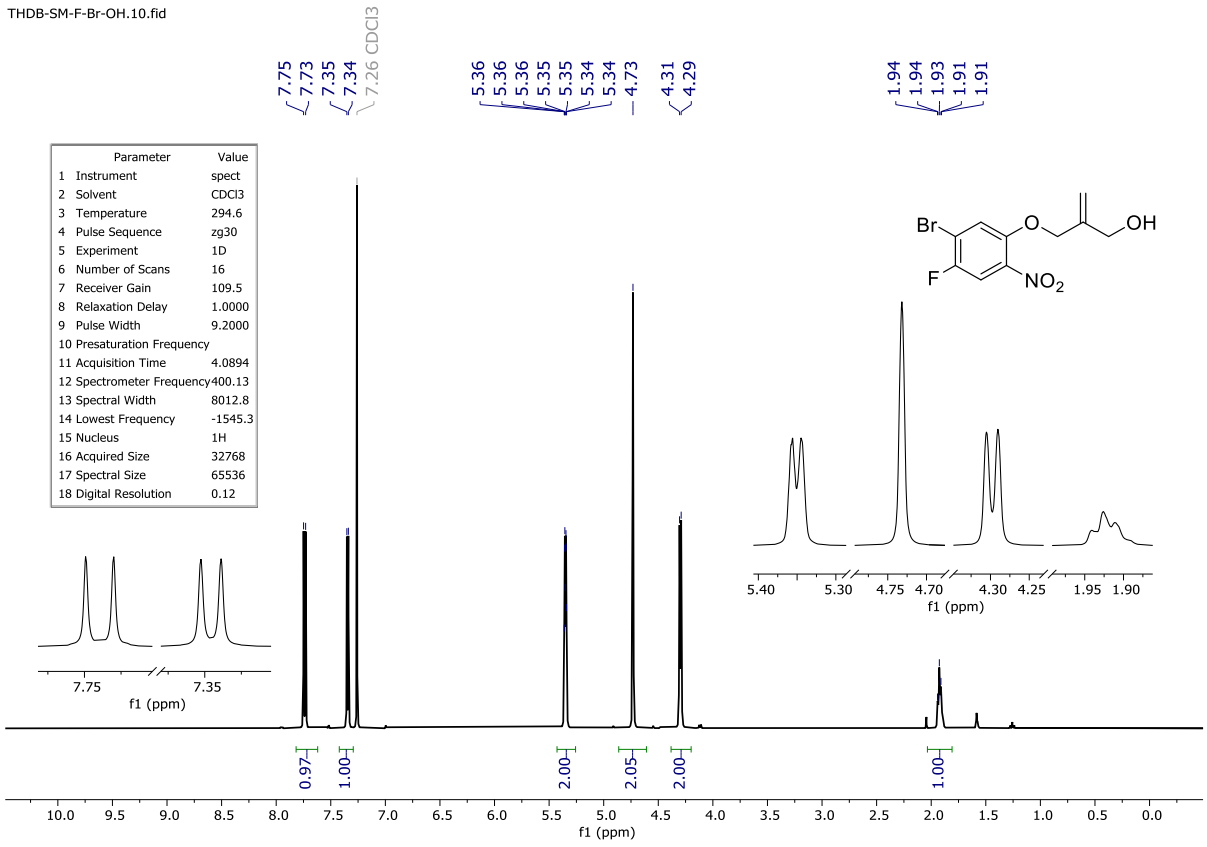

Figure S33. ^{1}H NMR spectrum ($CDCl_3$, 400 MHz) of 2-((5-bromo-4-fluoro-2-nitrophenoxy)methyl)prop-2-en-1-ol – **1h**

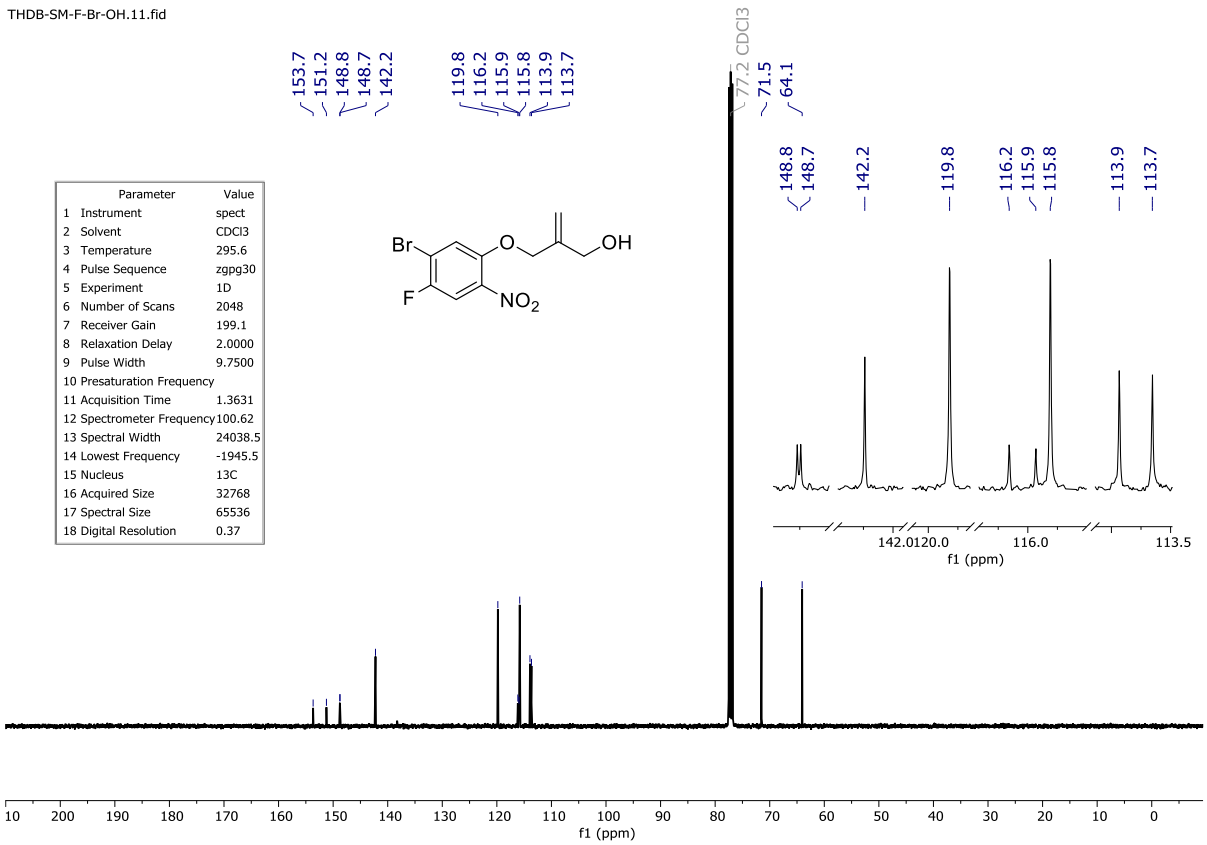

Figure S34. ^{13}C NMR spectrum ($CDCl_3$, 101 MHz) of 2-((5-bromo-4-fluoro-2-nitrophenoxy)methyl)prop-2-en-1-ol – **1h**

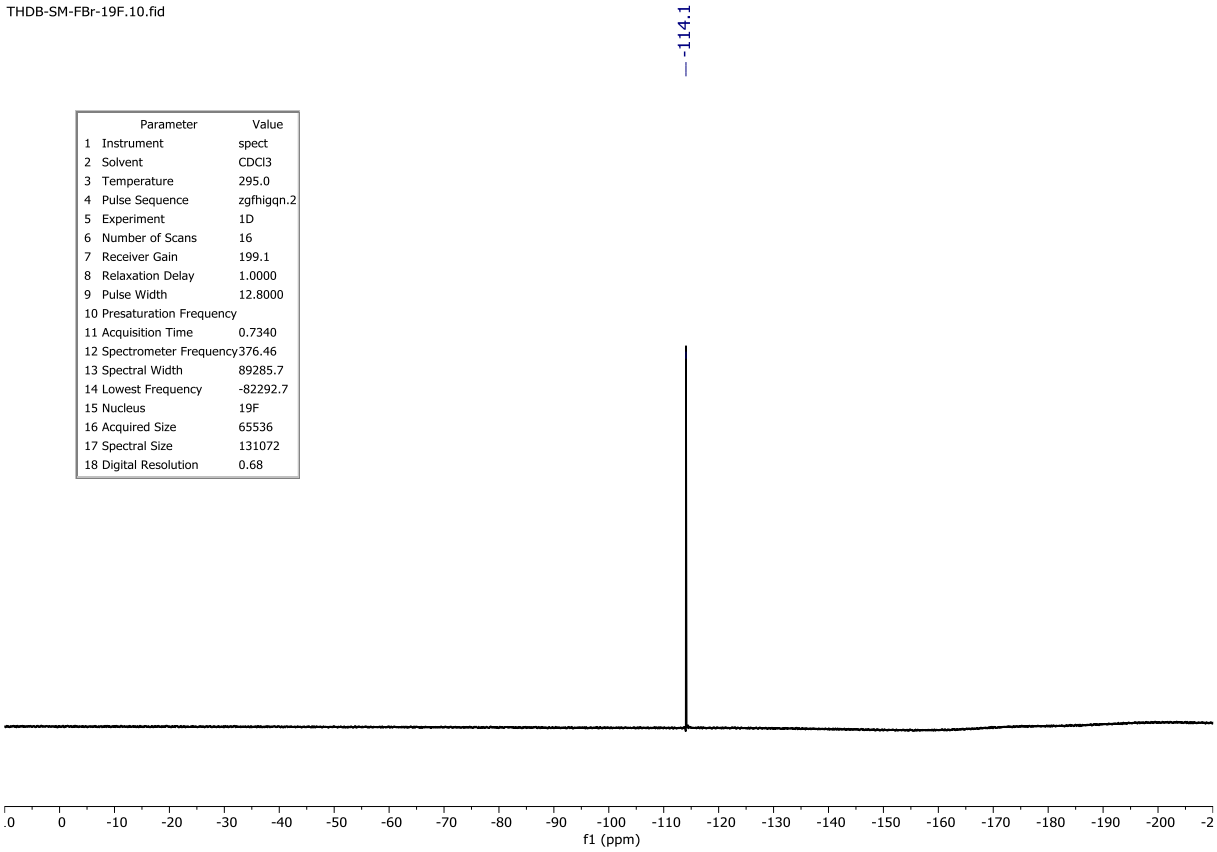

Figure S35. ^{19}F NMR spectrum (376 MHz, $CDCl_3$) of 2-((5-bromo-4-fluoro-2-nitrophenoxy)methyl)prop-2-en-1-ol – **1h**

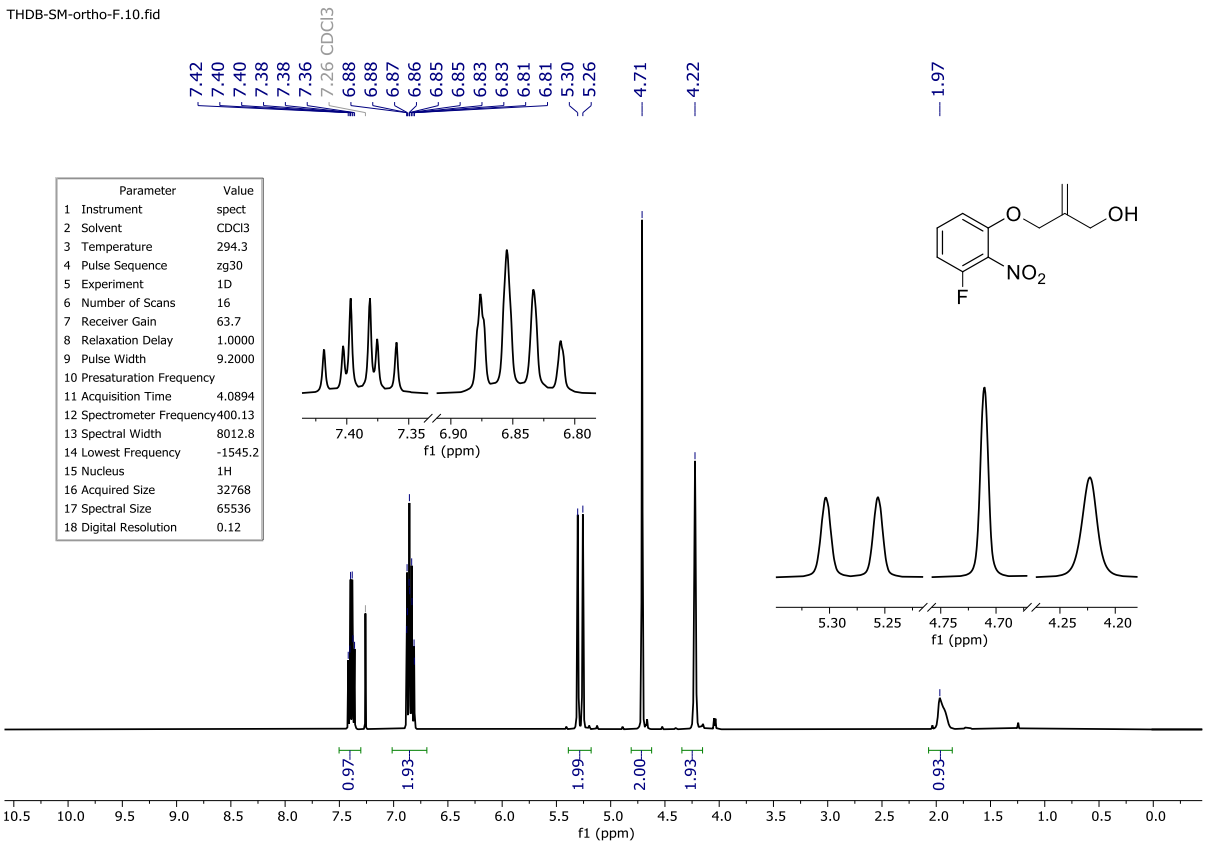

Figure S36. ^{1}H NMR spectrum ($CDCl_3$, 400 MHz) of 2-((3-fluoro-2-nitrophenoxy)methyl)prop-2-en-1-ol – **1i**

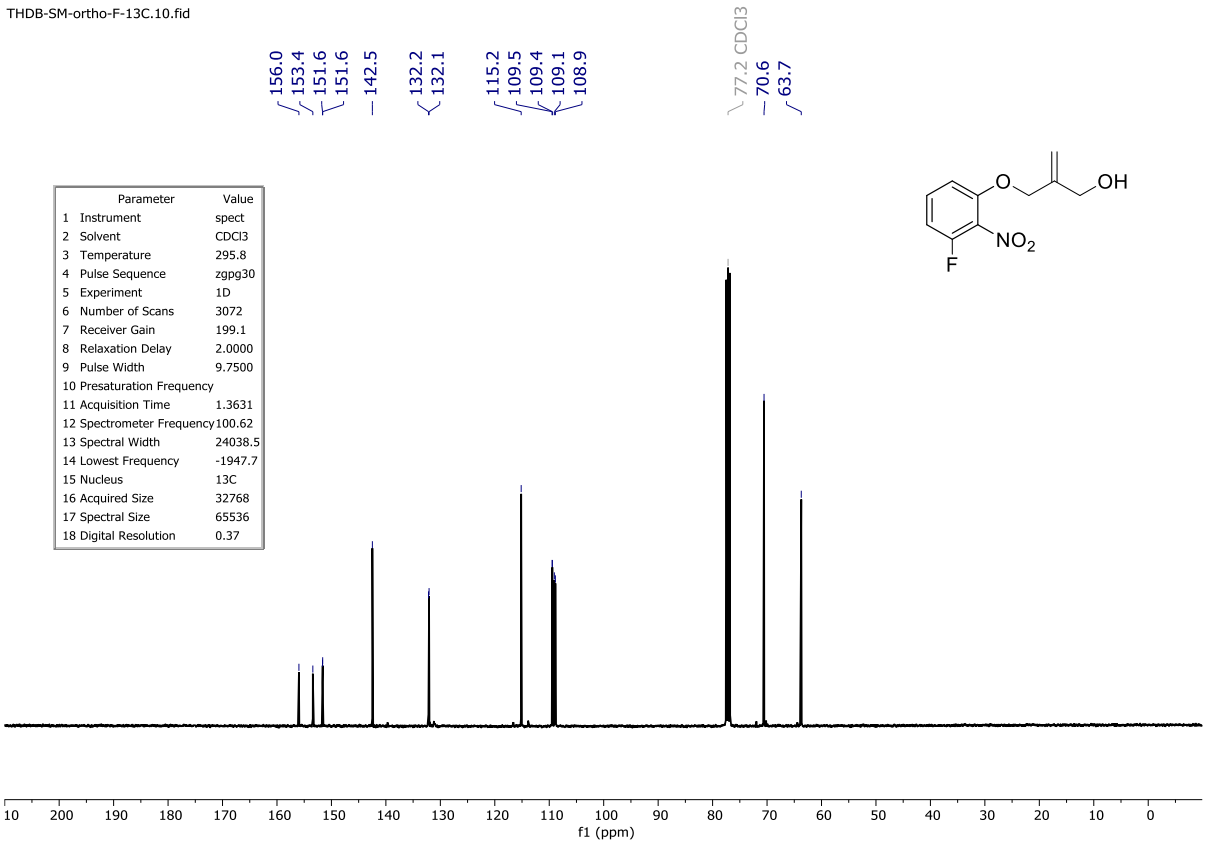

Figure S37. ^{13}C NMR spectrum ($CDCl_3$, 101 MHz) of 2-((3-fluoro-2-nitrophenoxy)methyl)prop-2-en-1-ol – **1i**

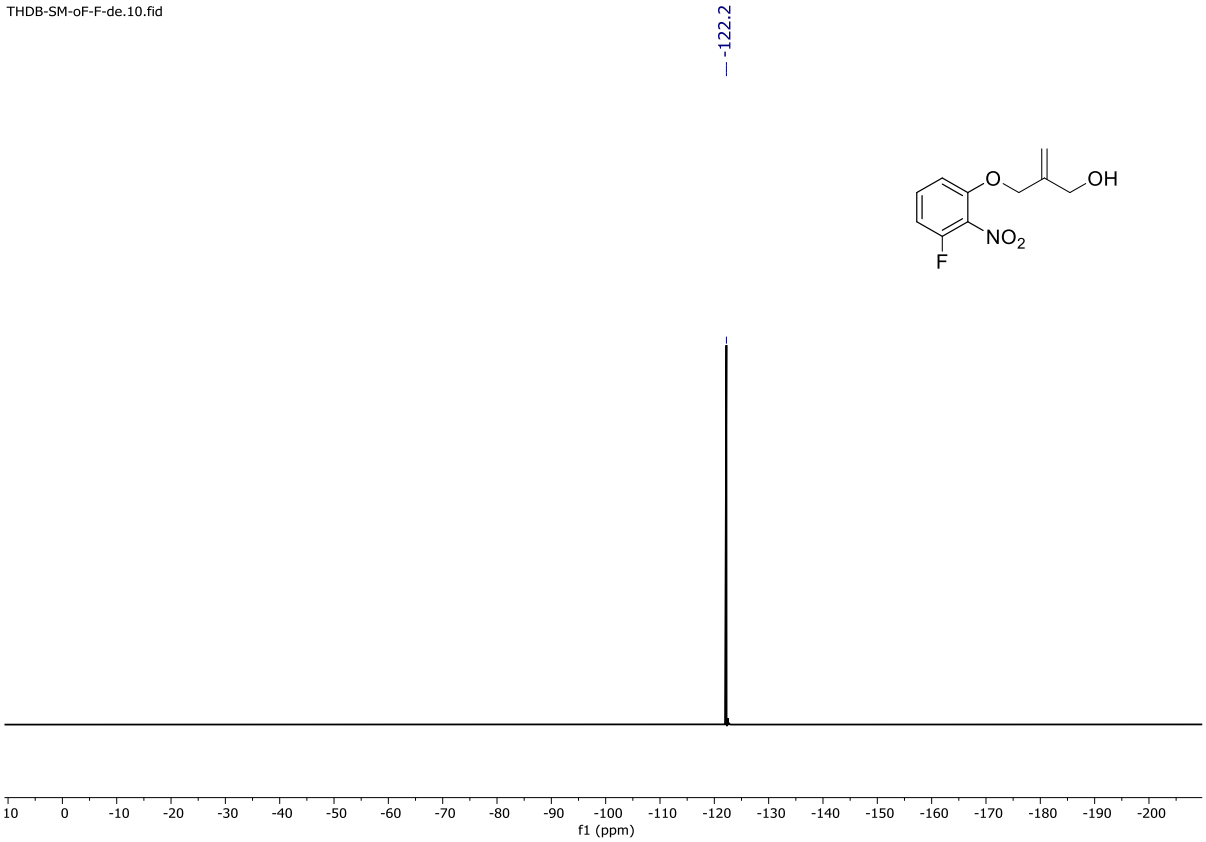

Figure S38. ^{19}F NMR spectrum (376 MHz, $CDCl_3$) of 2-((3-fluoro-2-nitrophenoxy)methyl)prop-2-en-1-ol – **1j**

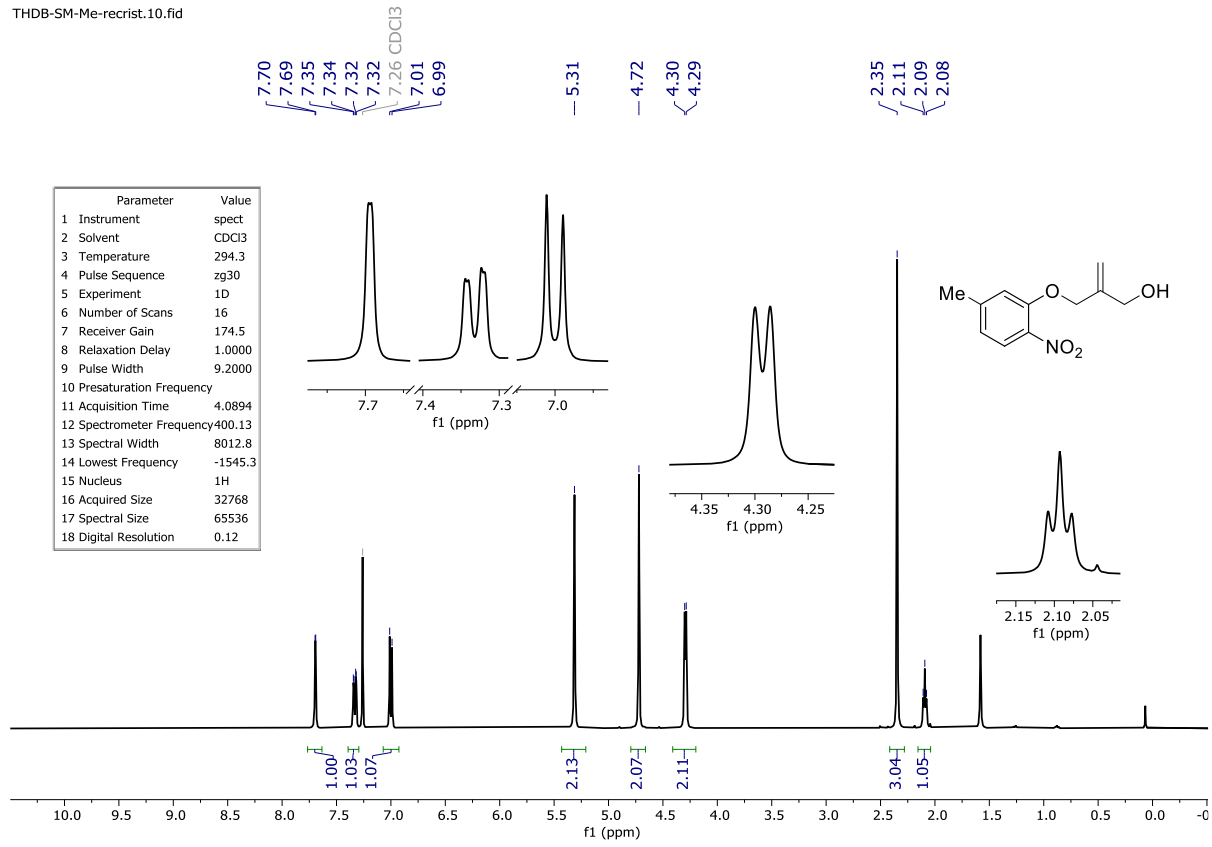

Figure S39. ^{1}H NMR spectrum ($CDCl_3$, 400 MHz) of 2-((5-methyl-2-nitrophenoxy)methyl)prop-2-en-1-ol – **1j**

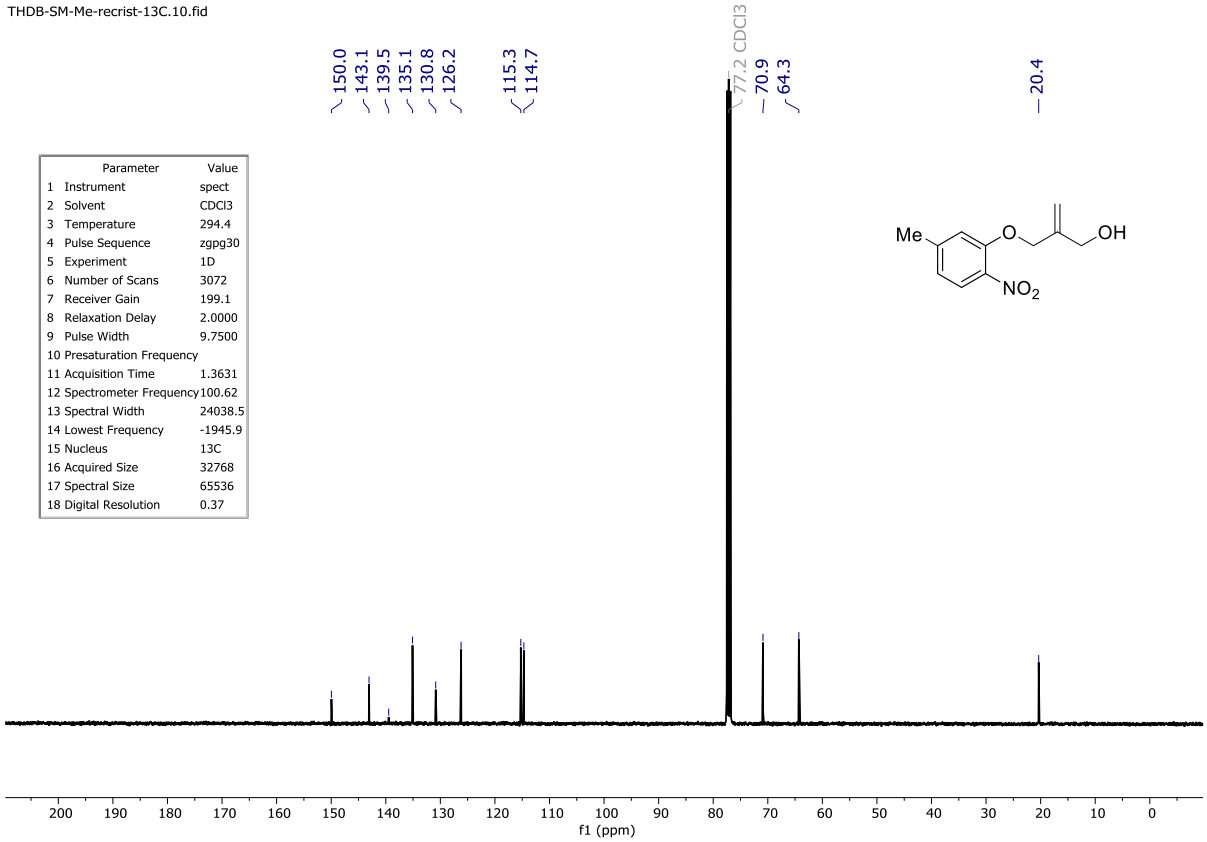

Parameter	Value
1 Instrument	spect
2 Solvent	CDCl3
3 Temperature	294.4
4 Pulse Sequence	zgpg30
5 Experiment	1D
6 Number of Scans	3072
7 Receiver Gain	199.1
8 Relaxation Delay	2.0000
9 Pulse Width	9.7500
10 Presaturation Frequency	
11 Acquisition Time	1.3631
12 Spectrometer Frequency	100.62
13 Spectral Width	24038.5
14 Lowest Frequency	-1945.9
15 Nucleus	13C
16 Acquired Size	32768
17 Spectral Size	65536
18 Digital Resolution	0.37

Figure S40. ^{13}C NMR spectrum ($CDCl_3$, 101 MHz) of 2-((5-methyl-2-nitrophenoxy)methyl)prop-2-en-1-ol – **1j**

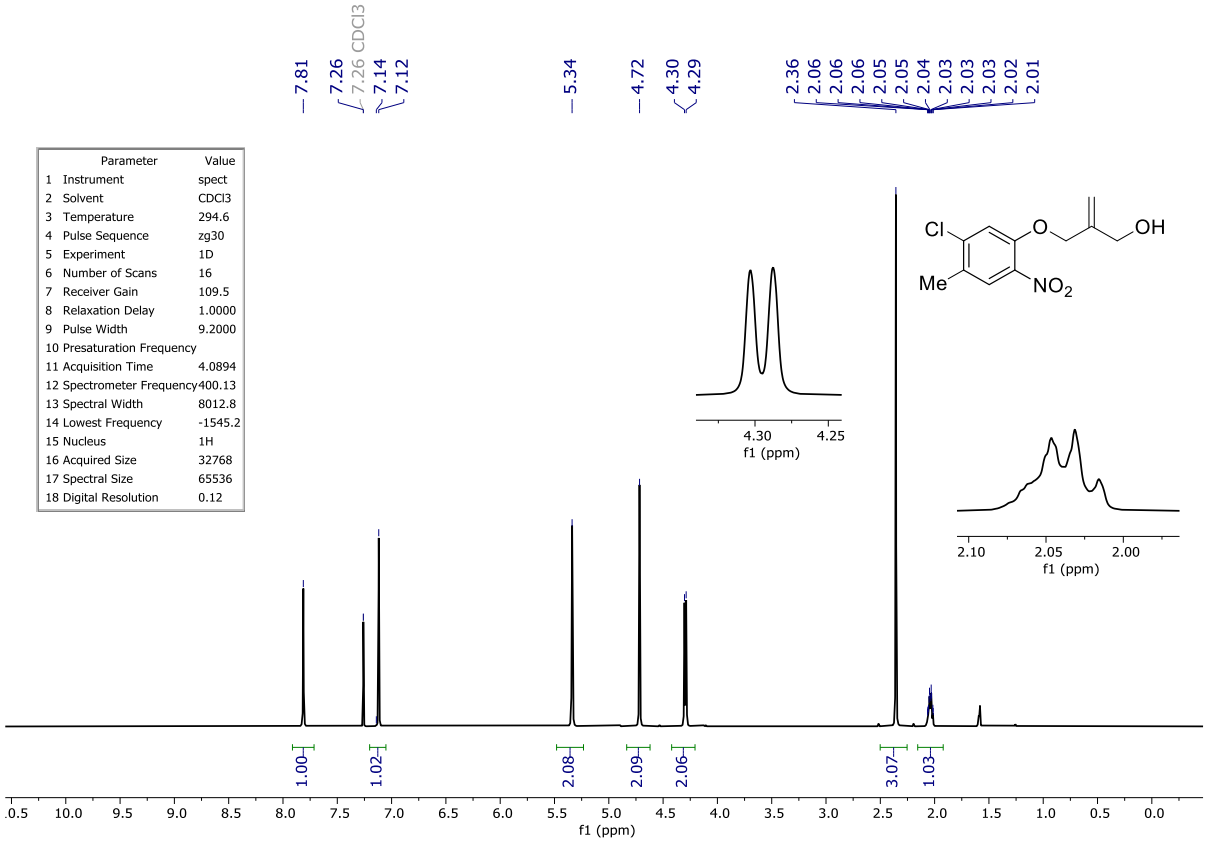

Parameter	Value
1 Instrument	spect
2 Solvent	CDCl3
3 Temperature	294.6
4 Pulse Sequence	zg30
5 Experiment	1D
6 Number of Scans	16
7 Receiver Gain	109.5
8 Relaxation Delay	1.0000
9 Pulse Width	9.2000
10 Presaturation Frequency	
11 Acquisition Time	4.0894
12 Spectrometer Frequency	400.13
13 Spectral Width	8012.8
14 Lowest Frequency	-1545.2
15 Nucleus	1H
16 Acquired Size	32768
17 Spectral Size	65536
18 Digital Resolution	0.12

Figure S41. ^{1}H NMR spectrum ($CDCl_3$, 400 MHz) of 2-((5-chloro-4-methyl-2-nitrophenoxy)methyl)prop-2-en-1-ol **– 1k**

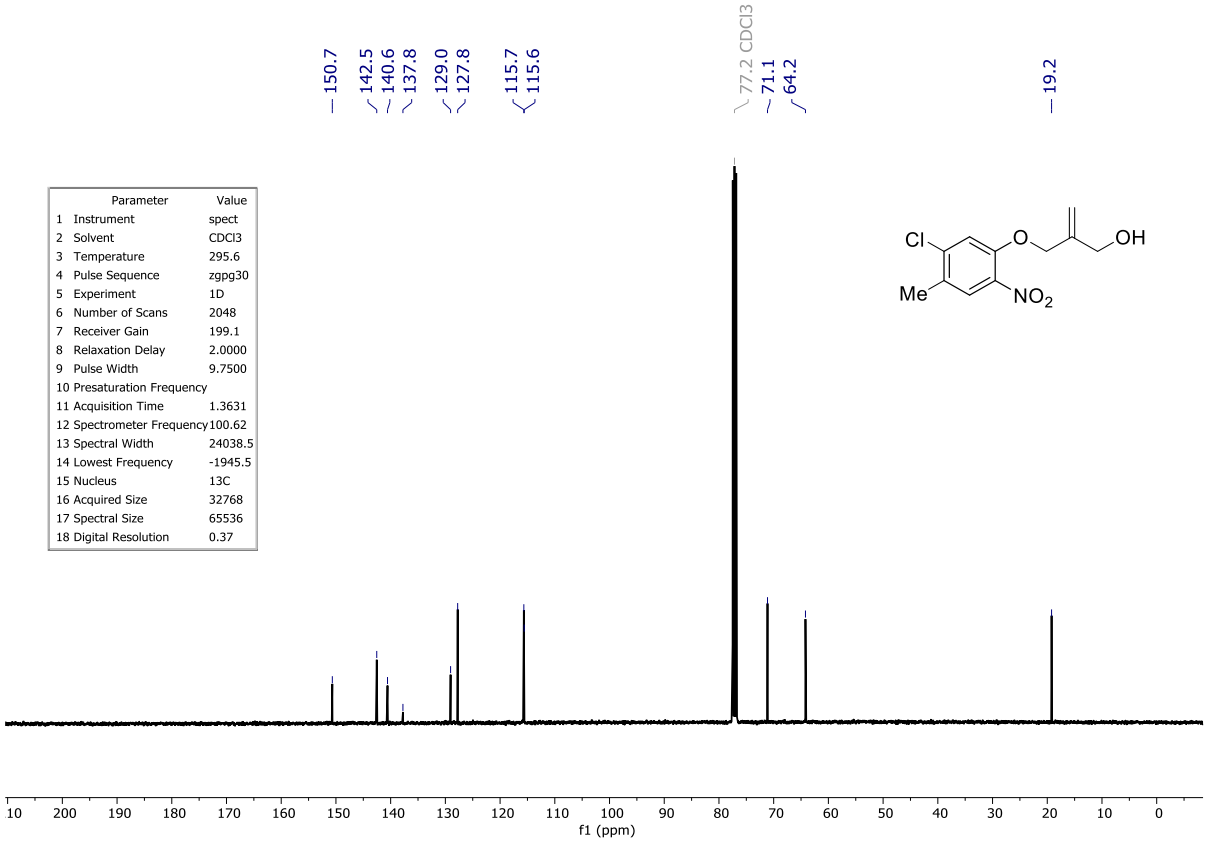

Figure S42. ^{13}C NMR spectrum ($CDCl_3$, 101 MHz) of 2-((5-chloro-4-methyl-2-nitrophenoxy)methyl)prop-2-en-1-ol **– 1k**

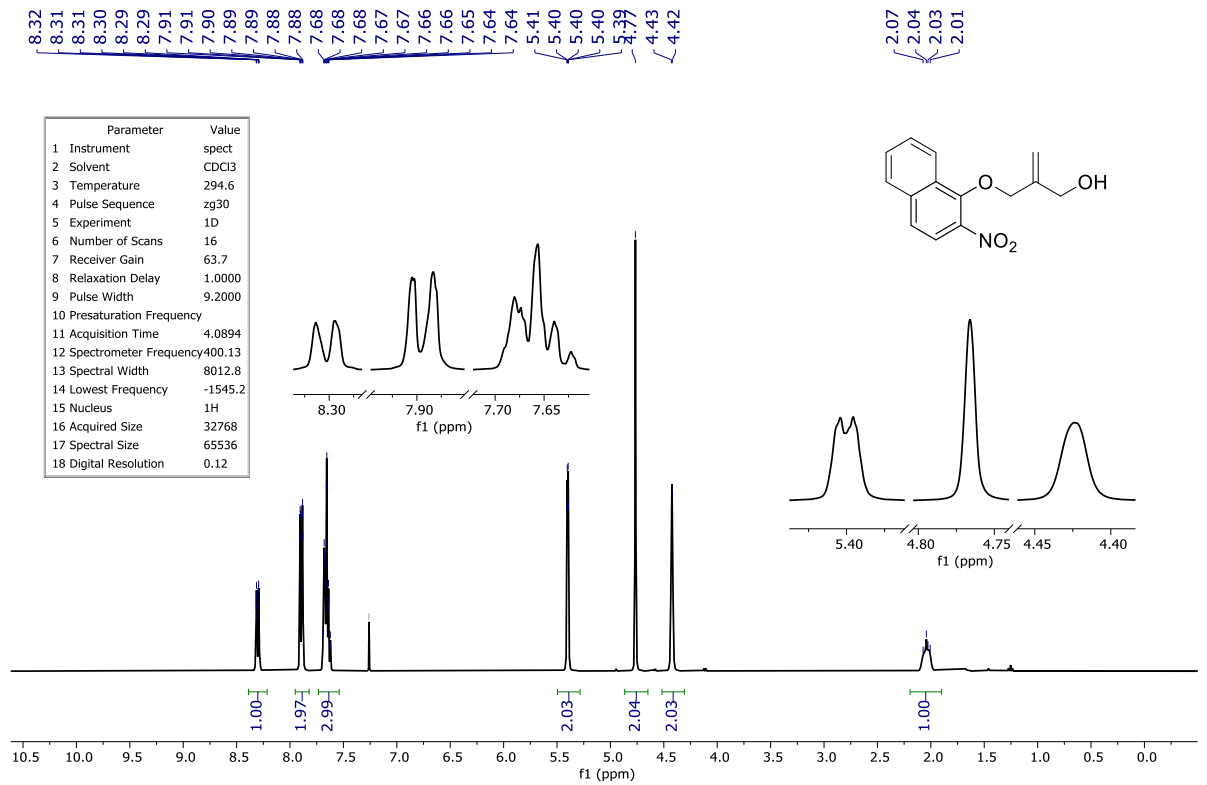

Figure S43. ^{1}H NMR spectrum ($CDCl_3$, 400 MHz) of 2-(((2-nitronaphthalen-1-yl)oxy)methyl)prop-2-en-1-ol – **1l**

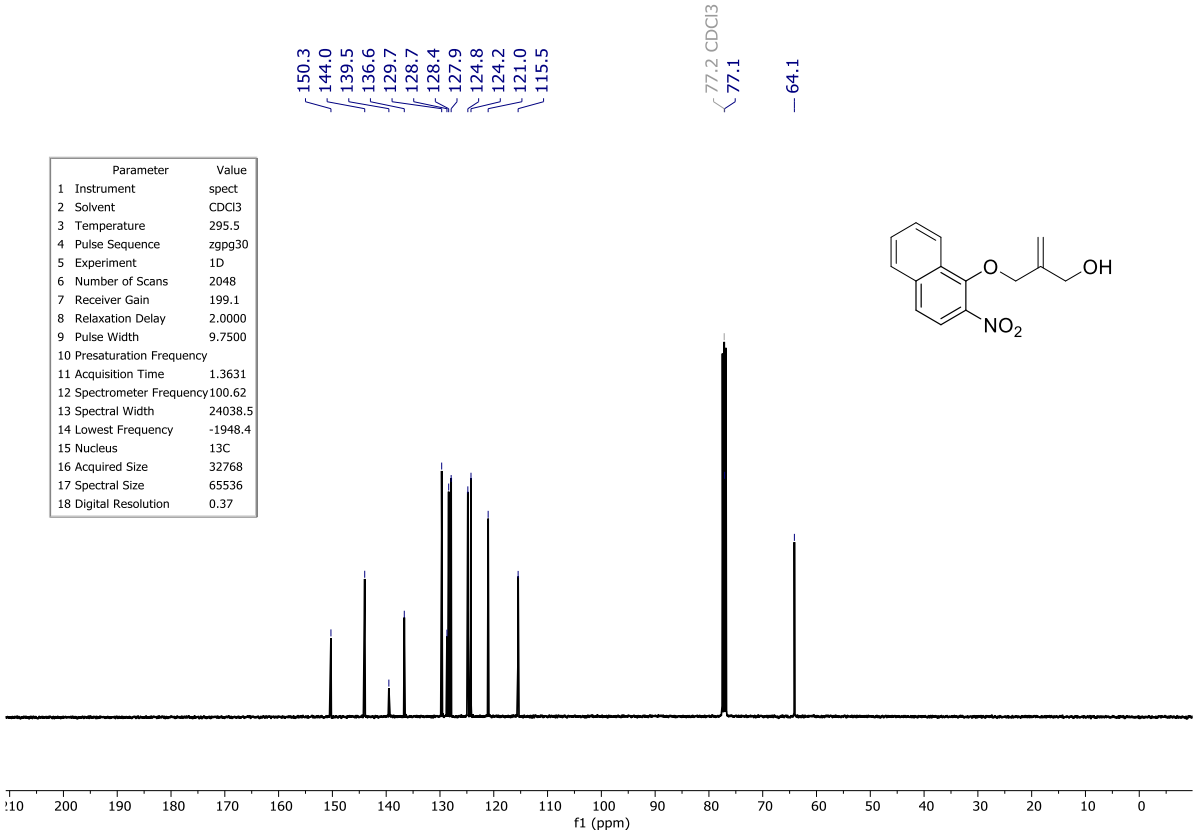

Figure S44. ^{13}C NMR spectrum ($CDCl_3$, 101 MHz) of 2-(((2-nitronaphthalen-1-yl)oxy)methyl)prop-2-en-1-ol – **1l**

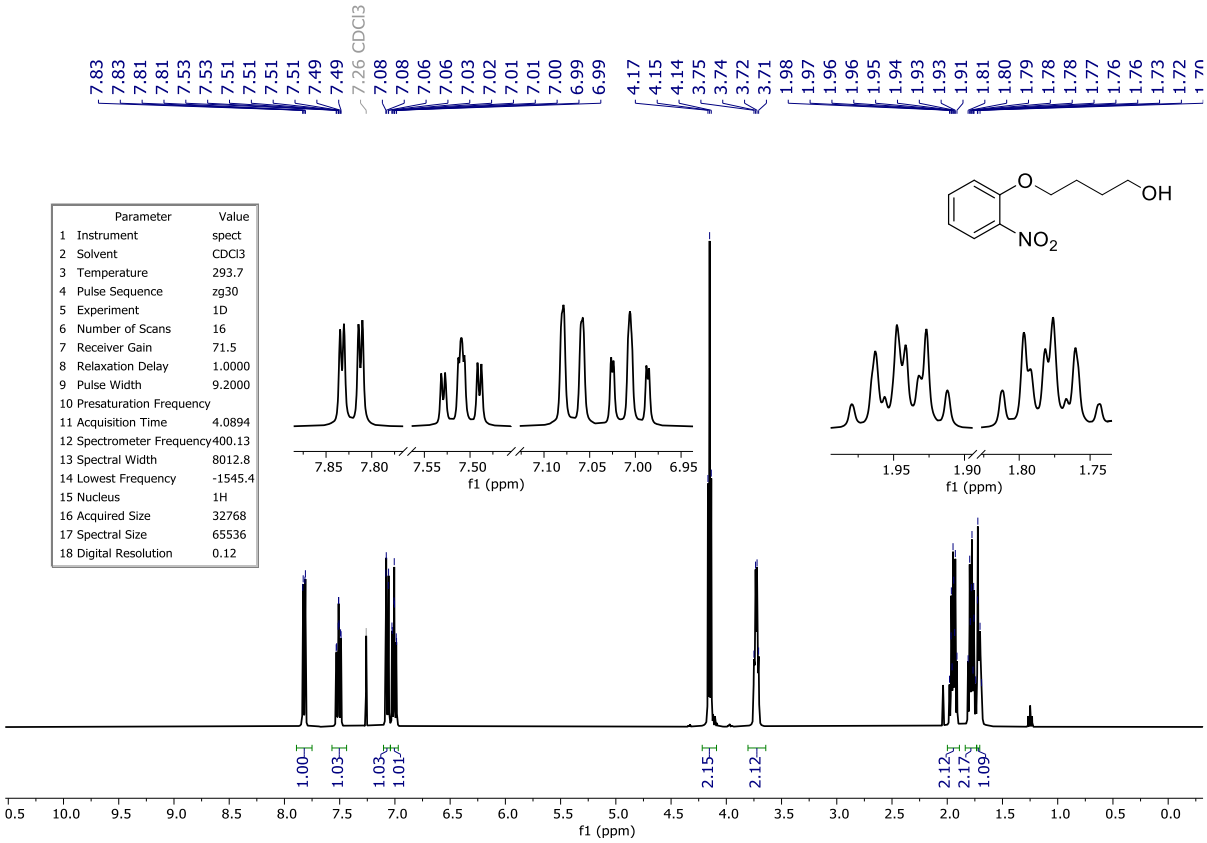

Figure S45. ^{1}H NMR spectrum ($CDCl_3$, 400 MHz) of 4-(2-nitrophenoxy)butan-1-ol – **S1**

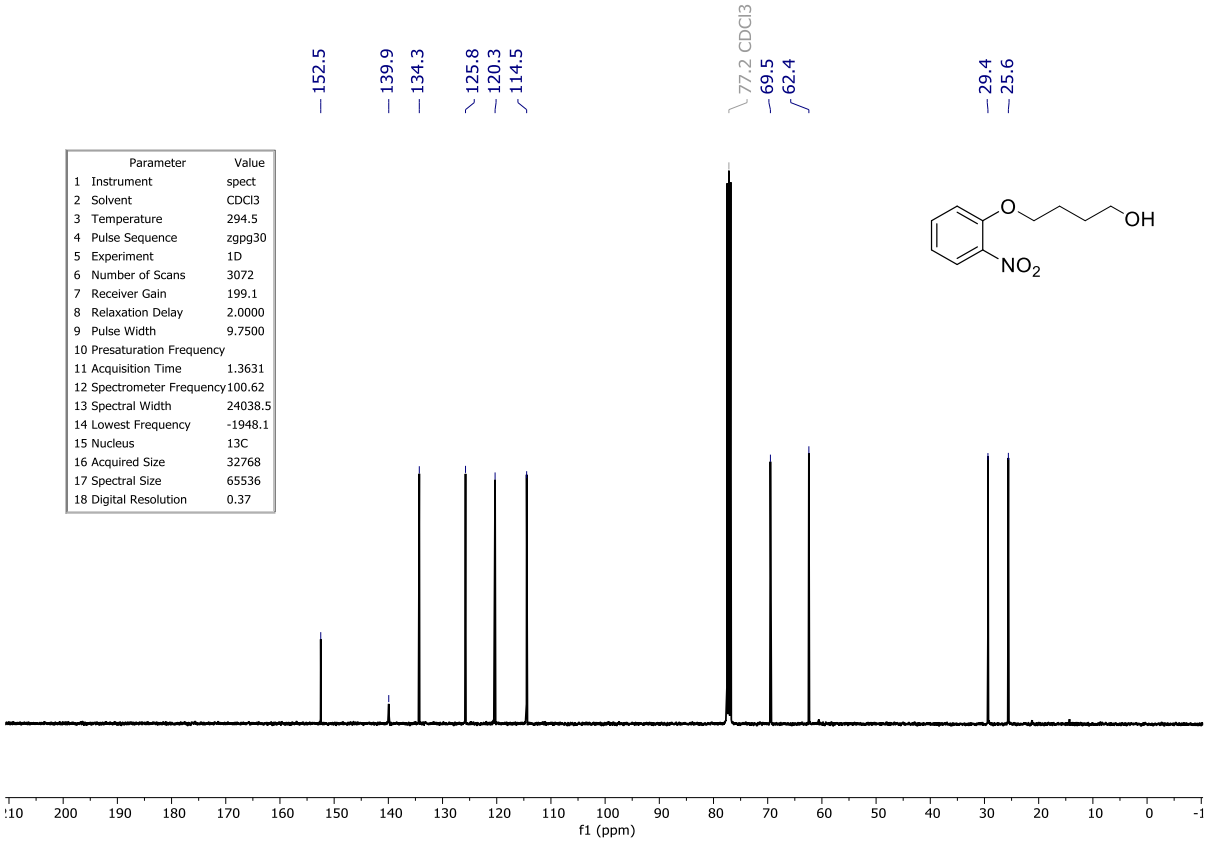

Figure S46. ^{13}C NMR spectrum ($CDCl_3$, 101 MHz) of 4-(2-nitrophenoxy)butan-1-ol – **S1**

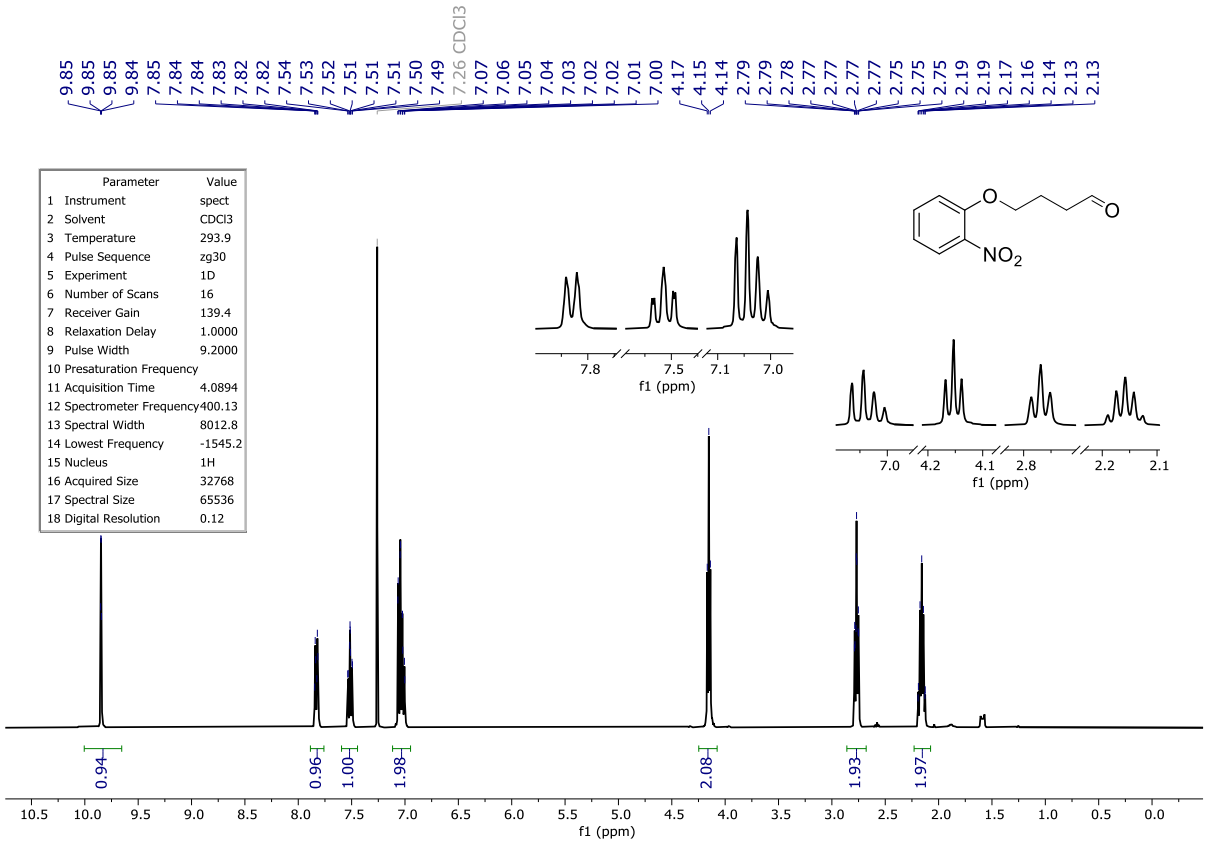

Figure S47. ^{1}H NMR spectrum ($CDCl_3$, 400 MHz) of 4-(2-nitrophenoxy)butanal – **S2**

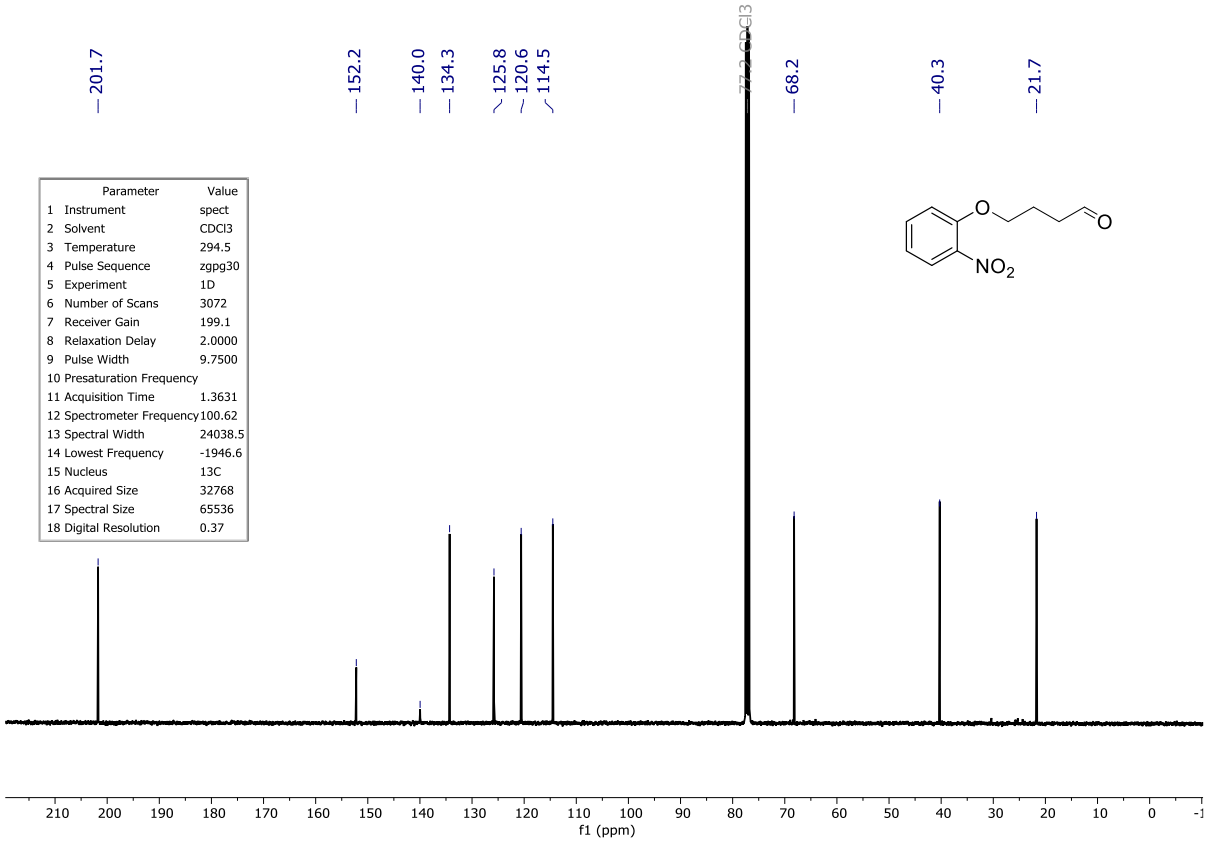

Figure S48. ^{13}C NMR spectrum ($CDCl_3$, 101 MHz) of 4-(2-nitrophenoxy)butanal – **S2**

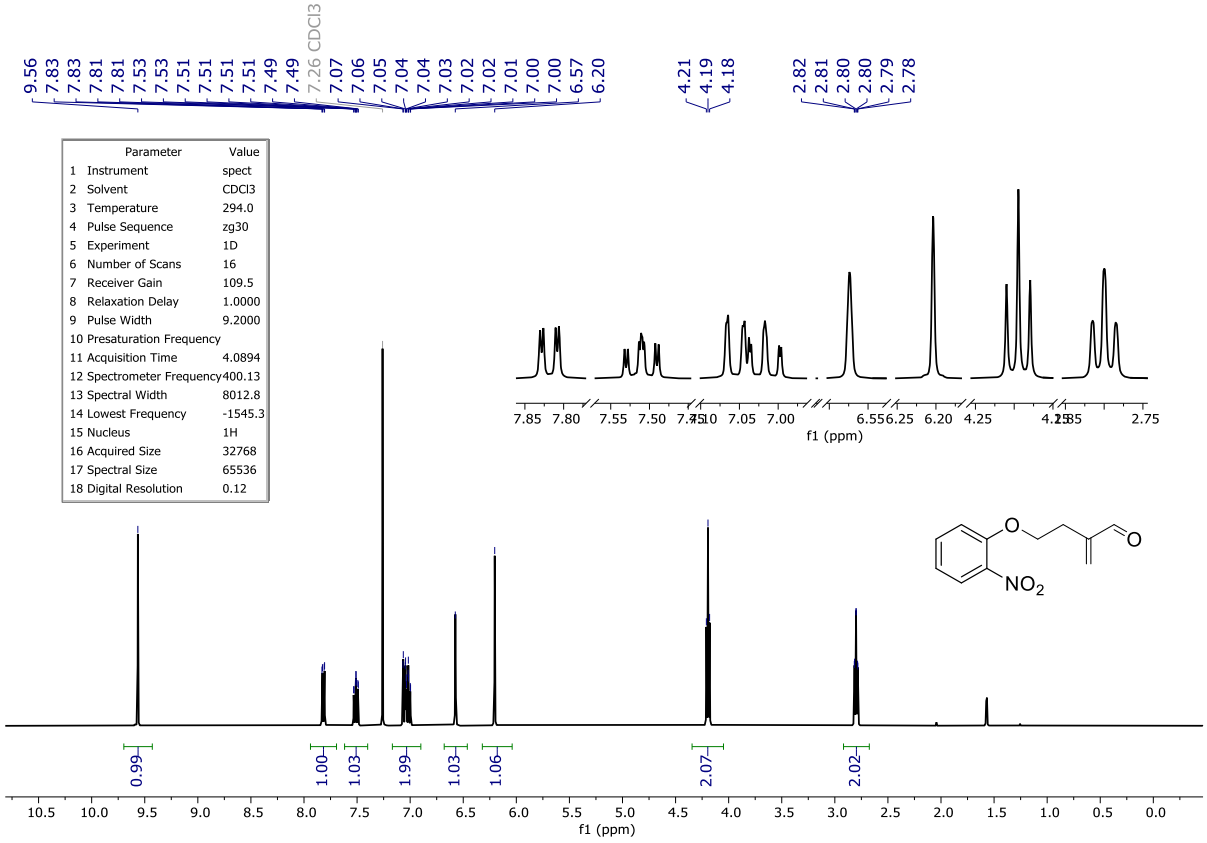

Figure S49. ^{1}H NMR spectrum ($CDCl_3$, 400 MHz) of 2-methylene-4-(2-nitrophenoxy)butanal – **S3**

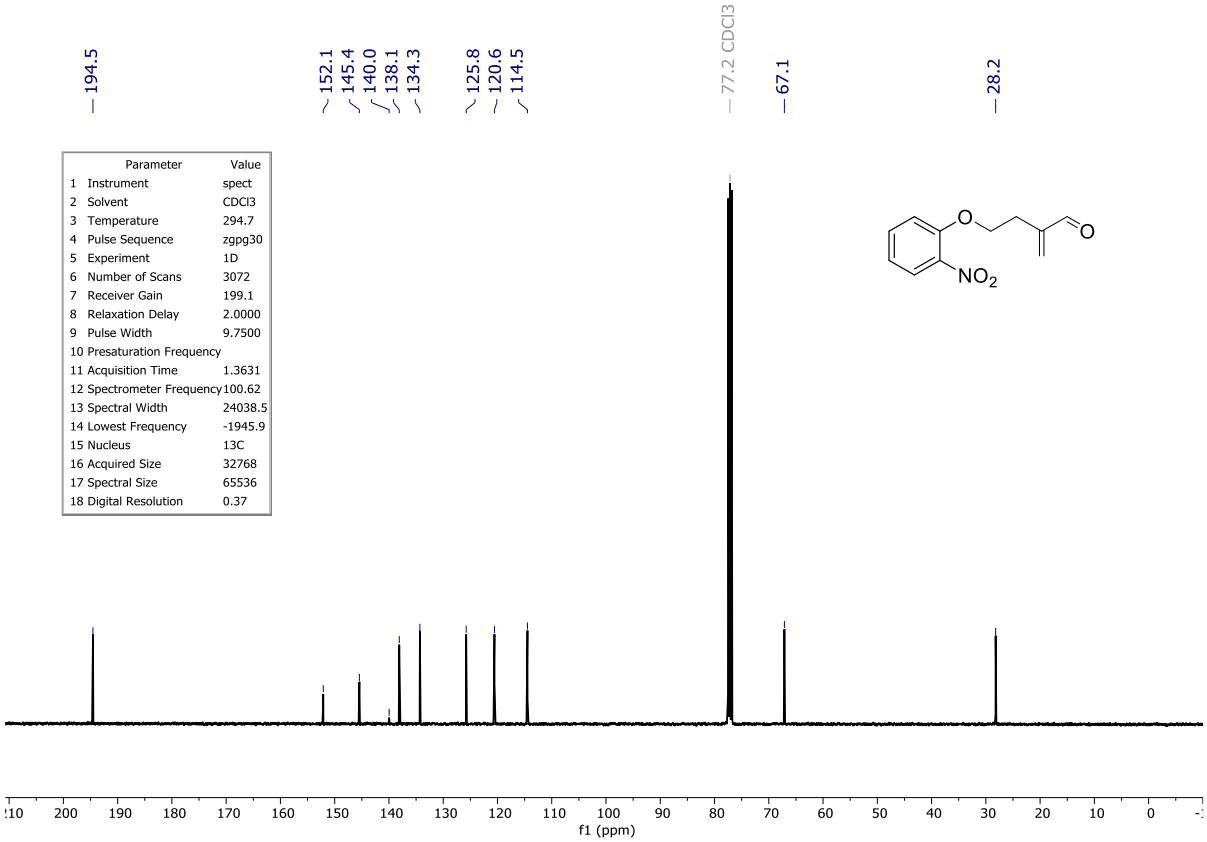

Figure S50. ^{13}C NMR spectrum ($CDCl_3$, 101 MHz) of 2-methylene-4-(2-nitrophenoxy)butanal – **S3**

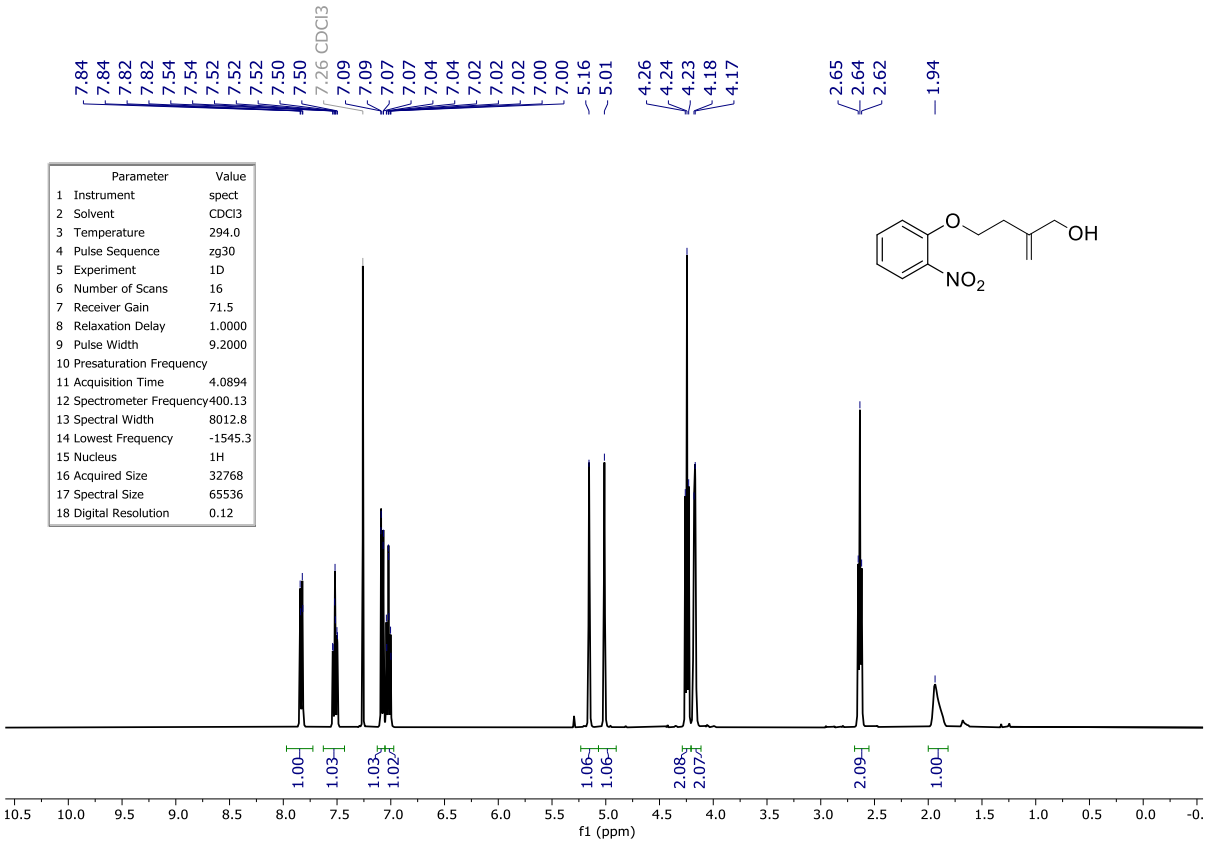

Figure S51. ^{1}H NMR spectrum ($CDCl_3$, 400 MHz) of 2-(((2-nitrobenzyl)oxy)methyl)prop-2-en-1-ol – **1m**

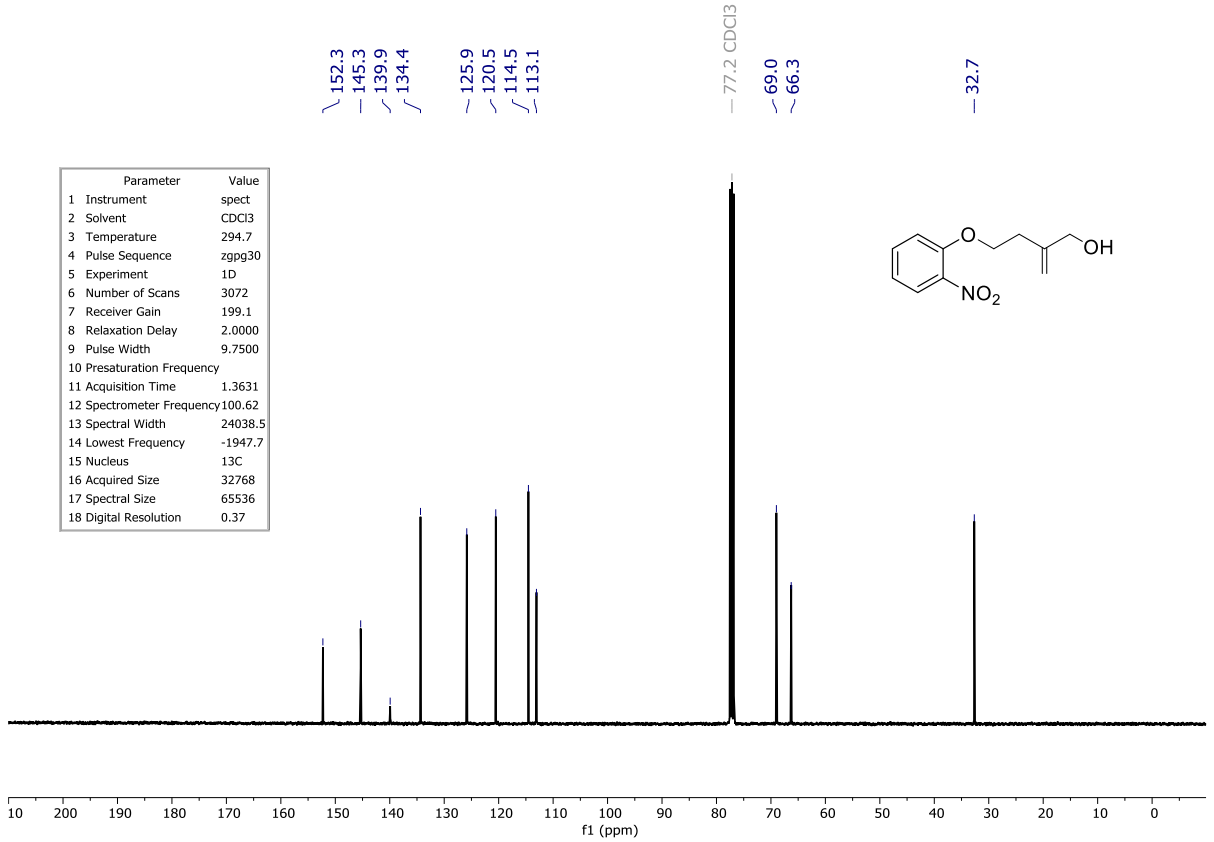

Figure S52. ^{13}C NMR spectrum ($CDCl_3$, 101 MHz) 2-(((2-nitrobenzyl)oxy)methyl)prop-2-en-1-ol – **1m**

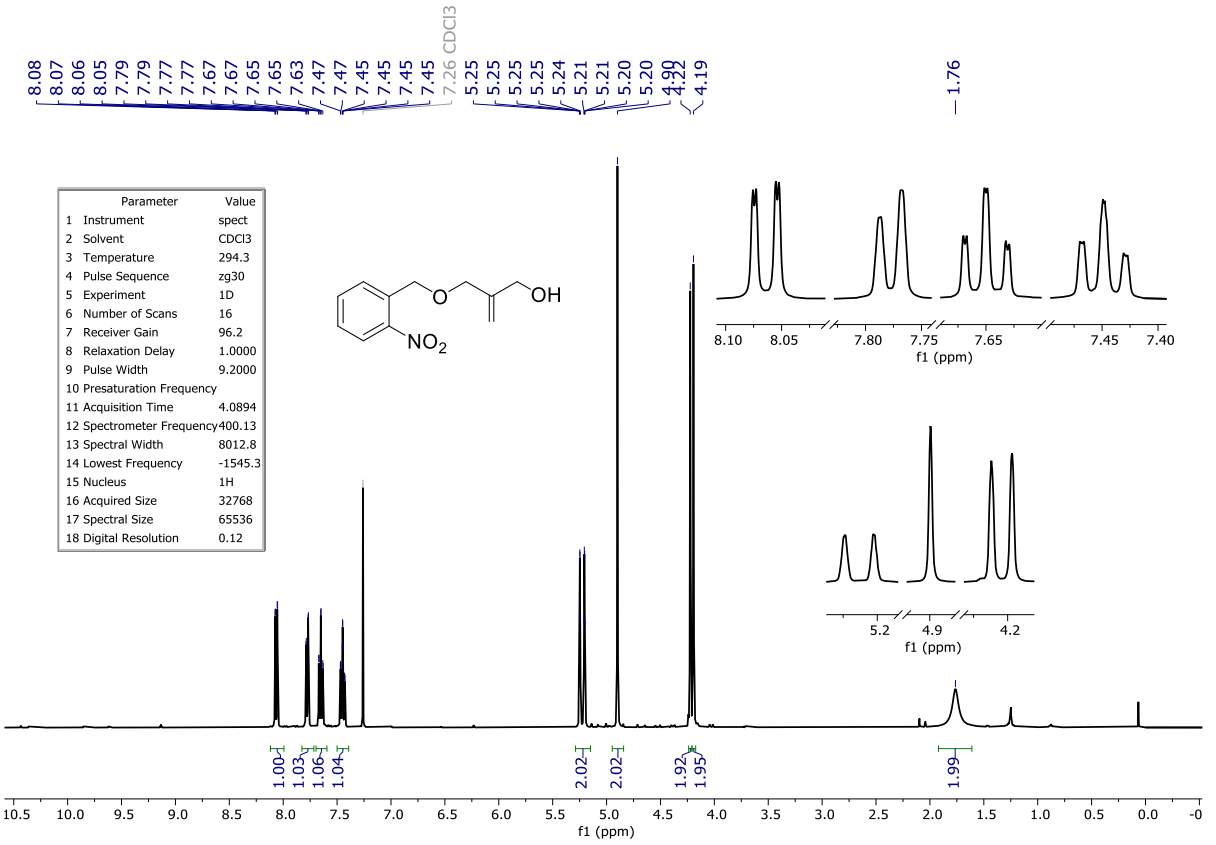

Figure S53. ^{1}H NMR spectrum ($CDCl_3$, 400 MHz) of 2-(((2-nitrobenzyl)oxy)methyl)prop-2-en-1-ol – **1n**

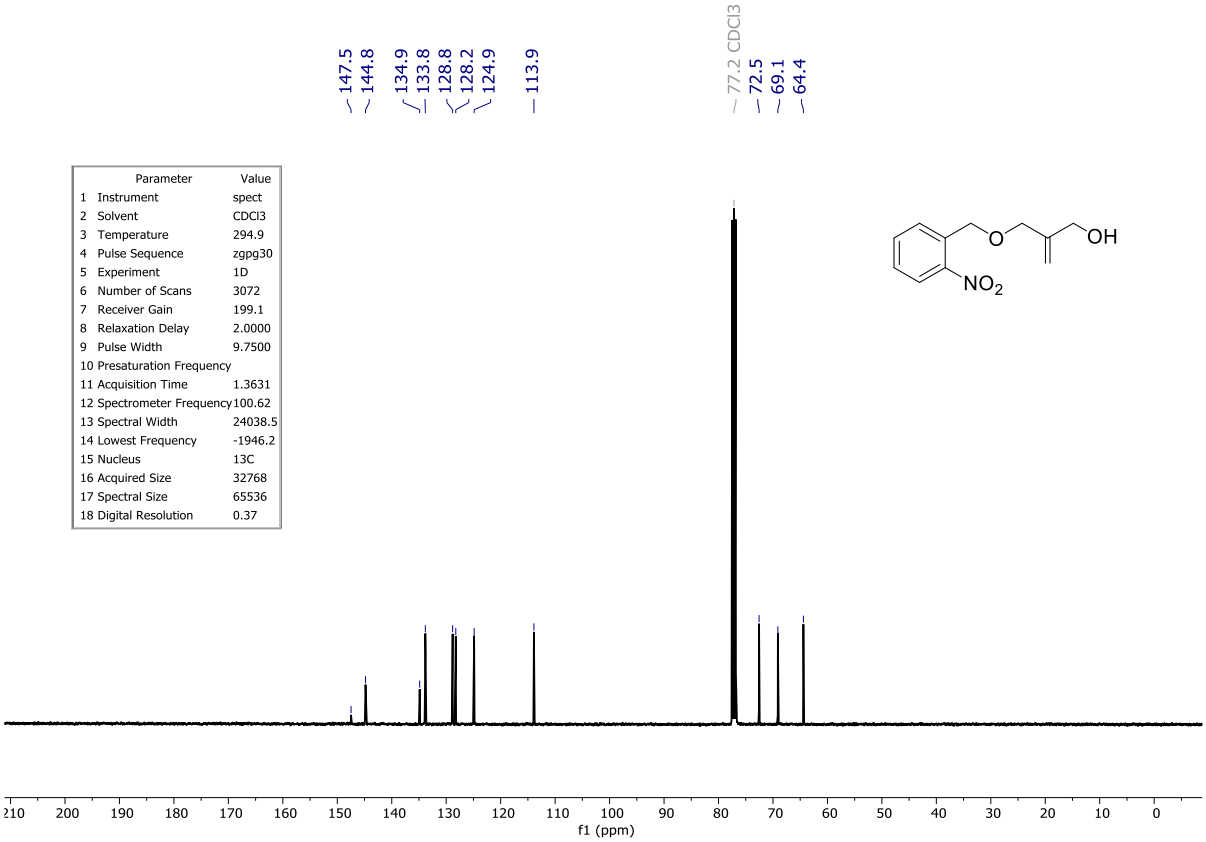

Figure S54. ^{13}C NMR spectrum ($CDCl_3$, 101 MHz) of 2-(((2-nitrobenzyl)oxy)methyl)prop-2-en-1-ol – **1n**

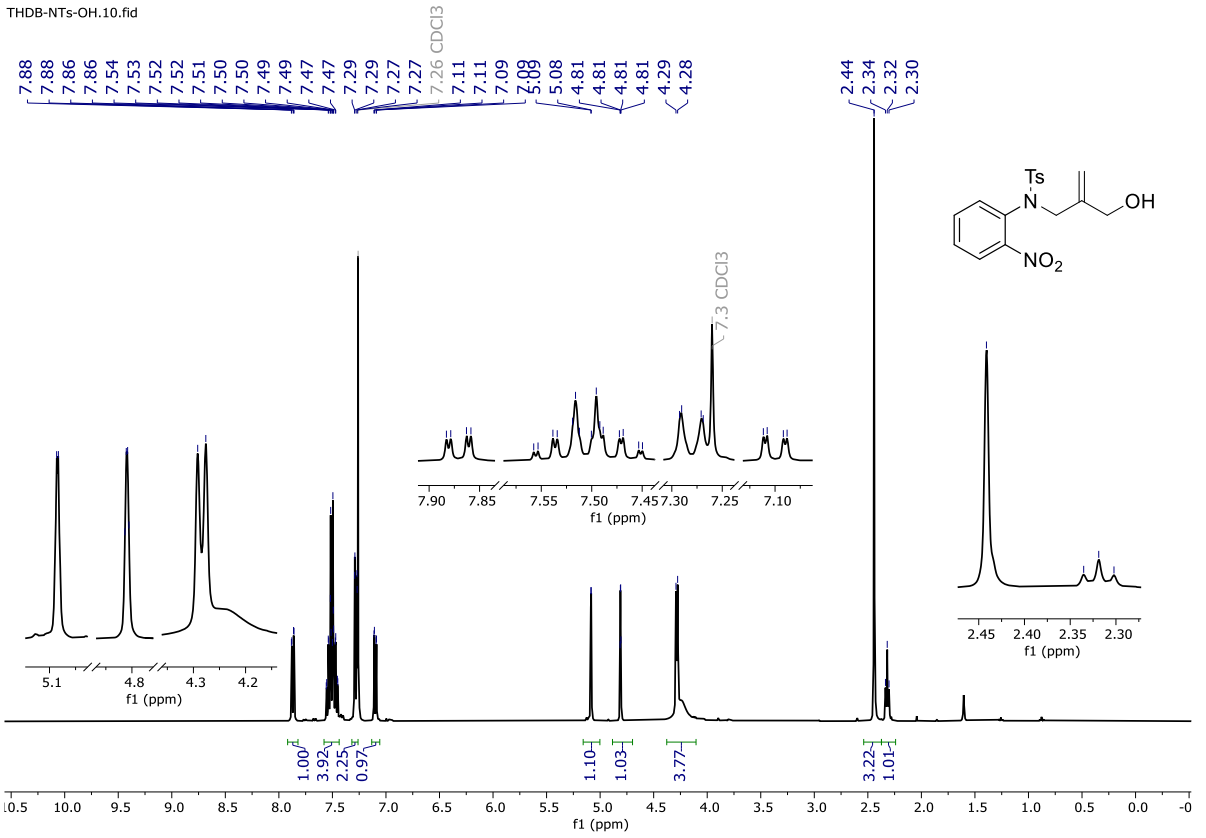

Figure S55. ^{1}H NMR spectrum ($CDCl_3$, 400 MHz) of *N*-(2-(hydroxymethyl)allyl)-4-methyl-*N*-(2-nitrophenyl)benzenesulfonamide – **1o**

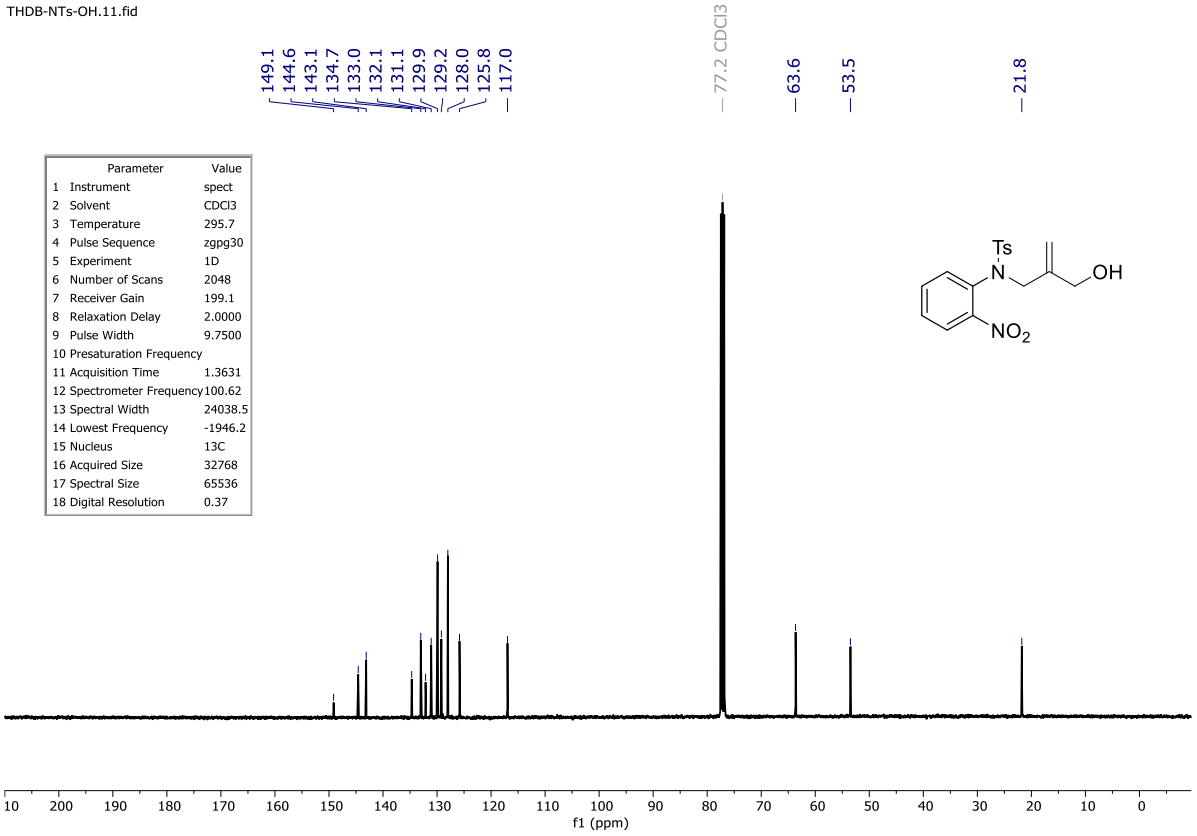

Figure S56. ^{13}C NMR spectrum ($CDCl_3$, 101 MHz) of *N*-(2-(hydroxymethyl)allyl)-4-methyl-*N*-(2-nitrophenyl)benzenesulfonamide – **1o**

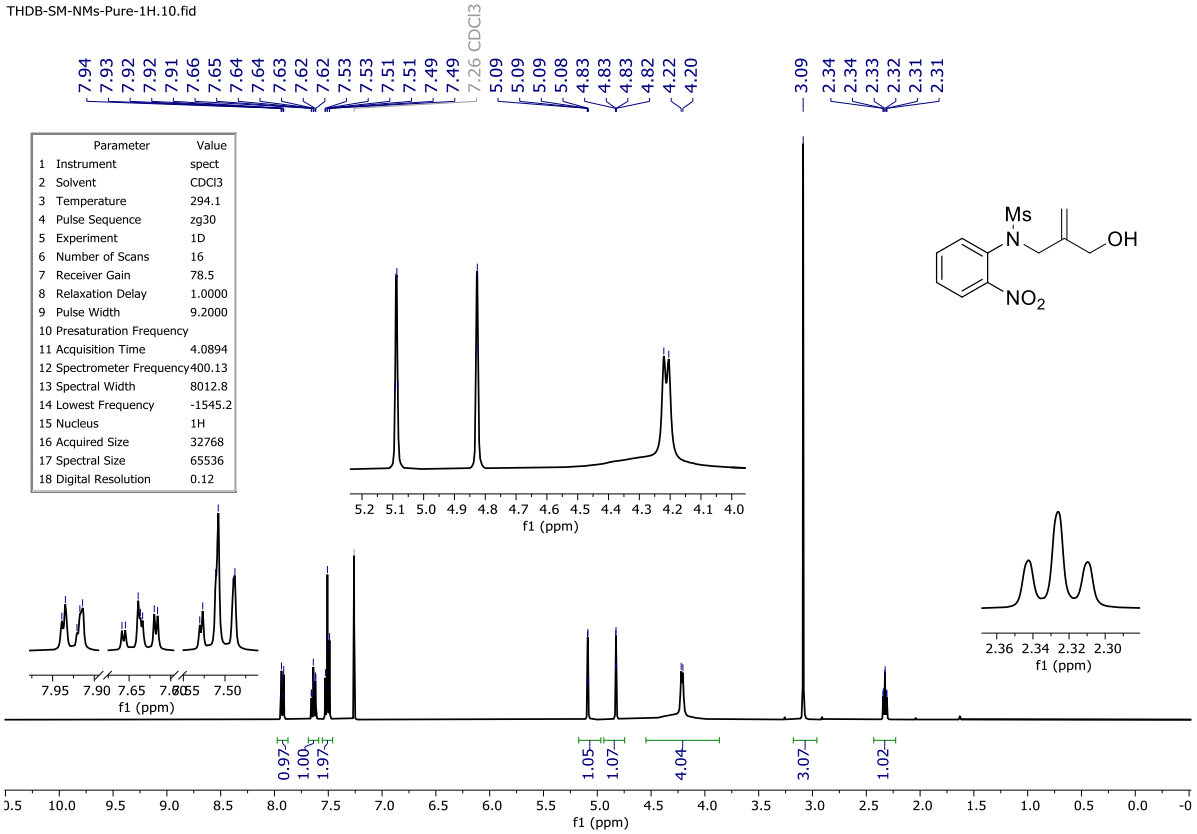

Figure S57. ^{1}H NMR spectrum ($CDCl_3$, 400 MHz) of *N*-(2-(hydroxymethyl)allyl)-*N*-(2-nitrophenyl)methanesulfonamide – **1p**

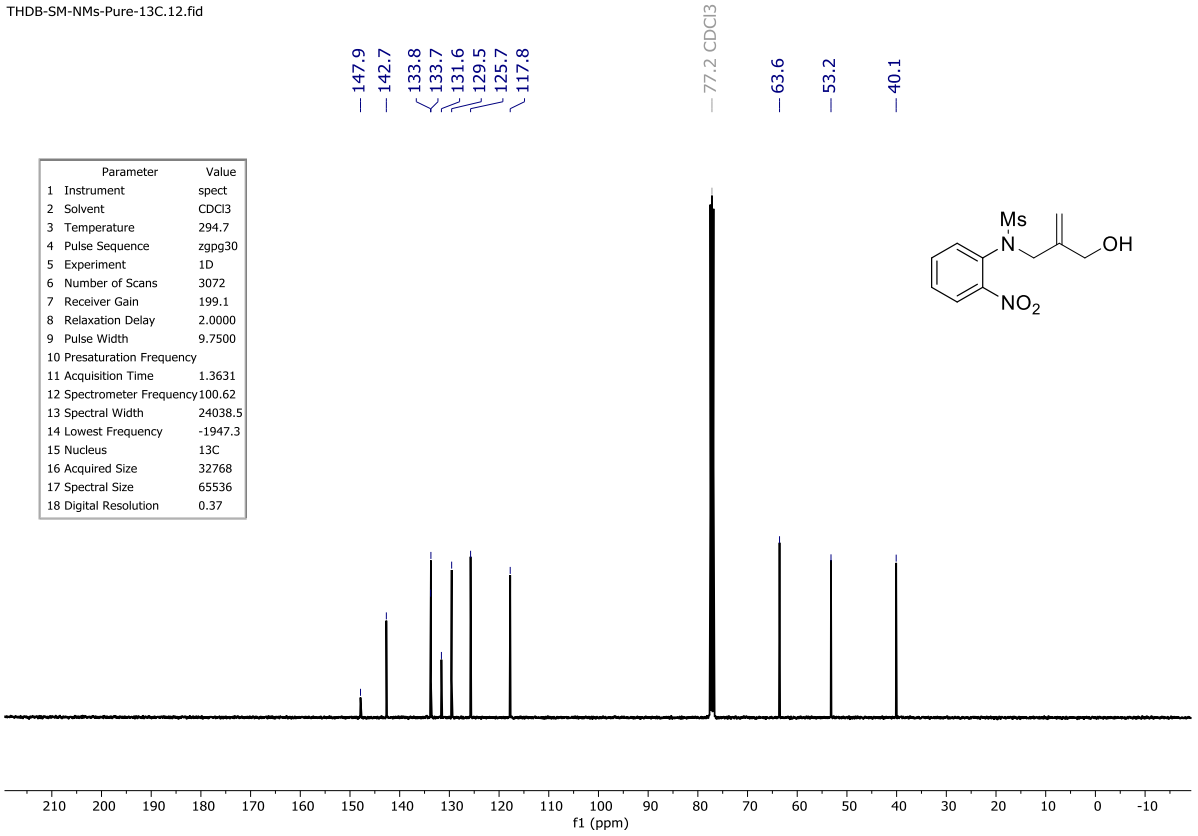

Figure S58. ^{13}C NMR spectrum ($CDCl_3$, 101 MHz) of *N*-(2-(hydroxymethyl)allyl)-*N*-(2-nitrophenyl)methanesulfonamide – **1p**

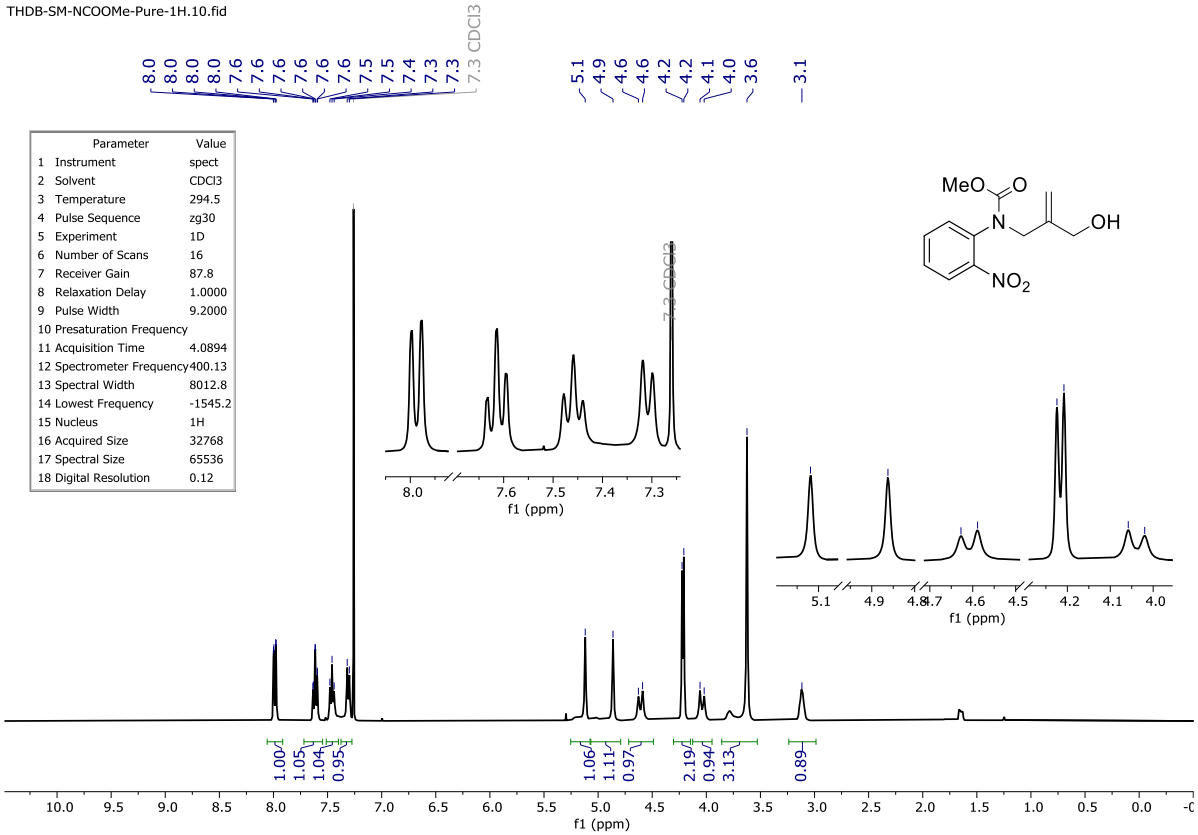

Figure S59. ^{1}H NMR spectrum ($CDCl_3$, 400 MHz) of Methyl (2-(hydroxymethyl)allyl)(2-nitrophenyl)carbamate – **1q**

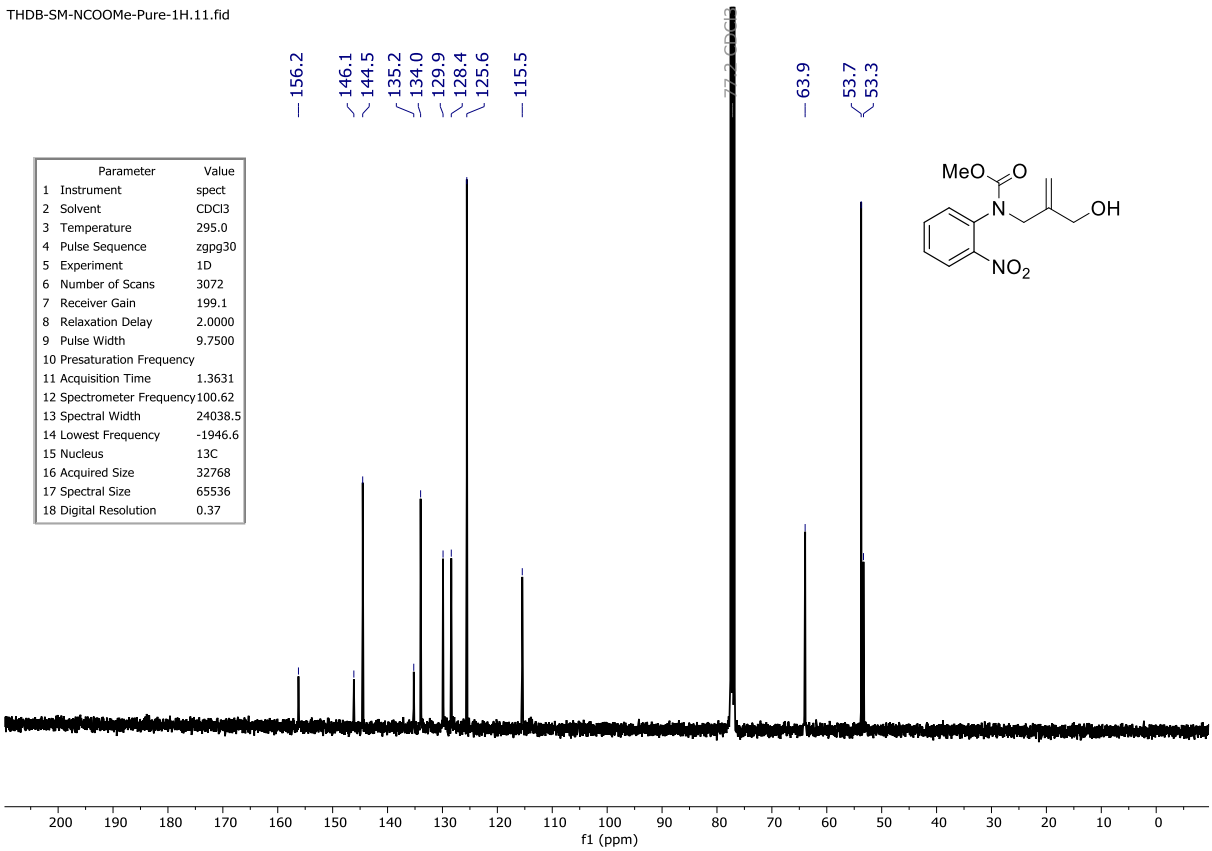

Figure S60. ^{13}C NMR spectrum ($CDCl_3$, 101 MHz) of Methyl (2-(hydroxymethyl)allyl)(2-nitrophenyl)carbamate – **1q**

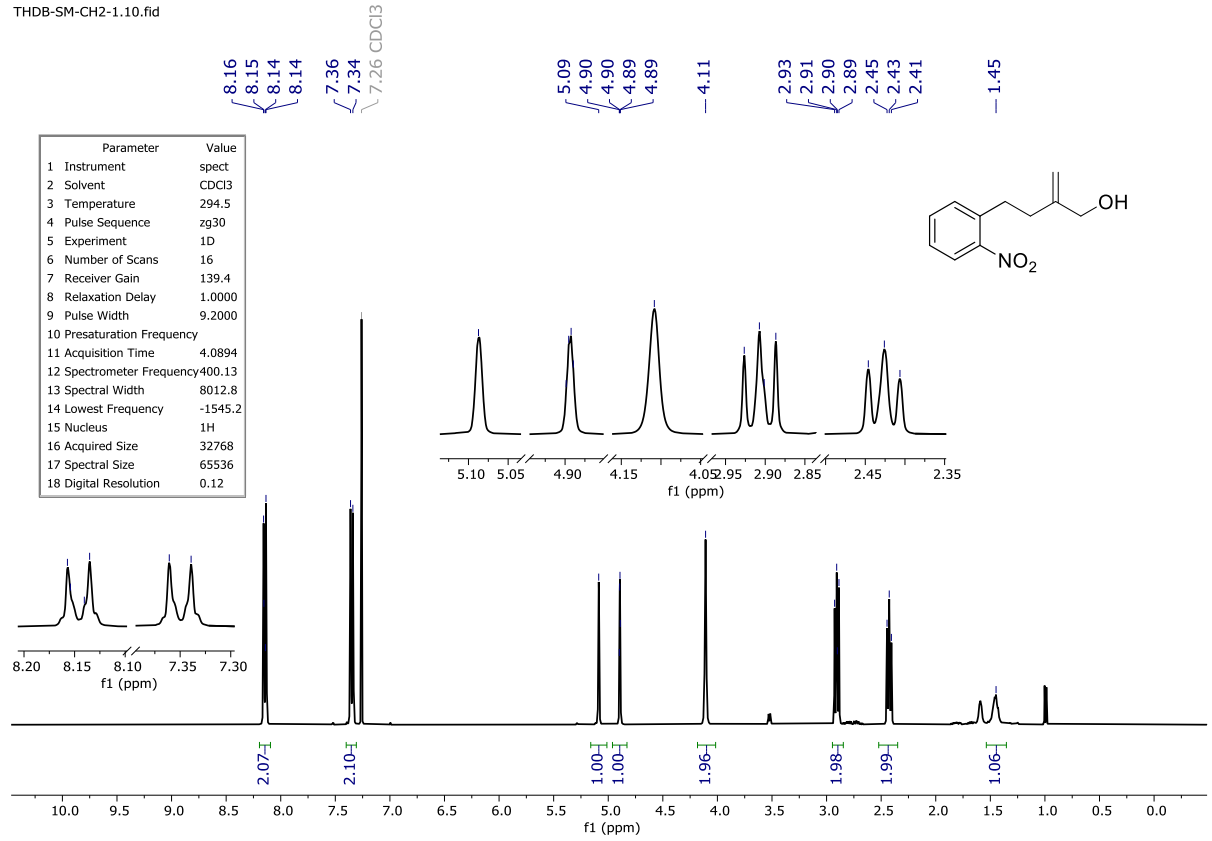

Figure S61. ^{1}H NMR spectrum ($CDCl_3$, 400 MHz) of 2-methylene-4-(2-nitrophenyl)butan-1-ol – **1r**

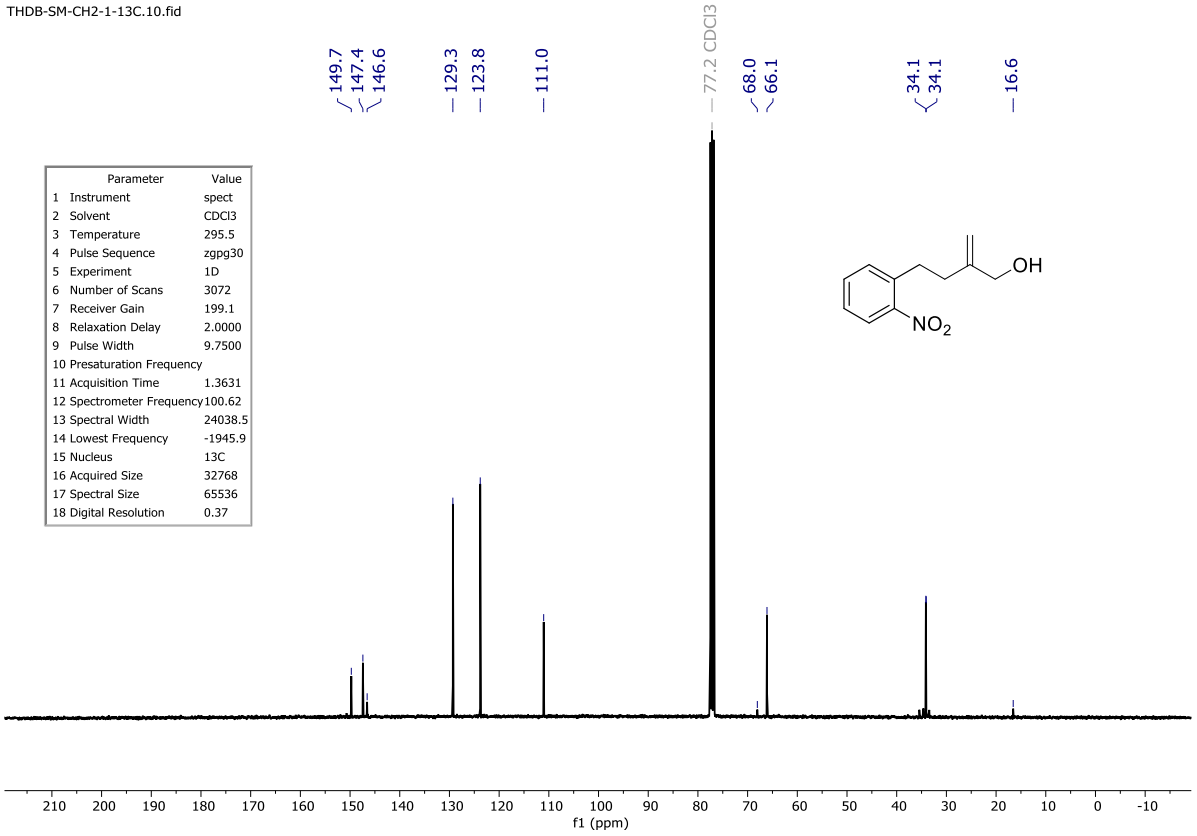

Figure S62. ^{13}C NMR spectrum ($CDCl_3$, 101 MHz) of 2-methylene-4-(2-nitrophenyl)butan-1-ol – **1r**

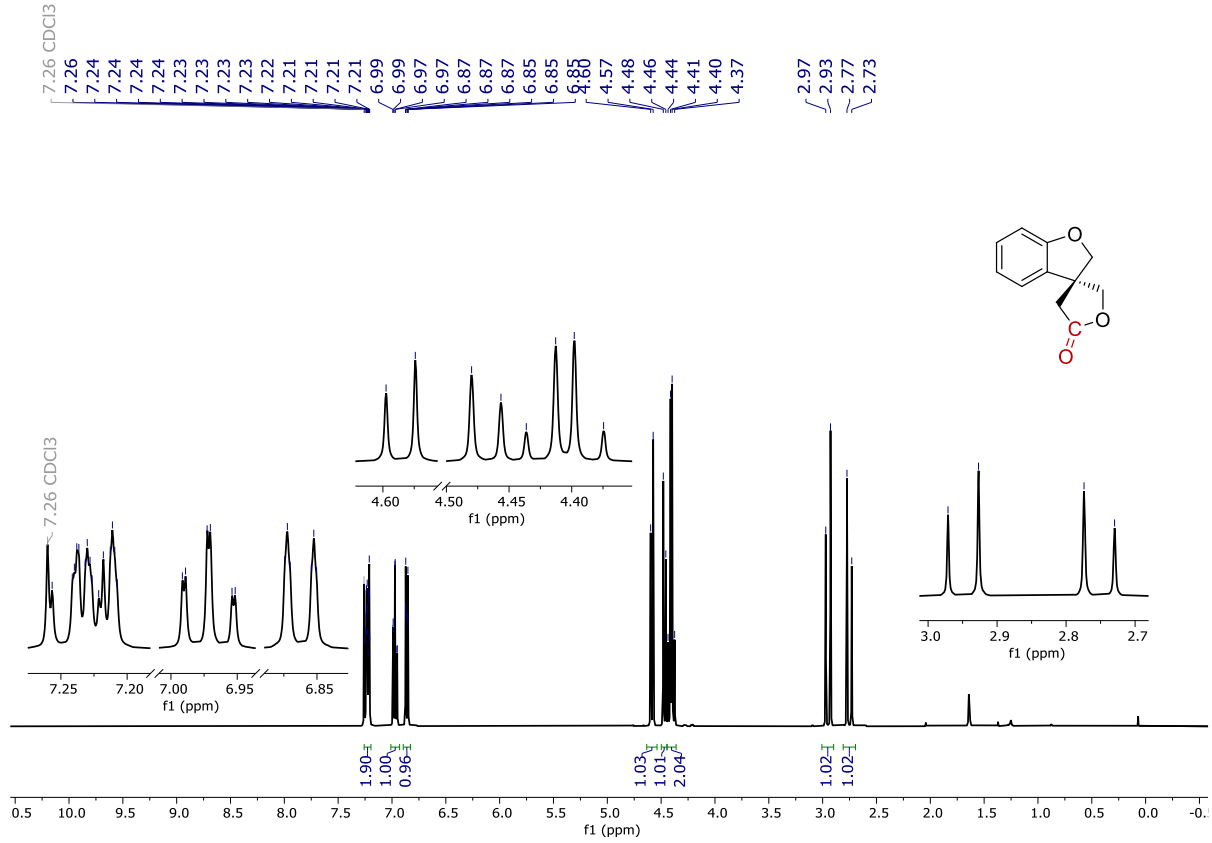

Figure S63. ^{1}H NMR spectrum ($CDCl_3$, 400 MHz) of (*R*)-2*H*,2'*H*-spiro[benzofuran-3,3'-furan]-5'(4'*H*)-one – **3a**

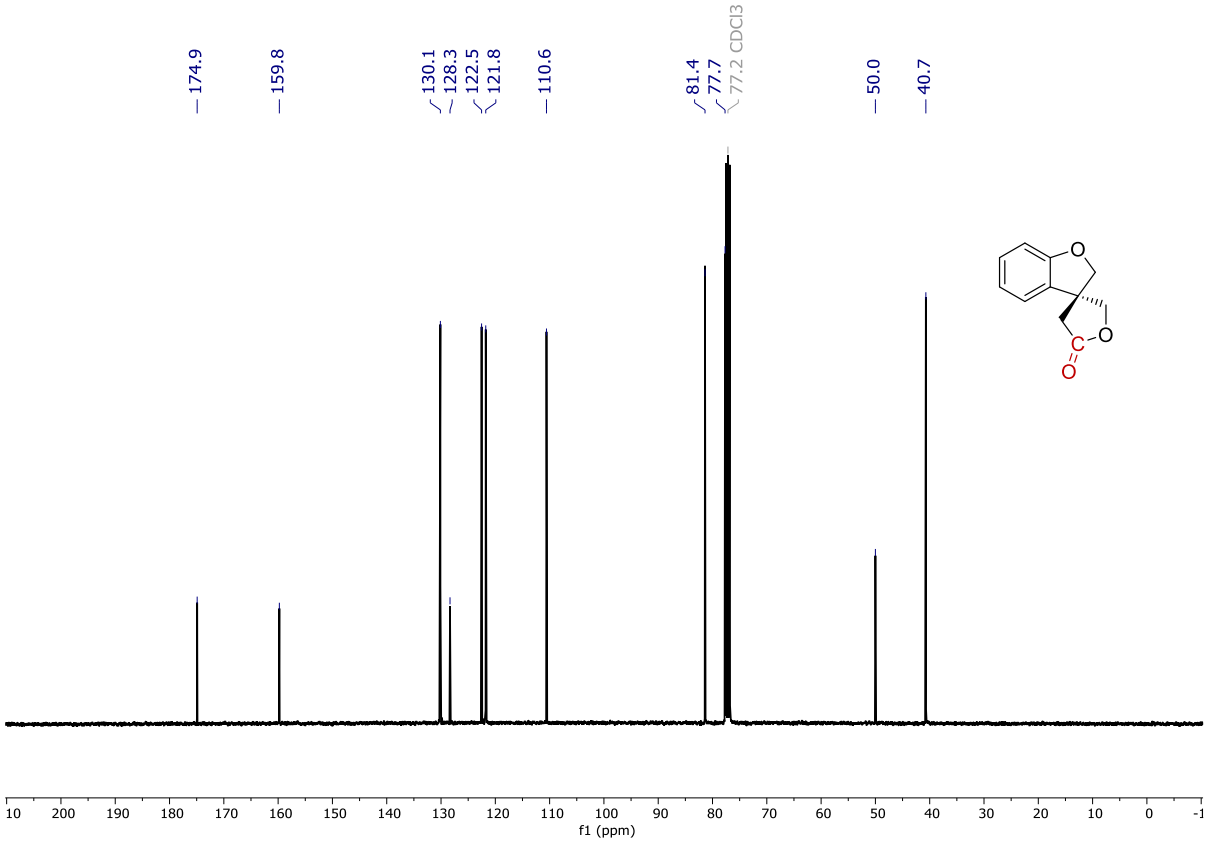

Figure S64. ^{13}C NMR spectrum ($CDCl_3$, 101 MHz) of (*R*)-2*H*,2'*H*-spiro[benzofuran-3,3'-furan]-5'(4'*H*)-one – **3a**

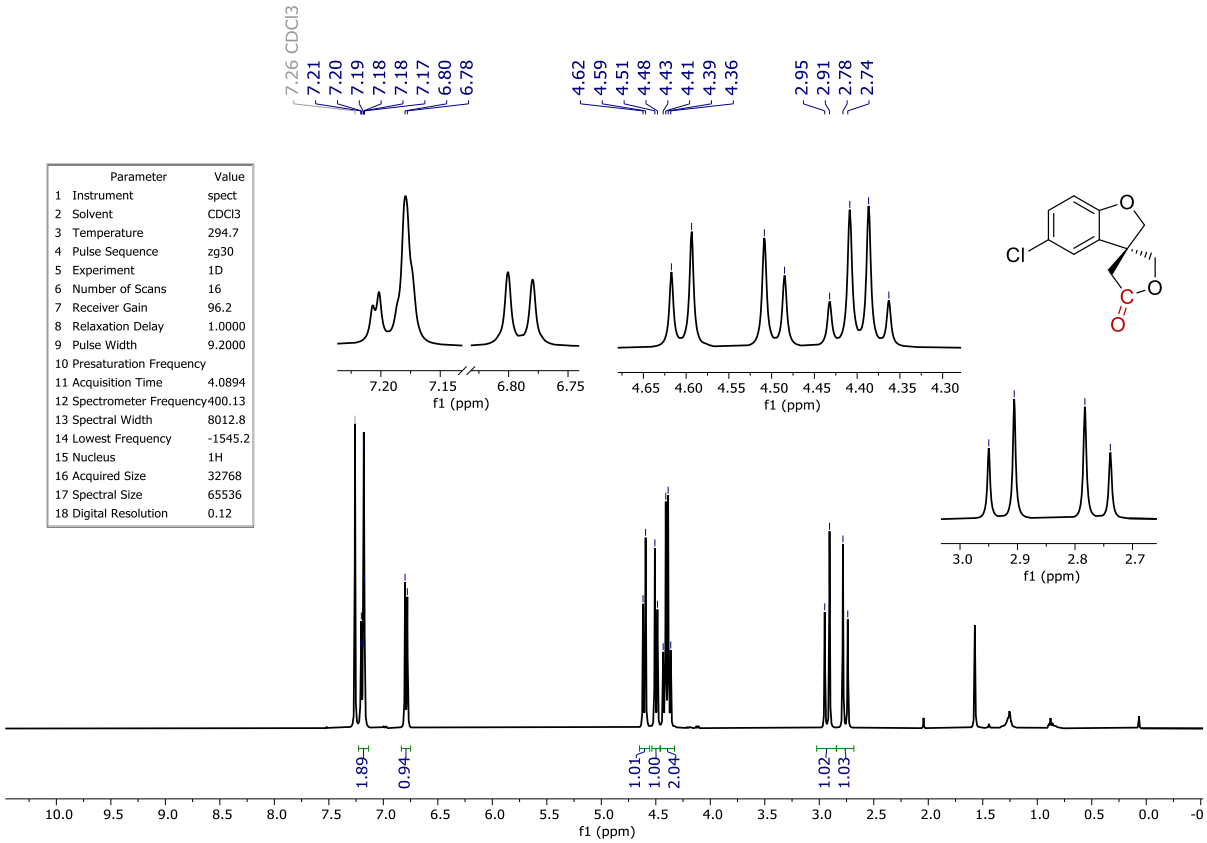

Figure S65. ^{1}H NMR spectrum ($CDCl_3$, 400 MHz) of (*R*)-5-chloro-2H,2'H-spiro[benzofuran-3,3'-furan]-5'(4'H)-one – **3b**

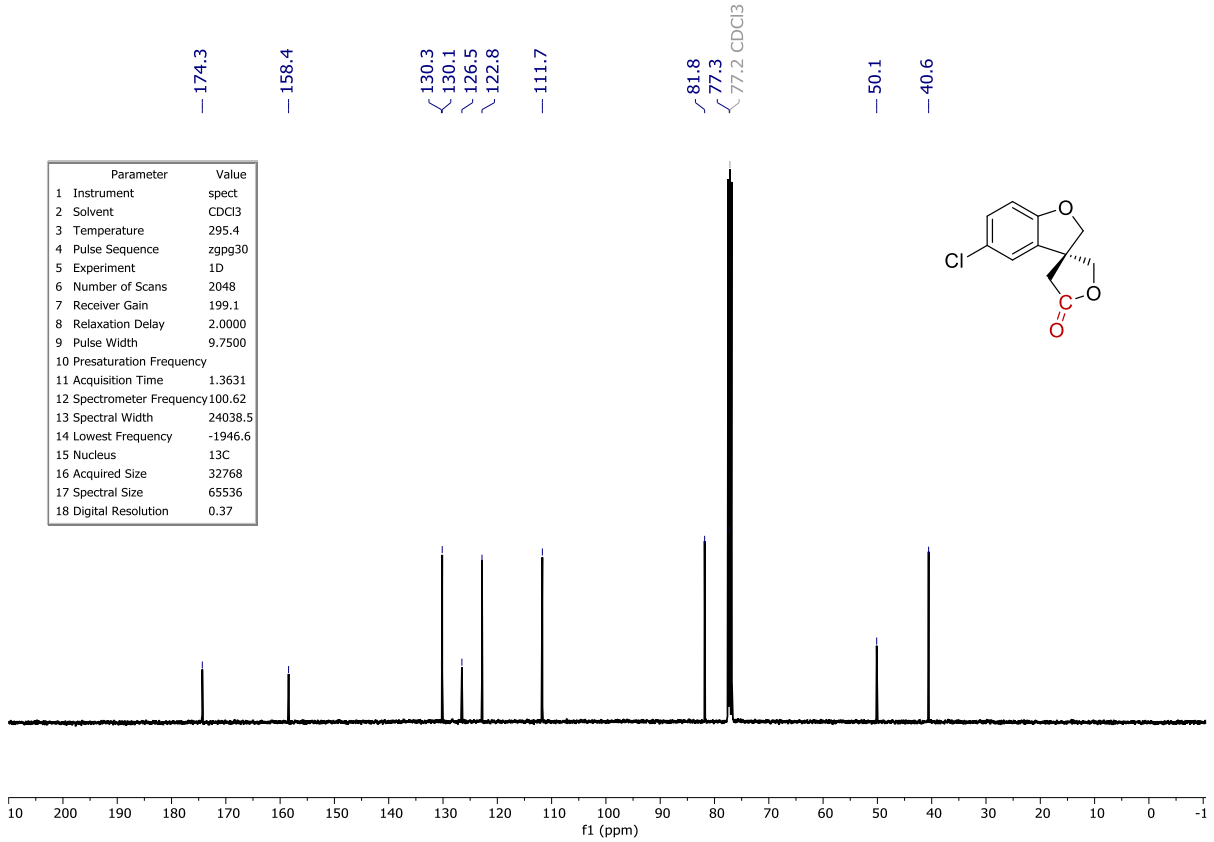

Figure S66. ^{13}C NMR spectrum ($CDCl_3$, 101 MHz) of (*R*)-5-chloro-2H,2'H-spiro[benzofuran-3,3'-furan]-5'(4'H)-one – **3b**

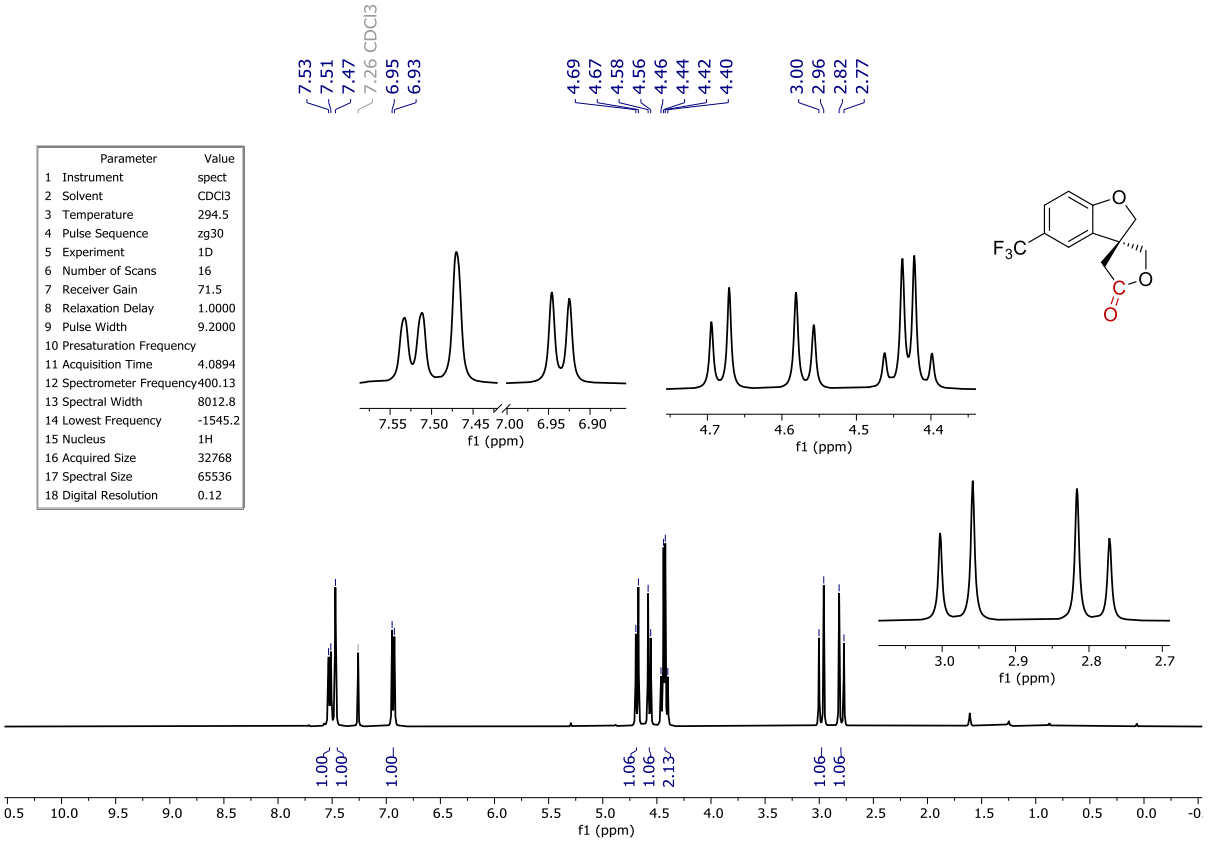

Figure S67. ^{1}H NMR spectrum ($CDCl_3$, 400 MHz) of (*R*)-5-(trifluoromethyl)-2*H*,2'*H*-spiro[benzofuran-3,3'-furan]-5'(4'H)-one – **3c**

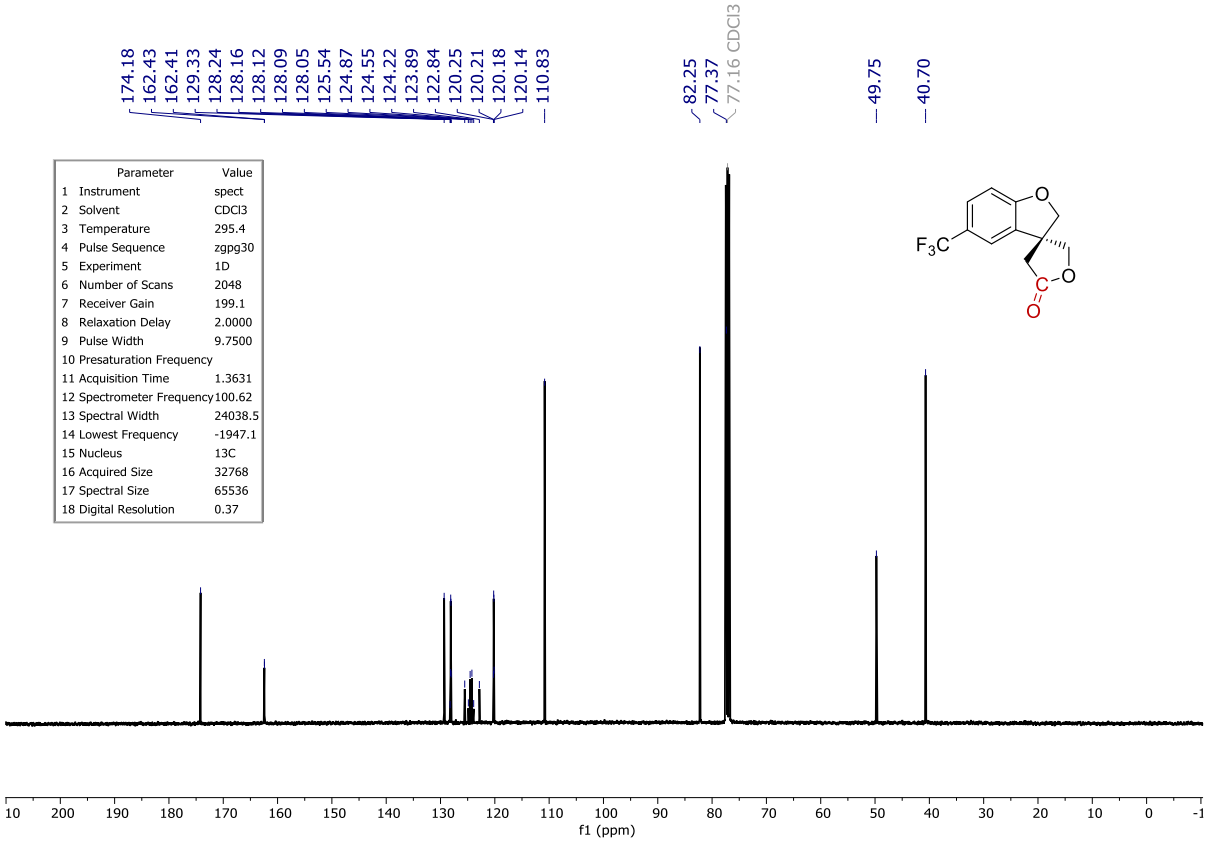

Figure S68. ^{13}C NMR spectrum ($CDCl_3$, 101 MHz) of (*R*)-5-(trifluoromethyl)-2*H*,2'*H*-spiro[benzofuran-3,3'-furan]-5'(4'H)-one – **3c**

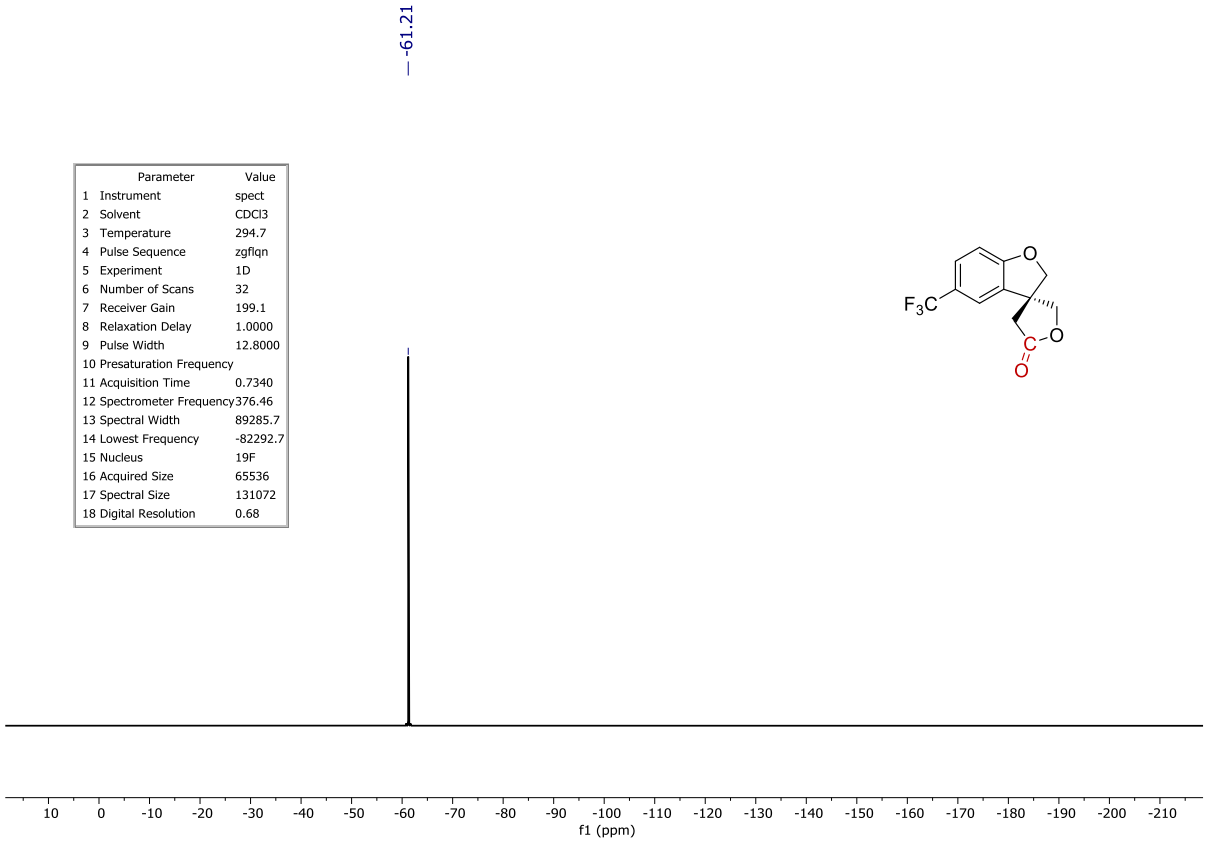

Figure S69. ^{19}F NMR spectrum (376 MHz, $CDCl_3$) of (*R*)-5-(trifluoromethyl)-2*H*,2'*H*-spiro[benzofuran-3,3'-furan]-5'(4'H)-one – **3c**

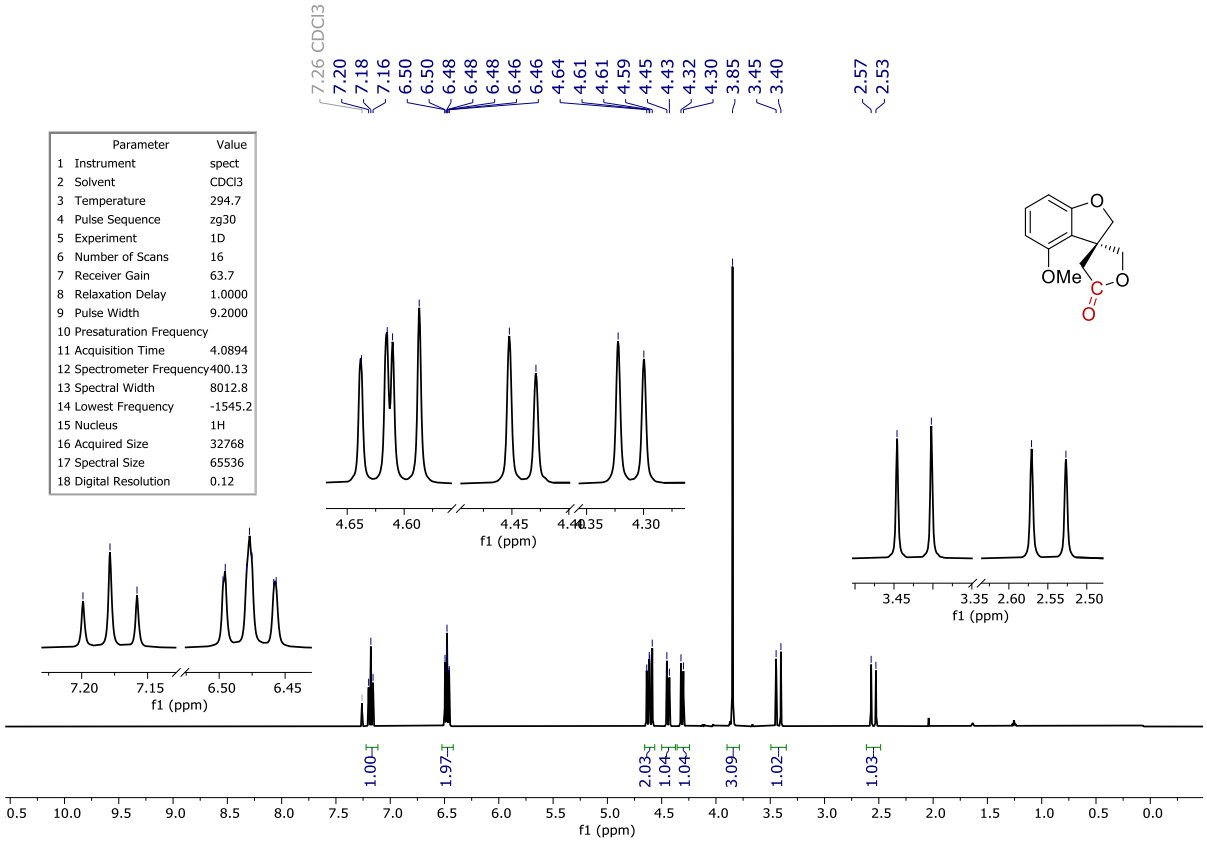

Figure S70. ^{1}H NMR spectrum ($CDCl_3$, 400 MHz) of (*R*)-4-methoxy-2*H*,2'*H*-spiro[benzofuran-3,3'-furan]-5'(4'*H*)-one – **3d**

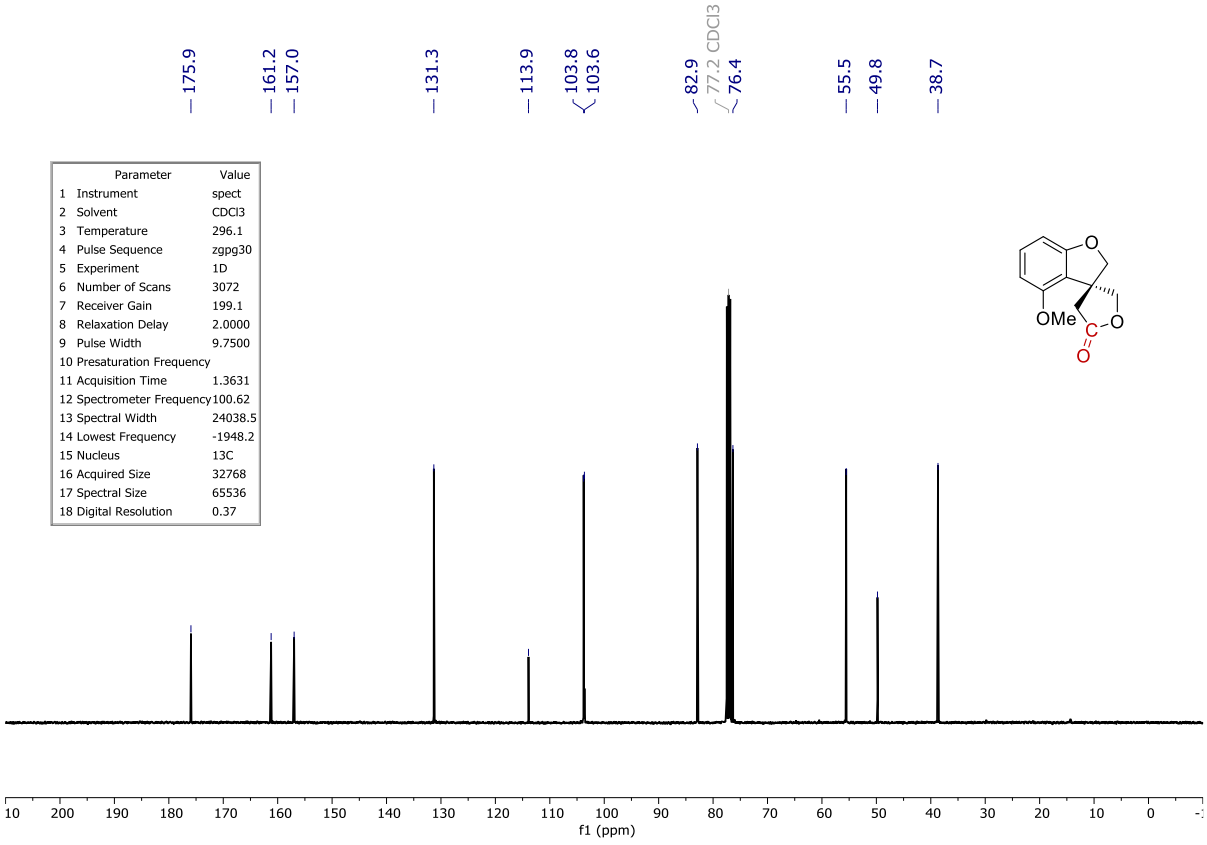

Figure S71. ^{13}C NMR spectrum ($CDCl_3$, 101 MHz) of (*R*)-4-methoxy-2*H*,2'*H*-spiro[benzofuran-3,3'-furan]-5'(4'*H*)-one – **3d**

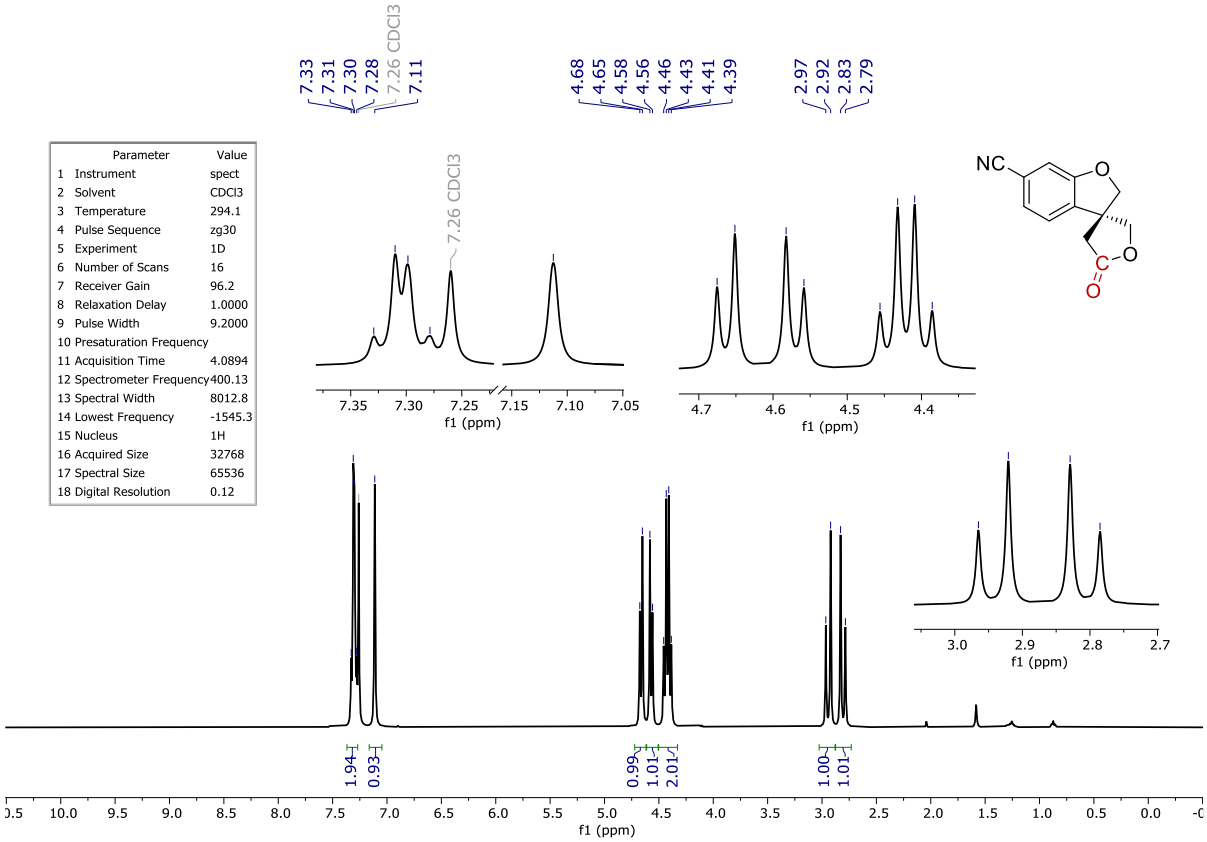

Figure S72. ^{1}H NMR spectrum ($CDCl_3$, 400 MHz) of (*R*)-5'-oxo-4',5'-dihydro-2*H*,2'*H*-spiro[benzofuran-3,3'-furan]-6-carbonitrile – **3e**

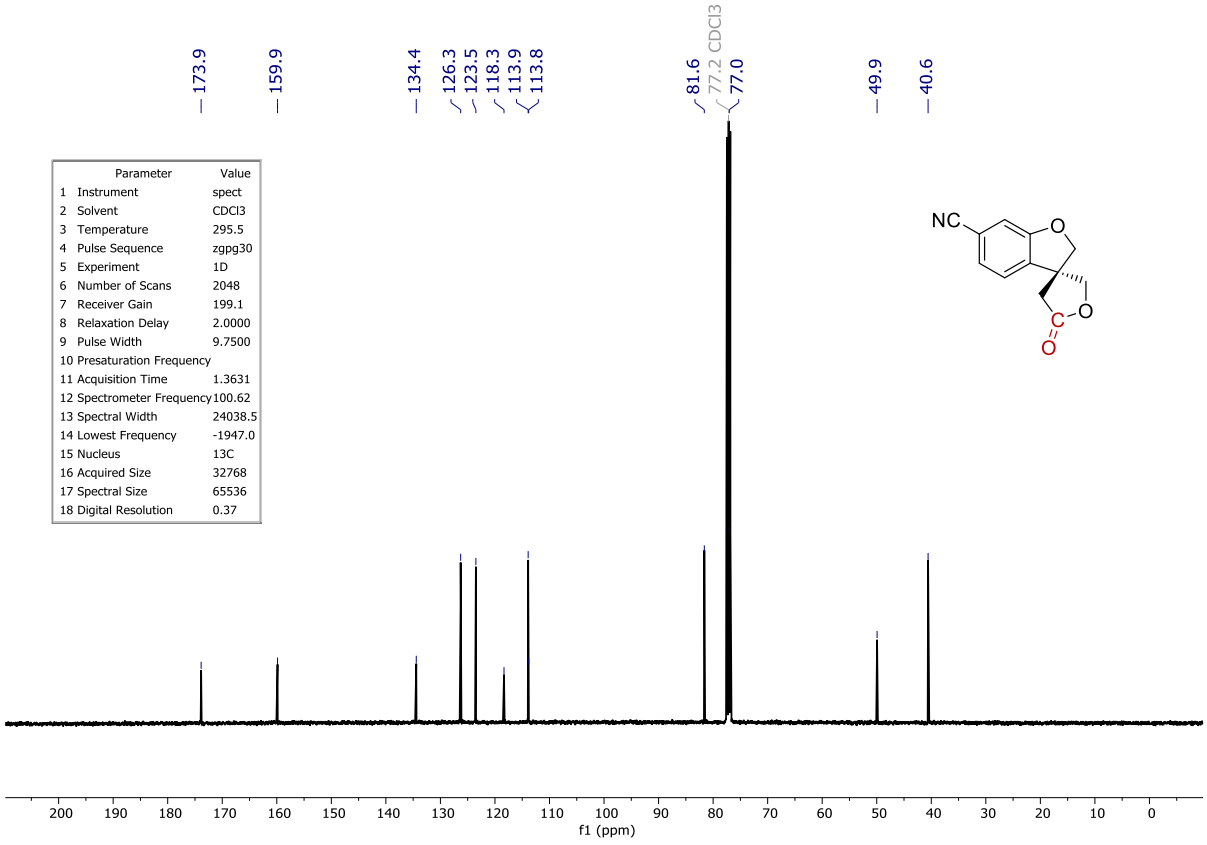

Figure S73. ^{13}C NMR spectrum ($CDCl_3$, 101 MHz) of (*R*)-5'-oxo-4',5'-dihydro-2*H*,2'*H*-spiro[benzofuran-3,3'-furan]-6-carbonitrile – **3e**

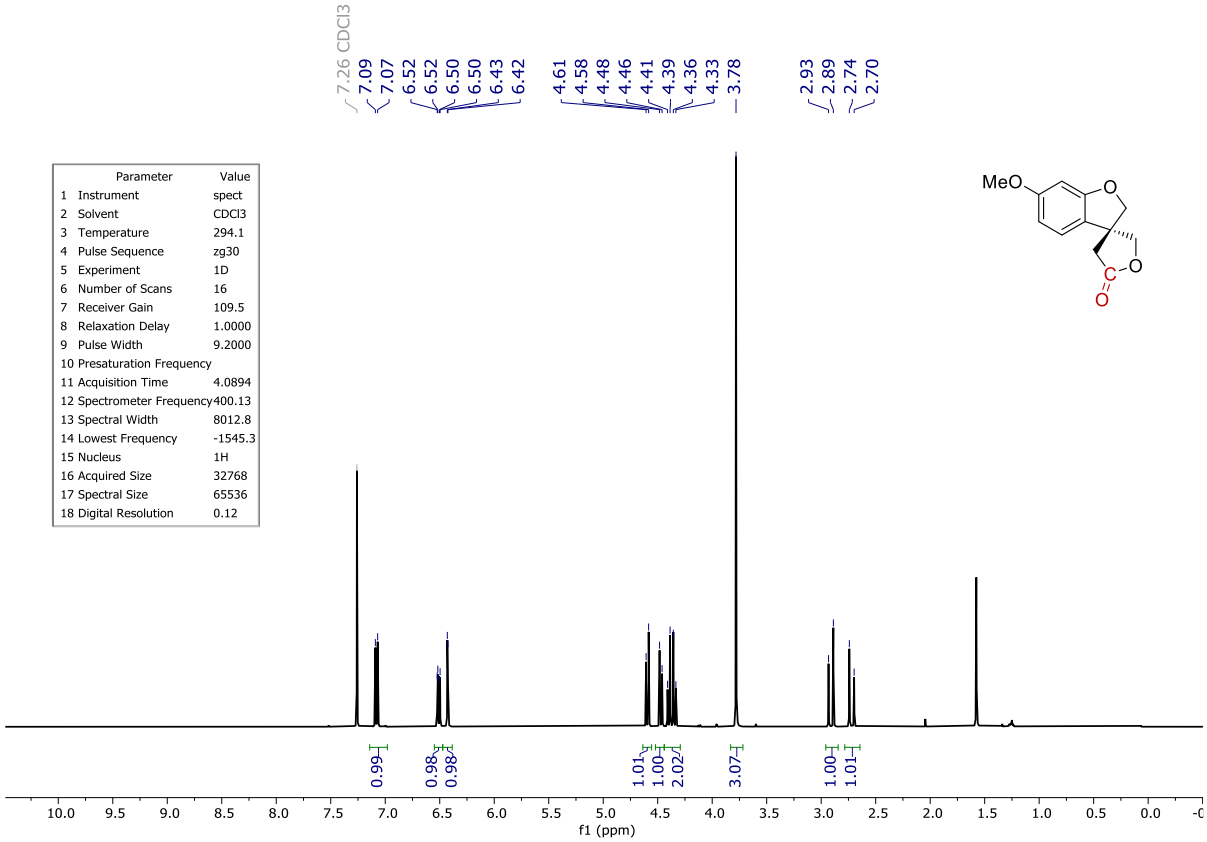

Figure S74. ^{1}H NMR spectrum ($CDCl_3$, 400 MHz) of (*R*)-6-methoxy-2*H*,2'*H*-spiro[benzofuran-3,3'-furan]-5'(4'*H*)-one – **3f**

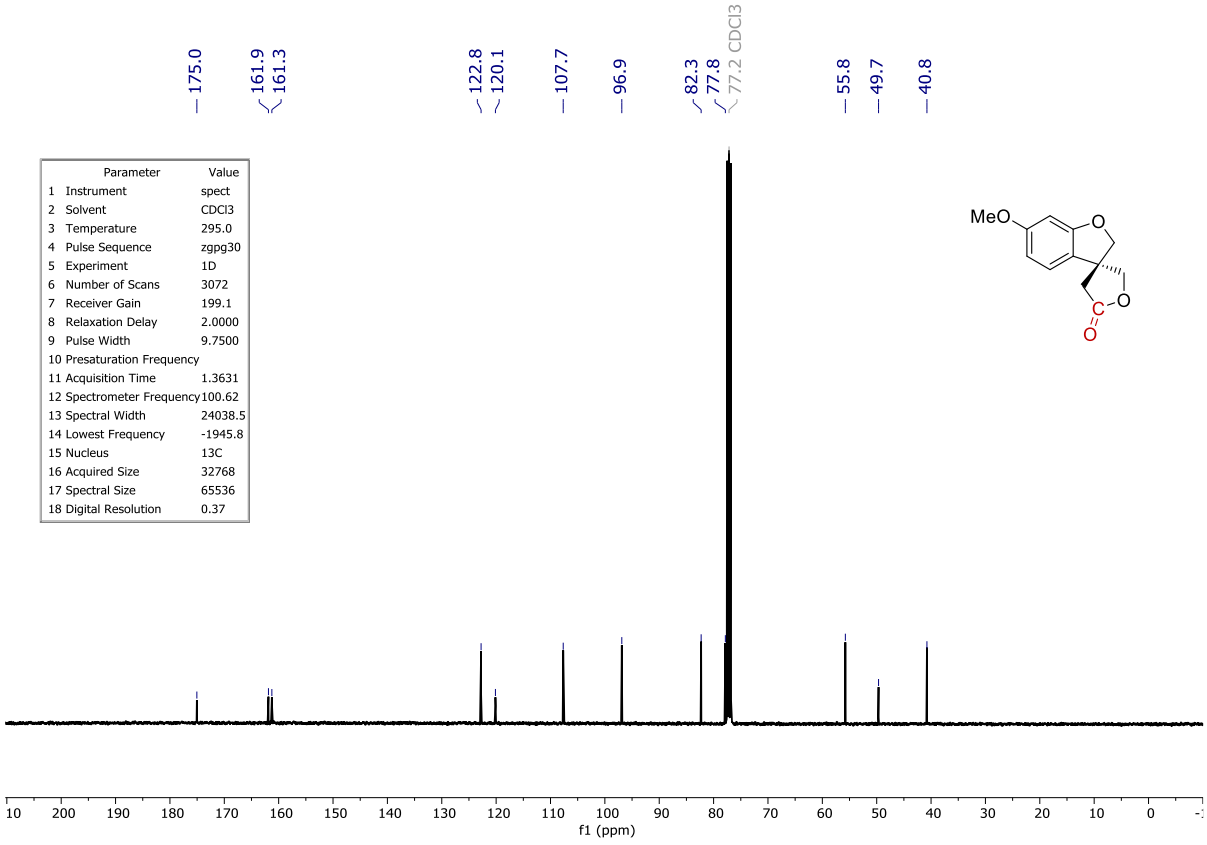

Figure S75. ^{13}C NMR spectrum ($CDCl_3$, 101 MHz) of (*R*)-6-methoxy-2*H*,2'*H*-spiro[benzofuran-3,3'-furan]-5'(4'*H*)-one – **3f**

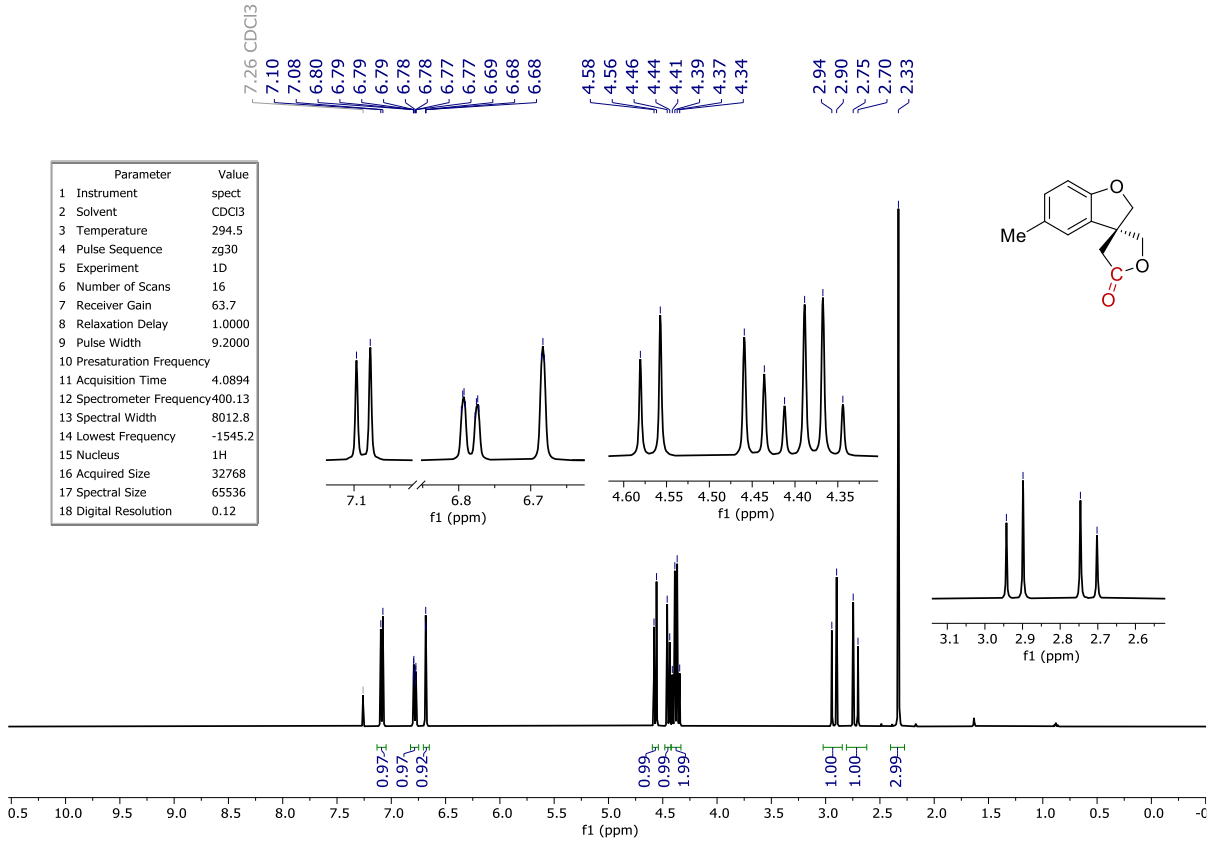

Figure S76. ^{1}H NMR spectrum ($CDCl_3$, 400 MHz) of (*R*)-5-methyl-2*H*,2'*H*-spiro[benzofuran-3,3'-furan]-5'(4'*H*)-one – **3g**

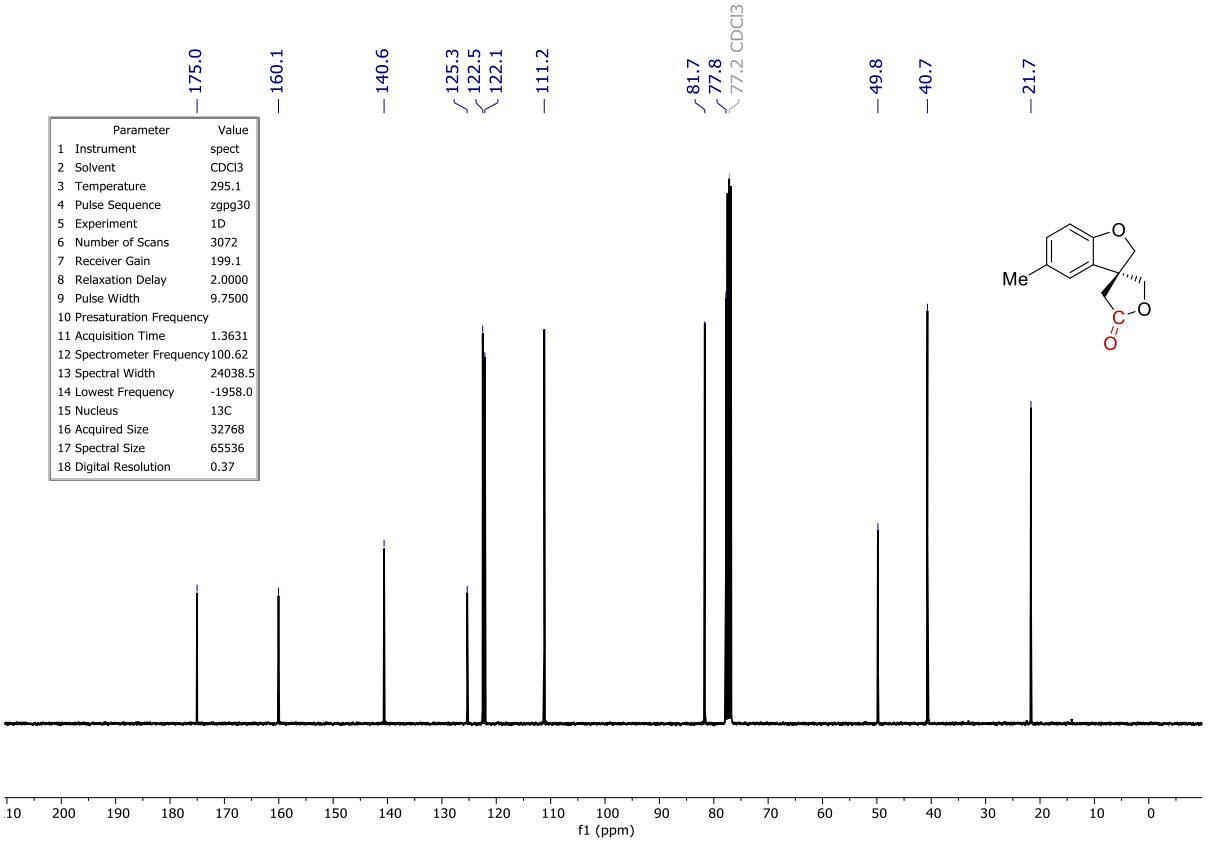

Figure S77. ^{13}C NMR spectrum ($CDCl_3$, 101 MHz) of (*R*)-5-methyl-2*H*,2'*H*-spiro[benzofuran-3,3'-furan]-5'(4'*H*)-one – **3g**

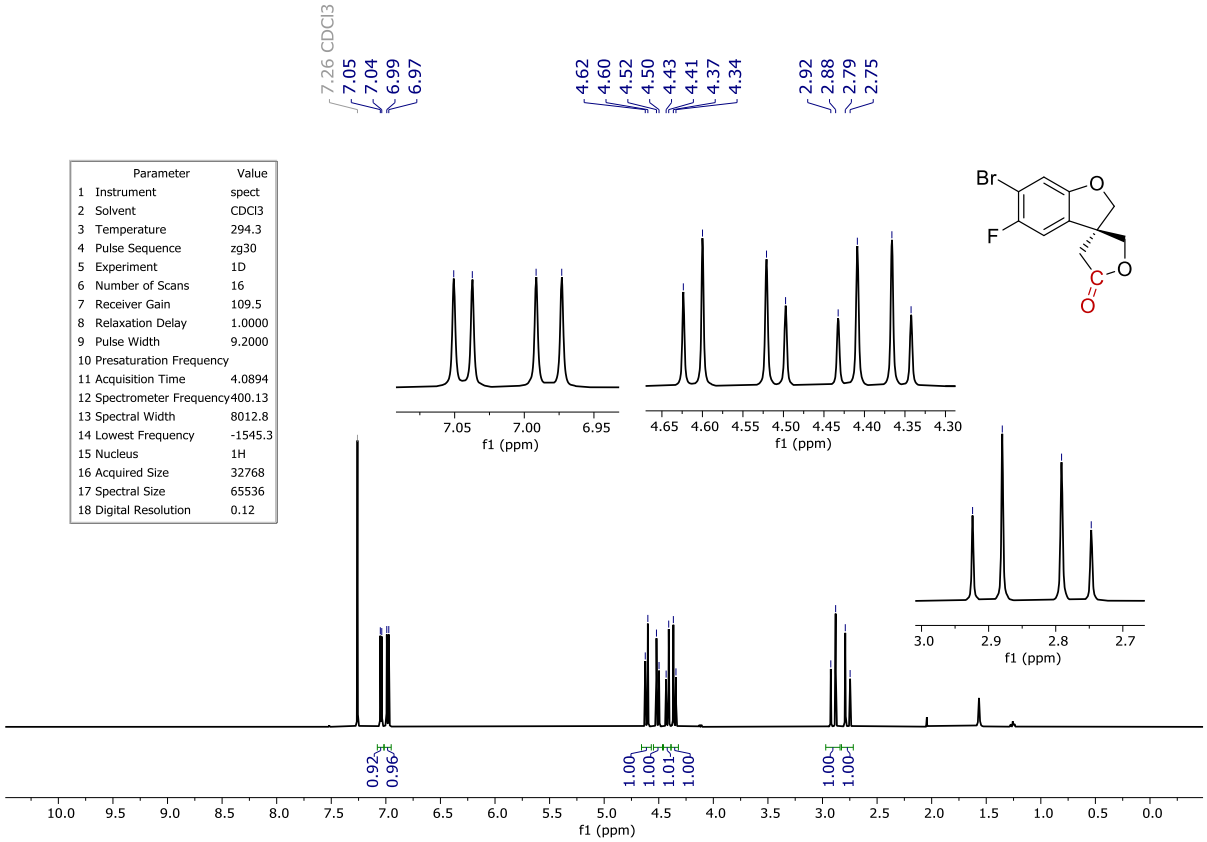

Figure S78. ^{1}H NMR spectrum ($CDCl_3$, 400 MHz) of (*S*)-6-bromo-5-fluoro-2*H*,2'*H*-spiro[benzofuran-3,3'-furan]-5'(4'*H*)-one – ***ent*-3h**

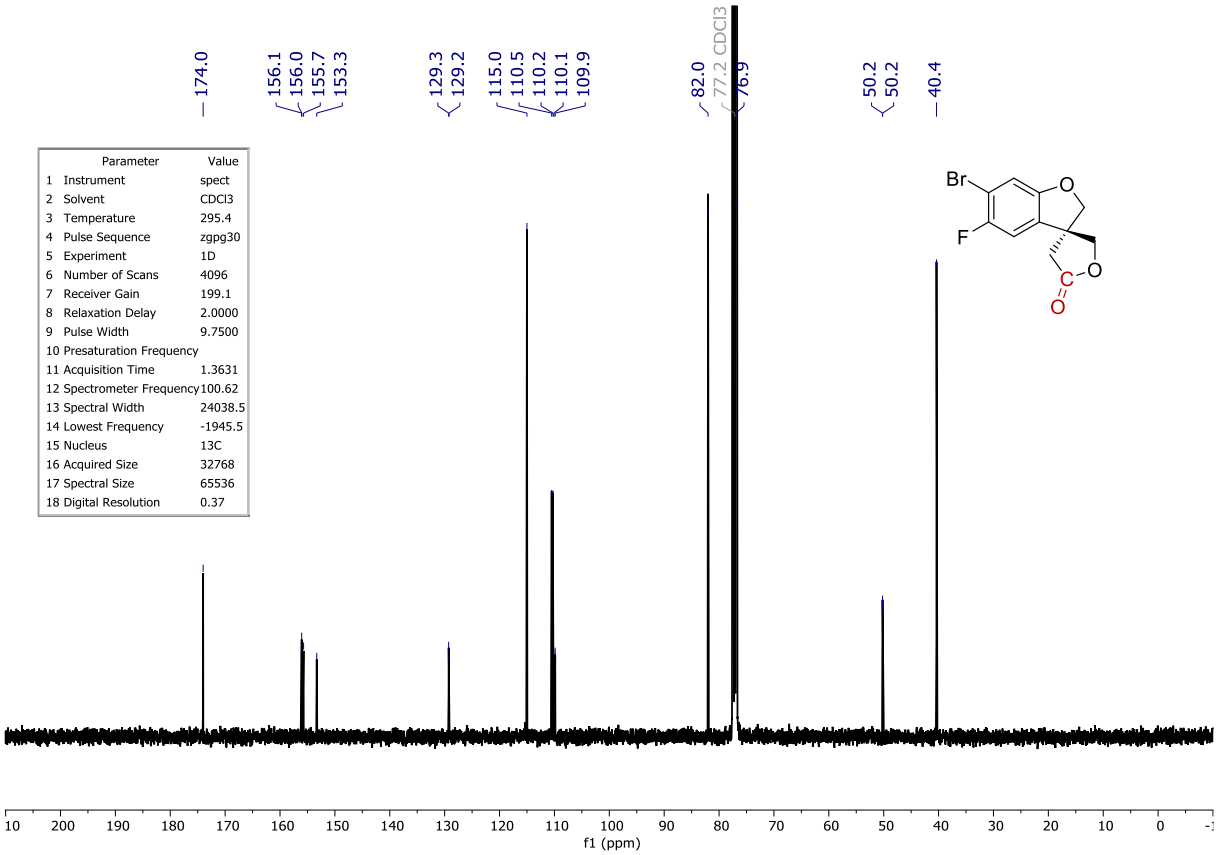

Figure S79. ^{13}C NMR spectrum ($CDCl_3$, 101 MHz) of (*S*)-6-bromo-5-fluoro-2*H*,2'*H*-spiro[benzofuran-3,3'-furan]-5'(4'*H*)-one – ***ent*-3h**

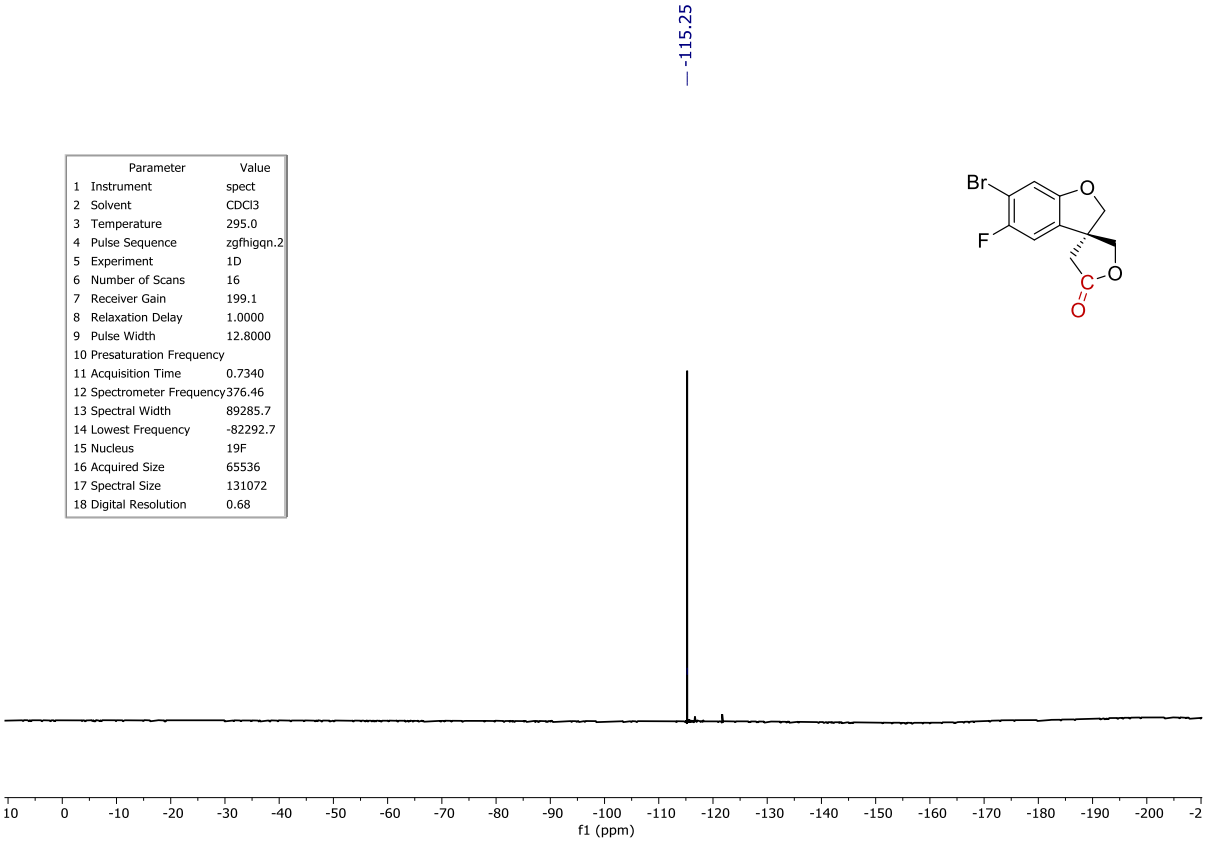

Figure S80. ^{19}F NMR spectrum (376 MHz, $CDCl_3$) of (*S*)-6-bromo-5-fluoro-2*H*,2'*H*-spiro[benzofuran-3,3'-furan]-5'(4'*H*)-one – ***ent*-3h**

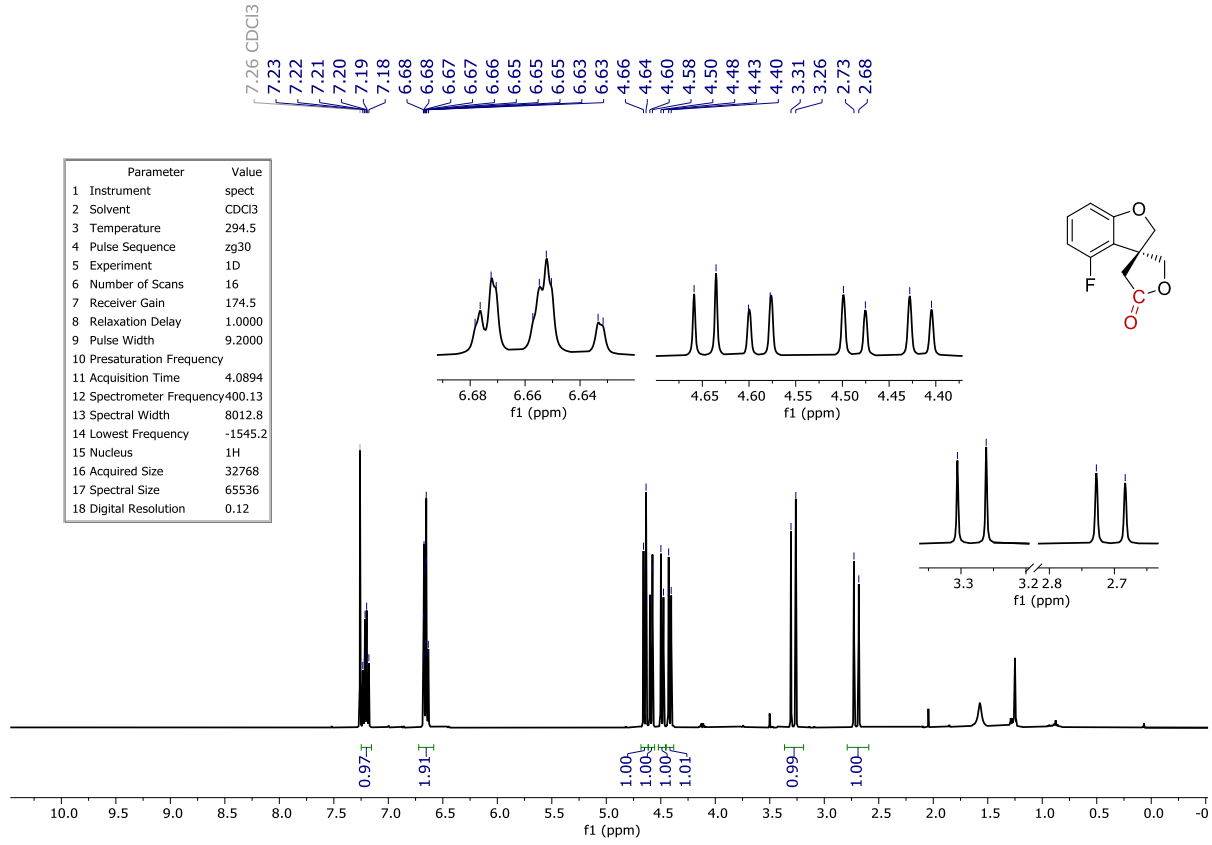

Figure S81. ^{1}H NMR spectrum ($CDCl_3$, 400 MHz) of (*R*)-4-fluoro-2*H*,2'*H*-spiro[benzofuran-3,3'-furan]-5'(4'*H*)-one – **3i**

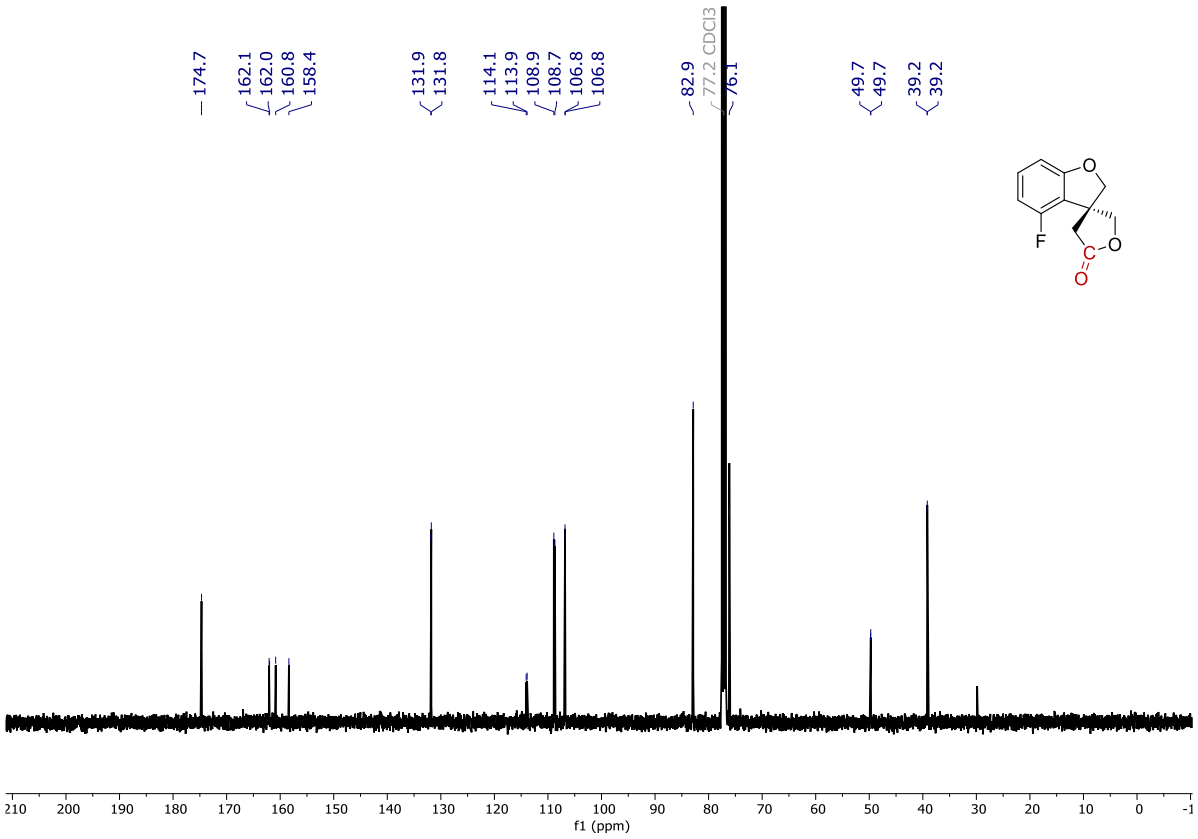

Figure S82. ^{13}C NMR spectrum ($CDCl_3$, 101 MHz) of (*R*)-4-fluoro-2*H*,2'*H*-spiro[benzofuran-3,3'-furan]-5'(4'*H*)-one – **3i**

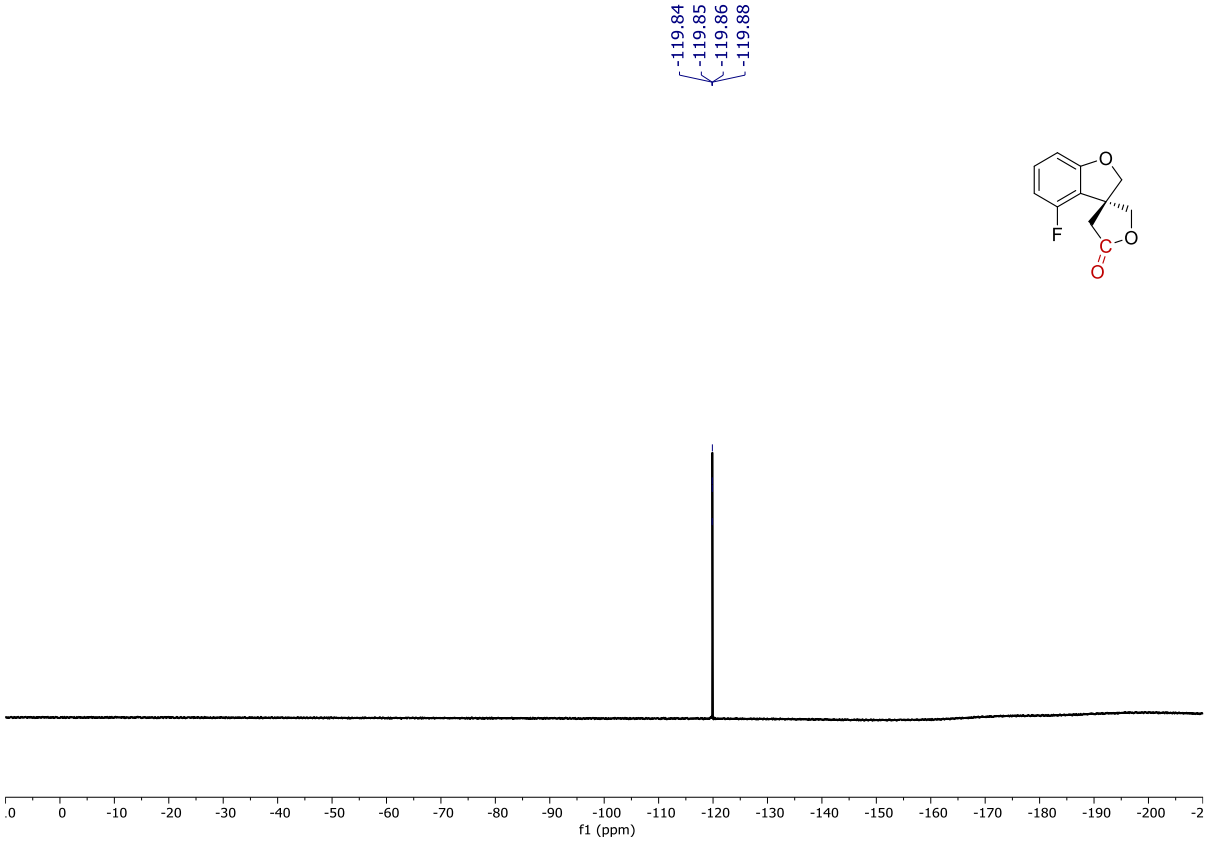

Figure S83. ^{19}F NMR spectrum (376 MHz, $CDCl_3$) of (*R*)-4-fluoro-2*H*,2'*H*-spiro[benzofuran-3,3'-furan]-5'(4'*H*)-one – **3i**

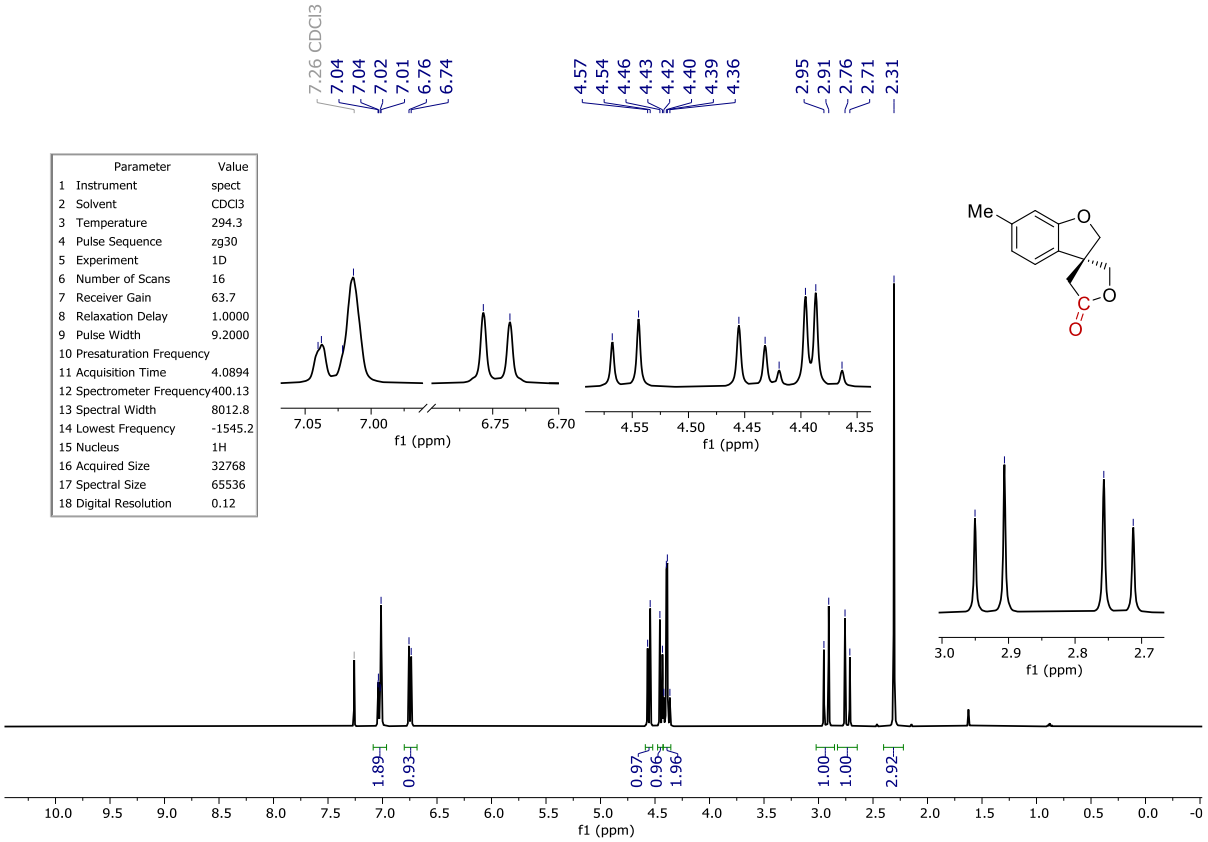

Figure S84. ^{1}H NMR spectrum ($CDCl_3$, 400 MHz) of (*R*)-6-methyl-2*H*,2'*H*-spiro[benzofuran-3,3'-furan]-5'(4'*H*)-one – **3j**

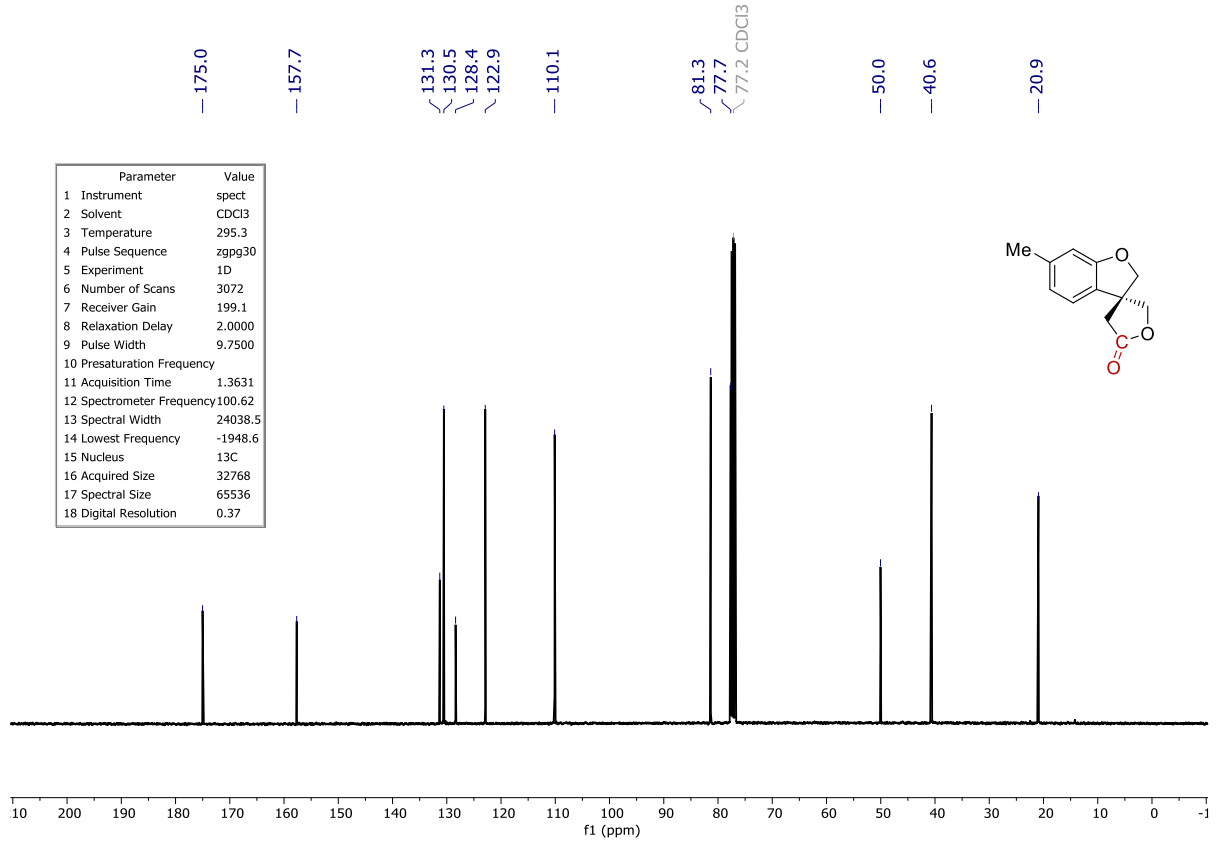

Figure S85. ^{13}C NMR spectrum ($CDCl_3$, 101 MHz) of (*R*)-6-methyl-2*H*,2'*H*-spiro[benzofuran-3,3'-furan]-5'(4'*H*)-one – **3j**

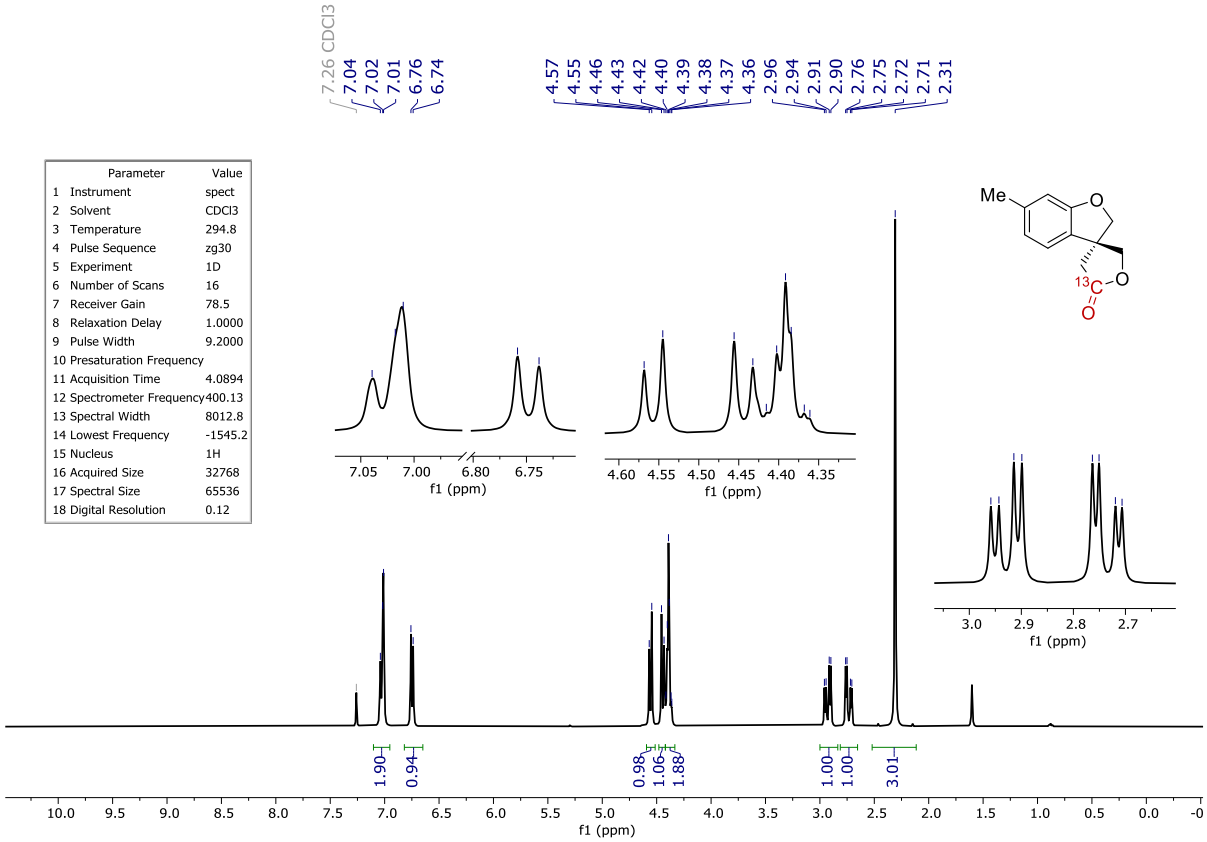

Figure S86. ^{1}H NMR spectrum ($CDCl_3$, 400 MHz) of (*R*)-5-methyl-2H,2'H-spiro[benzofuran-3,3'-furan]-5'(4'H)-one-5'-^{13}C – **^{13}C-3j**

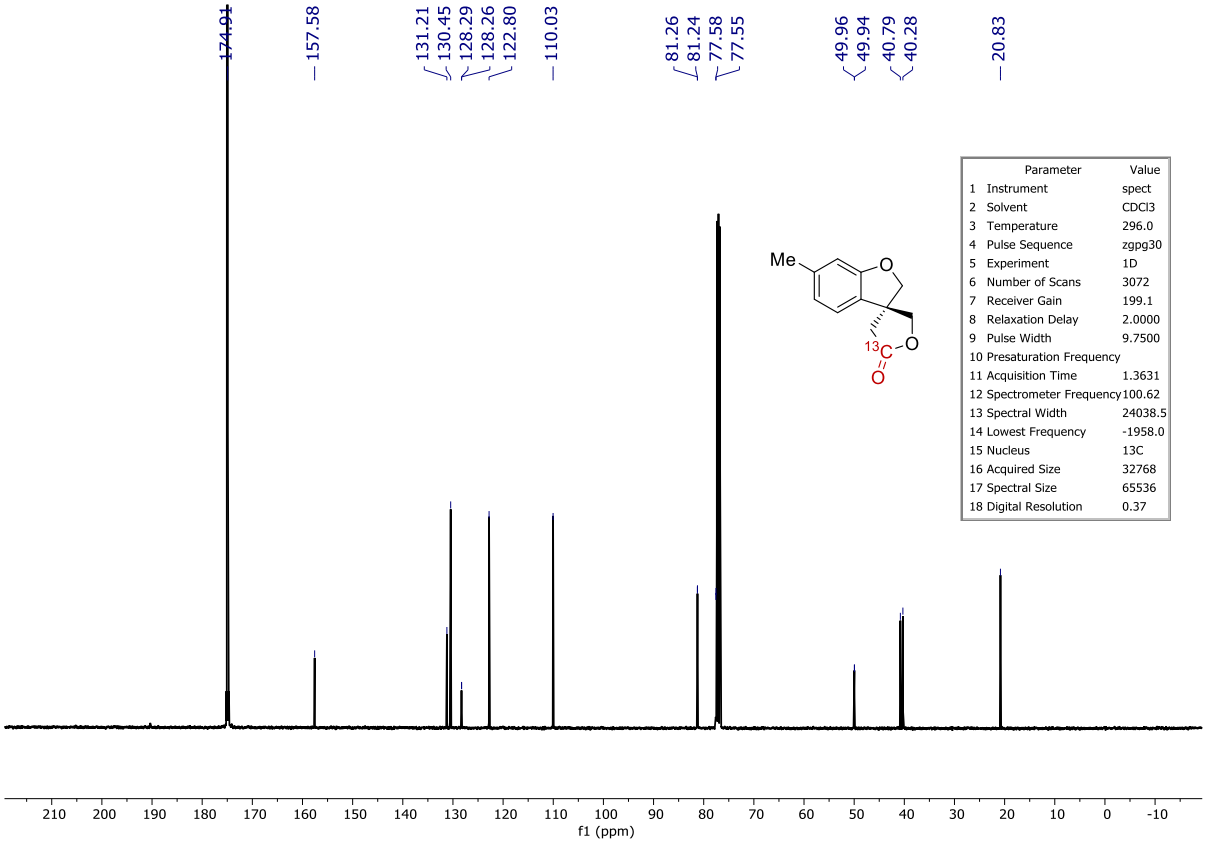

Figure S87. ^{13}C NMR spectrum ($CDCl_3$, 101 MHz) of (*R*)-5-methyl-2H,2'H-spiro[benzofuran-3,3'-furan]-5'(4'H)-one-5'-^{13}C – **^{13}C-3j**

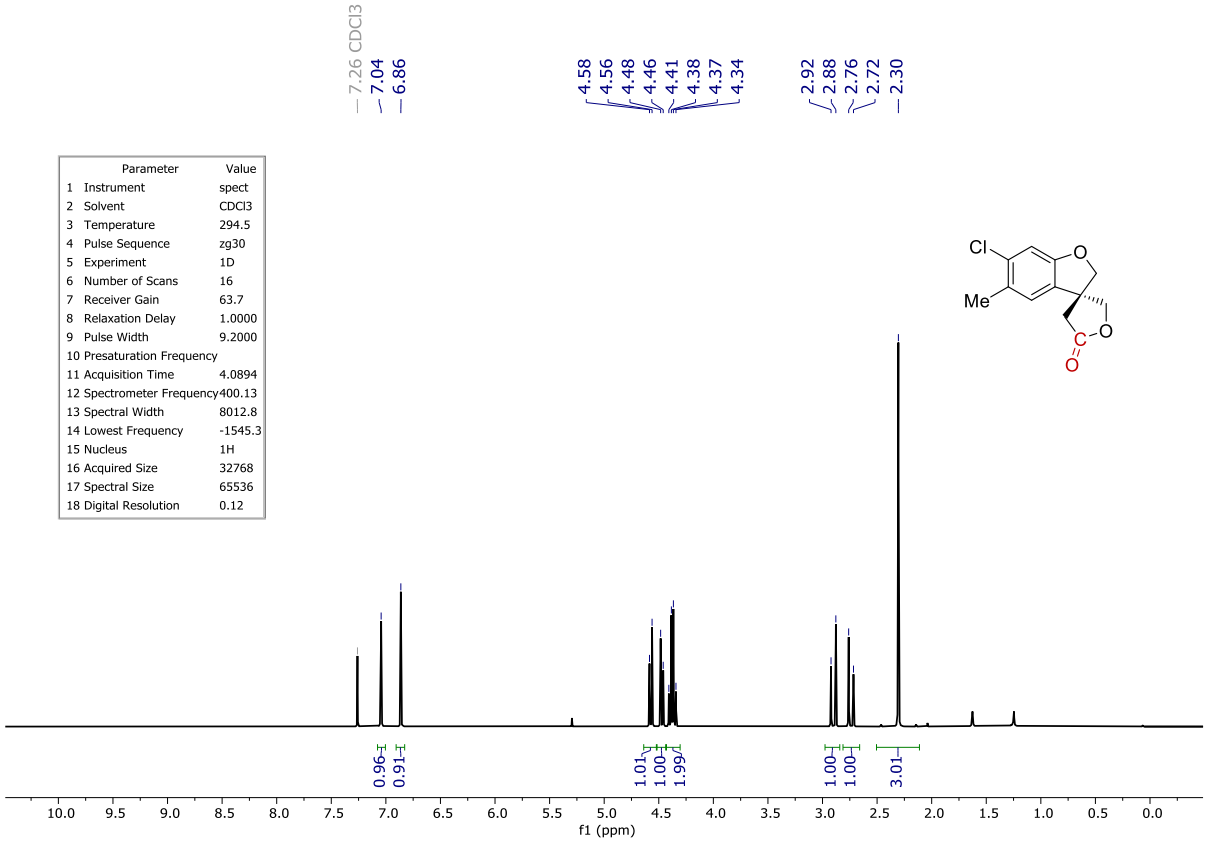

Figure S88. ^{1}H NMR spectrum ($CDCl_3$, 400 MHz) of (*R*)-6-chloro-5-methyl-2*H*,2'*H*-spiro[benzofuran-3,3'-furan]-5'(4'*H*)-one – **3k**

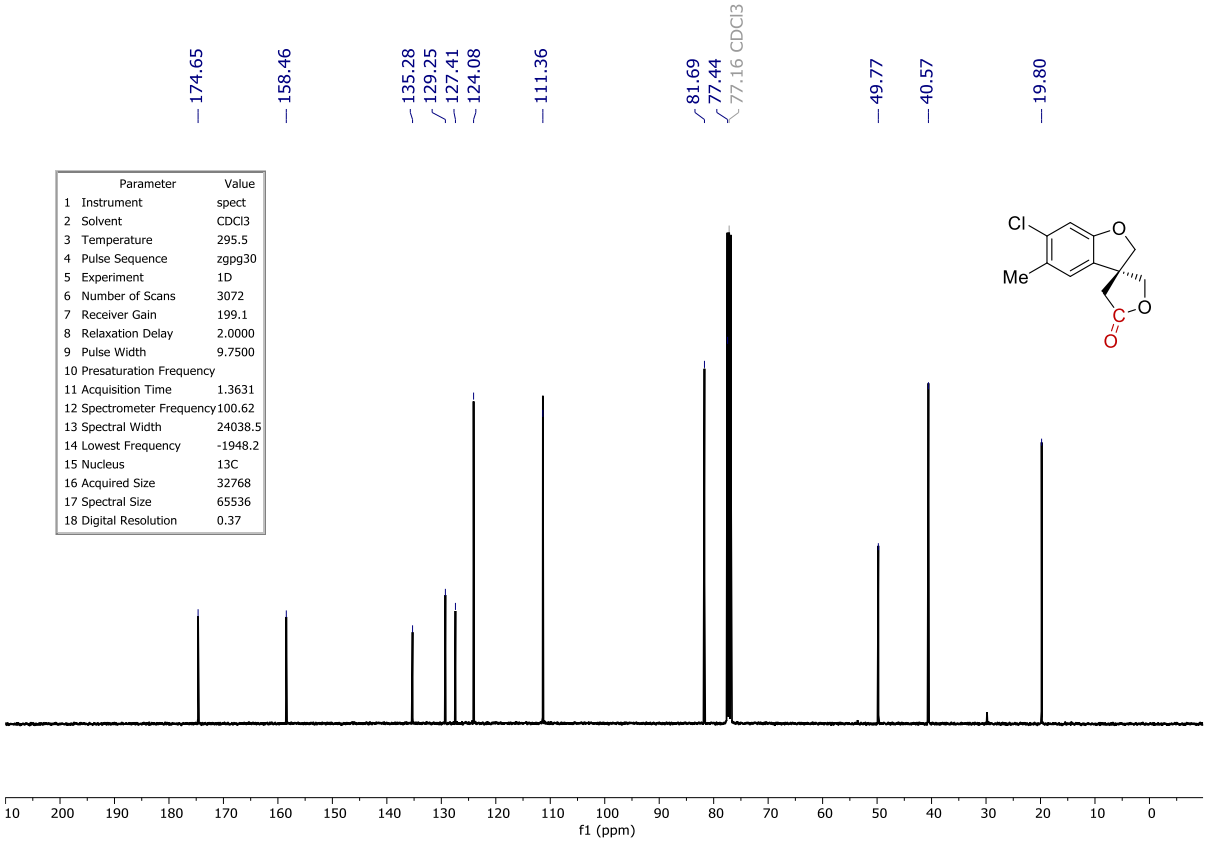

Figure S89. ^{13}C NMR spectrum ($CDCl_3$, 101 MHz) of (*R*)-6-chloro-5-methyl-2*H*,2'*H*-spiro[benzofuran-3,3'-furan]-5'(4'*H*)-one – **3k**

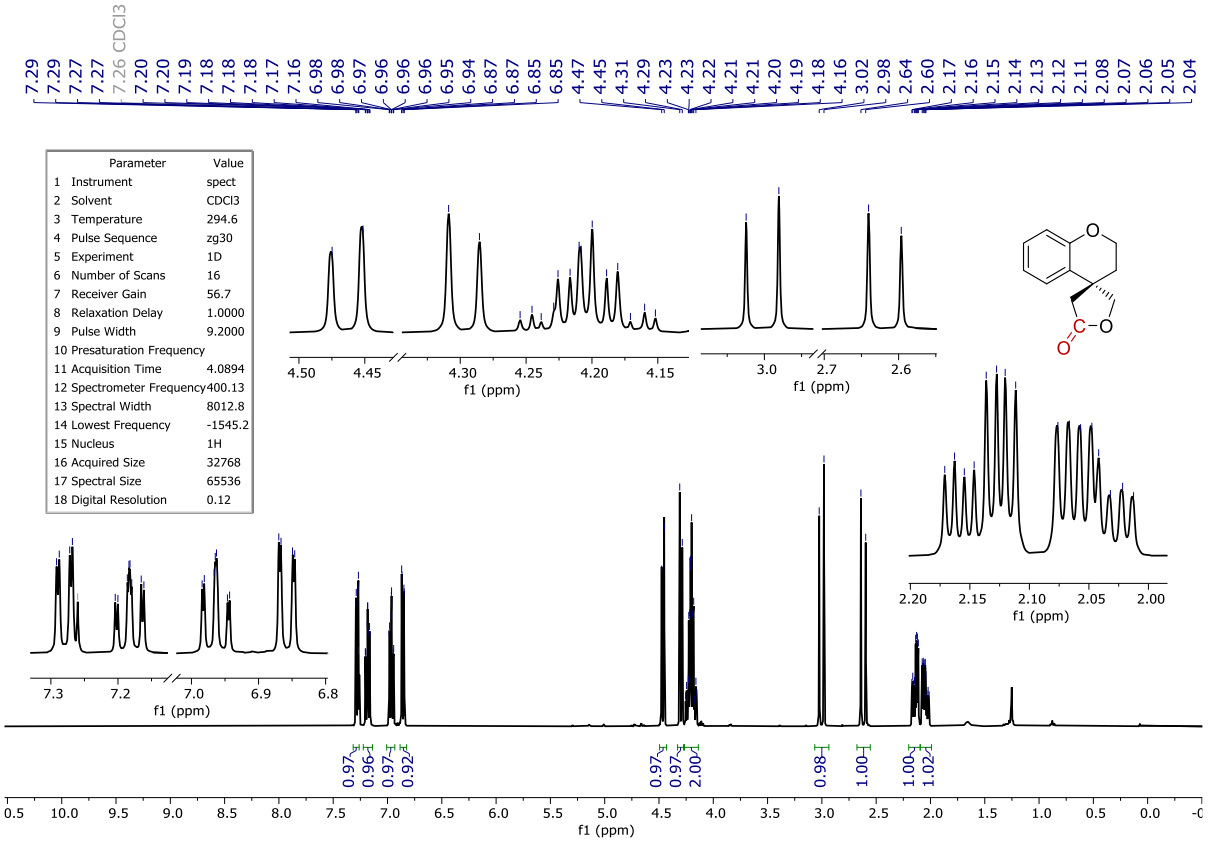

Figure S90. ^{1}H NMR spectrum ($CDCl_3$, 400 MHz) of (*R*)-2'*H*-spiro[chromane-4,3'-furan]-5'(4'*H*)-one – **3m**

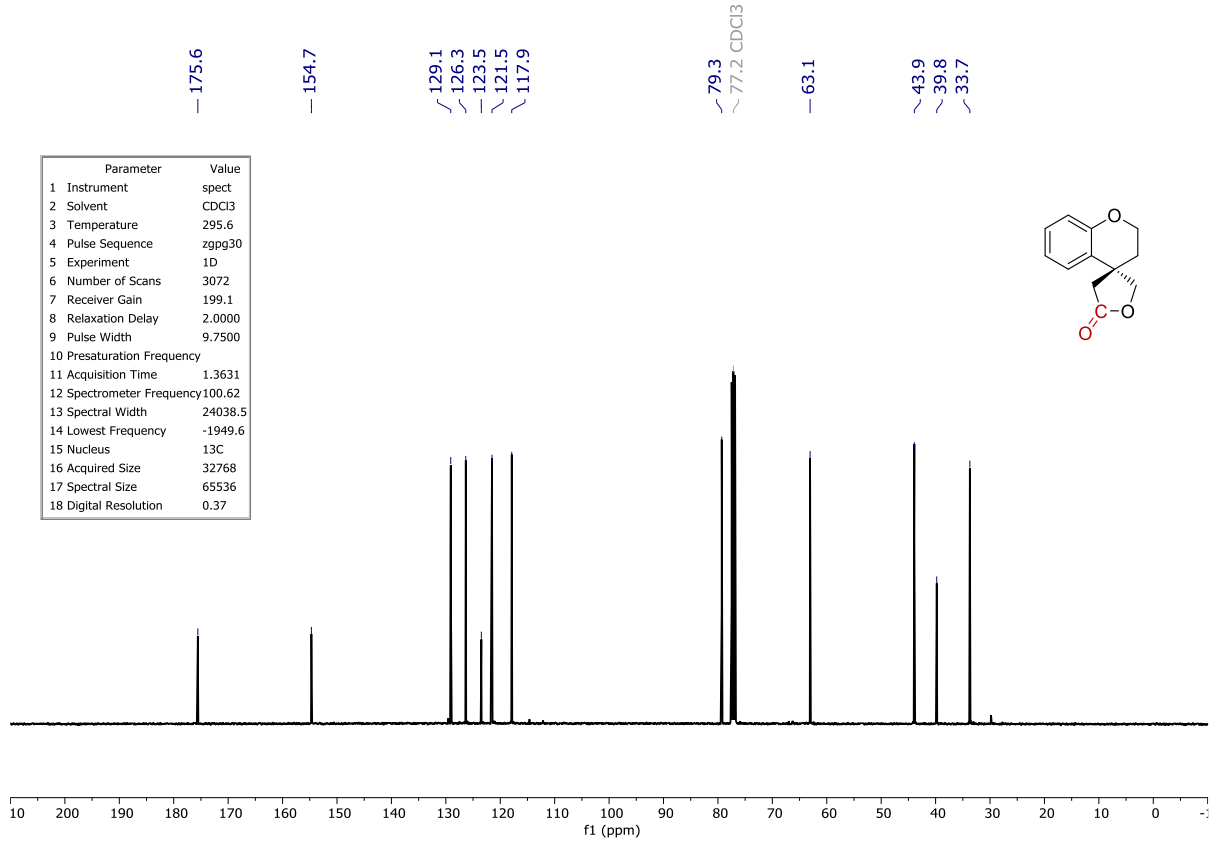

Figure S91. ^{13}C NMR spectrum ($CDCl_3$, 101 MHz) of (*R*)-2'*H*-spiro[chromane-4,3'-furan]-5'(4'*H*)-one – **3m**

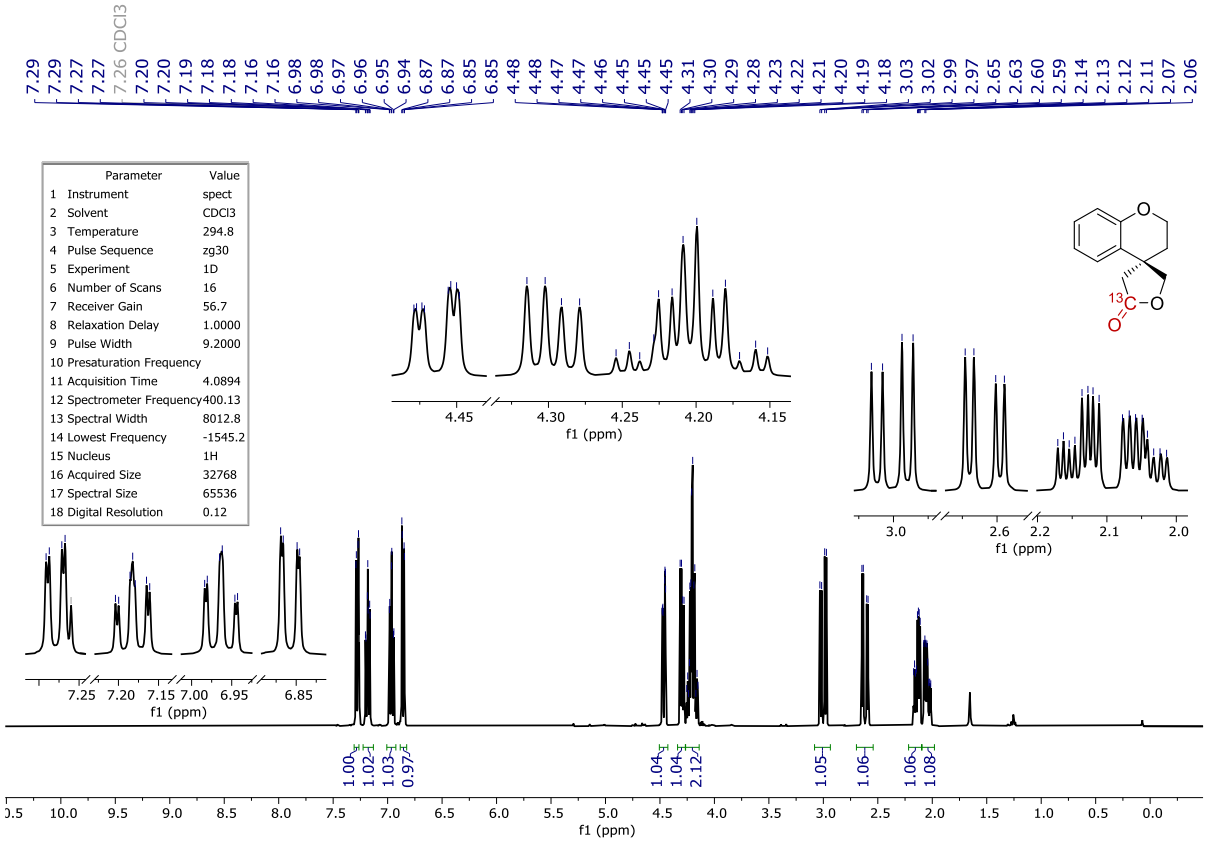

Figure S92. ^{1}H NMR spectrum ($CDCl_3$, 400 MHz) of (*S*)-2'*H*-spiro[chromane-4,3'-furan]-5'(4'*H*)-one-5'-^{13}C – **^{13}C-*ent*-3m**

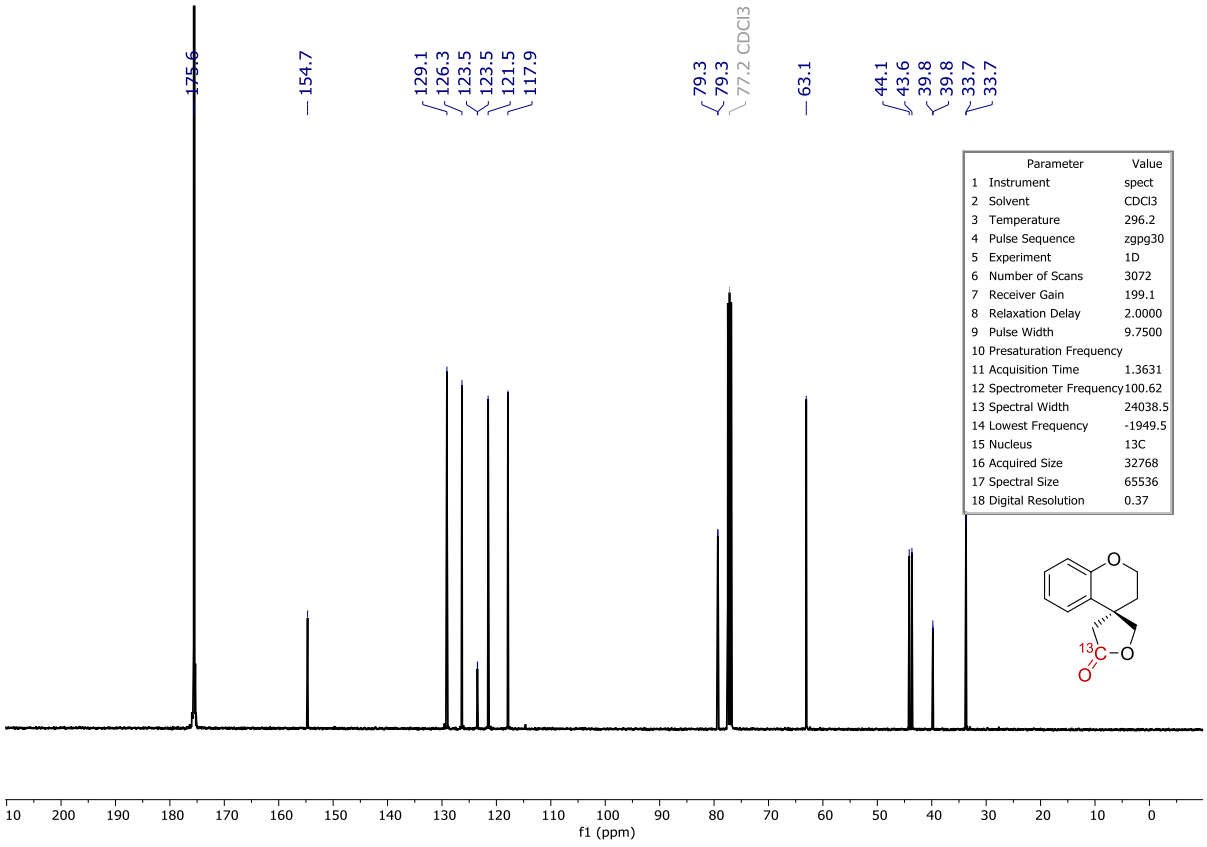

Figure S93. ^{13}C NMR spectrum ($CDCl_3$, 101 MHz) of (*S*)-2'*H*-spiro[chromane-4,3'-furan]-5'(4'*H*)-one-5'-^{13}C – **^{13}C-*ent*-3m**

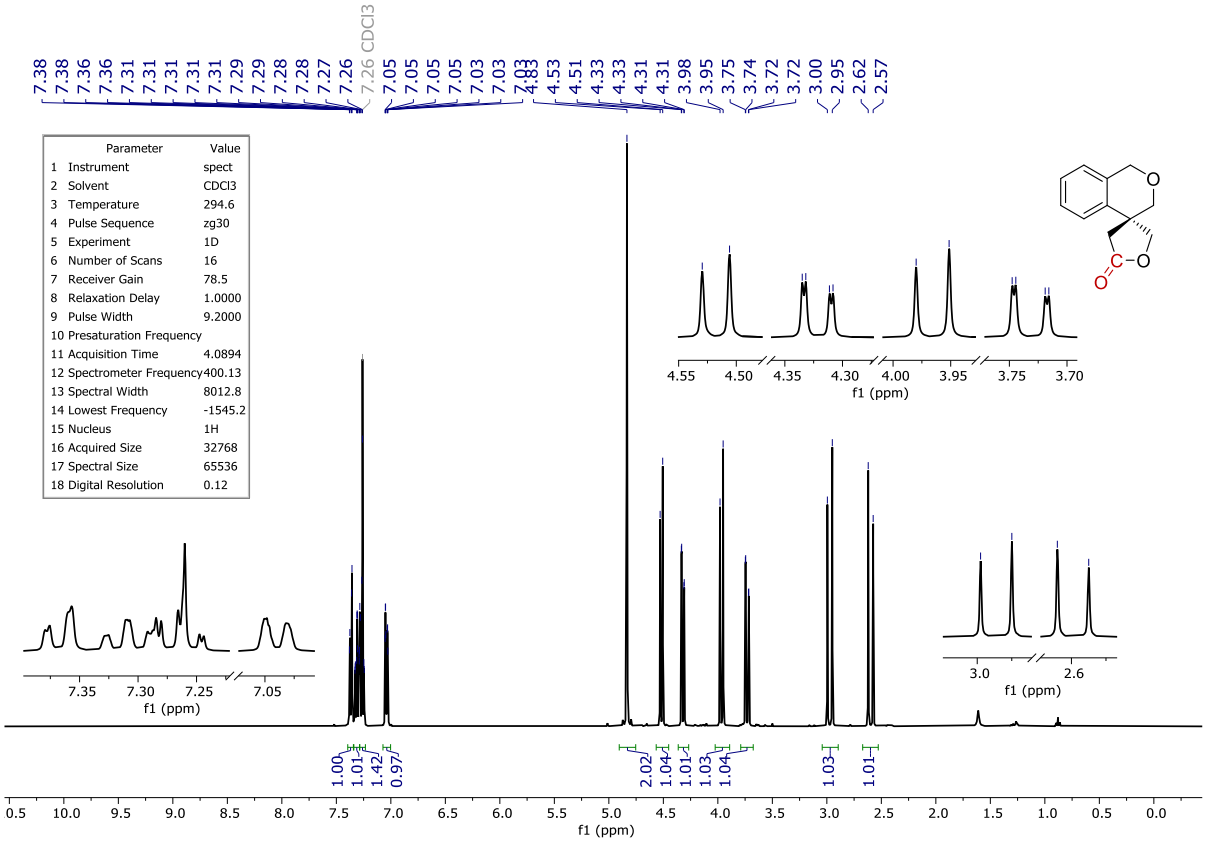

Figure S94. ^{1}H NMR spectrum ($CDCl_3$, 400 MHz) of (*R*)-2*H*-spiro[furan-3,4'-isochroman]-5(4*H*)-one – **3n**

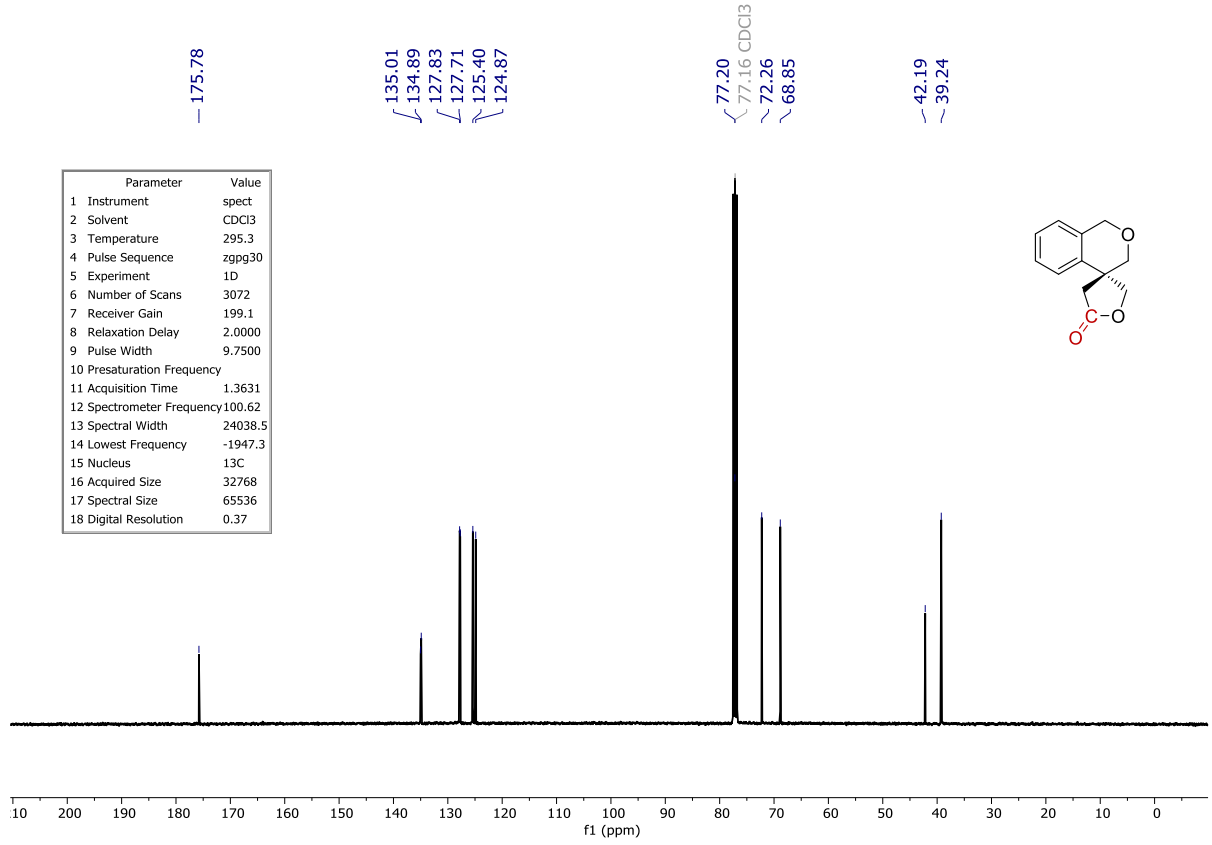

Figure S95. ^{13}C NMR spectrum ($CDCl_3$, 101 MHz) of (*R*)-2*H*-spiro[furan-3,4'-isochroman]-5(4*H*)-one – **3n**

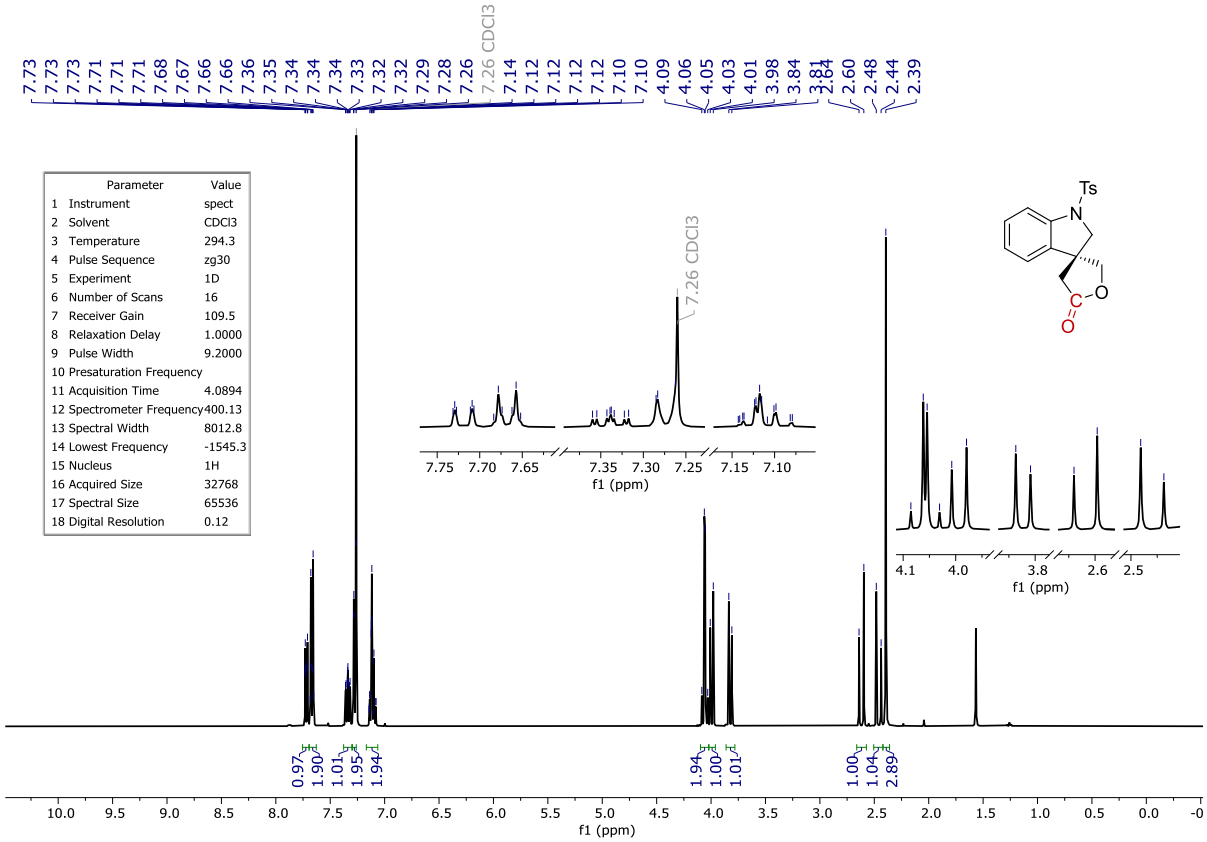

Figure S96. ^{1}H NMR spectrum ($CDCl_3$, 400 MHz) of (*R*)-1'-tosyl-2*H*-spiro[furan-3,3'-indolin]-5(4*H*)-one – **3o**

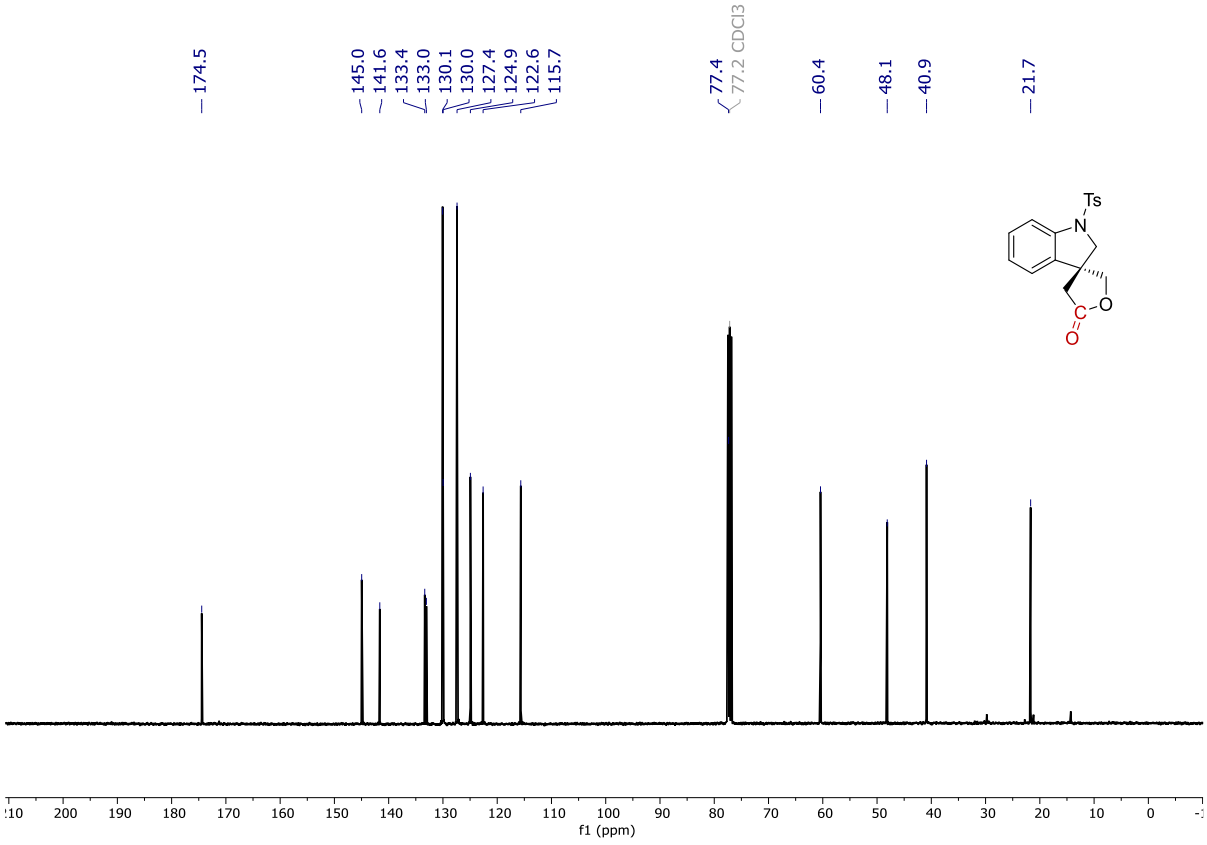

Figure S97. ^{13}C NMR spectrum ($CDCl_3$, 101 MHz) of (*R*)-1'-tosyl-2*H*-spiro[furan-3,3'-indolin]-5(4*H*)-one – **3o**

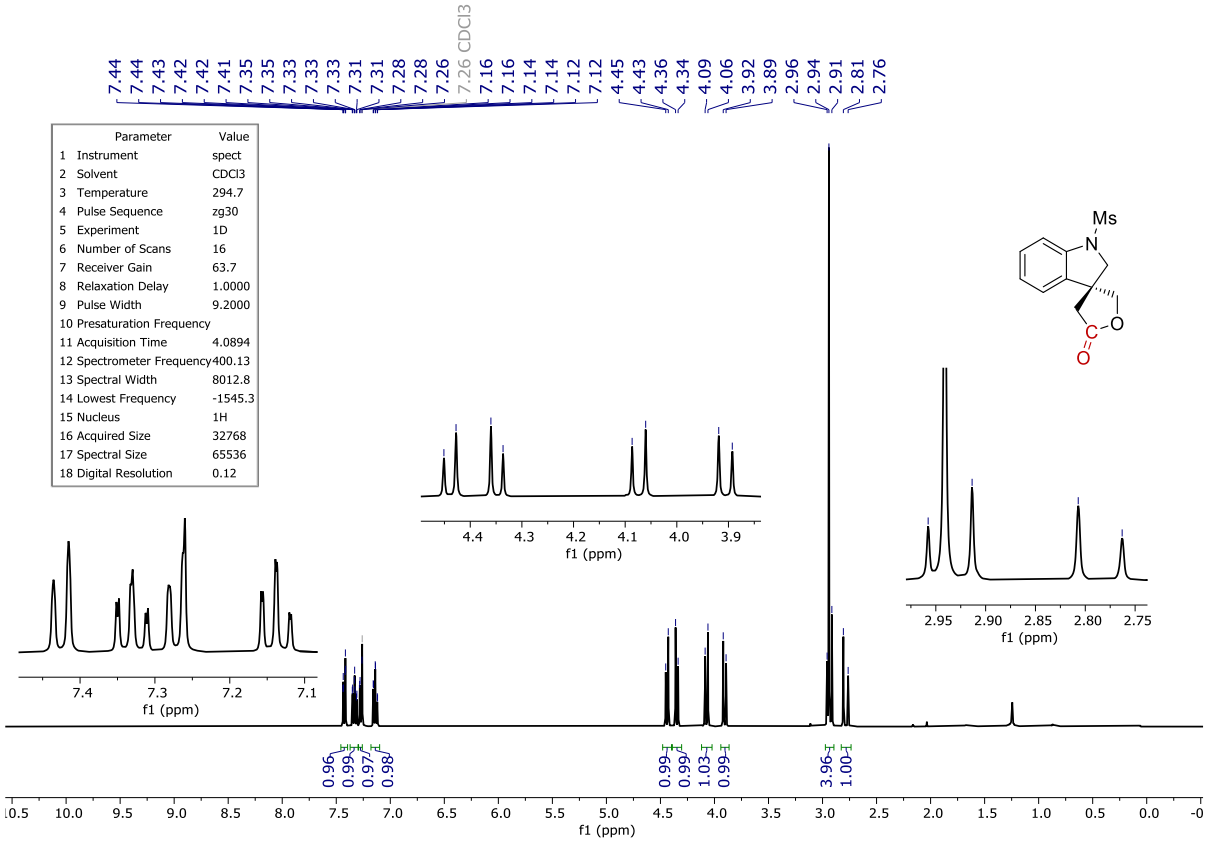

Figure S98. ^{1}H NMR spectrum ($CDCl_3$, 400 MHz) of (*R*)-1'-(methylsulfonyl)-2*H*-spiro[furan-3,3'-indolin]-5(4*H*)-one – **3p**

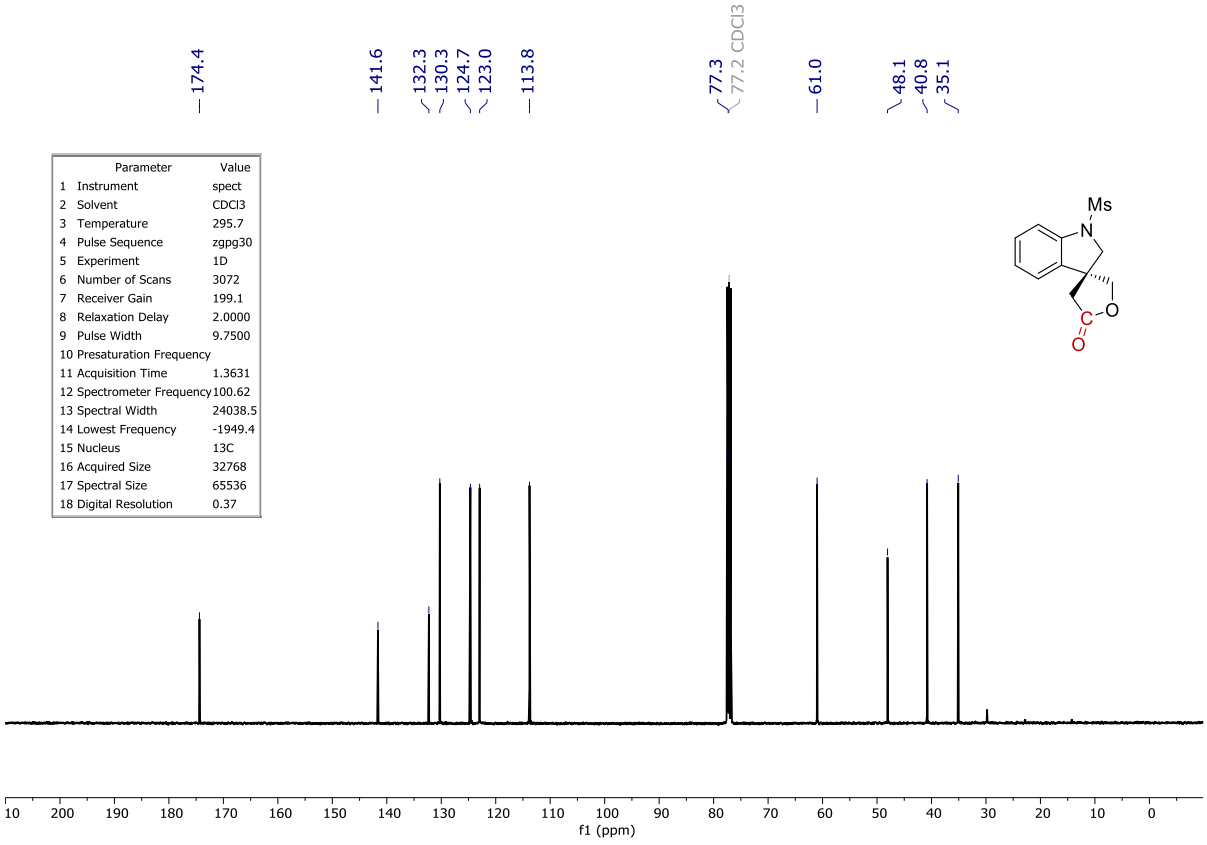

Figure S99. ^{13}C NMR spectrum ($CDCl_3$, 101 MHz) of (*R*)-1'-(methylsulfonyl)-2*H*-spiro[furan-3,3'-indolin]-5(4*H*)-one – **3p**

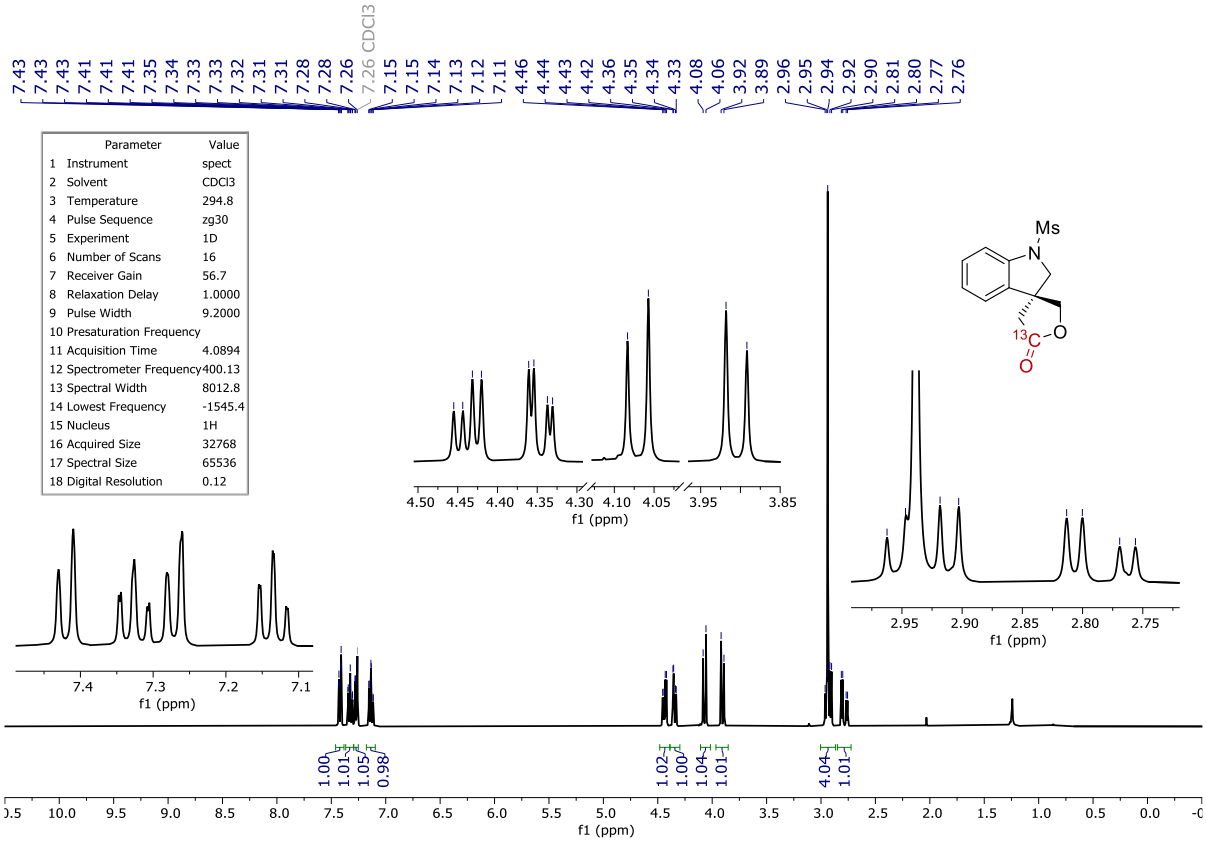

Figure S100. ^{1}H NMR spectrum ($CDCl_3$, 400 MHz) of (*S*)-1'-(methylsulfonyl)-2*H*-spiro[furan-3,3'-indolin]-5(4*H*)-one – **^{13}C-*ent*-3p**

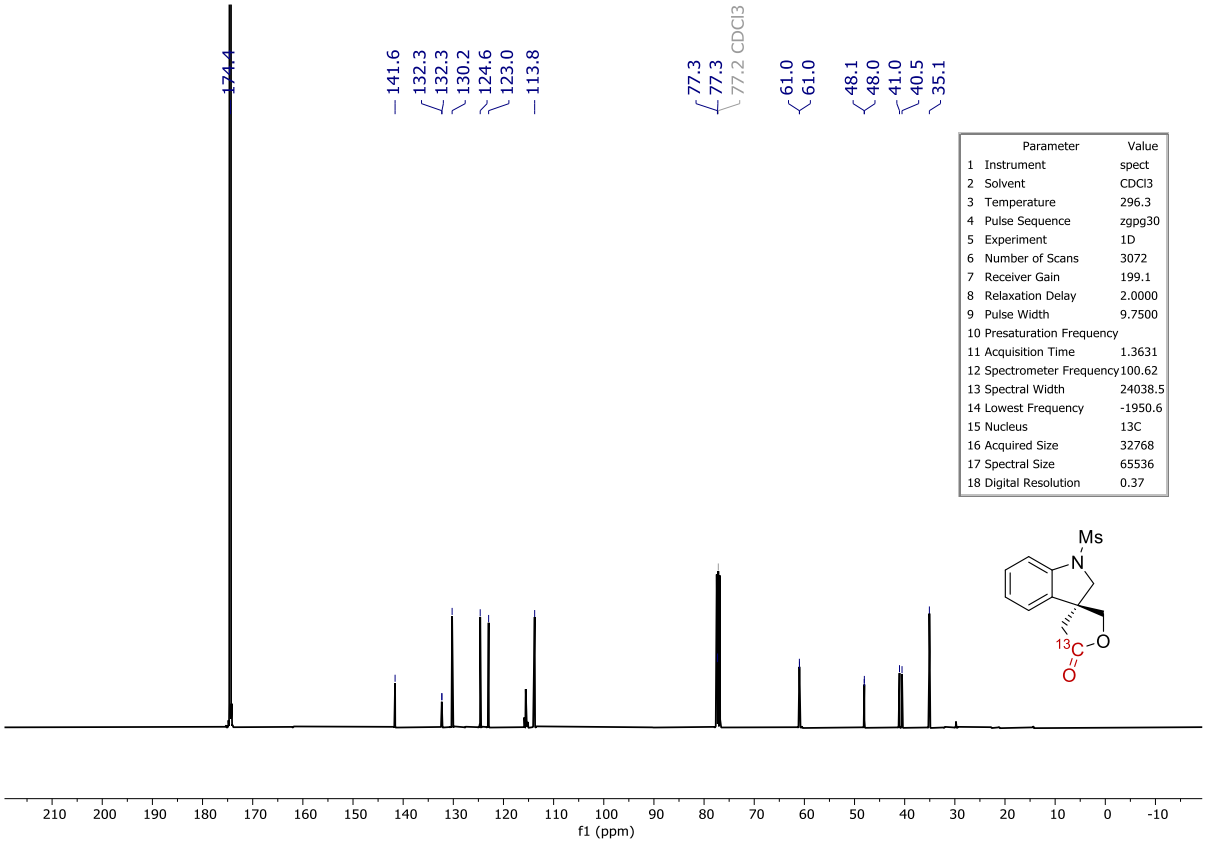

Figure S101. ^{13}C NMR spectrum ($CDCl_3$, 101 MHz) of (*S*)-1'-(methylsulfonyl)-2*H*-spiro[furan-3,3'-indolin]-5(4*H*)-one – **^{13}C-*ent*-3p**

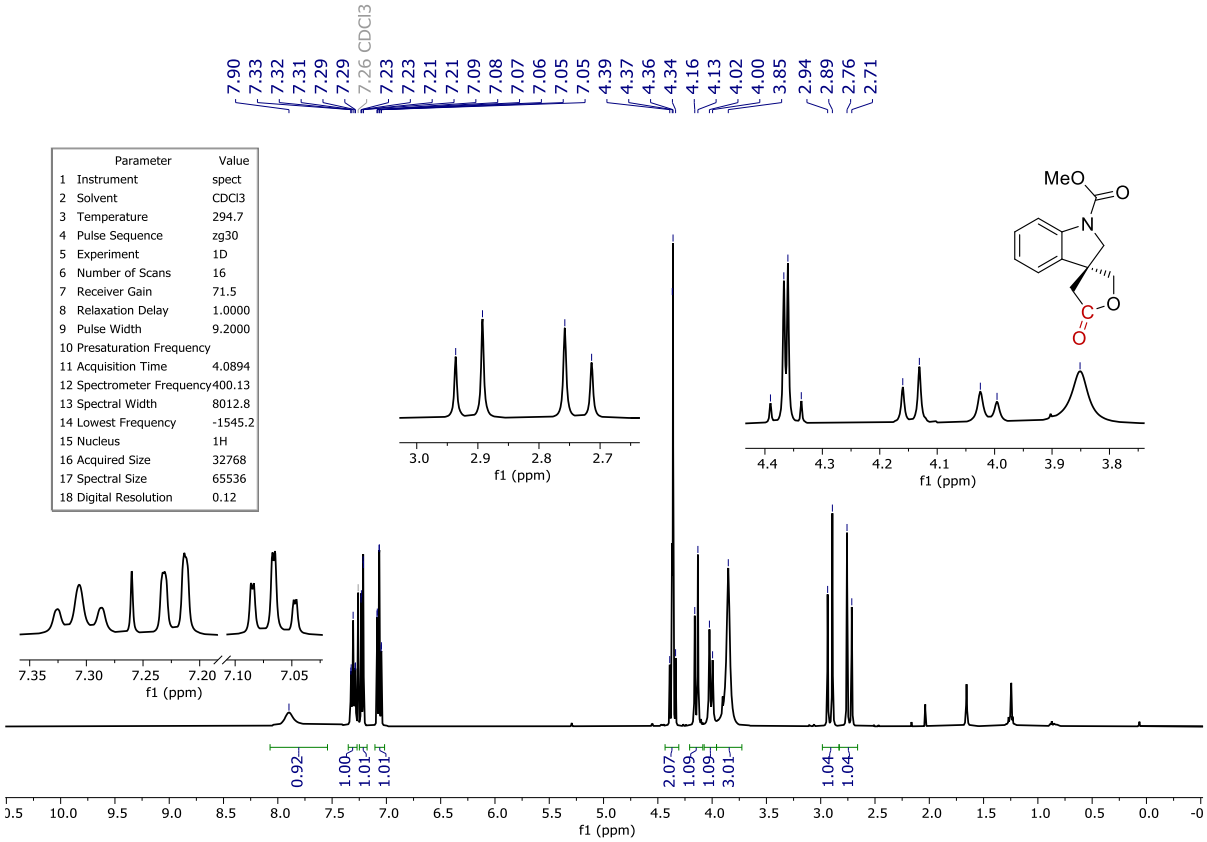

Figure S102. ^{1}H NMR spectrum ($CDCl_3$, 400 MHz) of Methyl (*R*)-5-oxo-4,5-dihydro-2*H*-spiro[furan-3,3'-indoline]-1'-carboxylate – **3q**

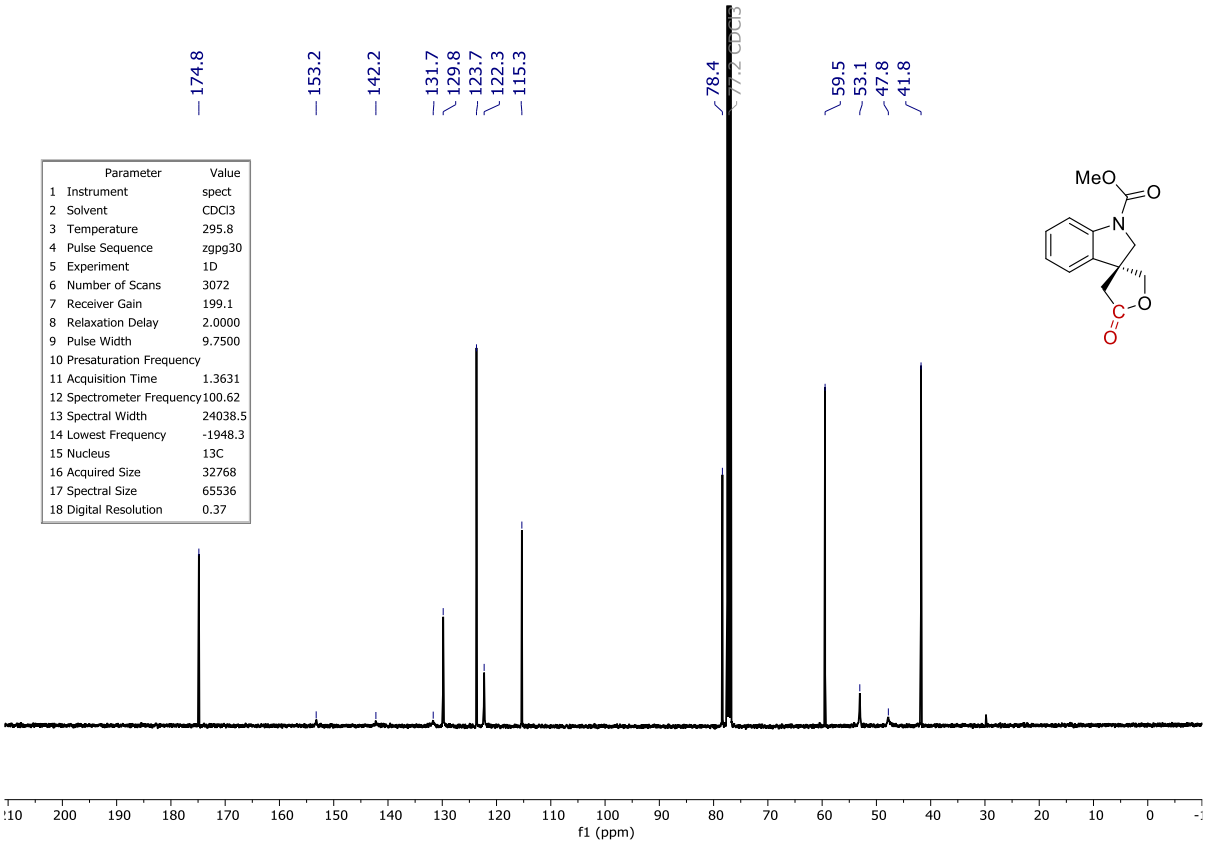

Figure S103. ^{13}C NMR spectrum ($CDCl_3$, 101 MHz) of Methyl (*R*)-5-oxo-4,5-dihydro-2*H*-spiro[furan-3,3'-indoline]-1'-carboxylate – **3q**